INFRA-RED and ELECTRO-OPTICS

development components
research systems
manufacture instruments

BARNES ENGINEERING COMPANY
30 Commerce Road Stamford, Connecticut

BEC PROJECT 3744

BARNES ENGINEERING COMPANY
30 Commerce Road
Stamford, Connecticut

PHASE IA STUDY REPORT

EARTH/LUNAR HORIZON SENSOR PROGRAM

PREPARED BY:

Frank Schwarz
Frank Schwarz
Project Manager

Thomas Falk
Thomas Falk
Project Engineer

WITH ASSISTANCE FROM:

Newton N. Chapnick
Gerald Falbel
M. Monty Merlen
Peter E. Spangenberg
Kenneth A. Ward

APPROVED BY:

Frank Schwarz
Frank Schwarz
Head, Advanced Development Department

Robert W Astheimer
Robert W. Astheimer
Technical Director
DEFENSE AND SPACE DIVISION

DATE: September 14, 1965

TABLE OF CONTENTS

Contents (cont.)

LIST OF ILLUSTRATIONS

Illustrations (cont.)

Illustrations (cont.)

Illustrations (cont.)

1. INTRODUCTION

This Phase IA report of the Earth/Lunar Horizon Sensor program discusses the technical aspects of the various types of horizon sensors which may be considered for possible use in the Apollo Extension System space missions. It attempts to narrow down the choice from a fair variety of sensor types to the one which is thought to satisfy the design goals which have been specified and which can be implemented within the scope of the program, both from the standpoint of demonstrating the performance characteristics and doing so within the specified time and budget.

In this report we will discuss principally the technical considerations guiding this choice and will do so only in the limited sense of covering the special aspects of sensor technology which we consider vital for the present program. We will not discuss the broad subject and fundamentals of horizon sensors which have been covered adequately elsewhere but only those characteristics which are pertinent to the choice of an optimum system.

Thus we will assume that the reader has a general familiarity with the basic horizon sensor concepts and state

of the art. We will further assume that certain choices have already been made in specific components and elements of the system. The unique advantages of thermal detectors such as the thermistor and solid-backed thermopile have already been well established, as have various elements of the optics, mechanical design, and electronic processing. We have also avoided any concepts which we consider beyond attainment within the scope of a one-year program.

This report discusses three basic horizon sensor system concepts, with variations of each. These three are:

(1) Conical Scan Sensors

(2) Electronically Scanned Sensors

(3) Edge Trackers

Not all of the system concepts which we have analyzed were found to be capable of meeting the requirements for lunar use. However, as a matter of general interest, we have included discussions of these concepts in this report.

Section 2 discusses the spectral and optical considerations applicable to the earth-lunar horizon sensor design.

Section 3.1 discusses general signal processing concepts relative to the problem of horizon edge angular definition with high precision. This discussion is primarily applicable to conical scan sensors.

Conical scan sensors suitable for lunar use can be divided into space scan and normal conical scan types. In a space scan system, the horizon is always intersected from space to planet; while in a normal conical scanner, both the space-to-planet and planet-to-space scans are used. The signal processing approaches designed to maximize the angular definition of the horizon edge intersection for both space scan and normal conical scan horizon sensors are discussed in Paragraphs 3.1.1 through 3.1.4.

For the normal conical scan type of horizon sensor on the moon, the planet pulse must be differentiated or the edge gradient must be sensed. The problem in this scan for lunar use is recognition of the pulse defining the leading and trailing lunar horizons. The signal processing concepts applicable to the normal conical scan sensor when used on the moon are discussed in Paragraph 3.1.5.

Section 3.2 discusses the design considerations applicable to electronically scanned horizon sensors for earth-lunar use.

Section 3.3 discusses the design considerations applicable to various types of edge trackers. At least one of these concepts using field switching at the edge of the planet and which is described in Section 3.3.2.4 appears to meet all the requirements for the Earth/Lunar Horizon Sensor System. Some other approaches are described which are not considered satisfactory.

Section 4 is a review of the significant characteristics of the various horizon sensor concepts described in Section 3. In it are discussed various advantages and disadvantages of the several approaches considered and their relationship to the mission requirements.

Section 5 discusses the reliability considerations of the various horizon sensor approaches. In this section we have tabulated Mean Time Before Failure figures for tentative designs of the three systems which are capable of meeting the design goals of sensitivity and accuracy for the present program.

In Section 6 we present our conclusions and recommendations for Phases IB and II of this program.

2. SPECTRAL AND OPTICAL CONSIDERATIONS

The horizon of the earth as seen from space is not an abrupt discontinuity; there is a region of gradual transition from the zero radiance of space to full radiance. This region is from about 60 km above the earth's surface to the surface itself. The shape of this plot of radiance versus altitude depends upon the temperature, pressure, water vapor content, etc. of the air at that particular point on the earth and also upon the band of wavelengths to which the horizon sensor is sensitive. Variations in these plots cause uncertainty in the exact horizon position for a horizon sensor and therefore directly affect the sensor accuracy.

Three independent groups of investigators have established their own computer programs for determining these profiles. The groups are (1) Hanel, Bandeen, and Conrath at Goddard Space Flight Center, (2) Burn and Oppel at Lockheed MSC, Sunnyvale, California, and (3) Wark, Alishouse, and Yamamoto of the U. S. Weather Bureau. The work of Dr. Wark is particularly useful in that he has published tables of radiance versus altitude for a large number of narrow wavelength intervals (in general,

intervals of 25 cm^{-1}) for each of eight model atmospheres. By multiplying the radiance in a given interval by the transmission of a particular optical system in that interval and summing the resulting products, a profile of radiance versus altitude can be calculated for that optical system. Identical calculations with data for another model atmosphere yield another profile.

Profiles for Dr. Wark's model atmospheres A, B, C, and D have been computed as outlined above for a system sensitive only between 20 and 40 microns. These are shown in Figure 2-1. The interesting features of this plot are the following:

(1) Radiance variations for the worst case conditions to be encountered in viewing the earth's atmosphere in the 20 to 40 micron band (in the range of elevations around 200 nautical miles) are only about two to one.

(2) At a low level of radiance at the upper layers of atmosphere, the variations in altitude at which identical radiance levels are encountered are very small.

These observations warrant certain conclusions with regard to the system accuracy obtainable with a sensor operating in this spectral interval and sensing the earth's atmosphere.

(1) The dynamic range requirements are not excessive (two-to-one variations in energy are expected).

(2) Since the total energy available in this broad spectral region is greater than would be obtained in a narrow region in the shorter wavelengths (e.g., 15 micron CO_2 band), we can expect to obtain a reasonably high signal-to-noise ratio.

(3) At a low threshold level (comfortably above the system noise level), we can register a scan crossover point which is reasonably independent of the climatic and seasonal conditions of the region scanned. For example, at a radiance level of 1/20 of the highest value which could be encountered according to the model atmosphere studied, the maximum variation in altitude for the different atmospheric models are of the order of 5 km. For a conical scan sensor which may be considered and at the 300 nautical mile altitude, this corresponds to an error of about 0.1°. This error is, of course, averaged over two crossover positions for the horizon sensor system.

(4) Since the sensor would be measuring attitude with reference to positions in the upper atmosphere, there are no serious cloud problems in evidence. The data plotted is based

on atmospheric models which include the effects of normal cloud conditions. The curves shown in Figure 2-1 are rather similar to the radiance profiles of a 15 micron CO_2 band centered earth atmosphere.

In a recent flight test of an experimental horizon sensor, radiometric data were gathered for an optical bandpass very similar to that proposed here. The spectral band of this sensor was 14-16 microns and 18-35 microns using silicon as the optical material. The energy in the 14-16 micron region is only about 1/7 of the total so that this system is very similar to the 20-40 micron band. Results of this flight were reported in the Proceedings of the First Symposium on Infrared Sensors for Spacecraft Guidance and Control in a paper by Lt. Col. W. T. Jones and K. A. Ward titled "Performance of Horizon Sensor Systems in Earth Orbit." Extensive radiometric data were obtained in polar, temporate, and equatorial regions of the earth. These results show no more than 2:1 contrast ratio and in general confirm the theoretical predictions.

Since the results of the investigation of the earth's radiance in the 20-40 micron spectral region appear to be quite

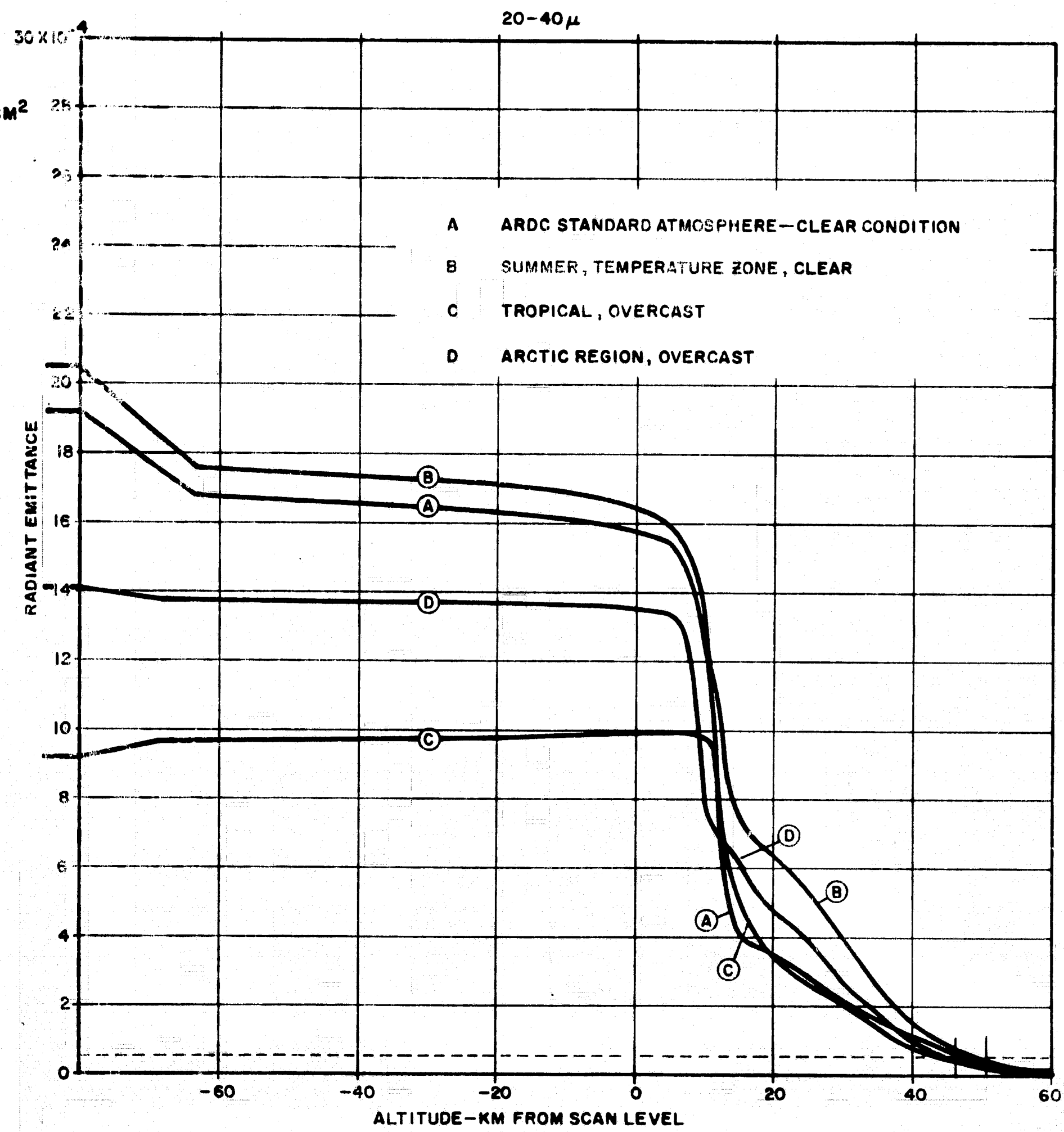

Figure 2-1 EARTH RADIANCE PROFILES FOR VARIOUS ATMOSPHERES IN THE 20-40 MICRON BAND.

favorable, we recommend that the optical system of the present sensor be designed for use of that spectral interval and that it optimize the efficiency of the various optical and detector elements to provide a high signal-to-noise ratio for all target conditions expected.

An added and powerful advantage of this choice is that the 20-40 micron spectral interval is well suited for the lunar application of this sensor. We therefore feel that the sensor can be designed with an identical detector/optical system for either lunar or earth missions, requiring no interchange of detectors or filters for a specific mission. A further advantage of this choice of spectral interval is that the relative energy from the sun and the planet is more favorable for the long wavelength sensitive system than would be the case for one which is made to operate in a shorter wavelength region closer to the peak radiance of the sun.

In addition to determining an optimum spectral region in which the Earth/Lunar Horizon Sensors will operate, we must give some consideration to the characteristics of the optical materials to be used and the detector's sensitivity in the

spectral band of interest. It will be desirable, wherever possible, to use reflecting components. Certain conical scan sensors, some versions of edge trackers, and the electronically sampled horizon sensors all may be designed to use reflecting elements for at least some of the optical components. As a rule, it will be found that optically immersed detectors will be preferable from the standpoint of sensitivity and detector size reduction.

The detector to be used, a thermistor, can be shown to have a reasonably high and uniform sensitivity in the spectral region of interest, 20-40 microns. This is seen in Figure 2-2, in which a thermistor bolometer's spectral response is limited only by the detector's long wavelength absorptance and the window used (KRS-5).

Were we to use a germanium-immersed detector, the long wavelength absorption characteristics of the thick germanium element would severely reduce the energy received by the detector and the sensitivity would be degraded. Typical of the spectral sensitivity of a germanium-immersed thermistor is the curve shown in Figure 2-3. Figure 2-4 shows the spectral

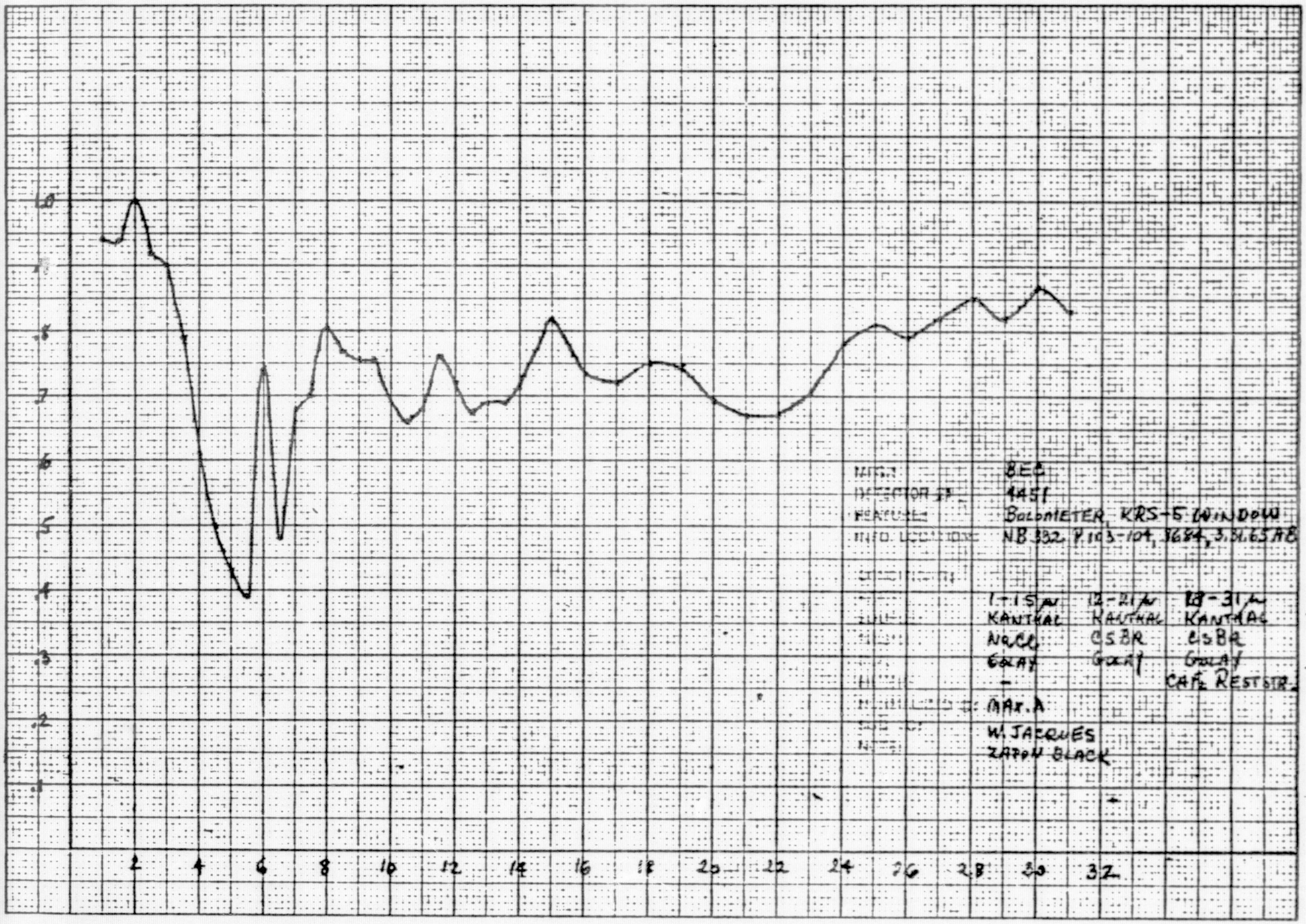
BE
1451
BOLOMETER, KRS-5 WINDOW
NB 332, P. 103-104, 3684, 3.31.65 AB
1-15 μ
KANTHAL
NaCl
GOLAY
12-21 μ
KANTHAL
CSBR
GOLAY
18-31 μ
KANTHAL
CSBR
GOLAY
CaF2 RESTSTR.
MAX. A
W. JACQUES
ZAPON BLACK
BE 1451, BOLOMETER, KRS-5 WINDOW, ZAPON
SAPPHIRE, NO M/LAR 3.31.65

Figure 2-2

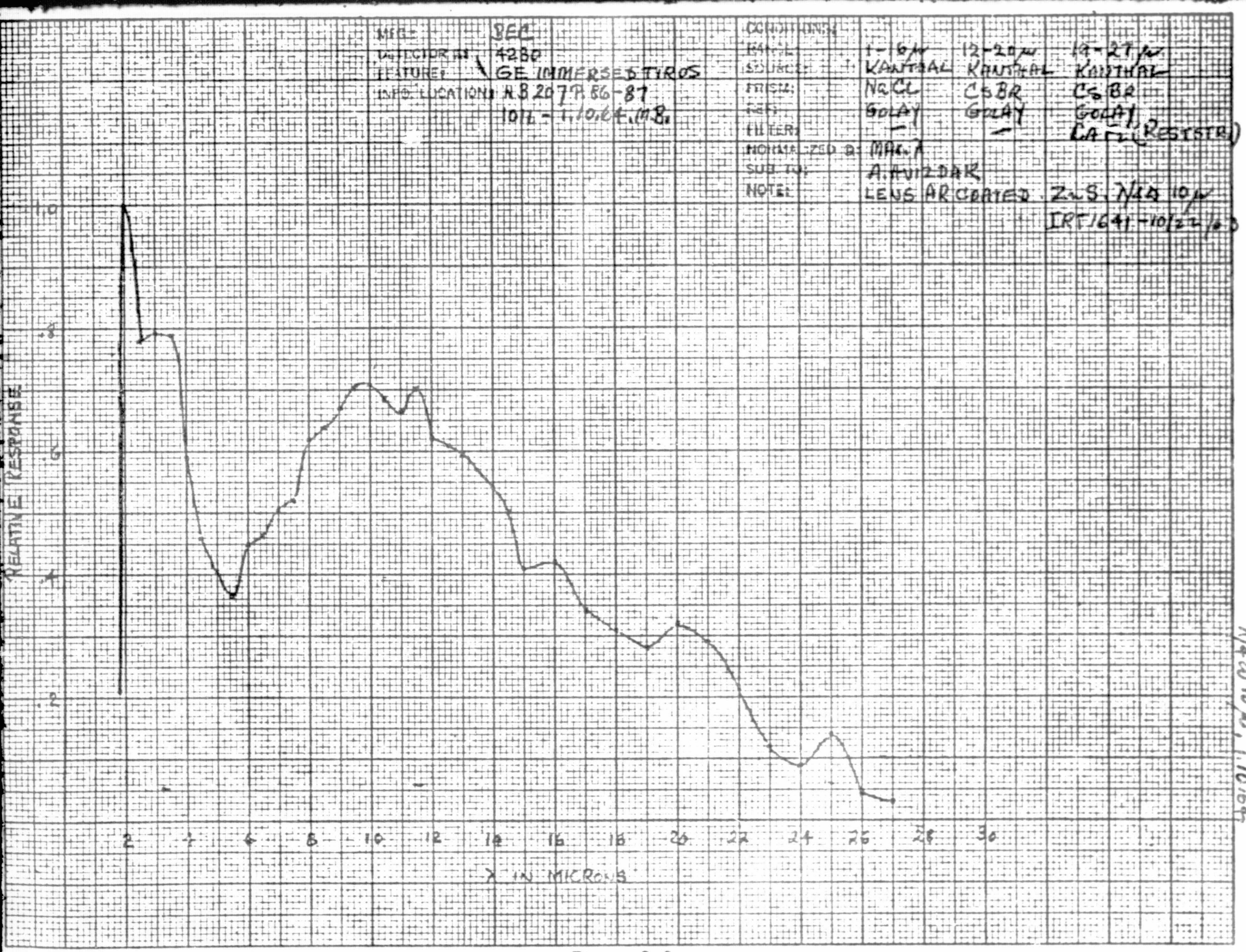
MFR- SEC
DETECTOR: 4280
FEATURES: GE IMMERSED TIROS
INFO. LOCATION: RB 207 P. 86-87
10IL - 1, 10, 11, MB
CONDITIONS
1-6μ
12-20μ
19-27μ
SUBSTRATE: KANTHAL
KANTHAL
KANTHAL
FINISH: NaCl
CsBR
CsBR
GOLAY
GOLAY
GOLAY (RESISTR)
FILTER:
NORMALIZED @: MAX.
SUB TO: A. AVIZDAK
NOTES: LENS AR COATED ZnS N/4 10μ
IRT 641 -10/22/68
SEC 4280, SINGLE IMM. TIROS
N/4 @ 10μ, 1.10.64
RELATIVE RESPONSE
1.0
.8
.6
.4
.2
2
4
6
8
10
12
14
16
18
20
22
24
26
28
30
λ IN MICRONS

Figure 2-3

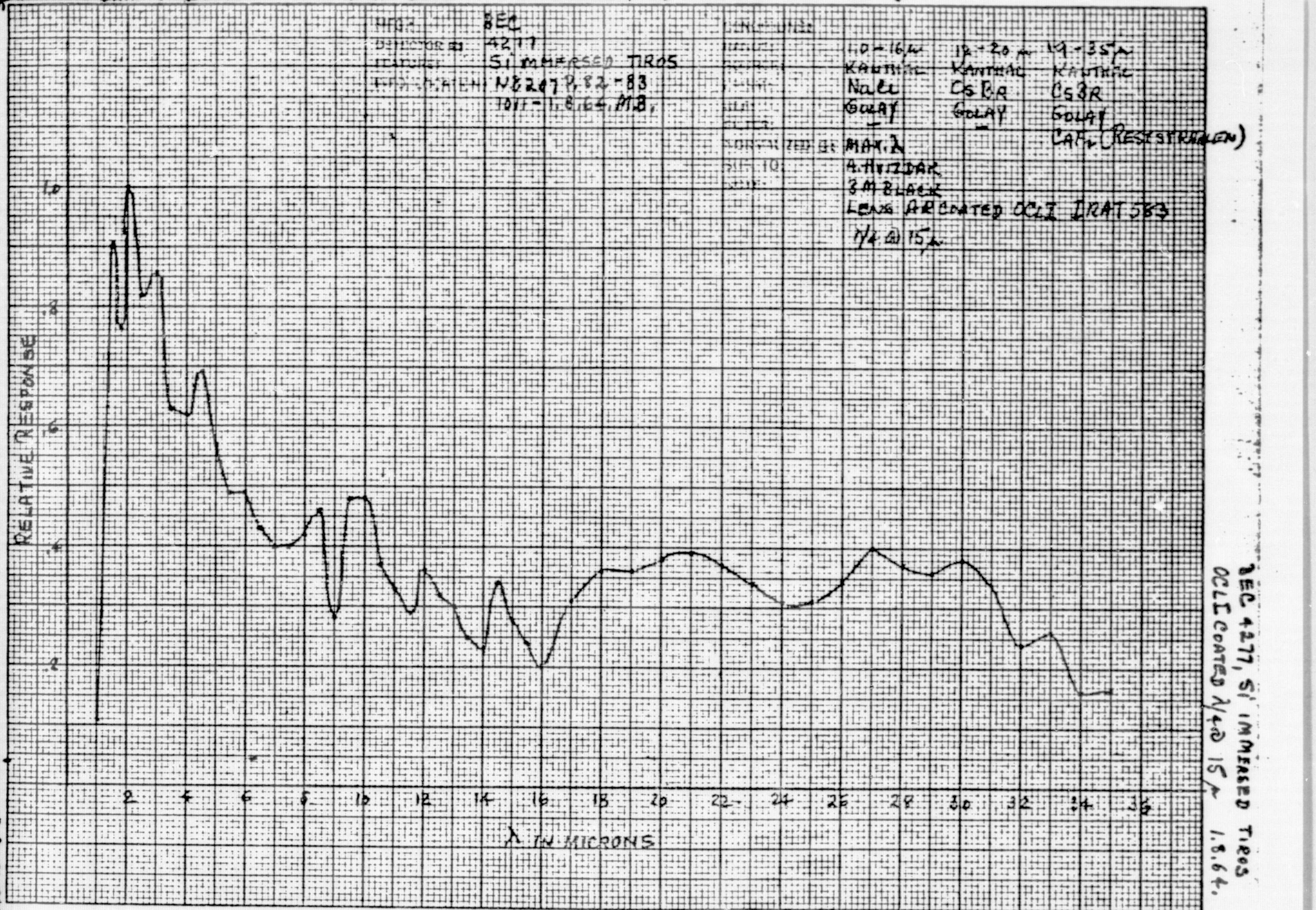
BEC
4277
Si IMMERSED TIROS
1.0 - 16μ
KANTHAL
NaCl
GOLAY
CsBr
CAF2 (RESTSTRAHLEN)
MAX. λ
3M BLACK
LENS AR COATED OCLI IRAT 583
λ/4 @ 15μ
RELATIVE RESPONSE
λ IN MICRONS
BEC 4277, Si IMMERSED TIROS
OCLI COATED λ/4 @ 15μ 1.8.64.

Figure 2-4

response of a thermistor detector immersed in a silicon hyper-hemisphere which is seen to be sensitive to the longer wavelengths, although with some losses. Our calculations in later sections of this report take into account the detector sensitivity averaged over the spectral region of interest.

While the 20-40 micron spectral region appears to offer certain advantages in this application in avoiding the need for a change in optics for various missions and seems to provide the desired accuracy, it would be unfair to overlook the value of the 15 micron CO_2 band for earth missions. Although the desired 0.1° accuracy seems to be achievable with the 20-40 micron spectral band, the horizon profile curves for the various atmospheres are more uniform in the 15 micron CO_2 band than in the 20-40 micron band. This may be seen by comparing Figure 2-1 in this report with Figure 1 of a paper by F. Schwarz, K. Ward, and T. Falk, "A High Accuracy Conical Scan Infrared Horizon Sensor Operating in the 15 Micron CO_2 Band," presented at the Symposium on Infrared Sensors for Spacecraft Guidance and Control held at Barnes Engineering Company, May 1965. Therefore, it is to be expected that a

somewhat higher accuracy can be achieved for earth missions by operating in the 15 micron CO_2 band with nearly all the horizon sensor systems we have studied.

In the analysis of various systems in the next section, we will occasionally call attention to the improvements in accuracy which are made possible through use of the relatively homogeneous earth atmosphere as viewed in the 15 micron CO_2 band and to a slightly lesser extent in the 20-40 micron band, with its reasonably low radiance contrast and a dynamic range in radiance of only about two to one.

3.0 DISCUSSION OF SYSTEM CONCEPTS

Apart from radiation balance sensors which generally have a rather limited accuracy and horizon crossover indicators used with spinning type vehicles, both of which are unsuitable for the present application, infrared horizon sensors may be placed into three basic categories: conical scan horizon sensors, electronically sampled no-moving-parts horizon sensors, and edge tracking horizon sensors.

We believe that ultimately, with sufficient development and time, various versions in each of these categories can be made to meet the design goals for the earth/lunar horizon sensor required for this program with one limitation: the specification of reliability cannot be met by any of these systems without redundancy and scrupulous attention to all aspects of reliability in the design of the sensors and choice of components.

The system selected for this program must meet these design goals but do so within the specified time limit of less than one year and a budget limit, all with a reasonably high confidence factor so that no new unresolved problems are

encountered which may interfere with the successful completion of the program.

It will be instructive, therefore, to set down the principal differences and the advantages and disadvantages of each of the horizon sensor concepts and later discuss each in more detail and thus resolve the possible problem areas in advance of the execution of the design and construction phase of this program. In all this we will assume that the reader has a familiarity with basic infrared horizon concepts and the operating principles of each. We will therefore not repeat what we feel has been adequately covered in the literature in the form of individual papers on specific horizon sensor systems or in two presently available works which treat these subjects in great detail.[1,2]

3.0.1 Conical Scan Horizon Sensors

Conical scan horizon sensors are characterized by the fact that they contain a scanning mechanism which causes

---

[1]Symposium on Infrared Sensors for Spacecraft Guidance and Control, held at Barnes Engineering Company, May 1965.

[2]John Duncan, William Wolfe, George Oppel, and James Burn. "Infrared Horizon Sensors," IRIA State-of-the-Art Report, Institute of Science and Technology, The University of Michigan, April 1965.

the detector to view a finite size elemental field in a continuously rotating conical pattern. As a rule, the rotational rates are fairly high (motor speeds of 7200 rpm being common) and friction and lubrication may present problems. The electronics are, as a rule, rather simple, since there is no need to separate a search and track function. Use of the conical scan results in a wide possible acquisition field but wastes a considerable portion of the scan time in traversing over space and planet where no useful information is derived. The only useful information is the time of planet crossover at the leading and trailing edges of each scan. As a result, the electrical bandwidth requirements may be higher than desirable and the signal-to-noise ratio may be degraded.

Conical scan sensors can thus provide both search and track functions with each scan and, since the mechanical motion is constrained in bearings, the system can function during launch or powered flight in an environment with high vibration levels. For missions in which the altitude range is limited to small variations, one can adjust the scan cone angle to a position which minimizes the amount of time in

which the sensor views regions which provide no useful information (e.g., space). Reliability of motors and rotating components is intimately tied to the parameters of operation such as speed of rotation, mission life, number of bearings, etc., which will be discussed in later sections.

3.0.2 Electronically Sampled No-Moving-Parts Horizon Sensor

A formidable advantage of the electronically sampled system is the complete avoidance of any moving parts and a consequent potential for missions requiring a very long operating life. A no-moving-parts system on the other hand, like a d.c. amplifier, requires a high degree of long-term stability which is usually difficult to achieve. The accuracy of the system becomes a function of either the field of view subtense (resolution) of the individual detectors (for a digital type system) or the degree to which it may be possible to resolve the position of the target within each detector field of view element (in the case in which analog target position interpolation is used). Both these methods of obtaining a high degree of resolution require rather complex electronic circuitry using many active and passive components,

For the present application the advantage gained through elimination of all mechanical components is weakened by the need for a large number of detectors and associated low-level sampling switches required to achieve the desired resolution. In time, such a multi-element system can be simplified and constructed in an integrated circuit form which may improve the reliability. In considering the sensitivity and signal-to-noise ratio of this system, we must also take into account the long-term drift and the requirement for maintaining a constant or zero output when all active detectors view outer space losing heat to the background. This dictates use of either a detector array with exceedingly good responsivity matching between elements or the solution we have adopted--provision of a controlled heat source within the optical system which insures that all detectors viewing space will experience no net heat gain or loss with respect to its reference junctions. Thus all detectors, regardless of their absolute responsivities, must produce equal outputs (or zero output) when viewing outer space. Insofar as signal-to-noise ratio and bandwidth are concerned, this system has the advantage

that the detectors "stare" at their target area almost continuously and may have a slow response and the bandwidth requirement is low.

3.0.3 Edge Tracking Horizon Sensors

3.0.3.1 With Small Field Scan

Edge tracking horizon sensors have the advantage over the conical scan sensor that they waste little time looking at regions other than the edge of the planet which they must track, except for the time during which they search for their target. The search time is thus normally longer than for the conical scan sensor. However, once the planet edge is acquired, little time is wasted in scanning other regions and the electronic bandwidth may be narrow. A complicating factor is the need for a tracking servo loop and, in some systems, two separate field scans: wide field tracking and a small field fine oscillation. In some systems (e.g., the "Positor" of the ATL edge tracker), these two movements may be performed by the same mechanical component.

The searching function is usually performed by some type of servo drive. The fine tracking may be a small field

"dithering" movement about a normal planet edge field of view position or it may be a small cone scanned at the planet edge and, in some systems, it may be a field switching action in which a detector is exposed alternately to the edge of the planet and to outer space which may serve as the reference. This field switching system, since it does not waste any time in scanning an area on the planet and in space, allows further restriction of electrical bandwidth.

To produce the small dithering motion usually requires mechanical components. These may consist of a flexing type device or a rotating type device. The former do not require lubrication and are usually non-friction devices. They generally have resonances at low frequencies and may be unsatisfactory in applications in which they may experience vibration forces. The latter rotational or bearing constrained devices are essentially unaffected by the usual external vibrational forces but do require lubrication. Thus one must consider the requirements of the mission before reaching a conclusion as to the suitability of a specific scanner system.

3.0.3.2 Field Switching Edge Trackers

Edge trackers in which a field of view at the edge of the planet is compared with a field in space by optical chopping may use modulators of three basic types: choppers of the Frustrated Internal Reflection Modulators (FIRM) using imperceptibly small movement to effect modulation, vibration type choppers, and rotating chopper modulators.

The FIRM type shows a negligible amount of wear, can be free from mechanical resonances in the range of frequencies normally encountered in space vehicles, and if the design is well executed should have a very high reliability.

The vibration type field chopper (e.g., tuning fork moving vane type modulator) usually has a high reliability for the small movement required but usually is subject to disturbance through external vibrations. It may be designed to have its mechanical resonance at a very high frequency. However, in that case, it would require considerably higher drive power to cause it to vibrate at the desired low frequency chop rate. This type system is therefore preferably used in missions operating in free flight with low vibration forces.

The rotating chopper type field switching modulator can be designed to be unaffected by normal vibration forces in a spacecraft. Its reliability can be reasonably high, provided that the mechanism is made to operate at low speeds and the lubrication problem is satisfactorily solved.

All of the field switching edge tracker types have the common advantage of requiring the lowest signal bandwidth of all sensor types, since the noise bandwidth need only be as wide as the information bandwidth required by the system. The modulation frequency may be selected conveniently within the time constant which is typical of the detector to be used. Like the other edge trackers this type also requires the servo drive system to operate the tracking mirror (or lens). It is to be expected that this method of sensing provides the best signal-to-noise ratio. The design for this type sensor must make provision for possible sun in one of the primary fields of view, which usually requires an auxiliary guard detector field of view.

In general, we see from the above that the considerations guiding the choice of an appropriate earth/lunar

horizon sensor system should include not only the specific numbers indicating achievable signal-to-noise ratio and accuracy but also some more poorly defined criteria involving confidence level, design and fabrication time, cost, and some considerations which are characteristic of specific missions. The precise form of the sensor is further influenced by the location of the sensor package in the spacecraft. Thus, if prime space is available where the sensor can view regions nearly 180° apart, the sensor can be designed in such a way that pitch and roll data may be obtained with one integrated sensor head.

It is for reasons such as these that we counsel a joint discussion of the mission requirements and any interface problems.

3.1 Conical Scan Sensors

Of all the various approaches to horizon sensing, the conical scan type is the one which has been developed to the highest degree and used most widely in the US space program. More than 200 conical scan sensors built by Barnes Engineering Company have been flown in various space vehicles and rockets--more than all other types of horizon sensors combined.

In view of the present requirement for greater accuracy than is required for other existing missions, capability of operating with a high accuracy in an orbit around the moon, and a reliability figure far beyond anything achieved to date, we have reviewed in some detail the various possibilities for improvement in these areas insofar as the conical scan concept is concerned and the relative potential of this technique vis-a-vis other horizon sensing methods. Because the conical scan sensor is a fairly well established device and has had much space experience, it will obviously be desirable to explore to the utmost its value in the present application. The advantage of using it is the greater if one bears in mind the factor of time and cost. Therefore, if it is found that relatively small changes will make the system meet the design goals for the present sensor, then the factors of experience, cost, and time may carry much weight in deciding on the choice of the most desirable system.

Looking at the basic problem areas with the various types of sensors as discussed in Section 3.0, we find that the main weaknesses of existing conical scan sensors lie in the

use of high speed rotating parts, an unfavorable ratio of dwell time on space versus planet, and possible electronic processing difficulties in obtaining high accuracy and satisfactory signal-to-noise ratios.

If the vehicle dynamics and system requirements are such that an integration time of 5 seconds is allowed for attitude error output, as appears to be the case, then a slowing down of scan rate to around 1 rps is possible. This leads to a number of improvements in reliability and crossover time determination as discussed in greater detail below. The error dependence on scan time is summarized in Figure 3-0. We will discuss only those aspects of conical scan horizon sensing not already covered adequately in the literature.

A review and study of the conical scan horizon sensor was conducted to recommend possible changes and improvements to the present designs. The areas investigated include basic system concept and design, choice of optics, and electronic processing. The study includes a preliminary technical discussion of several basic concepts of the conical scan horizon sensor.

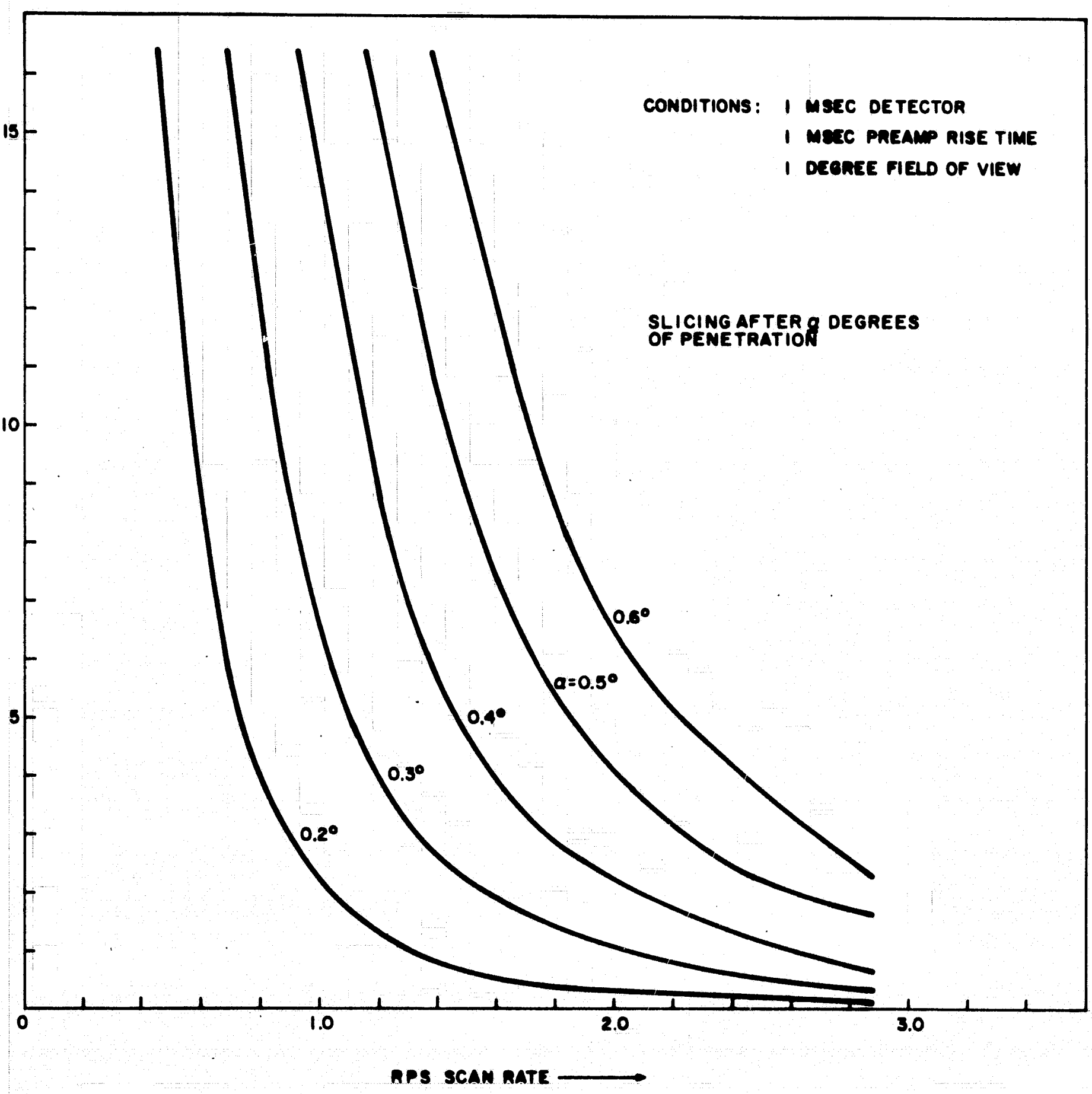

21749

Figure 3-0 INFLUENCE OF SCAN RATE ON DESIRED SLICE LEVEL (FOR 1° FOV)

For a general discussion of the conical scan horizon sensing concept, refer to the following papers:

(1) John Duncan, William Wolfe, George Oppel, and James Burn. "Infrared Horizon Sensors," IRIA State-of-the-Art Report, Institute of Science and Technology, The University of Michigan, April 1965.

(2) Morris H. Arck and M. Monty Merlen. "Horizon Sensors for Vertical Stabilization of Satellites and Space Vehicles," Proceedings of the National Specialists Meeting on Guidance of Aerospace Vehicles, May 25-27, 1960.

(3) Frank Schwarz, Kenneth Ward, and Thomas Falk. "A High Accuracy Conical Scan Infrared Horizon Sensor Operating in the 15 Micron CO_2 Band," presented at the 12th National Infrared Information Symposium, January 12-14, 1965, at Fort Belvoir, Virginia.

(4) Eric M. Wormser and Morris H. Arck. "Infrared Navigation Sensors for Space Vehicles," presented at American Rocket Society Conference, Stanford University, Stanford, California, August 7-9, 1961.

3.1.1 Qualitative Aspects of Edge Determination

3.1.1.1 Radiation Considerations

To accurately determine the horizon edge using conical scan horizon sensors, the slope, at a particular

point, of a pulse edge of a waveform must be maximized. Figure 3-1b shows the slope of the radiation pulse perceived by the bolometer of an infrared scanner when its field of view passes across an object of uniform temperature and emissivity against a uniform background of different temperature (Figure 3-1a).

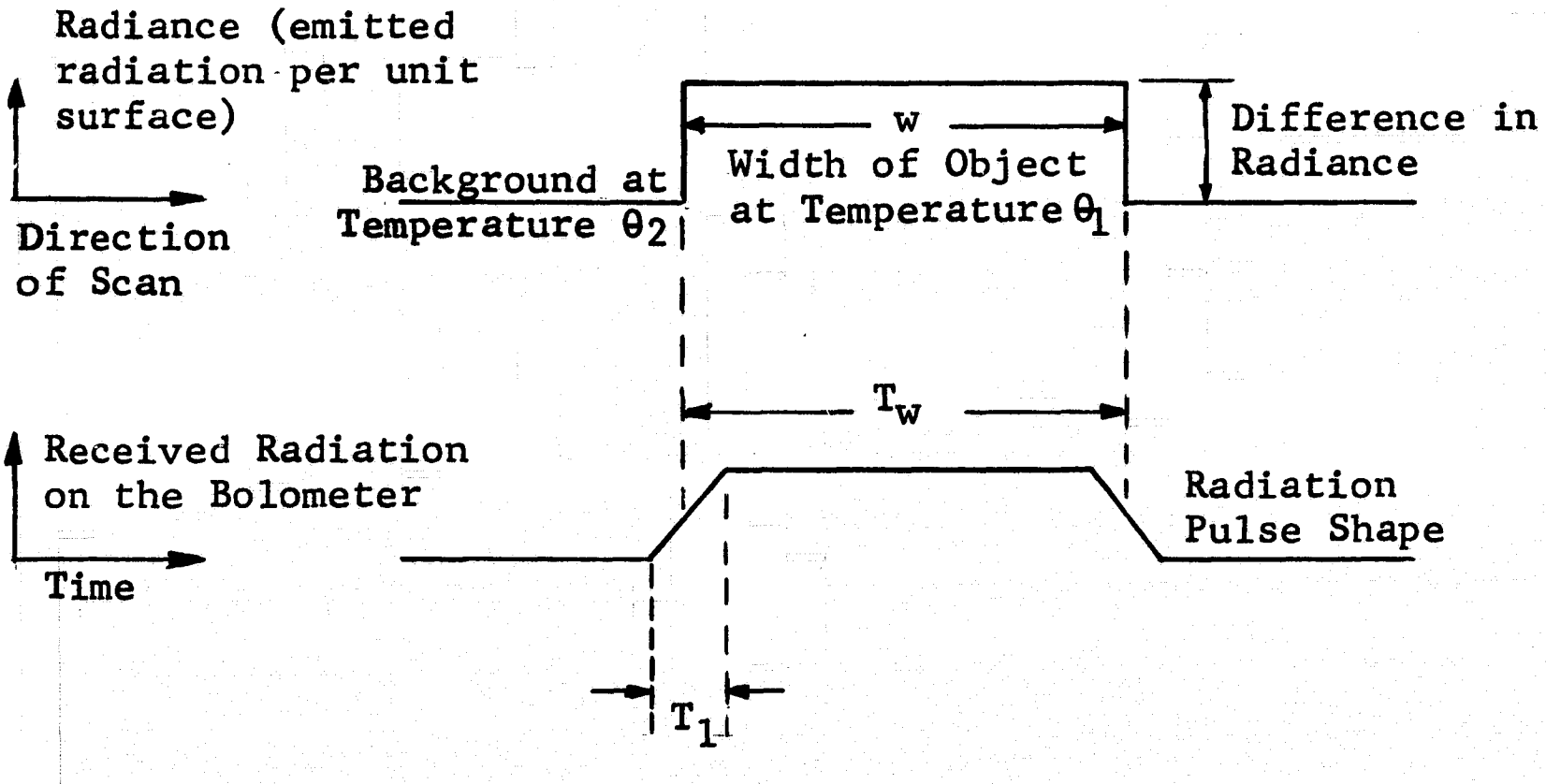

FIGURE 3-1a

FIGURE 3-1b

T_w: time necessary to scan across object of width w

T_1: time necessary to move field of view across sharp edge of object

The ramp-shaped edges of the pulse in Figure 3-1b are generated by moving an optical field of view of non-zero width across a step discontinuity in radiance. (T_1 is the time required to move the field of view across the step discontinuity.) The straight ramp of Figure 3-1b is developed by a rectangular field of view moving with uniform scanning velocity across a discontinuity parallel with one of its sides. In this case, the fractional illumination during crossover is a linear function of time. With other field of view geometries (such as circular) and/or other field of view orientations with respect to the radiation edge (for example the diagonal of a rectangular field of view parallel with the radiation discontinuity) the fractional illumination is not a linear function of time. The generated pulse edge is, of course, still monotonic, but not a straight ramp.

3.1.1.2 Electronic Processing Considerations

Further deterioration (deviation from a rectangle) occurs when the received radiation pulse is converted into an electrical pulse and amplified as such. There are two fundamental contributions to this latter distortion:

(a) A low pass in the transfer function between the received radiation pulse and the electrical output of the radiation detector: In the case of a thermistor bolometer, the received radiation will raise the temperature of the bolometer flake (unbalancing the resistance bridge into which it is connected and thereby producing an electrical signal). However, the bolometer temperature changes only at a rate less than or equal to that permitted by the heat capacity, C_b, of the bolometer flake and the thermal resistance, R_b, from the flake through its backing to the heat sink. (T_2 is the time constant determined by R_b and C_b.) The designer has some freedom in determining R_b for a given C_b (C_b is a function of the bolometer material and flake size) by varying the thickness of the backing. Reduced backing thickness permits faster response, but it also reduces the sensitivity of the bolometer.

(b) A low pass in the amplifier to which the output of the bolometer bridge is applied: The introduction of this low-pass is intentional; the high frequency cut-off is set at a convenient frequency, as low as compatible with pulse-shaping

requirements, in order to reduce the noise bandwidth. The time constant that corresponds to the amplifier high frequency cut-off is denoted by T_b.

Figure 3-2 shows a typical pulse shape at the amplifier output.

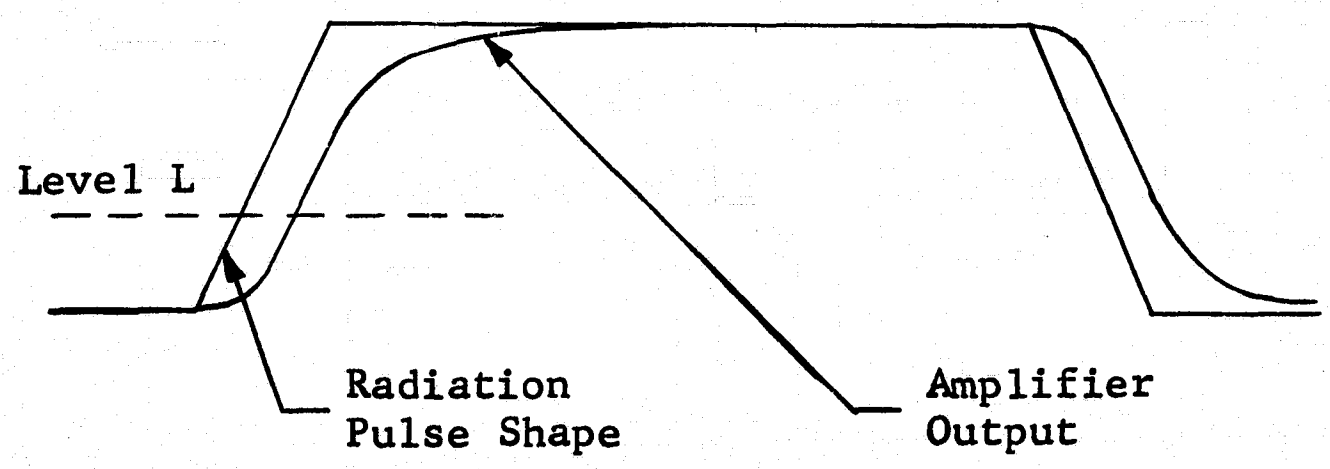

FIGURE 3-2

NOISELESS PULSE SHAPE AT AMPLIFIER OUTPUT

3.1.1.3 Noise Considerations

Since, in practical instruments, the amplifier output contains additive gaussian noise, the entire preceding discussion on pulse edge distortion must be considered in this light. Infrared scanners are used to determine the position of objects that emit radiation different from that of their backgrounds. If it were not for the noise, it would be possible to accurately determine the position of the radiation discontinuity in spite of the distortion of the pulse shape. This could be done by determining the instant at which the amplifier output passes above level L (Figure 3-2) and discounting the known delays introduced by finite field of view, detector time constant, and amplifier high frequency cut-off.

With noise, the instant at which level L is crossed is no longer precisely determined. Rather, there are fluctuations in the crossover instant, with a gaussian distribution around a mean determined by level L and the noiseless amplifier output of Figure 3-2. In fact, multiple crossings of level L are possible if the noise correlation time (largely determined by the amplifier high frequency cut-off) is much

shorter than the field of view crossover time or the detector time constant. (The word "largely" is used because one portion of the additive noise may have a $(1/f)^n$ spectral distribution.)

The mean deviation of these fluctuations in crossover time is directly proportional to the rms value of the additive gaussian noise and inversely proportional to the slope of the amplifier output of Figure 3-2 at the reference level L.[3] If T_1 (field of view crossover time) and T_b (detector time constant) are fixed (that is, as in given optical head), the slope of the pulse at level L is a function of only T_b (the high frequency roll-off of the amplifier). The slope is a monotonically decreasing function of T_b. Since the rms value of the additive gaussian noise is also a decreasing function of T_b, the ratio of the two (proportional to the mean deviation of the crossover time fluctuations) is a minimum for some value of T_b. This value determines the optimum simple roll-off amplifier for a given optical system.

---

[3]Harold S. Black, Modulation Theory. VanNostrand, 1953.

3.1.2 Mathematical Approach to Edge Definition Problem

Keeping the aforementioned statement of the edge definition problem in mind, it is possible to derive expressions which permit optimizing the time response and bandwidth of a system to achieve the best results in terms of edge definition, thus obtaining the highest accuracy in local vertical determination for a specific system. Several approaches are considered. One assumes the use of high frequency boost and a ramp forcing function; the second is worked out for a second-order system with no boost, again using a ramp input with sufficient latitude for the placement of a slice level. Later sections introduce time domain equalization techniques.

3.1.3 Analysis of Conical Scan Horizon Sensor Systems with and without High Frequency Boost

3.1.3.1 Analysis of System using Detector High Frequency Boost

Considering a system scanning always from space to planet, we are faced with a number of choices: using a slow or a fast detector, boosting the high frequency or not, establishing a cut-off frequency for the amplifier, etc. Bear in mind that in this system we are interested only in the leading edge of a pulse and not the trailing edge.

Insofar as the sensor is concerned, the time definition of this crossover point can occur with a minimum error if the rise time of the detector and amplifier is extremely fast (there is no pulse rise delay time) and at the same time the detector and system noise is so low as to preclude the possibility of noise peaks being mistaken for planet signals. These two requirements are obviously in conflict since fast response requires a wide bandwidth which, in turn, results in increased noise. Indeed, the matter may be complicated by the need for a detector which is inherently slow and may require electronic compensation (high frequency boosting) in order to make its rise time rapid enough. Such boosting also increases noise.

In a system whose input signal (planet radiation intensity) is uniform, a time delay introduced by the sluggish response of the detector or amplifier could be offset. However, if the input varies greatly (due to temperature non-uniformities on the planet), a threshold or slicing level must be established above the maximum expected noise peak and the time at which this threshold is exceeded must be determined.

This time, or the pulse edge position which represents that time, is used in deriving the attitude readout.

It should be emphasized that the bandwidth optimization discussed here is not applicable to a system in which both the leading and trailing edges of a highly non-uniform planet are to be determined. This is so because we will be forced to set a threshold (or slicing level) at a very low value just slightly above the noise level, essentially converting the system to a space-scanning type. For a planet profile which may yield radiation values varying by orders of magnitude, it would be impossible to accurately establish the position of the trailing edge. The detector decay time to the low threshold value would be strongly dependent on the radiation from the trailing edge of the planet. (A later section on equalization techniques tackles this difficulty.) It is for this reason that the counter-rotating scanner system is considered as one possible method of improving the edge definition capability.

It is the interaction between noise bandwidth and threshold level setting which we wish to optimize. For a

given detector response time, if we could set the threshold level infinitely low, there would be negligible time error in defining the crossover point. To allow operation at such a low threshold would require an infinitely small noise bandwidth which is also improbable.

The optimum frequency response can be determined by minimizing the following quantity:

$$\frac{V_n}{\frac{dV_s}{dt}}$$

where

V_n = rms noise fluctuations (the peak value of which must be restricted to fall below the threshold level)

$\frac{dV_s}{dt}$ = slope of signal pulse at the threshold level

Expressions for the signal time response and the system noise response must be obtained. In order to make the analysis general, break points for high frequency boost and decay networks are assumed.

In block form, the networks are assumed as sketched below, and the frequency response in Bode diagram form identifies the break-point frequencies.

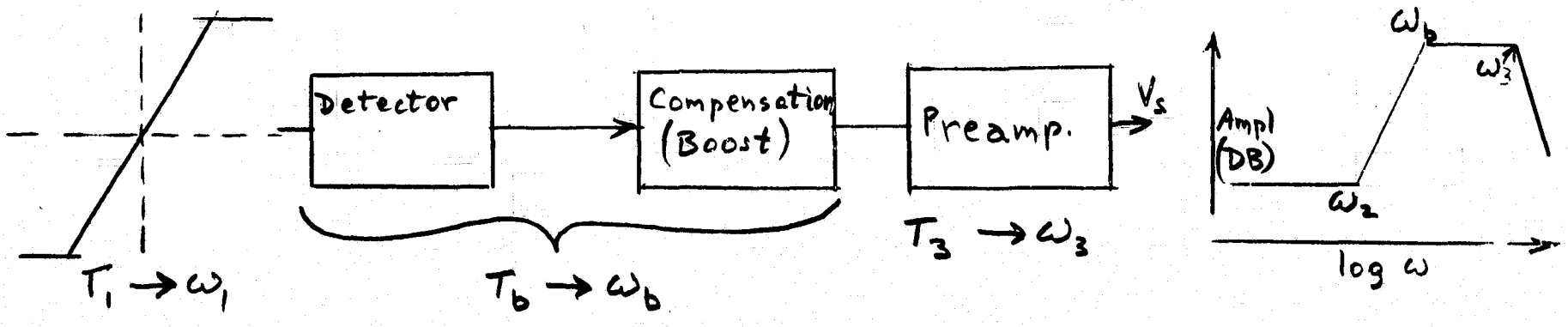

$$\frac{dV_s}{dt} \cong \frac{1}{T_1 + T_b + T_3^*} = \frac{1}{\frac{1}{\omega_1} + \frac{1}{\omega_b} + \frac{1}{\omega_3}} = \frac{\omega_1\omega_b\omega_3}{\omega_b\omega_3 + \omega_1\omega_3 + \omega_1\omega_b}$$

(T_1 is the detector field of view crossover time.)

---

*The use of the sums of the various time constants in the expression for the signal leading edge slope is, of course, an approximation. For a system in which the slice level is placed fairly high in a range of uniform and maximum slope (for example, a CO_2 band system with appropriate parameters), the approximation will lead to small errors. For a system having a very low slice level, the approximation is not as dependable.

The network transfer function is:

$$\frac{T_2 s + 1}{T_b s + 1} \times \frac{1}{(T_1 + T_b)\, S + 1} = \frac{1 + j\omega T_2}{1 + j\omega T_b} \times \frac{1}{1 + j\omega(T_1 + T_b)}$$

(Let $T_1 + T_b = T_3$.)

$$\bar{V}_n^2 \propto \int_o^\infty \frac{1 + \omega^2 T_2^2}{1 + \omega^2 T_b^2} \times \frac{d\omega}{1 + \omega^2 T_3^2} = \frac{1}{T_3^2 T_b^2} \int_o^\infty \frac{d\omega}{(1/T_b^2 + \omega^2)(1/T_3^2 + \omega^2)}$$

$$+ \frac{T_2^2}{T_3^2 T_b^2} \int_o^\infty \frac{\omega^2 d\omega}{(\frac{1}{T_b^2} + \omega^2)(\frac{1}{T_3^2} + \omega^2)}$$

$$\bar{V}_n^2 \propto \omega_3^2 \omega_b^2 \int_o^\infty \frac{d\omega}{(\omega_b^2 + \omega^2)(\omega_3^2 + \omega^2)}$$

$$+ \frac{\omega_3^2 \omega_b^2}{\omega_2^2} \int_o^\infty \frac{\omega^2 d\omega}{(\omega_b^2 + \omega^2)(\omega_3^2 + \omega^2)}$$

The denominator is now simplified, using partial fraction expansion, as follows:

$$\frac{A}{\omega_b^2 + \omega^2} + \frac{B}{\omega_3^2 + \omega^2} \qquad A = \frac{1}{\omega_3^2 - \omega_b^2} \qquad B = -A = \frac{1}{\omega_b^2 - \omega_3^2}$$

$$\overline{V}_n^2 \propto \omega_3^2\omega_b^2 \left[\frac{1}{\omega_3^2 - \omega_b^2} \int_0^\infty \frac{d\omega}{\omega_b^2 + \omega^2} + \frac{1}{\omega_b^2 - \omega_3^2} \int_0^\infty \frac{d\omega}{\omega_3^2 + \omega^2}\right]$$

$$+ \frac{\omega_3^2\omega_b^2}{\omega_2^2} \left[\frac{\omega_b^2}{\omega_2^2 - \omega_3^2} \int_0^\infty \frac{d\omega}{\omega_b^2 + \omega^2} + \frac{\omega_3^2}{\omega_3^2 - \omega_b^2} \int_0^\infty \frac{d\omega}{\omega_3^2 + \omega^2}\right]$$

$\left(\frac{dv}{v^2 + a^2} = \frac{1}{a} \arctan \frac{v}{a} + C\right)$ as obtained from tables of LaPlace transforms)

$$\therefore \int_0^\infty \frac{d\omega}{\omega_b^2 + \omega^2} = \left[\frac{1}{\omega_b} \tan^{-1} \frac{\omega}{\omega_b}\right]_{\omega=\infty} - \left[\frac{1}{\omega_b} \tan^{-1} \frac{\omega}{\omega_b}\right]_{\omega=0} = \frac{1}{\omega_b} \times \frac{\pi}{2}$$

$$(\tan^{-1} \infty = \tfrac{\pi}{2}) \qquad (\tan^{-1} 0 = 0)$$

$$\overline{V}_n^2 \propto \omega_3^2\omega_b^2 \left[\frac{1}{\omega_3^2 - \omega_b^2} \frac{1}{\omega_b} \frac{\pi}{2} + \frac{1}{\omega_b^2 - \omega_3^2} \frac{\pi}{2\omega_3}\right]$$

$$+ \frac{\omega_3^2\omega_b^2}{\omega_2^2} \left[\frac{\omega_b^2}{\omega_b^2 - \omega_3^2} \frac{\pi}{2\omega_b} + \frac{\omega_3^2}{\omega_3^2 - \omega_b^2} \frac{\pi}{2\omega_3}\right]$$

$$\overline{V}_n^2 \propto \frac{\pi}{2} \left[\frac{\omega_3^2\omega_b}{\omega_3^2 - \omega_b^2} - \frac{\omega_3\omega_b^2}{\omega_3^2 - \omega_b^2} - \frac{\omega_3^2\omega_b^3}{\omega_2^2(\omega_3^2 - \omega_b^2)} + \frac{\omega_3^3\omega_b^2}{\omega_2^2(\omega_3^2 - \omega_b^2)}\right]$$

$$= \frac{\pi\ \omega_3\omega_b}{2\omega_2^2(\omega_3^2 - \omega_b^2)} (\omega_2^2\omega_3 - \omega_2^2\omega_b - \omega_3\omega_b^2 + \omega_3^2\omega_b)$$

Leaving out $\pi/2$:

$$\overline{V}_n^2 \propto \frac{\omega_3\omega_b}{\omega_3^2 - \omega_b^2}\left(\omega_3 - \omega_b - \frac{\omega_3\omega_b^2}{\omega_2^2} + \frac{\omega_3^2\omega_b}{\omega_2^2}\right)$$

$$= \frac{\omega_3\omega_b(\omega_3 - \omega_b)}{\omega_3^2 - \omega_b^2}\left[1 + \frac{\omega_3\omega_b}{\omega_2^2}\right] = \frac{\omega_3\omega_b}{\omega_3 + \omega_b}\left[1 + \frac{\omega_3\omega_b}{\omega_2^2}\right]$$

The rms noise is proportional to:

$$V_n \propto \sqrt{\frac{\omega_3\omega_b}{\omega_3 + \omega_b}\left(1 + \frac{\omega_3\omega_b}{\omega_2^2}\right)}$$

To get the optimum S/N as a function of the bandwidth, boost, etc., minimize the following:

$$\frac{V_n}{dVs/dt} = \sqrt{\frac{\omega_3\omega_b}{\omega_2 + \omega_b}\left(1 + \frac{\omega_3^2\omega_b^2}{\omega_2^2}\right)} \times \frac{\omega_b\omega_3 + \omega_3 + \omega_1\omega_b}{\omega_1\omega_b\omega_3} \qquad (1)$$

Using the criterion derived above, it is possible, although difficult, to find a minimum value for the quantity $V_n/dV_s/dt$. The difficulty arises from the fact that the expression contains a number of parameters (such as detector

time constant, amount of high frequency boosting, and final high frequency cut-off) which may be chosen by the designer. Therefore, it was decided to evaluate this figure of merit for a number of possible combinations. These combinations include some which appear desirable for use with a CO_2 band system which may use a relatively fast detector and a modest amount of high frequency boost.

The figures of merit arrived at and listed in Table 3-1 show that it is desirable to use the fastest detector obtainable and minimize boosting.

3.1.3.2 Analysis of System without High Frequency Boost

To facilitate the optimization of the detector time constant and the amplifier bandwidth of a system having a ramp input but using no high frequency boosting, the technique used in Paragraph 3.1.3.1 can again be used. The technique consists of differentiating the transfer function with respect to time (to obtain dV_s/dt) and then dividing this function by the system noise. This procedure yields the system figure of merit, the optimum value of which may then be found.

TABLE 3-1

Detector Time Constant Used	f_1*	f_2	f_b	f_3	Figure of Merit $V_n/dV_s/dt$ (Eq. 1)	Type System Using These Parameters
1 msec	160	160	320 (boosted to 0.5 msec equivalent response)	400	280	CO_2 Band System**
0.5 msec	160	320	320	480	155	---
1 msec	160	160	240	320	150	Alternate Choice for CO_2 Band System
4 msec	160	40	320	480	1660	---
2.25 msec	160	70	800	1800	1220	---

*In this table we have used frequency as a parameter. In equation (1) ω_1 refers to the ramp input, and a crossover time of 1 msec has been assumed. $\omega_1 = 1/T_1 = 2\pi f_1 = 1000$.

**In this system, which uses a modest amount of boosting, the preamplifier cut-off occurs just above the frequency to which it is desired to compensate the detector. An abrupt cut-off may be provided by a low pass filter such as UTC LMI 400.

The time response of a ramp applied to a detector of time constant $1/\gamma$ and a preamp with a high frequency cut-off of α radian/second is:

$$v = t - \frac{\gamma + \alpha}{\alpha\gamma} + \frac{\gamma^2 e^{-\alpha t} - \alpha^2 e^{-\gamma t}}{\alpha\gamma(\gamma - \alpha)}$$

(As may be obtained from tables for second-order systems.[4])

$$\frac{dv}{dt} = 1 - \frac{\gamma}{\gamma - \alpha} e^{-\alpha t} + \frac{\alpha}{\gamma - \alpha} e^{-\gamma t}$$

The noise, V_n, is proportional to $\sqrt{\alpha}$, since it is a function of the square root of frequency.

---

[4]E. M. Grabbe, S. Ramo, and D. E. Wooldridge, Handbook of Automation, Computation, and Control, Vol. 1, p. 20-35. John Wiley & Sons, Inc., 1958.

$$\frac{\frac{dv}{dt}}{\sqrt{\alpha}} = \left(1 - \frac{\gamma}{\gamma - \alpha} e^{-\alpha t} + \frac{\alpha}{\gamma - \alpha} e^{-\gamma t}\right) \frac{1}{\sqrt{\alpha}}$$

Maximizing this function with respect to α:

$$\frac{d\left(\frac{dv/dt}{\sqrt{\alpha}}\right)}{d\alpha} = \left[- \frac{\gamma}{(\gamma - \alpha)^2} e^{-\alpha t} + \frac{\gamma t}{\gamma - \alpha} e^{-\alpha t} + \frac{1}{\gamma - \alpha} e^{-\gamma t} + \frac{\alpha}{(\gamma - \alpha)^2} e^{-\gamma t}\right] \frac{1}{\sqrt{\alpha}} - \frac{1}{2} \frac{1}{\sqrt[3]{\alpha}} \left[1 - \frac{\gamma}{\gamma - \alpha} e^{-\alpha t} + \frac{\alpha}{\gamma - \alpha} e^{-\gamma t}\right] = 0$$

Multiplying by $2\sqrt[3]{\alpha}$:

$$- \frac{2\alpha\gamma}{(\gamma - \alpha)^2} e^{-\alpha t} + \frac{2\alpha\gamma t}{\gamma - \alpha} e^{-\alpha t} + \frac{2\alpha}{\gamma - \alpha} e^{-\gamma t} + \frac{2\alpha^2}{(\gamma - \alpha)^2} e^{-\gamma t}$$

$$- 1 + \frac{\gamma}{\gamma - \alpha} e^{-\alpha t} - \frac{\alpha}{\gamma - \alpha} e^{-\gamma t} = 0$$

Collecting terms with the same exponentials:

$$e^{-\alpha t} \left[- \frac{2\alpha\gamma}{(\gamma - \alpha)^2} + \frac{2\alpha\gamma t + \gamma}{\gamma - \alpha}\right] + e^{-\gamma t} \left[\frac{\alpha}{\gamma - \alpha} + \frac{2\alpha^2}{(\gamma - \alpha)^2}\right] - 1 = 0$$

$$e^{-\alpha t}\left[\frac{-2\alpha\gamma + 2\alpha\gamma^2 t + \gamma^2 - 2\alpha^2\gamma t - \alpha\gamma}{(\gamma - \alpha)^2}\right]$$

$$+ e^{-\gamma t}\left[\frac{2\alpha^2 + \gamma\alpha - \alpha^2}{(\gamma - \alpha)^2}\right] - 1 = 0$$

$$e^{-\alpha t}\ \frac{-3\alpha\gamma + 2\alpha\gamma^2 t + \gamma^2 - 2\alpha^2\gamma t}{(\gamma - \alpha)^2} + e^{-\gamma t}\frac{\alpha^2 + \gamma\alpha}{(\gamma - \alpha)^2} - 1 = 0$$

$$e^{-\alpha t}\ \gamma(2\alpha\gamma t - 3\alpha + \gamma - 2\alpha^2 t) + e^{-\gamma t}\ \alpha(\alpha + \gamma) - (\gamma - \alpha)^2 = 0$$

Expanding the exponentials, taking only the first two terms:

$$e^{-\alpha t} = 1 - \alpha t$$

$$e^{-\gamma t} = 1 - \gamma t$$

$$\gamma(1 - \alpha t)(2\alpha\gamma t - 3\alpha + \gamma - 2\alpha^2 t) + \alpha(1 - \gamma t)(\alpha + \gamma) - (\gamma - \alpha)^2 = 0$$

$$2\alpha\gamma^2 t - 3\alpha\gamma + \gamma^2 - 2\alpha^2\gamma t - 2\alpha^2\gamma^2 t^2 + 3\alpha^2\gamma t - \alpha\gamma^2 t + 2\alpha^3\gamma t^2 + \alpha^2$$

$$+ \gamma\alpha - \alpha^2\gamma t - \alpha\gamma^2 t - \gamma^2 + 2\alpha\gamma - \alpha^2 = 0$$

$$-2\alpha^2\gamma^2 t^2 + 2\alpha^3\gamma t^2 = 0$$

Dividing by $2\alpha^2 t^2$:

$$\alpha\gamma - \gamma^2 = 0$$

$$\alpha = \gamma$$

It can now be seen that the optimum condition requires a preamplifier bandwidth approximately equal to the equivalent bandwidth of the detector.

For an unequalized system of this type, the trailing edge error would be severe. However, for a leading edge tracker, the edge definition for an uncompensated system will lead to acceptably small errors. The optics of a system of this type is shown in Figure 3-2a. A block diagram of the electronics for such a system is shown in Figure 3-2b.

3.1.4 Detector Time Response Equalization

With conical scan horizon sensors it is possible to achieve the desirable effects of electronic detector speed boosting without increasing system noise as it is in the case with the RC lead network presently in use.

Consider the planet radiance distribution of Figure 3-3. Assume a field of view crossover time small compared to the detector time constant. Then the bolometer output voltage will be shown by the dotted trace on the same figure. If low level slicing is desired (to be able to handle the smallest expected

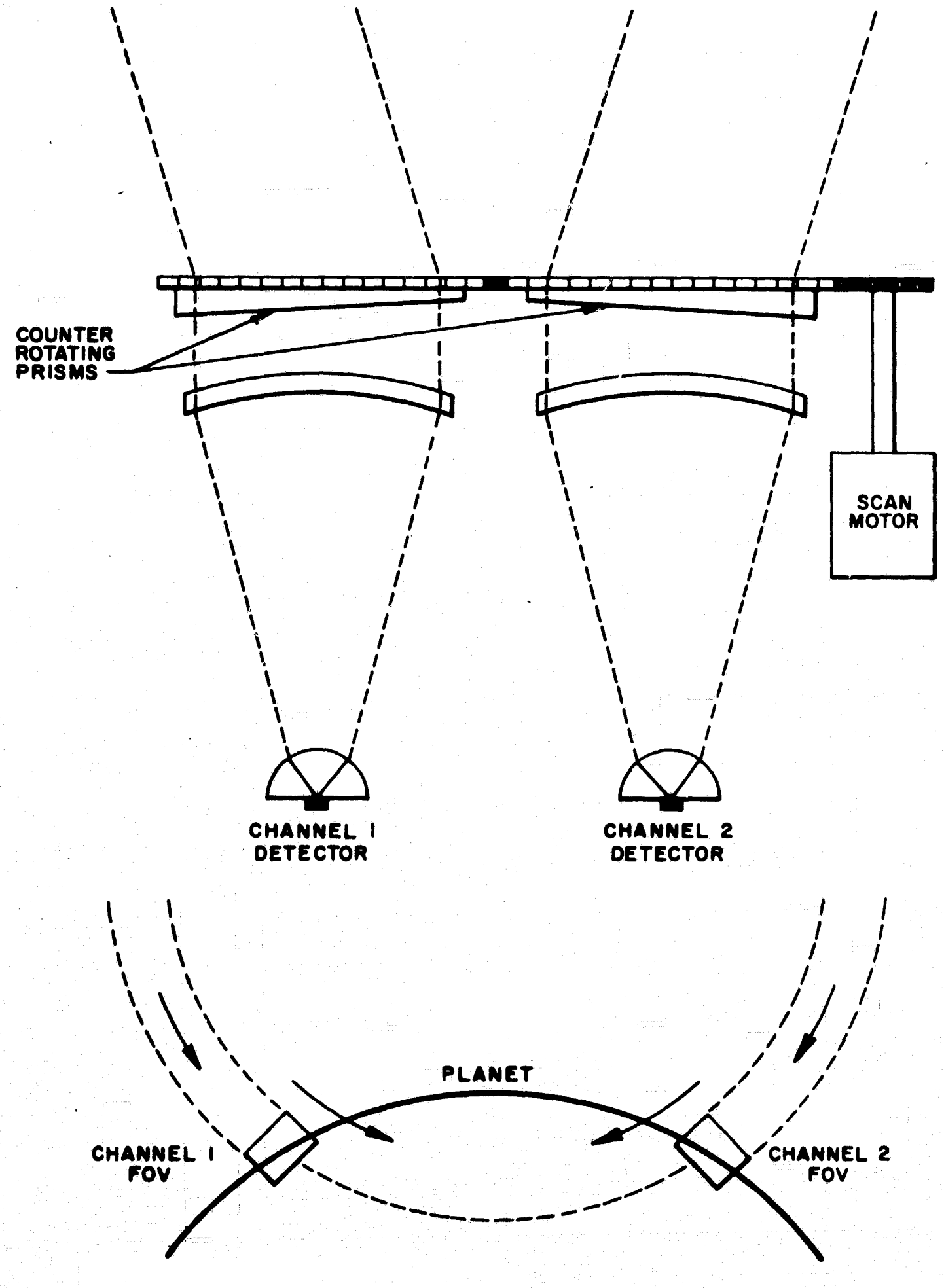

Figure 3-2a SKETCH OF LEADING EDGE TYPE CONICAL SCAN SENSOR

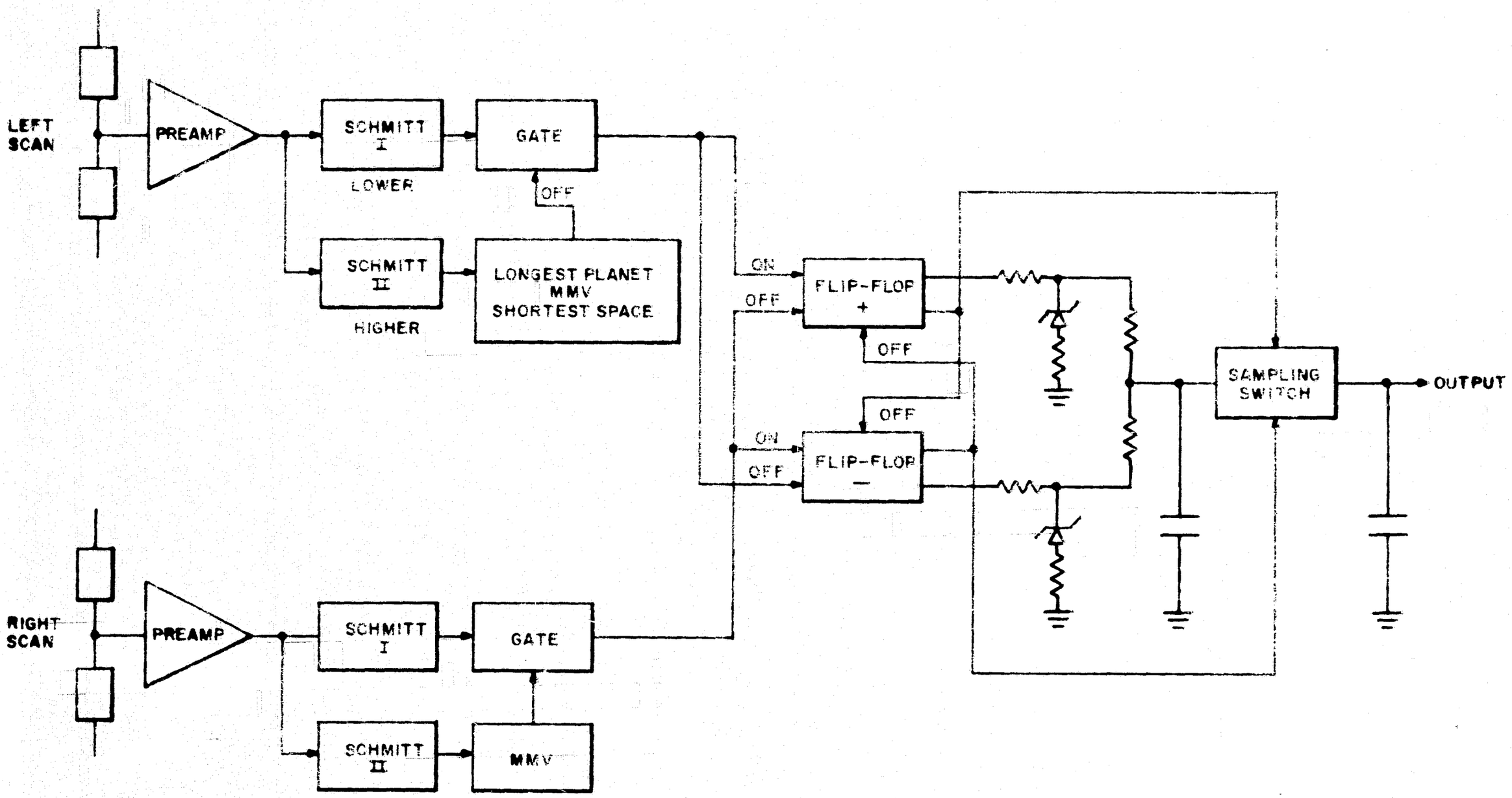

21750

Figure 3-2b CALIPER SCAN BLOCK DIAGRAM

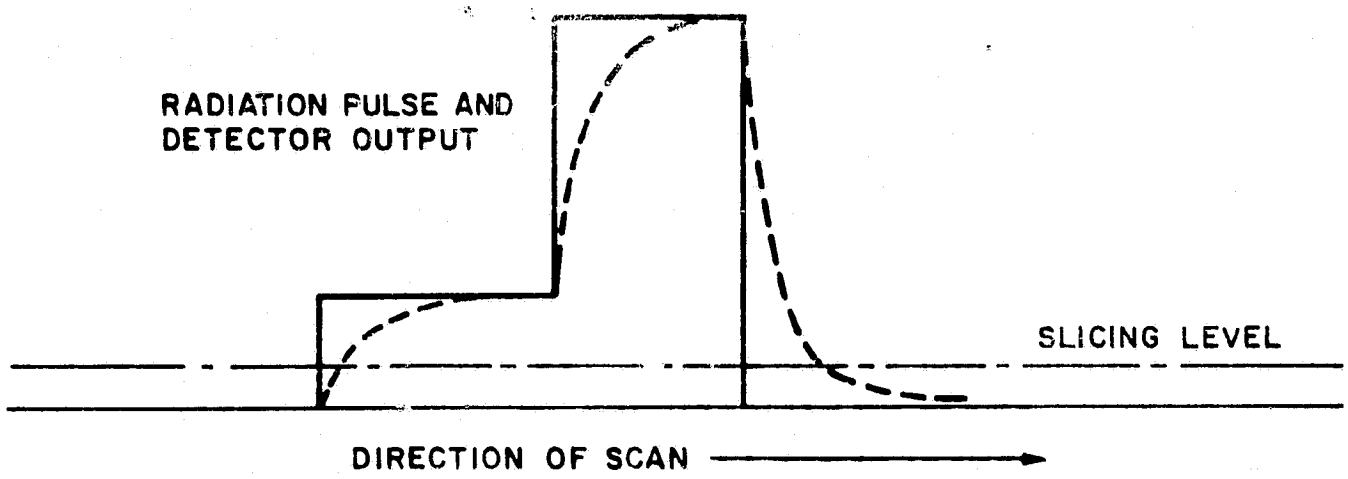

Figure 3-3

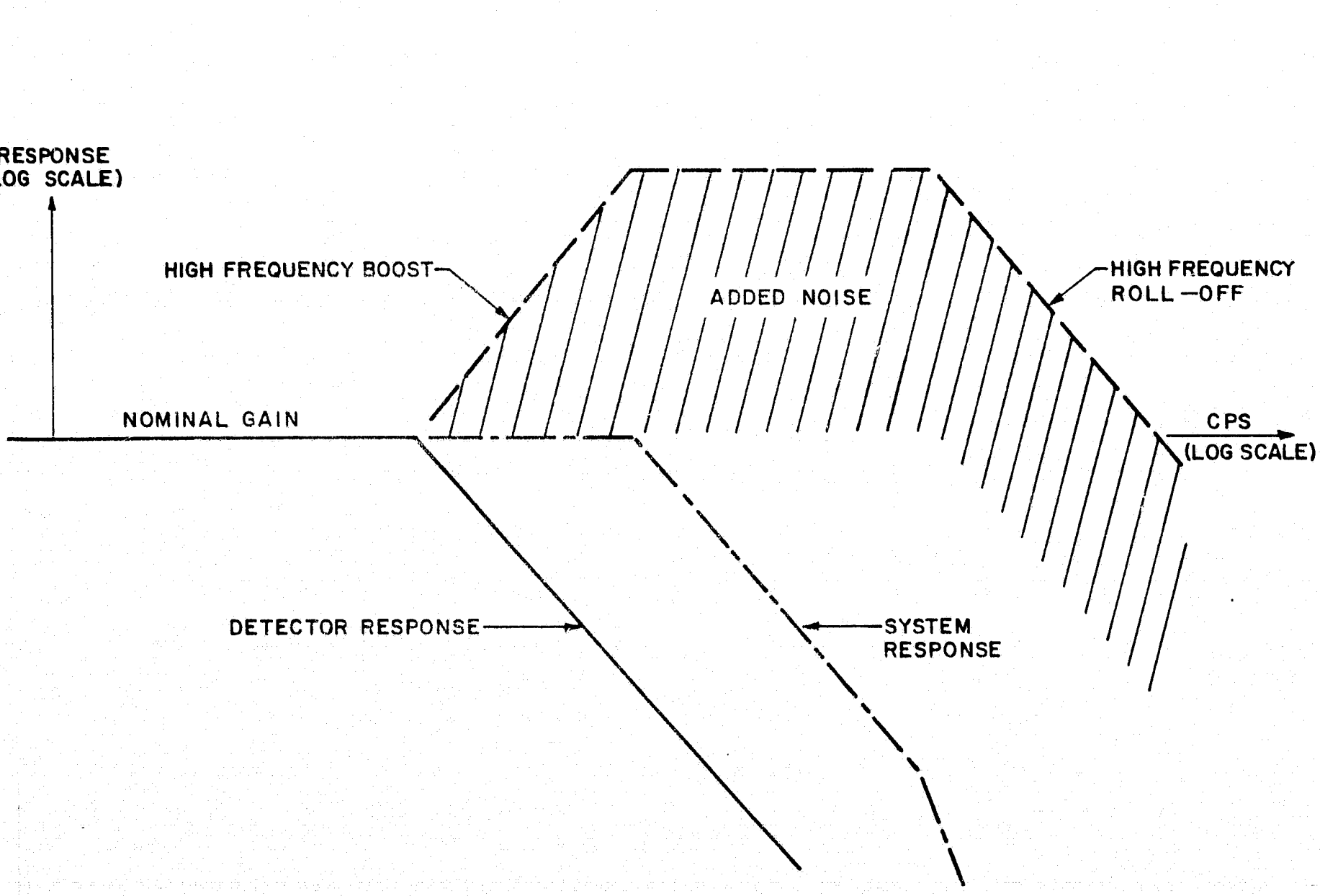

Figure 3-4

signal), a large error, possibly several detector time constants, will result at the falling edge of the planet pulse.

To avoid such error, electronic high frequency boost is applied. This reduces the effective time constant so that, although it still takes the same number of time constants for a large signal to decay to the slicing level, this will result in a smaller absolute error.

Such boost of speed of response increases system noise by a rather strong factor, as will be evident from Figure 3-4.

Yet it is not really necessary to boost up the response. It would serve equally well to straighten out the detector response characteristics, starting out with about the same slope but continuing on a straight line instead of on an exponential decay curve. (Figure 3-5.) Then it is guaranteed that trailing edge error cannot exceed one detector time constant regardless of signal intensity.

Such correction is possible with an equalizer network and it does not result in an increase in noise.

In the usual terminology of the LaPlace transformation, the response of a detector of time constant τ to a step change in radiation is

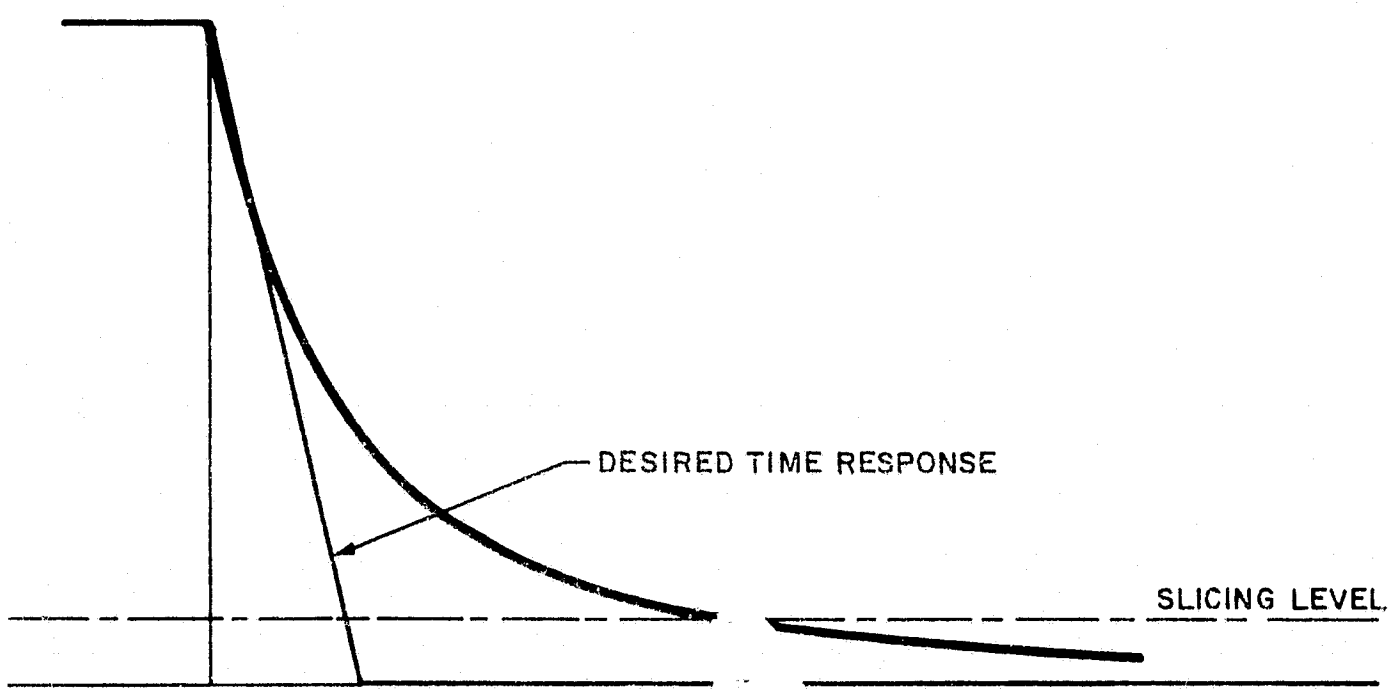

Figure 3-5

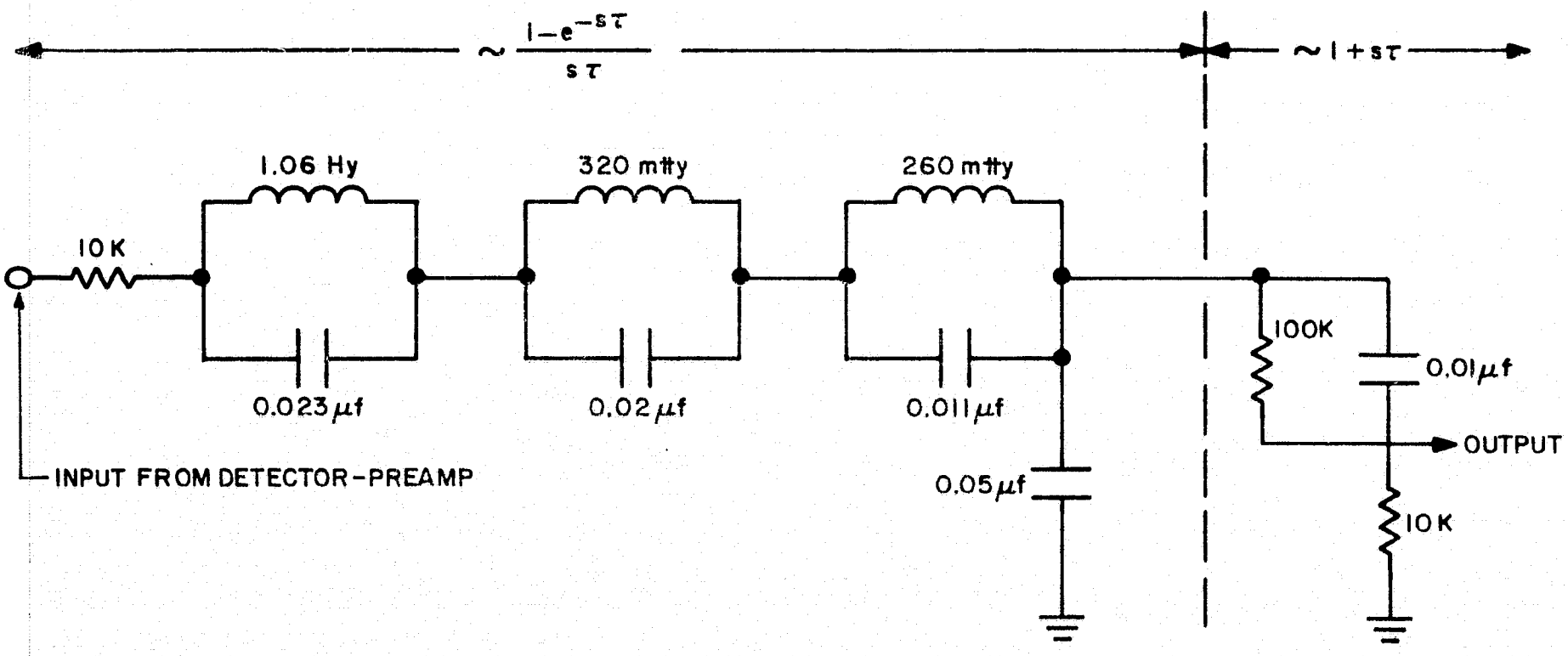

Figure 3-6

$$E(s) = \frac{1}{s} \frac{1}{1 + s\tau}$$

representing an exponential rise and decay characteristic in the time domain. The desired response (having the same initial slope and thus implying about the same bandwidth) is the broken ramp of Figure 3-5.

$$E_{desired}(s) = \frac{1}{s^2\tau} (1 - e^{-s\tau})$$

We want to insert an equalizer transfer function which is the ratio of:

$$\frac{E_{desired}(s)}{E(s)} = \frac{1 + s\tau}{s\tau} (1 - e^{-s\tau}) = T(s)$$

A network with such response will transform the exponential detector response into a broken ramp. Such networks had been synthesized by Corrington of RCA using tapped delay lines[5], but it is possible to approximate such response by using rather simple lumped networks. Break up T(s) into two factors:

$$T(s) = (1 + s\tau) \frac{1 - e^{-s\tau}}{s\tau}$$

---

[5]M. S. Corrington, et al. "Equalization in the Time Domain," IRE Convention Record, 1954.

The second factor is the Laplace transform of a rectangular pulse of height $1/\tau$ and duration τ. Consequently, the second factor would be realized by a network that responds to a delta function with a rectangular pulse of width τ. The approximate synthesis of such networks has been described in the literature.[6] We have built one such network containing three inductors.

The first factor can be approximated by a simple RC network.

The first factor is a lead network and thus enhances noise, but the second is a low pass and the net result is actually a slight reduction in noise, as shown in a later paragraph (3.1.4.1).

Figure 3-6 shows the equalizer network that approximates in its response T(s) for a 1 msec detector. Figure 3-7 is an oscillogram of the response of the laboratory breadboard network built for a higher frequency range (80 microsecond detector) upon application of a typical detector response

---

[6]H. J. Langer. Stetige Mittelwertbildung mit Hilfe von passiven Netzwerken. Frequenz, Bd. 16/1962, No. 1.

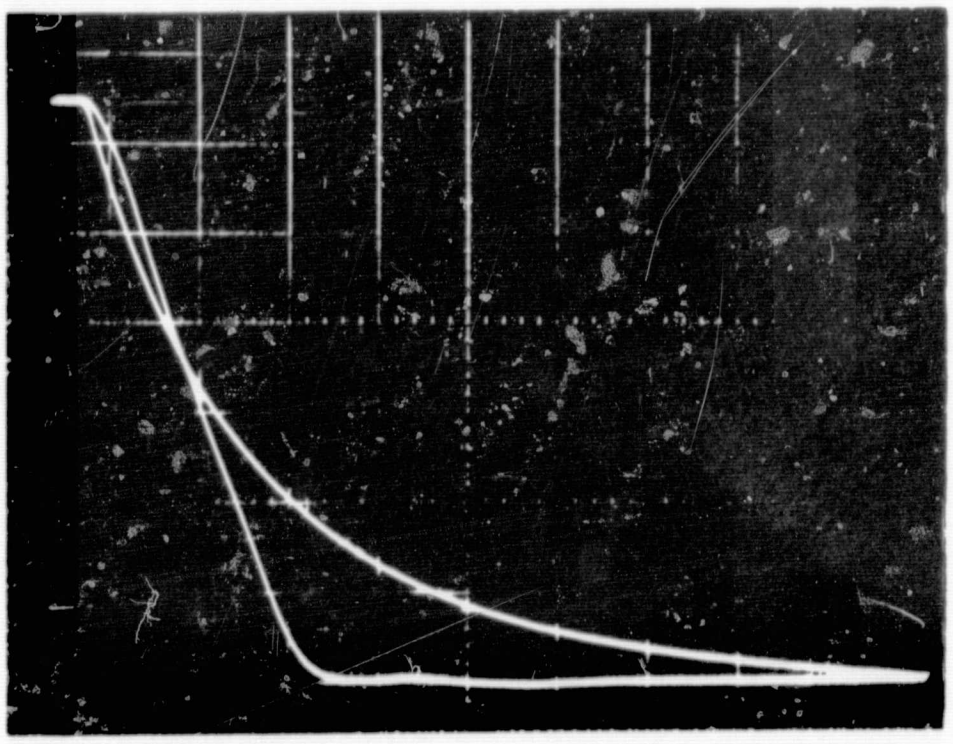

Time Scale: 40 msec/cm

Detector Decay and Equalized Detector Decay. For a ±20% variation in detector time constant there is a 3% undershoot or overshoot. The slight time lag of the equalized response should be observed.

FIGURE 3-7

voltage curve at its input. The response is a rather straight ramp with very little overshoot or ripple.

With field of view crossover times that are not negligible compared to the detector time constant, similar improvements are obtained.

Figure 3-8 is the measured frequency response of the network equalizing a 1 msec detector compared to the frequency response of an RC high frequency boost network that achieves "detector speed-up" by a factor of three. Of course, the latter response would be rolled off beginning at 1.5-2.0 KC, but additional roll-off could be introduced at the same frequency with the equalizer network as well. The signal-to-noise improvement is about three.

3.1.4.1 Noise Power of the Equalizer Network

The frequency response of a network is equal to the Fourier transform of its impulse response. The impulse response of the low pass portion is a square pulse of duration $2t_o$ (if matched to a detector of time constant $2t_o$). The corresponding frequency response with

$$f_o = \frac{1}{2\pi t_o}$$

is:

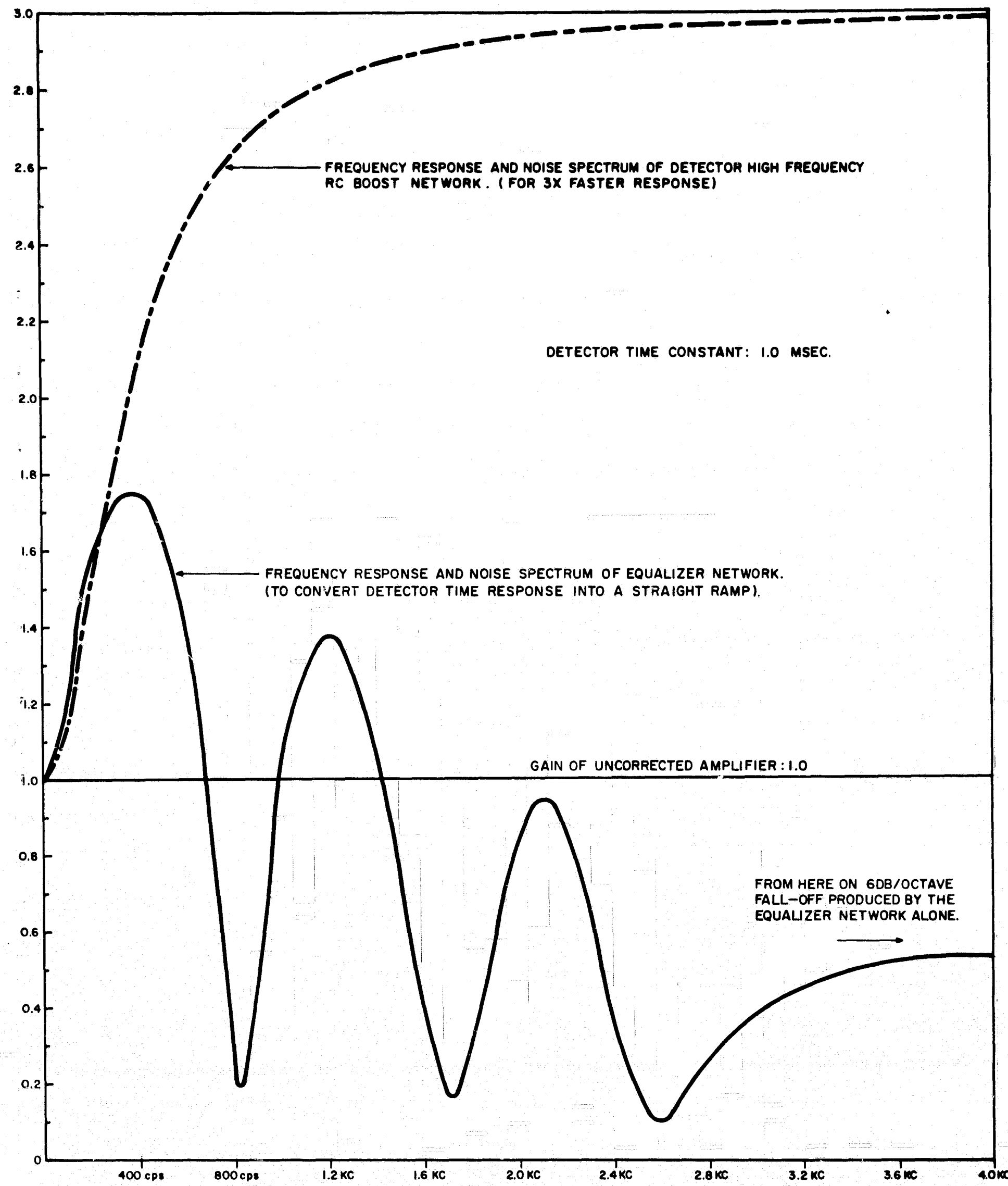
3.0
2.8
2.6
2.4
2.2
2.0
1.8
1.6
1.4
1.2
1.0
0.8
0.6
0.4
0.2
0
FREQUENCY RESPONSE AND NOISE SPECTRUM OF DETECTOR HIGH FREQUENCY RC BOOST NETWORK. (FOR 3X FASTER RESPONSE)
DETECTOR TIME CONSTANT: 1.0 MSEC.
FREQUENCY RESPONSE AND NOISE SPECTRUM OF EQUALIZER NETWORK. (TO CONVERT DETECTOR TIME RESPONSE INTO A STRAIGHT RAMP).
GAIN OF UNCORRECTED AMPLIFIER: 1.0
FROM HERE ON 6DB/OCTAVE FALL-OFF PRODUCED BY THE EQUALIZER NETWORK ALONE.
400 cps
800 cps
1.2 KC
1.6 KC
2.0 KC
2.4 KC
2.8 KC
3.2 KC
3.6 KC
4.0 KC

Figure 3-8

$$\frac{\sin f/f_o}{f/f_o}$$

The power spectrum is:

$$\frac{\sin^2 f/f_o}{(f/f_o)^2}$$

In the equalizer, this is followed by an RC lead network, with the lead starting at

$$\frac{1}{2t_o} = \pi f_o$$

and ending at

$$\frac{\pi f_o}{\alpha}$$

where α is the d.c. attenuation of the lead network. The power spectrum of this is:

$$\frac{1 + 4 f^2/f_o^2}{1 + 4 \alpha^2 f^2/f_o^2}$$

To make the treatment more general, introduce an additional high frequency roll-off (as in fact it is practical) at a frequency f_h. The power spectrum of this is:

$$\frac{f_h^2}{f^2 + f_h^2}$$

The total noise output for white noise input is:

$$N_{out} = \alpha \sqrt{\int_o^\infty \frac{\sin^2 f/f_o}{(f/f_o)^2} \frac{1 + 4\,(f/f_o)^2}{1 + 4\,\alpha^2\,(f/f_o)^2} \frac{f_h^{\,2}}{f^2 + f_h^{\,2}}\, df}$$

Set $f/f_o = x$ and $f_h/f_o = \beta$, and the noise is:

$$N_{out} = \alpha\,\beta \sqrt{f_o \int_o^\infty \frac{\sin^2 x}{x^2} \frac{1 + 4\,x^2}{1 + 4\,\alpha^2\,x^2} \frac{1}{\beta^2 + x^2}\, dx}$$

With some manipulation and use of integral tables, this yields the rather awkward expression:

$$N_{out} = \sqrt{f_o \frac{\pi}{2} \frac{2\,\alpha^2\,\beta}{1 - 4\,\alpha^2\,\beta^2} \left[1 - 2\alpha\beta - 2\alpha^3\beta + 2\alpha^2\beta + \frac{1}{4\beta^2} - \frac{1}{2\beta} + e^{-1/\alpha}\,(2\alpha\beta - 2\alpha^3\beta) - e^{-2\beta}\,(1 + \frac{1}{4\beta^2})\right]}$$

To approximate the factor $(1 + s\tau)$ with some fidelity, the lead network has to introduce insertion loss: $\alpha << 1$. (In the case of the circuit built at Barnes, $\alpha = 0.1$.) Also, the gain cannot be rolled off at too low frequencies: $\beta >> 1$.

To compare with present systems using high frequency detector boost β would be about 10. Under these conditions and the restriction $\alpha\beta \neq 0.5$, the above expression can be approximated by:

$$N_{out} \cong \sqrt{f_o \frac{\pi}{2} \frac{\alpha^2}{1 - 4\alpha^2\beta^2} (2\beta - 4\alpha\beta^2 - 1)}$$

The signal is also attenuated by the insertion loss factor α. Thus for unity signal output, the normalized noise output is:

$$N_{out} \cong \sqrt{f_o \frac{\pi/2}{1 - 4\alpha^2\beta^2} (2\beta - 4\alpha\beta^2 - 1)}$$

If this is compared with the noise output of a simple roll-off at $f_h = \beta f_o$:

$$(N_{out})_{fh} = \sqrt{f_o \beta \frac{\pi}{2}}$$

$$\frac{N_{out}}{(N_{out})_{fh}} \cong \sqrt{\frac{1}{1 - 4\alpha^2\beta^2} (2 - 4\alpha\beta - \frac{1}{\beta})}$$

For $\alpha = 0.1$, this can be brought to the form:

$$\frac{N_{out}}{(N_{out})_{fh}} = \sqrt{\frac{1}{1 + 0.2\beta}\left[2 - \frac{1}{\beta(1 - 0.2\beta)}\right]}$$

This has been plotted for the range $7 \leq \beta \leq 15$ in Figure 3-9. It is seen that for practical values of high frequency roll-off there is a reduction rather than increase in noise due to the equalizer network. This is true for perfect approximation to the square pulse impulse response. Such network would have an infinite number of transmission zero's on the frequency axis. Still, even with the 3 zero network, the response of which is shown in Figure 3-8, the conclusion that there is no increase in noise is quite valid.

3.1.5 Introduction to Gradient Edge Determination

A method of determining the horizon crossover time at the leading and trailing edges of a scan uses various systems of differentiation including single differentiation (gradient sensing) and double differentiation (inflection point sensing).

3.1.5.1 Crossover Edge Definition through Double Differentiation

One method capable of more accurately defining the edge crossover time uses a technique of accentuating the signal

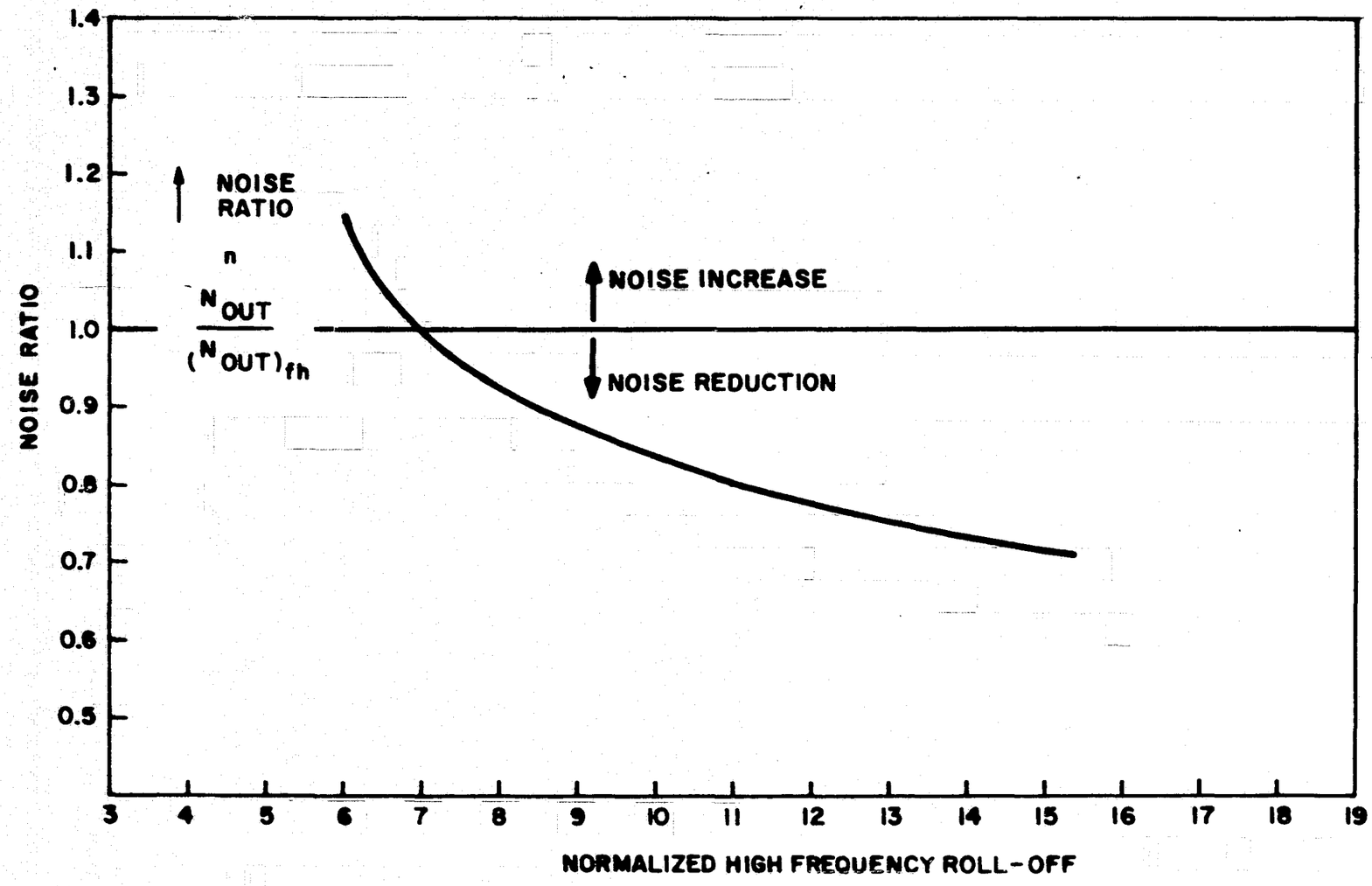

21752

Figure 3-9 RELATIVE NOISE PERFORMANCE OF EQUALIZED AND UNCORRECTED PROCESSING SYSTEMS

waveform slope variations and selecting only the first and last slope changes which occur during each scan across the earth. To accomplish this, it doubly differentiates the incoming signal and defines the crossover time as the first and last zero crossing position of a set of positive and negative going pulses which represent the inflection points of the pulse at the leading and trailing edges of the earth scan.

This scheme is best understood by sketching an assumed complex radiance pattern and showing the expected signal waveforms for the horizon scanner after linear amplification, after a first and then a second differentiator network (Figure 3-10.) In this system we would, in all likelihood, choose a slow detector to obtain more clearly defined inflection points and zero crossover definition which results from the double differentiation of these signals.

The logic circuitry required to reject all but the first and last zero crossover points during any one earth scan is not discussed in this report, although the circuit functions have been worked out in detail. If further interest is expressed in this system, the details of the necessary

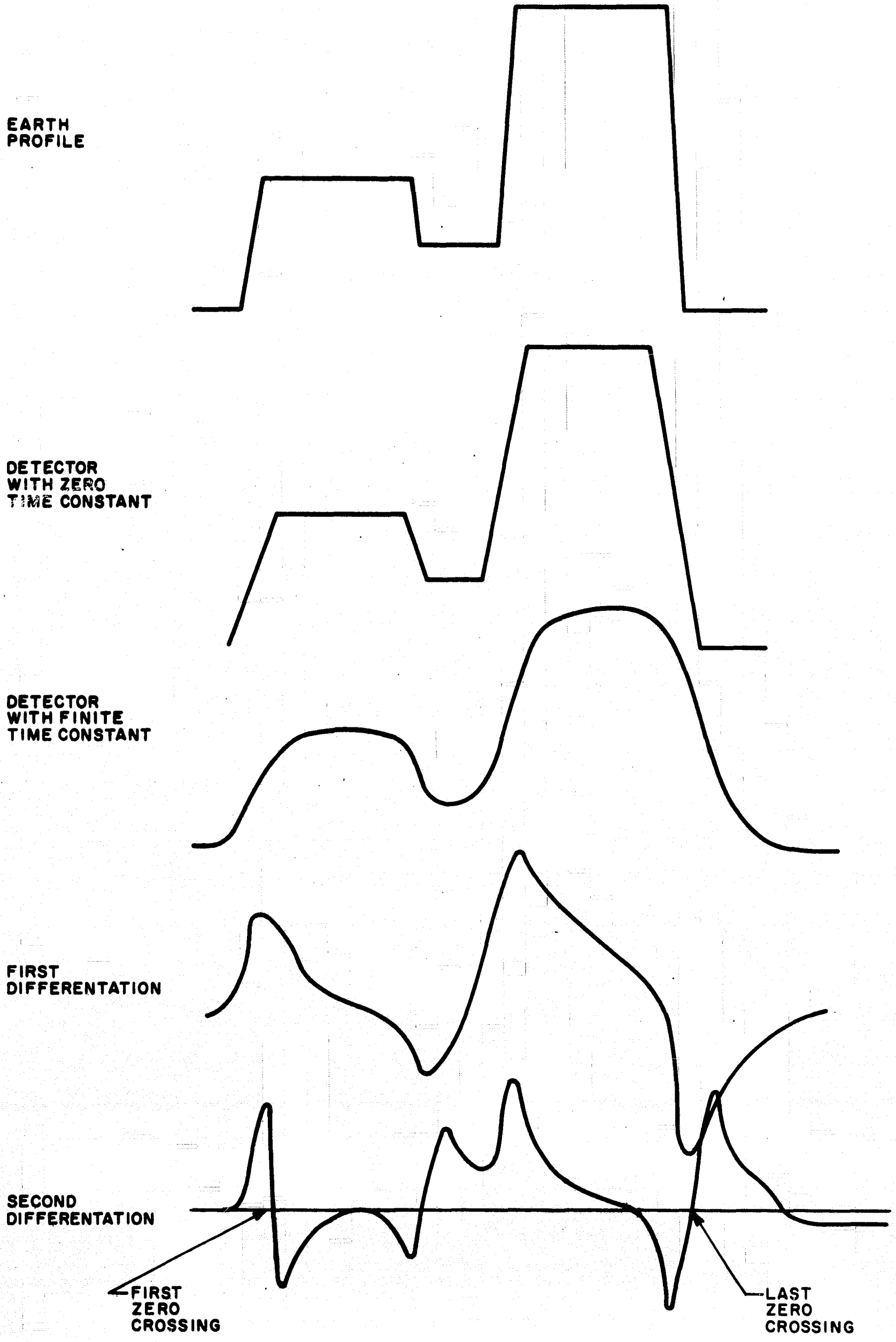

Figure 3–10 SIGNAL WAVEFORMS FOR DOUBLE DIFFERENTATION HORIZON EDGE DEFINITION SYSTEM

circuitry can be supplied. The block diagram shown in Figure 3-11 shows the basic approach. Of course, this system like the others discussed in this report are all adaptable and, indeed, simplified for the case in which the horizon scanner operates in the 15 micron CO_2 band.

3.1.5.2 Pulse Edge Correction using Single Slice Level and Single Differentiator

In this system, in order to restore an accurate horizon crossover time for leading and trailing edges of a scan, the complete processing circuitry of the standard conical scan horizon sensor is used with the addition of a factor which corrects for the error introduced by an inadequate detector time constant.

The system, in its most elementary form, can be understood readily from an examination of the group of typical waveforms shown in Figure 3-12 and the block diagram shown in Figure 3-13. For the radiance profile assumed and the resulting normalized pulse as produced by the standard processing (in which the single slice level crossover determines the pulse duration of Schmitt trigger No. 1), the output pulse of Schmitt No. 1 is foreshortened by t_1 at the leading edge and prolonged

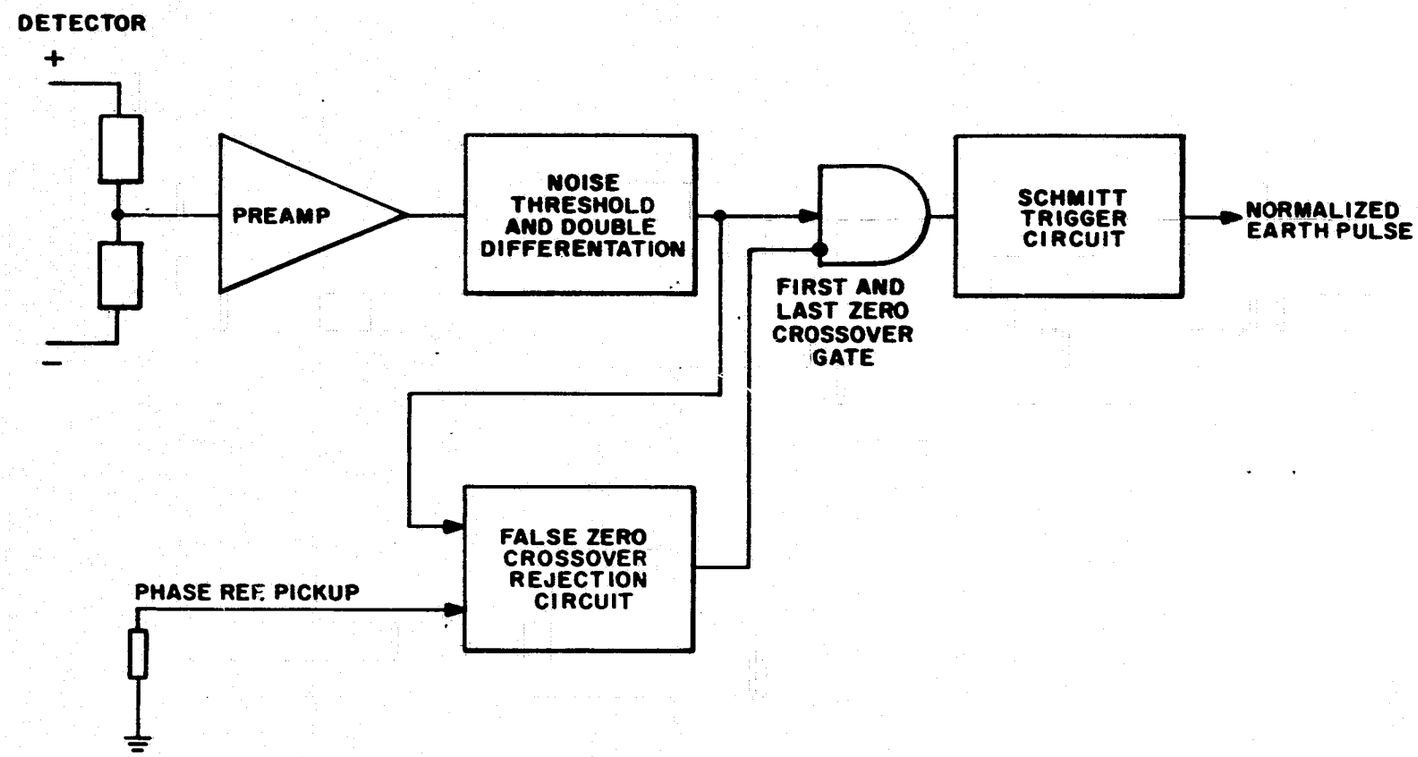

Figure 3-11 BLOCK DIAGRAM OF PROCESSING FOR DOUBLE DIFFERENTATION HORIZON EDGE DIFINITION SYSTEM

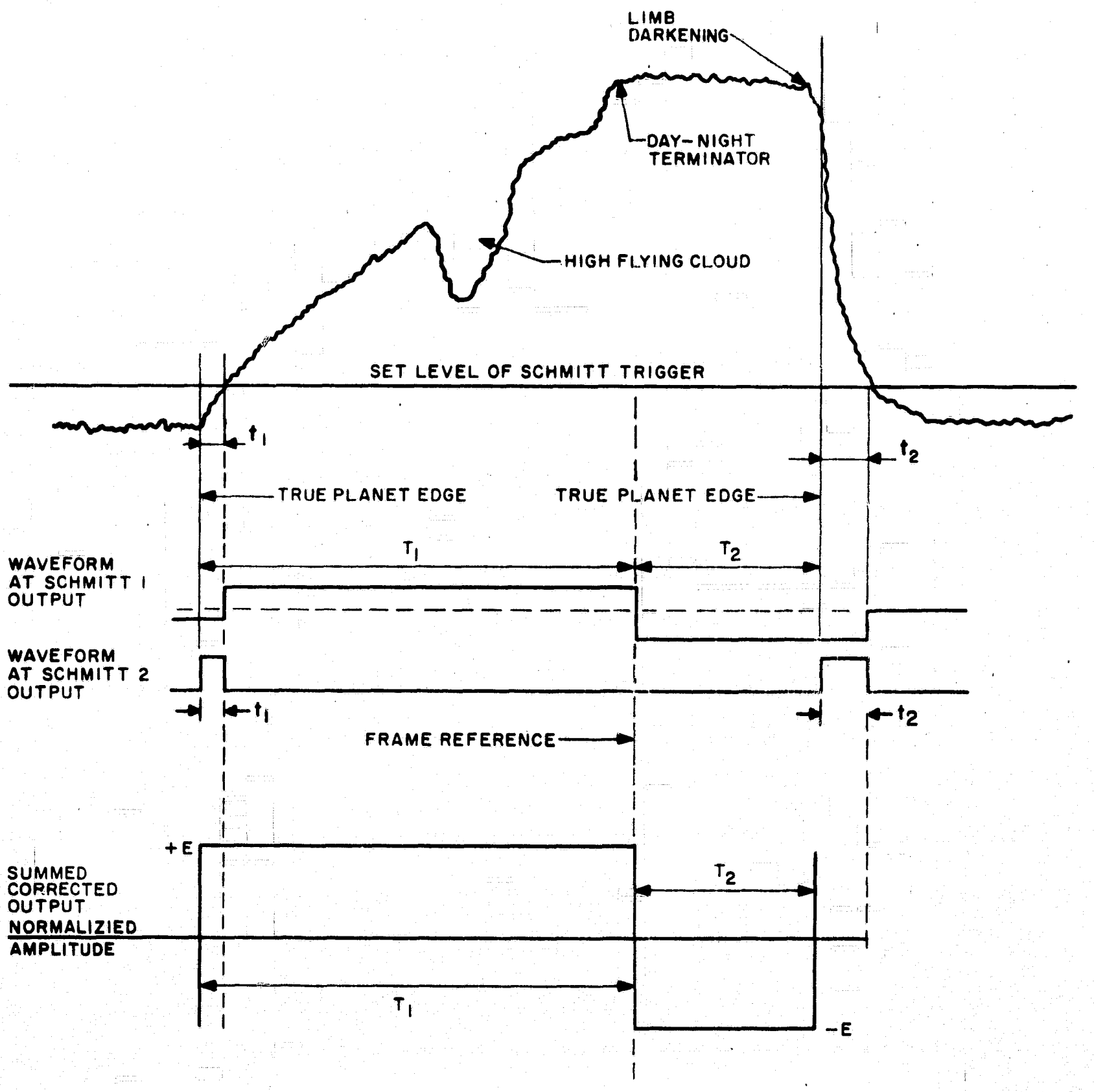

Figure 3-12 TYPICAL WAVEFORMS FOR SINGLE SLICE LEVEL, SINGLE DIFFERENTIATION HORIZON EDGE DEFINITION SYSTEM.

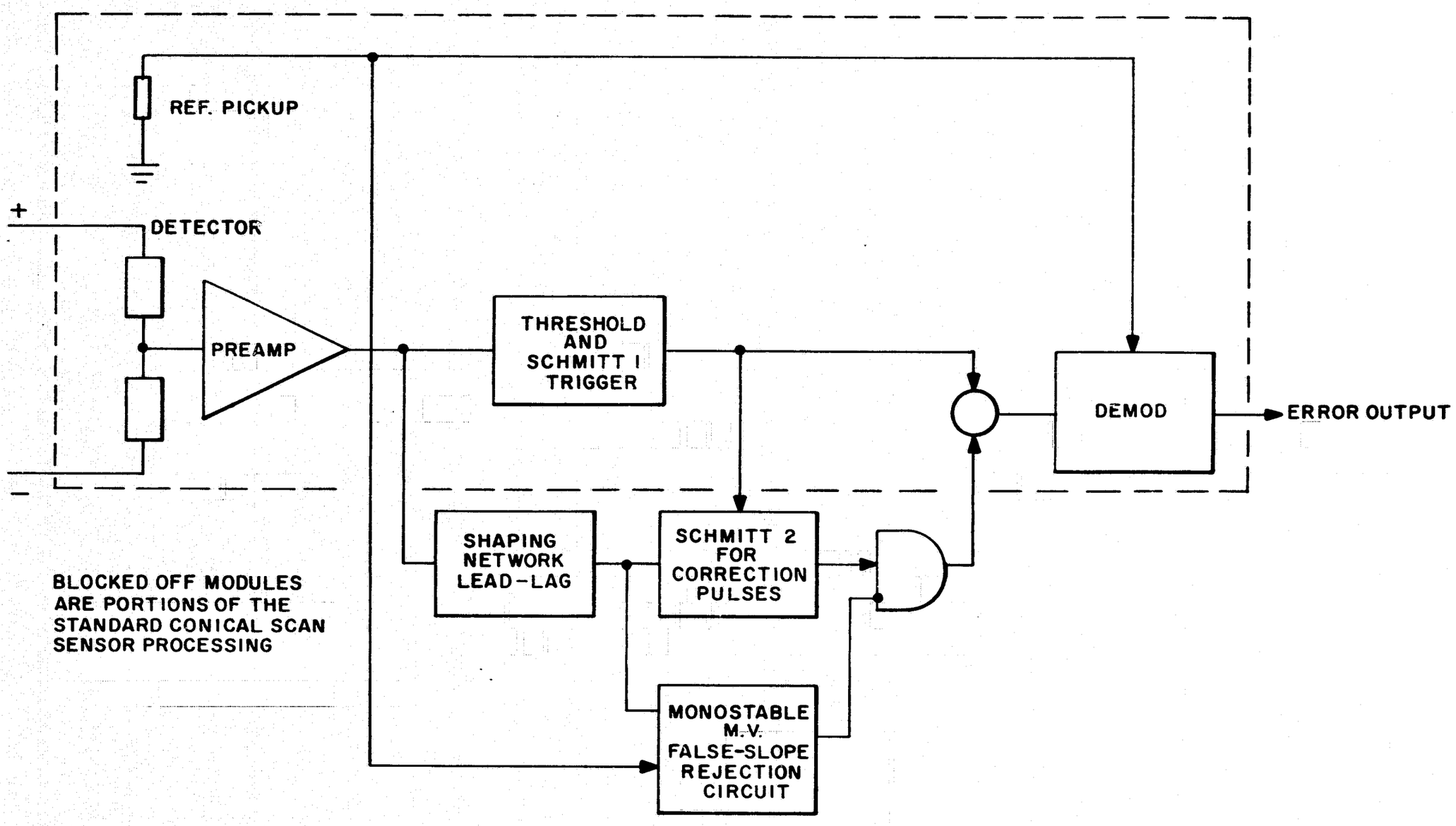

Figure 3-13 BLOCK DIAGRAM OF PROCESSING CIRCUITRY FOR SINGLE SLICE LEVEL/SINGLE DIFFERENTATION HORIZON EDGE DEFINITION SYSTEM

by t_2 at the trailing edge. Time t_1 and t_2 represent errors in the desired pulse duration and vary depending on the variations in radiance levels encountered at the leading and trailing edges of the scan.

A network, composed of a lead component and some lag components, on detecting a slope change activates Schmitt trigger No. 2, which is turned off when Schmitt No. 1 is actuated. This second Schmitt trigger thus produces correction pulses which may be combined with the output of Schmitt No. 1 and demodulated to produce the desired corrected error output signal. The corrected error output (with time duration $t_1 - t_2$) has a greater accuracy than that of the standard processing. The standard processing may now use a slow, uncompensated detector/preamplifier combination.

Circuits are also provided to gate out any correcting pulses which might arise from inflection points generated by cool clouds or other variations in radiance. The detailed circuitry for accomplishing this without excessive sensitivity to correction pulse time jitter is not shown in this study. These details have been worked out and a patent on the processing will

be issued shortly. The detailed circuitry can be supplied on request.

Like all the other configurations which have been discussed earlier, this technique too is aided and made less difficult and more accurate for a conical scan horizon sensor system operating in the 15 micron CO_2 band.

3.1.5.3 Predictor Delay Horizon Scanner

A scheme using predictors and delay lines makes it practical to handle irregularly shaped (clouds, terminator, etc.) planet pulses by gradient sensing but without some of the disadvantages of a differentiator, such as long decay time and overshoots which may interfere with subsequent pulses. Use of such techniques results in adequate signal-to-noise ratios to permit operation in applications in which the energy level detected is low (e.g., lunar sensing).

We will deal next with the nature of predictors. Wiener[7] and Doob[8] developed the theory of predicting future values of a random process (for example, electrical noise) from: (1) a knowledge of its statistics (that is, first

---

[7]N. Wiener. The Extrapolation, Interpolation, and Smoothing of Stationary Time Series, Wiley, N.Y., 1950.

[8]J. L. Dobb. Stochastic Processes, Wiley, N.Y., 1953.

and higher order autocorrelation functions) and (2) knowledge of its past values. Cartwright[9] treats the problem of "predicting future values of a function given its value and the values of certain of its derivatives at the instant t = 0." He shows that "the whole probability distribution of the function at some future time t > 0 can be deduced. The mean value of the distribution may be taken as the best predictable value and the variance of the distribution may be taken as a measure of the inaccuracy of the prediction."

It is not necessary to go into analytical details. Circuits have been built[10] that sum terms consisting of an input voltage function and some of its derivatives in the right proportion. At any given instant, t, a Taylor series of the voltage time function is formed with the aid of the derivatives measured at that instant and we may "predict" the value of the function at time $t + \Delta t$. The circuits are simple RC networks. The one we have built is given in Figure 3-14. The effectiveness and accuracy of the circuit in anticipating

---

[9]D. E. Cartwright. "The Prediction of a Random Function, Given Simultaneous Values of its First Few Derivatives," J. Math. Phys., Vol. 37, pp. 229-245, 1958.

[10]A. Schief. Vorausbestimmung von Signalen mit Hilfe eines einfachen RC-Netzwerkes. Archiv El. Ubertragung, 15, pp. 91-93, 1961.

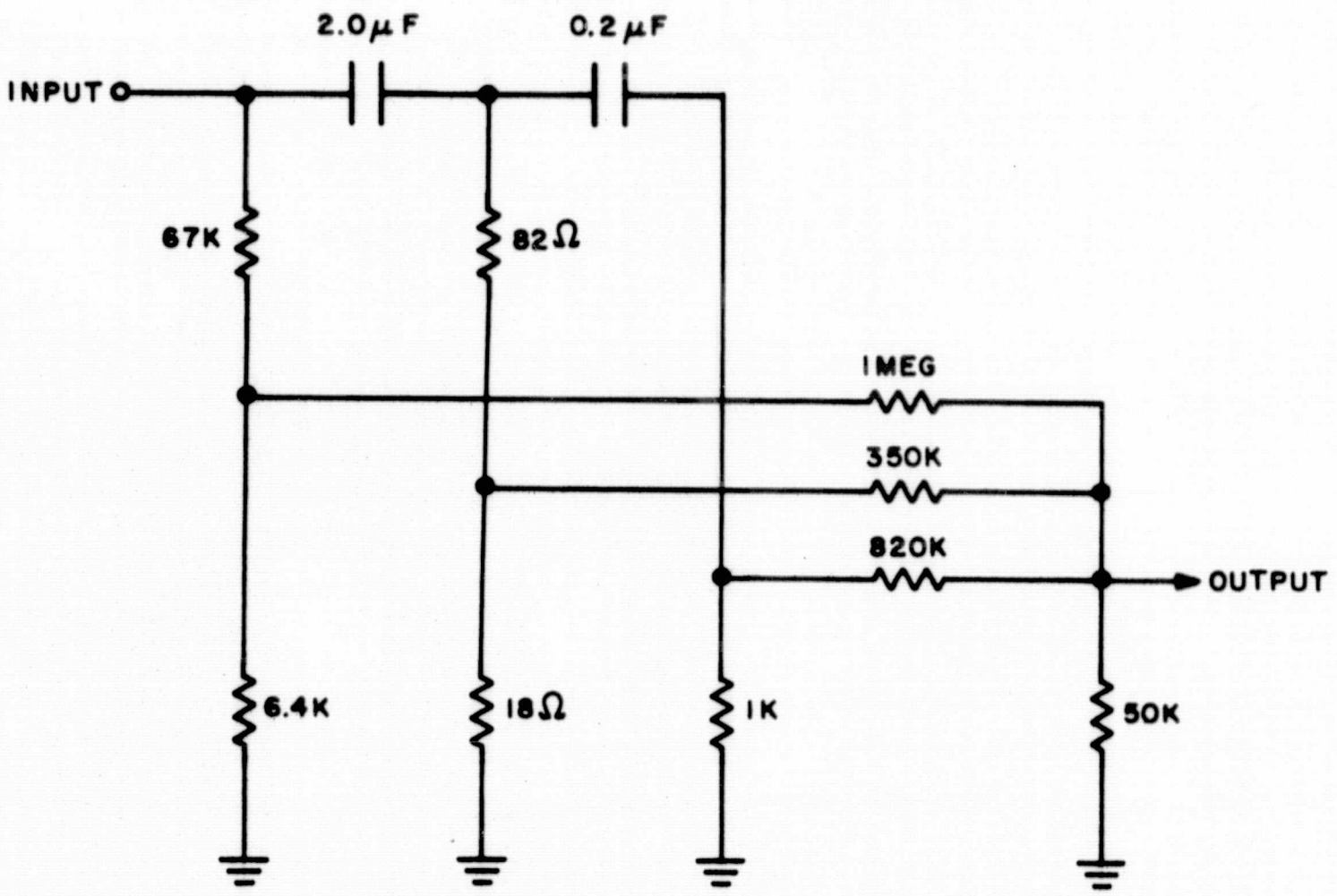

Figure 3-14 PREDICTOR NETWORK

by 1 millisecond the course of a 2-80 cps bandwidth random noise signal is shown in the oscillograms of Figure 3-15.

Considering the fidelity of the anticipation of the noise sample of Figure 3-15, it is reasonable to assume that, if the 1 millisecond predictor is followed by a 1 millisecond delay line and (1) the original noise and (2) the output of the delay line are applied to the two inputs of a difference amplifier (Figure 3-16), the amplifier output should be very small due to the close identity of its two inputs. Thus the predictor delay system will cancel low frequency noise.

Only stationary noise can be predicted. Stationary means that at any instant of time the signal statistics are the same. Thermal resistor noise and, in general, amplifier noise behave this way. (An exception would be "spiking" of a transistor.) At the beginning of a received planet pulse, the amplifier output is non-stationary. A predictor anticipating say 1 millisecond has, in the interval of 1 millisecond preceding the planet pulse, no means of "knowing" of the impending signal. On the other hand, if the spectrum of the rest of the signal following its edge is within the bandwidth

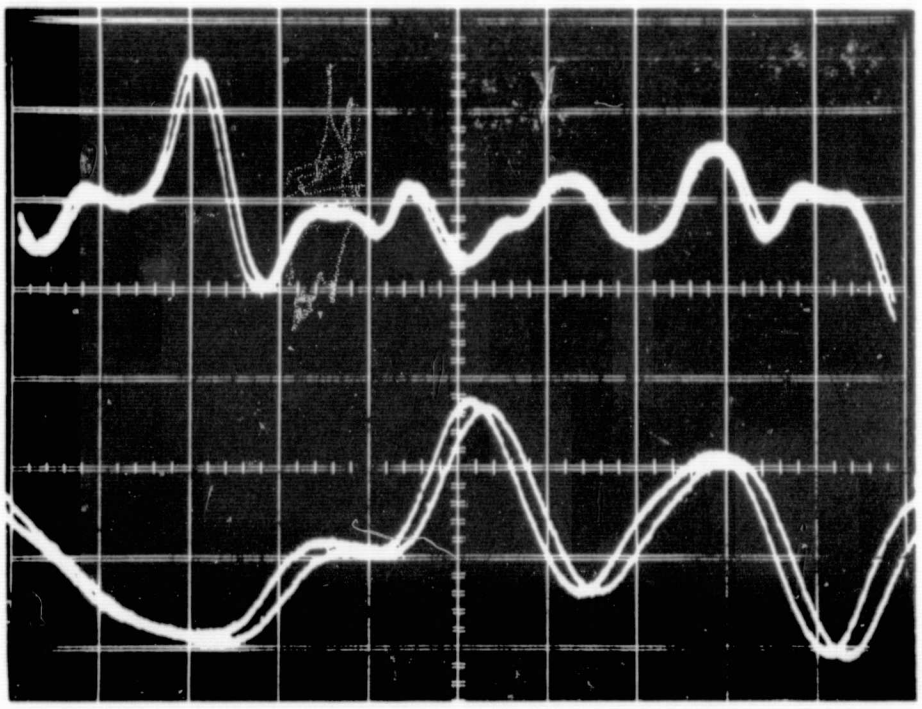

Noise voltage and anticipated noise voltage.

10 msec/cm

Noise voltage and anticipated noise voltage.

5 msec/cm

Bandwidth: 2-80 cps (Kron-Hite filter)

Prediction Time: 1 msec

FIGURE 3-15

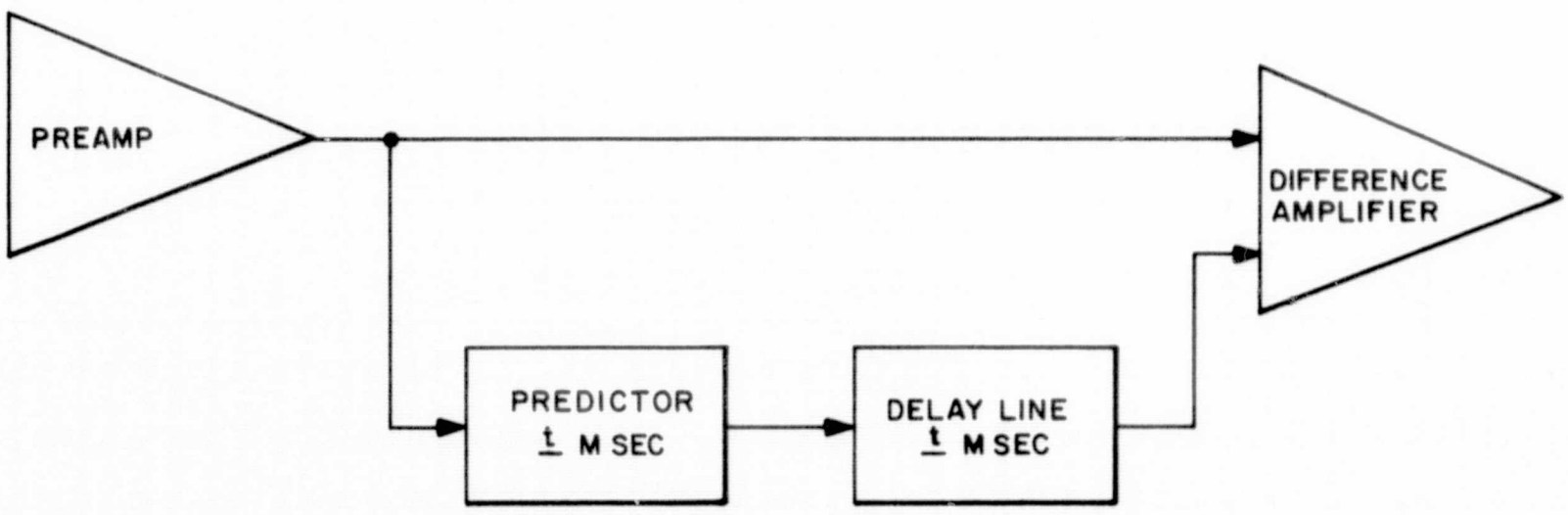

21753

Predictor - Delay System

FIGURE 3-16

that can be handled by a particular predictor, this, after a 1 millisecond embarrassment, will return to predict the signal, this time noise plus planet pulse until a new thermal gradient on the planet producing a new temporary (1 millisecond) non-stationary condition again upsets the predictor. At all these times of non-stationarity there will be an output from the difference amplifier of Figure 3-16, when, for the interval of one msec, the two inputs do not cancel. In fact, for 1 millisecond, there is a growing difference between the two inputs and it takes about another millisecond for the predictor to completely recover anticipation and thus for the output of the following delay line to cancel the primary signal. This effect is shown in the oscillograms of Figure 3-17. The difference, also shown in Figure 3-17, is our useful signal.

In this case, as in the case of a differentiator, useful signal is generated when there is an abrupt change in gradient of the planet signal. (In the case of the predictor delay, there is also response to an abrupt change in some higher order derivative.) Notice, however, (in Figure 3-18) the speed with which the output of the differentiator recovers

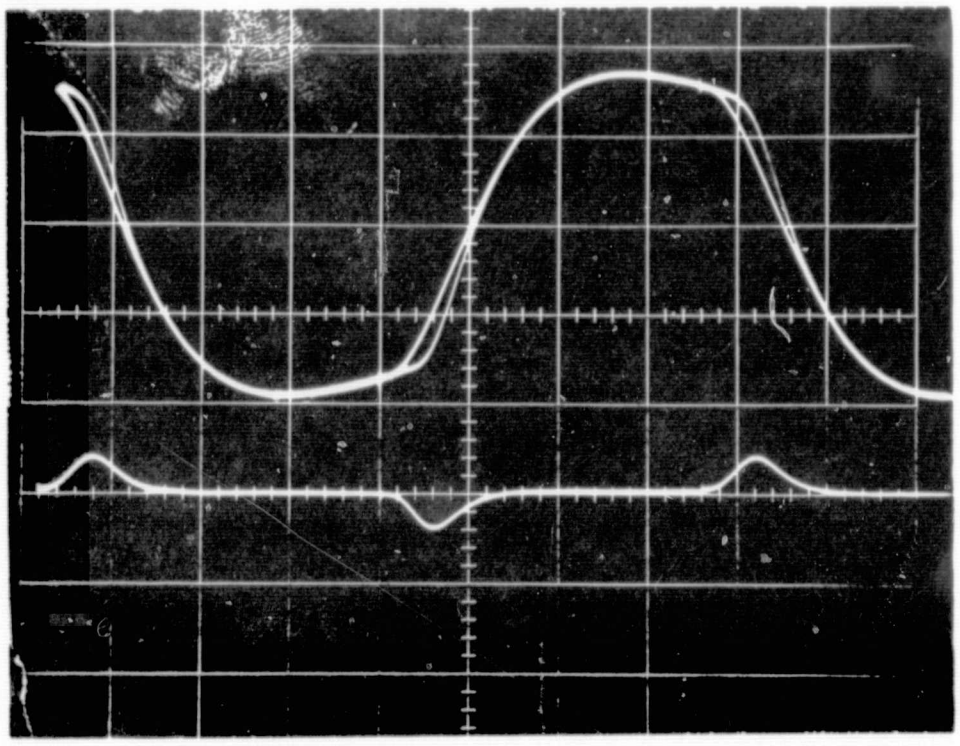

Earlier Trace: Preamp. output

Later Trace: Predictor-delay output

2.5 msec/cm

Difference amplifier output

Preamp Input: 50 cps square wave after 2 low-passes, 1 msec each.

Preamp. rise time: 1 msec.

FIGURE 3-17

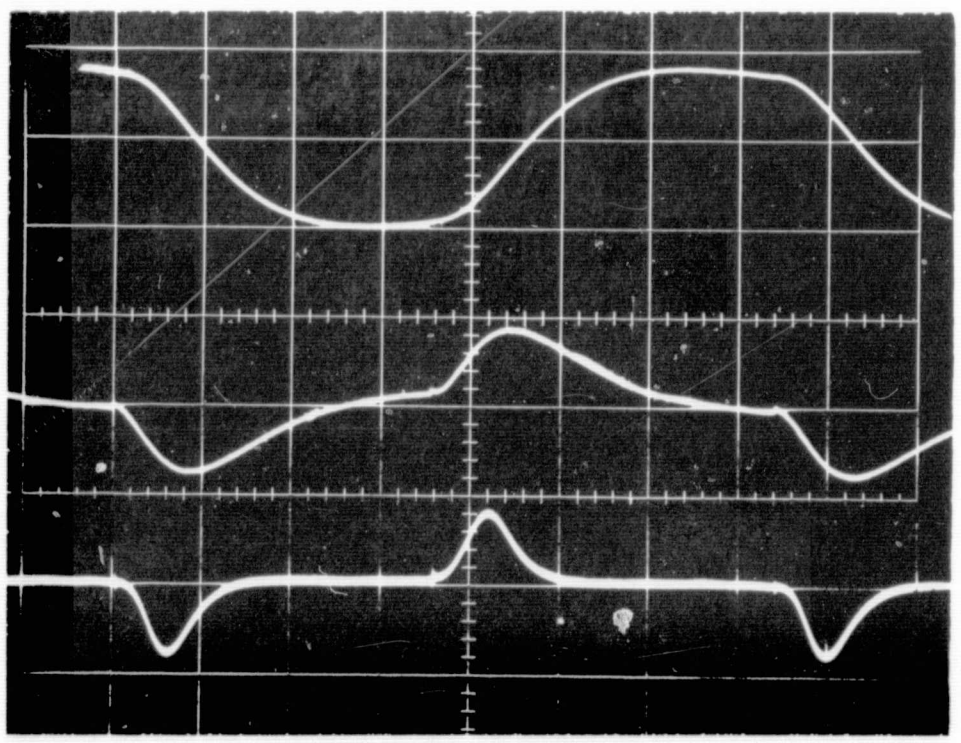

a) Preamp. output of Figure 5

b) Trace a) passed through a 200 μsec RC differentiator

c) Difference amplifier output

2.5 msec/cm

Observe the short decay time in trace c) as compared with trace b).

FIGURE 3-18

after a gradient change when compared with the recovery of the output of a differentiator of comparable peak-signal-to-noise ratio. The same information is amplified and expanded in Figure 3-19. There is very little or no overshoot in the case of the predictor delay, while there is considerable overshoot in the case of the differentiator. This feature will make the predictor delay system a preferred choice if rapidly following thermal gradients of wide dynamic range have to be resolved in the output.

Figure 3-20 is an oscillogram of noise samples--the first from an ordinary differentiator, the second from the predictor delay system. This latter exhibits the characteristics of relatively narrow band noise, centered around 500 cps. The spectral characteristics have been measured as curve (b) of Figure 3-21. In the same figure, curve A shows the Fourier spectrum of the signal output of this system. It can be appreciated that the system lends itself to spectral discrimination. In fact, a simple tuned circuit achieved the signal enhancement of Figure 3-22. It follows that, with some sacrifice in the sharpness of the pulse shape, it should be

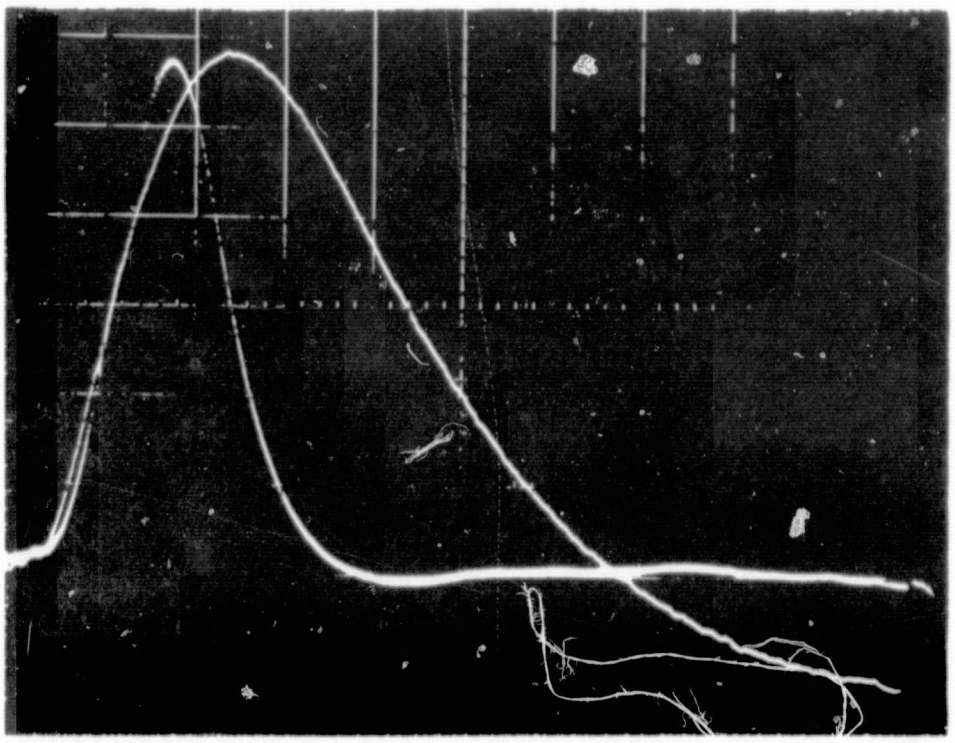

Traces b) and c) of Figure 3-20 amplified and expanded

Time Scale:

Approx. 1 msec/cm

FIGURE 3-19

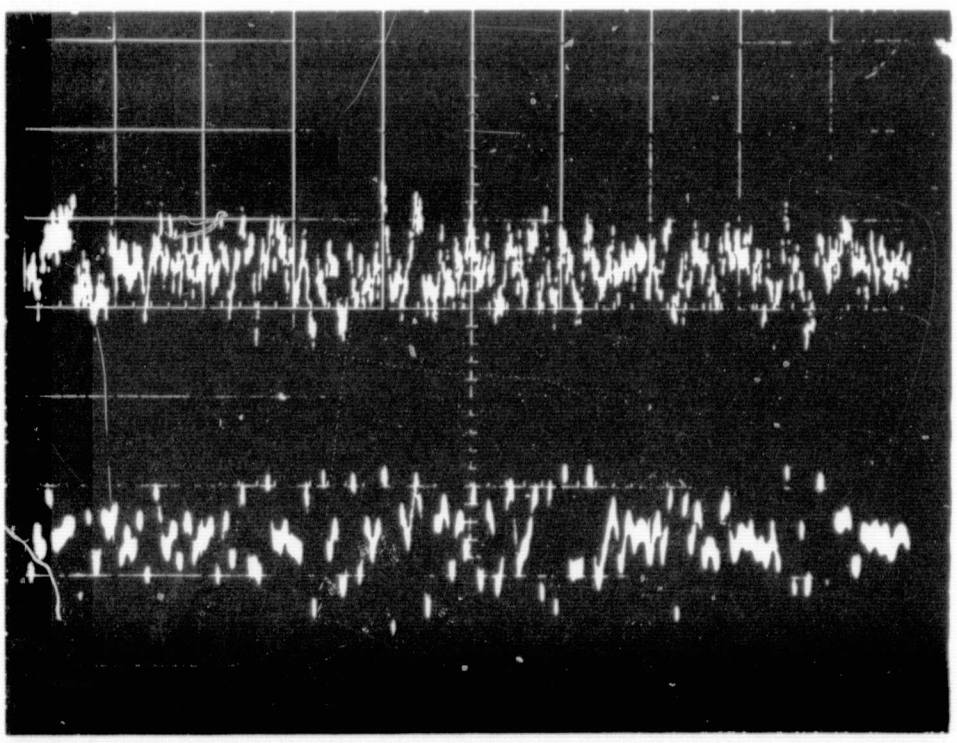

Noise output of 200 μsec R-C differentiator

Noise output of difference amplifier. Observe amplitude modulated narrow band character.

Preamplifier Bandwidth: 160 cps, simple roll-off

FIGURE 3-20

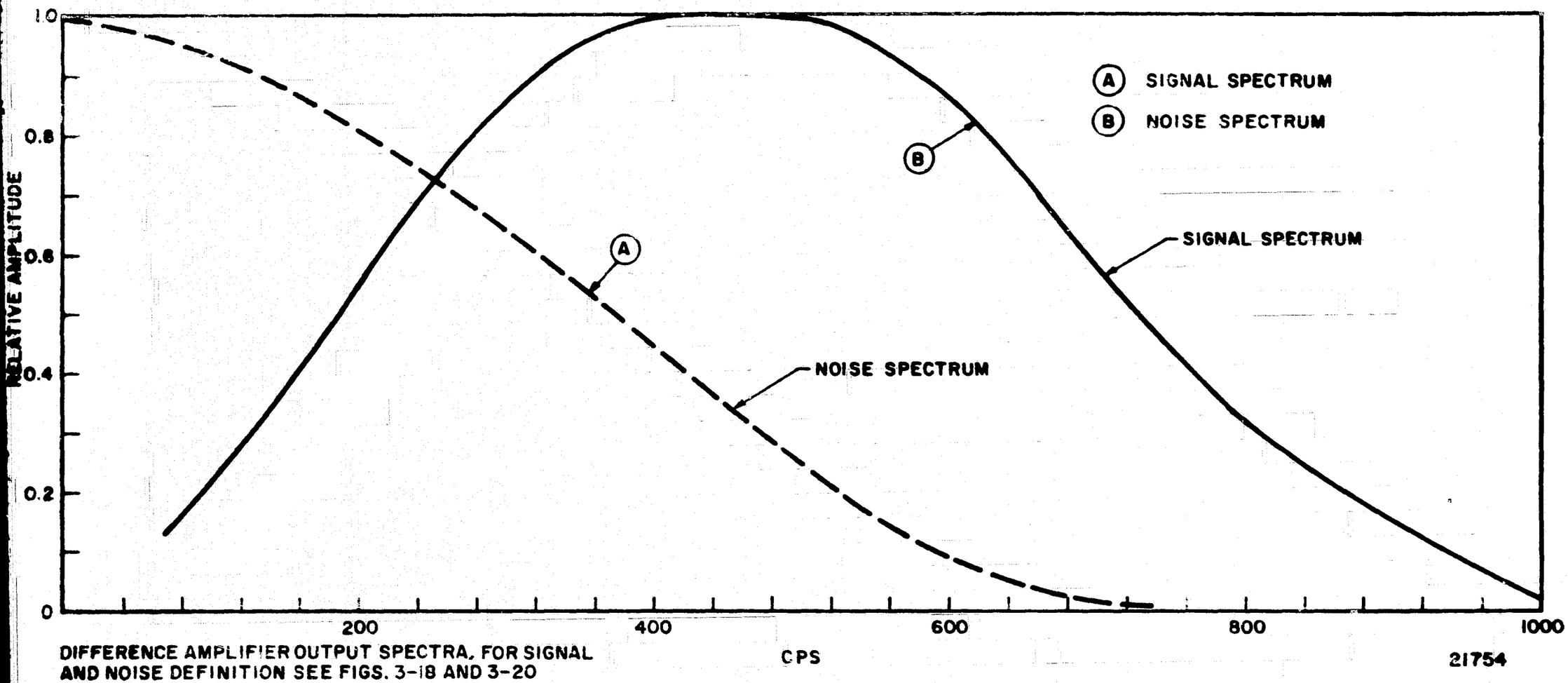

DIFFERENCE AMPLIFIER OUTPUT SPECTRA. FOR SIGNAL AND NOISE DEFINITION SEE FIGS. 3-18 AND 3-20

Figure 3-21 PREDICTOR-DELAY COMBINATION

possible to tailor an optimum filter for curves (A) and (B) of Figure 3-21 to obtain a signal-to-noise enhancement of about a factor of two.

The electronic circuitry necessary to implement the system represented in Figure 3-16 consists of the predictor circuit of Figure 3-14, a two-transistor amplifier to make up for the attenuation of about 200 of the predictor, and a delay line, the only circuit of any complexity in this system. The experimental work was performed with a delay circuit containing five inductors (Figure 3-23) taken from a paper published by L. Storch.[11] Simpler circuits should be investigated as to applicability.

Taking advantage of the fast decay characteristics of the predictor delay system output pulses, the following gradient sensing horizon scanner processing becomes practical:

(a) Horizon position is obtained in terms of the voltage reached by a ramp (or staircase) generator at an instant to be specified below under (d).

---

[11] L. Storch. "An Application of Modern Network Synthesis to the Design of Constant Time Delay Networks with Low-Q Elements," 1954 IRE Convention Record, Part 2, pp. 105-117.

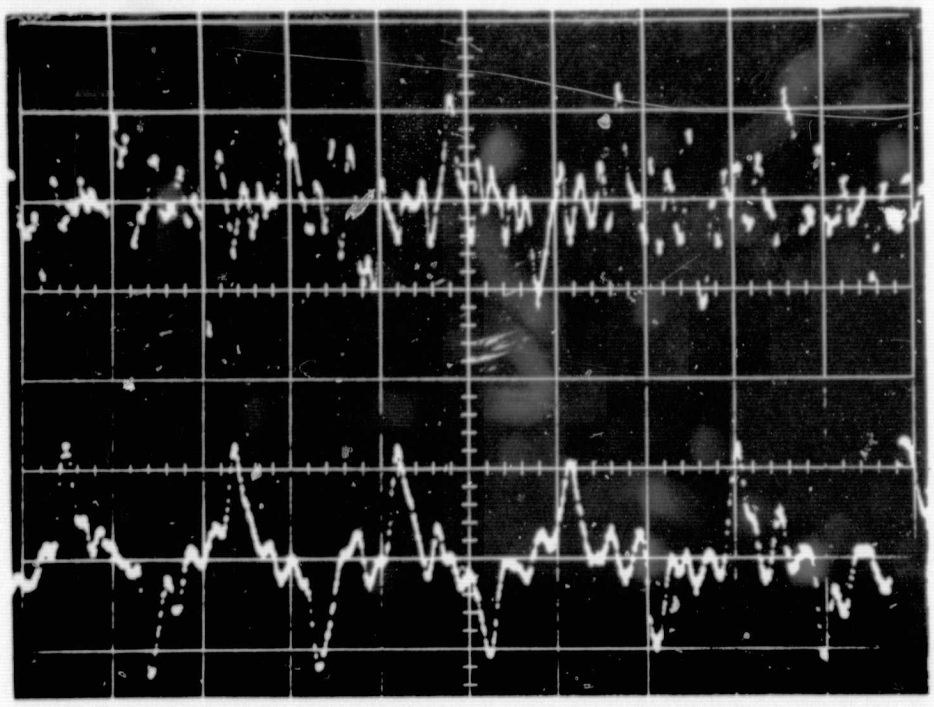

a) Noisy signal at difference amplifier output

b) As in a) with 1000 cps series L-C shunting difference amplifier input

Signal Enhancement with a Simple Filter

FIGURE 3-22 Effect of Filtering on S/N of Difference Amplifier

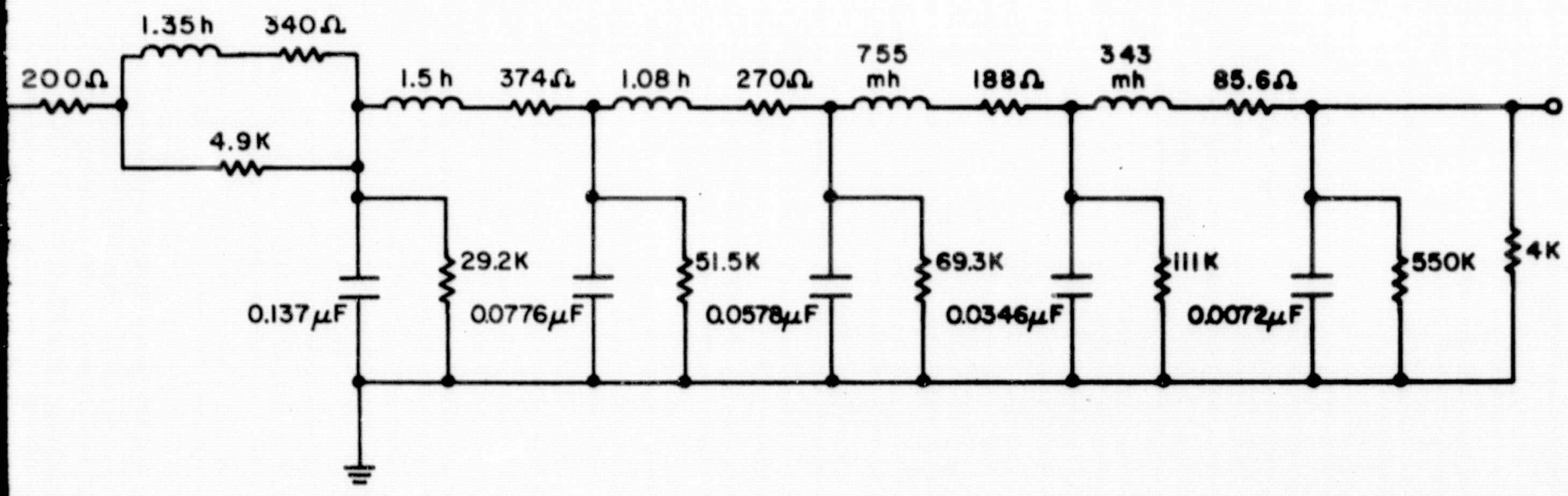

Storch 1.25 Millisec Delay Line

We built it with 10% tolerance resistors and capacitors and it worked well.

FIGURE 3-23 Delay Line Network

(b) Every negative-going signal pulse resets the ramp generator to zero and starts a new rising ramp.

(c) A reference pulse (connected with the horizon scanner frame and appearing in the center of the space scan when the scanner is at "null") reverses the slope of the ramp.

(d) The first positive pulse after the reference pulse stops the ramp generator. At this instant, its output is read out. A block diagram of this system is shown in Figure 3-23a.

It is seen that time is counted during the space scan. Item (b) insures that the true planet edge, leaving the planet being the last negative-going pulse, starts a fresh rising count. The first positive pulse, the one that stops the falling count, is the planet edge entering the planet. At null the reference pulse bisects the space scan, thus forcing equal lengths of rising and falling ramps, resulting in a net count of zero. See Appendix C for a detailed explanation.

Due to the rapid response of the predictor delay system, the scanner output will not be in error for thermal gradients separated by at least two detector fields of view from the horizon.

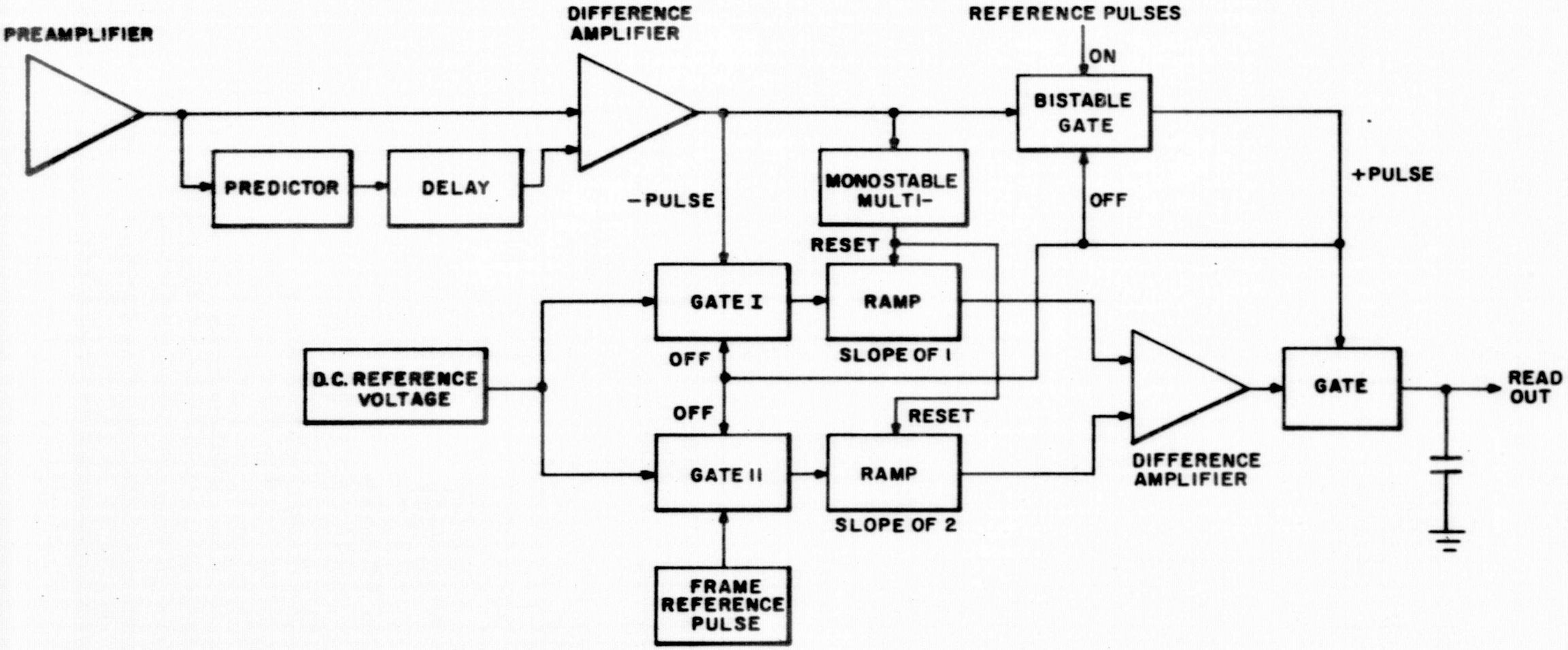

21755

Figure 3-23a PREDICTOR — DELAY SCANNER ELECTRONICS

Further work is required to establish the possibility of detecting an initial small fraction of a field of view crossover for horizon scanners of high angular resolution and accuracy. For such applications, the prediction should contain more terms with higher derivatives. The accuracy of the system just described with a 1° field of view and thresholding at one-quarter height of the minimum signal pulse is ±0.125°.

3.1.6 Sensitivity and Signal-to-Noise Ratio Considerations for Conical Scan Sensor

In order to arrive at a meaningful measure of the performance of a conical scan sensor with processing as described in the preceding paragraphs, we will base our calculations on parameters of a conical scan sensor which has recently been designed for an Air Force application and which is known as the Model 13-155 horizon sensor. The scan rate, processing electronics, and a number of other characteristics will, of course, require changes for the present application.

Parameters of the Optical Head

Optical System.....	Cassegrain reflecting system
Effective Collector Area.....	A_0 = 22 cm^2, 2.1 inch effective diameter

Field of View.....	$1° \times 2°$ ($\omega = 6.1 \times 10^{-4}$ ster)
Detector Dimensions.....	0.2 mm x 0.6 mm hyperimmersed
Optical Efficiency with 20 to 40 Micron Filter.....	$\epsilon \cong 0.6$
Detector NEP, assuming one msec time constant.....	$NEP = 6.3 \times 10^{-10} \sqrt{A/\tau}$ $= 6.3 \times 10^{-10} \sqrt{0.12/1}$ $= 2.2 \times 10^{-10}$ watts (for a single thermistor flake in a 1 cps bandwidth, τ = 1 msec; A = .2 x .6 mm = .12 mm)

For lunar sensing, assuming a 90°K crater, the effective radiance (ΔN) is:

$$\Delta N_{90°K(20-40\mu)} = \frac{4 \times 10^{-4}}{\pi} (0.31) = 4 \times 10^{-5} \frac{\text{watt}}{\text{cm}^2\text{-ster}}$$

The power on the detector is:

$$P_D = \Delta N \, \epsilon \, A_0 \, \omega$$

$$P_D = 4 \times 10^{-5} \times 0.4 \times 22 \times 6.1 \times 10^{-4} = 0.32 \ \mu\text{watts}$$

Allowing some degradation in detector sensitivity, we will assume a bolometer bridge (a load resistor equal to the

thermistor resistance). Degradation will be assumed as follows:

Bridge Factor	=	1.4
Bias Reduction for Safe High Temperature Operation	=	1.4
Noise Factor	=	1.5
Total	=	3

Assume a 200 cps bandwidth. Noise increase over that of a 1 cps bandwidth system is $\sqrt{200} = 14$ times.

The effective NEP is

$$NEP = 2.2 \times 10^{-10} \text{ watts} \times 3 \times 14$$

$$NEP \cong 9 \times 10^{-9}$$

and the signal-to-noise ratio is:

$$\frac{S}{N} = \frac{P_D}{NEP} = \frac{0.32 \times 10^{-6}}{9 \times 10^{-9}} \cong 35$$

For the expected detector resistance of 80K ohms (and 40 K Ω bridge resistance), the Johnson noise is:

$$V_J = \sqrt{4KTR\Delta f} \cong 0.36 \text{ microvolts}$$

With the assumed noise factor, we can expect to measure about 0.5 microvolt rms noise in the 200 cps bandwidth. The signal will be 35 x 0.5 = 17.5 microvolts rms, or about 35 microvolts peak.

If we set our slice level at a level 10 times below this signal amplitude (and still above peak values of noise), we can assess the crossover time error which would result for increases in radiance by a factor of 50 or more. Inspection of Figure 3-0 shows that, at 10% slice level with a 0.5 rps scan rate, the maximum attitude error is 0.2° or ±0.1° variation from the portion indicated for a nominal average radiance.

A similar approach may be applied for the case of the earth application. For the 20-40 micron spectral range, the lowest equivalent temperatures as seen from Figure 2-1 (radiance for various atmospheres in the 20-40 micron region) are about 200°K. The radiance in this spectral interval is

$$\Delta N_{200°K(20\text{-}40\mu)} = 2.9 \times 10^{-3} \times .35 = 10^{-3} \frac{\text{watt}}{\text{cm}^2\text{-ster}}$$

which is about 25 times higher than for a 90°K moon. The

signal developed at the detector will be about 1 millivolt. The error at a low slice level will be extremely small and is limited by phenomenological conditions rather than by the system errors to less than 0.05°.

3.2 Electronic Scan Horizon Sensor

3.2.1 General Considerations

One of the horizon sensor systems considered as a possibility for the earth/lunar horizon sensor application is the multi-element thermopile system using all-electronic sampling of individual detectors in order to define the position of the planet.

In view of the detailed descriptions which have already been prepared for this system, we will dispense with a discussion of the basic principles and performance of this horizon sensor system and instead append a paper which covers the necessary background material.[12] In addition, to show the most recent developments and improvements achieved, a

---

[12] M. Monty Merlen, Jerome M. Pasternak, and Denton Pearsall. "Electronic Scan Horizon Sensor," presented at the Symposium on Infrared Sensors for Spacecraft Guidance and Control, Barnes Engineering Company, May 1965.

discussion is presented in Appendix A of results of recent work on detector switching and sampling using MOS field effect transistors.

In this section of our study, we will confine ourselves to a discussion of the variations and modifications which would have to be undertaken in order to adapt the existing design to the application to be considered.

The primary differences in requirements of these two systems can be seen from a comparison of the performance features of the present system and the design goals given in Paragraph 3.1.2.1 of the work statement for this program.

Parameter	Design Goal	Present LPHS System
1. Weight	8 lbs.	25 lbs./system
2. Size	6" dia. x 10" long Vol. = 283 cubic in.	275 cubic inches
3. Power	15-20 watts	4 optical heads - ≈ 15 watts can be reduced
4. Reliability	0.997 for 90-day operation	MTBF is about two orders of magnitude less than desired without redundancy
5. Accuracy	0.1°	±0.5°

Parameter	Design Goal	Present LPHS System
6. Repeatability	±0.1°	±0.5°
7. Signal-to-Noise Ratio	10-12	threshold set at S/N_{rms} for 100°K moon
8. Spectral Region of Operation	20-40μ	14-50μ
9. Altitudes of Operation	100-300 n.m. for earth = 137° to 155° subtense with 50-150 n.m. for lunar orbit 137°-155° subtense	22° to 170° planet 10° x 81° FOV
10. Attitude Error for 2° of Vehicle Motion		±0.5°
11a. DC Error Signal	10 mv/deg. min.	300 msec/scan can be reduced to 0.1 sec.
11b. 5% Error Signal up to 10°	10 mv/deg. min.	digital output with positive indication over entire transfer function
11c. Noise not to Exceed Error of 0.01°	10 mv/deg. min.	±0.1° (for earth)

In reviewing the individual specifications, we find certain discrepancies which should be elaborated. Insofar as

the weight is concerned, the present system is seen to exceed the specified design goal. This is not considered to be a fundamental limitation since no major effort has been made to minimize the weight of the existing sensor. The single complete head which has been constructed uses an aluminum casting and employs individual photoconductor/neon sampling switch elements. An eventual flight system would be built with a magnesium casting and would use field effect transistor switches made in the form of an integrated circuit array which would result in a significant reduction in weight.

Likewise, unless major changes in the optics are undertaken to improve resolution or signal-to-noise ratio, the volume of the sensor can be kept within the design goals.

The power requirements listed can be, and would be, further reduced through use of field effect transistor sampling switches in place of the photomodulator/neon combination of the present unit.

It may be thought that the reliability of the all-electronic horizon sensor will be far greater than that of a system using moving parts, even if the mechanical system has

very slowly moving elements. This is somewhat deceiving because the multi-element, no-moving-parts system requires many more components (principally, the sampling switch elements and counters). Only if we can assume that high reliability integrated circuits are used for these components and that multiple redundancy is incorporated can we expect comparable reliability figures for this type sensor. The reliability comparison is carried out in greater detail in Section 5 of this report.

Another consideration is the nature of the output signal. Since the design requires that, if the output is digital, an analog signal should also be provided, additional circuitry must be used which further degrades the reliability of this system.

3.2.2 Accuracy Considerations of All-Electronic Horizon Sensor

The comparison chart in the preceding section shows that the accuracy of the present all-electronic horizon sensor is ±0.5°. This is established by the resolution of the sensor coupled with the mode of operation. In a digital system, as represented by the existing sensor, we obtain only one piece of

information: the sampling position at which we have crossed a threshold level, indicating wehther signal is present or absent. Therefore, with an elemental detector resolution of approximately 1°, the digital system can be made to respond in such a way that, if sufficient energy is received by one detector, planet presence is established for the one detector count. Thus the system is capable of detecting, in each co-ordinate (for each axis), two crossover positions within its detector resolution capability, resulting in an accuracy of ±0.5°. In order to improve the accuracy to the desired figure of 0.1°, it will be necessary to either increase the detector resolution by a factor of five without degradation in signal-to-noise ratio or to improve the existing signal-to-noise ratio by a factor of at least five and then resort to analog interpolation to define the position of the horizon more precisely with the existing detector subtense. Both of these approaches are difficult to carry out, as will be shown below.

3.2.3 Increase in Optical Resolution

The present all-electronic horizon sensor system uses a 5 cm focal length concentric optical system and has

detectors which subtend 0.9° by 10° fields of view. The detector size becomes f.1 x θ = 5 cm x 0.0157 = 0.079 cm (θ = 0.0157 radian for the 0.9° dimension). The length will be 11 times greater for a 10° subtense.

One way in which the resolution may be improved is through an increase in the focal length by a factor of five with a corresponding increase in aperture dimensions. However, a 25 cm focal length becomes rather unwieldy for this space application, particularly if we keep in mind the need for four optical heads. We have just examined the weight and volume design goals and have concluded that the present design comes close to the desired dimensions and leaves no reserve for the possible increase in the size of optics which could be considered.

An alternative possibility is to reduce the dimensions of the detector. In considering such a step we must remember that it is essential that the existing signal-to-noise ratio be maintained or exceeded in order to make the approach feasible. The construction of the present 21-element thermopile block is seen in the sketch following along with some of the performance characteristics.

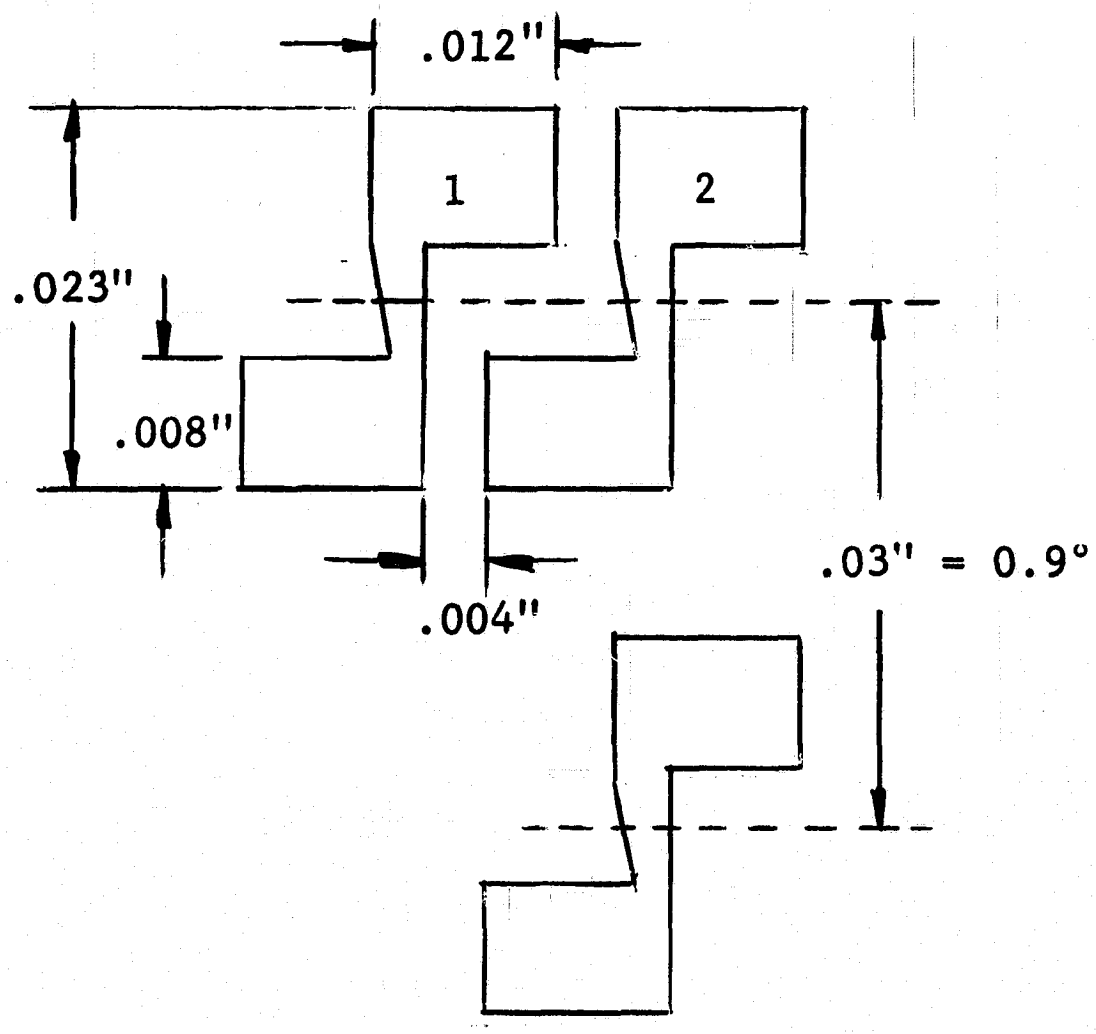

The minimum size elemental active area and separation between elements with existing techniques is considered to be 0.003 to 0.004. Since the existing detectors are larger than the minimum value, one would conclude that an area reduction can be used to increase the number of detectors and, consequently, the responsivity.

However, a closer examination reveals that this may not be accomplished so simply. The present design shown in the sketch above, while it does not use the smallest element size and separation, does provide an efficient thermal separation between adjacent fields of view through use of channels or grooves between rows of detector elements. Also, this form of construction permits some thermal isolation between the junctions and the aluminum blocks leading to a slower response, but also a higher responsivity.

A more standard serpentine arrangement of minimum size elements would afford neither of these advantages. We estimate that the latter geometry with an aluminum base 1/4 mil mylar substrate and minimum size elements would result in a responsivity approximately equal to that of the present system. However, there would be about 30% cross-talk between adjacent fields of view, i.e., if one elemental field of view alone were illuminated to produce an output of 1 microvolt change, the channel next to this would experience a 0.3 microvolt change, and so on.

This is considered to be an intolerable amount of cross-talk, since it would not be possible to obtain a 0.1°

resolution with such a system. Other compromises in terms of greater separation of elements to permit use of isolation channels or barriers would relieve this problem but would result in a reduction in responsivity which would make the S/N ratio too small for lunar horizon sensing.

Summarizing the foregoing considerations of the all-electronic horizon sensor, we find that the present system has a sensitivity just slightly below that required for satisfactory operation in a lunar horizon sensor. A factor of at least two improvement in S/N is required to insure operation for a target temperature of 90°K. Such a factor of two, it is believed, can be achieved through some improvement in thermopile efficiency presently being investigated, coupled with some reduction in noise and drift at the input which is also believed to be possible. However, these improvements may not be forthcoming in the time allowed for completion of an engineering model earth/lunar high accuracy horizon sensor.

It must also be remembered that the increased resolution requirement for such a system dictates an increase in the primary optics dimension with the consequent increase in volume and weight.

As a result of these considerations, we cannot presently recommend use of this approach in a system whose engineering model is to be built in a period of about 8 months. Considerations of cost, not covered in this study, may also dictate against the choice of this system.

In a later section we will explore the possibility of combining the advantageous features of the electronically sampled thermopile technique with an edge tracker through use of only three thermopiles. This would be a hybrid arrangement using a small number of electronically sampled thermopiles in combination with a servoed search movement as used in the edge tracker.

3.3 Edge Tracking Horizon Sensors

We can place edge tracking horizon sensors, as developed to date, in two basic categories: one in which we oscillate over a small angle in the vicinity of the horizon edge and a second type in which we switch fields and compare radiation from one field in outer space with that from another field at the edge of the horizon. The first of these is characterized by the fact that a null position or correct attitude

is established as the absence of second harmonic in the signal waveform. The angle of oscillation is normally small (of the order of 2°) in order not to stress unduly the mechanical components producing the oscillation and also to utilize a minimum of scanning time and electrical bandwidth.

The second type in which fields are switched uses the normally generated signal waveform for a servo drive and has an electronic bandwidth established by the chosen filter characteristics in a demodulator circuit. This bandwidth and the field switching rate are independent of the displacement of the fields of view being sampled.

Both systems include a search mechanism driven by a motor, usually in a closed loop system. The motion of this system is slow and, once the planet is acquired, only small and slow movements are required to maintain "lock" onto the planet edge. Frictional forces and wear are therefore not severe in either system. Both approaches are also adaptable to what has become known as "azimuth scan," a sweeping back and forth of the fields of view along the planet periphery which tends to average out the inhomogeneities in the radiance

emanating from different portions of the planet. Inevitably, such an "azimuth scan" requires a more complex mechanism with attendant decrease in reliability and increase in mechanical and electronic parts.

3.3.1 Scanning Edge Tracker

3.3.1.1 Second Harmonic Type Edge Tracker

Insofar as the potential performance is concerned, the second harmonic type edge tracking horizon sensor has some intriguing features.[13] The Advanced Technology Laboratories' edge tracker, using the "Positor" scan mechanism, is capable of the accuracy and other design requirements for the present system if we limit ourselves to operation in earth orbits. If one operates in the 15 micron CO_2 band of the spectrum with the second harmonic type processing, then it can be shown that acceptable accuracy is achievable when locking on to the earth's reasonably uniform CO_2 layer in the upper atmosphere.

Let us examine the case for operation in a lunar orbit. Regardless of the spectral band selected, the second

---

[13] Sheldon Knight. "Infrared Horizon Tracking for High Precision Attitude Measurement," presented at the 10th National Infrared Information Symposium, October 1-3, 1963, at Fort Monmouth, New Jersey.

harmonic type processing would cause the system to search for a null output from the second harmonic filter. Such a null would be as readily obtained at a crater edge somewhere within the confines of the lunar disc as at the edge. In fact, it would be difficult to obtain such a null at the edge in a region where the radiance level is very high and the dynamic range requirements are staggering. (50:1 variations in signal when viewing target temperatures of 350°K and 90°K.)

3.3.1.2 Edge Tracker with Azimuth Scan

It is felt that for lunar operation a wide angle "azimuth scan" would be indispensible in conjunction with the second harmonic type systems. A scan mechanism of this type, as developed by ATL, is not considered to be compatible with the high reliability goal of the present system. It has been estimated by ATL officials that the life of this system is about 500 hours and falls very far short of the goals set for this program.

Another possible drawback of the system as presently executed is the susceptibility of the flexural motion drive mechanism to vibrational forces. If used in powered flights

under heavy vibration, severe errors would result in the output signals, if not possible damage to the mechanism. Reliable operation is thus confined to earth missions in free flight and is severely limited for use in lunar orbits and in powered flights or during booster operation.

3.3.2 Field Switching Edge Tracker

The limitations ascribed to the system above do not apply to the field switching edge tracker, since it does not rely on a null in second harmonic and normally switches between two fields which are sufficiently separated (at least 5° to 6°) to insure that one field views outer space as a reference. While there are a number of possible ways in which the field switching edge tracker can be designed to operate, a simple form will be used by way of example to illustrate how the error in attitude determination may be kept within the desired limits. In the case of an earth orbiting mission, we will choose to operate in the 15 micron CO_2 band in order to avoid possible errors due to clouds at the edge of the horizon we wish to track. In the case of lunar operation, we will make the system capable of tracking on an edge of the

lowest conceivable temperature. The sketch below shows the errors which may be expected under the most extreme conditions.

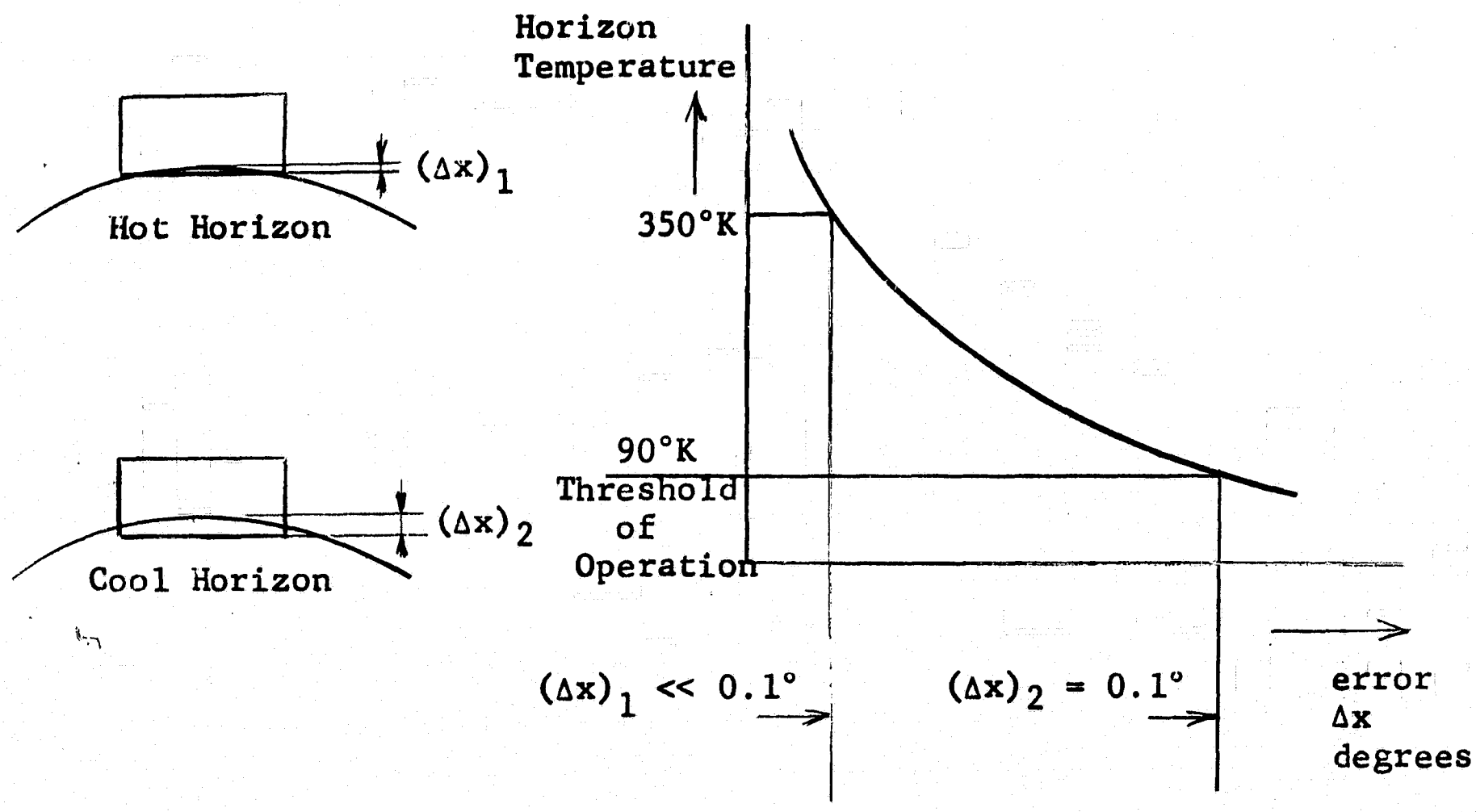

In this system, the tracking servo is made to lock on when a given threshold level is exceeded. For a 1-inch aperture system and a 1 cps bandwidth, we have computed a S/N of 100 for a 90°K target, which fully illuminates the detector. (See Table 4-1 for further parameters of this system.) If we set our threshold level at 10 times rms noise (about two

times peak-to-peak noise), we will exceed the threshold when 1/10 of the detector is illuminated. The error committed under this condition is thus 0.1° on one side of the planet. In practice, this error would be reduced as a result of the fact that it is averaged between the readings on both sides of the planet. If instead of a temperature of 90°K the planet edge to be tracked had a temperature of 350°K, then about 50 times more energy would be received for a totally illuminated detector field of view. The threshold level would then be exceeded at a point 1/500 of the vertical subtense or 1/500 of a degree, which is essentially at the very edge of the planet disc--a negligible error.

For a system operating in the 15 micron centered CO_2 band and viewing the earth's upper atmosphere, the maximum radiance variations which may be encountered are approximately two to one. The signal-to-noise ratio expected is about ten times larger than in the case of a 90°K lunar region. It is therefore possible to exceed the threshold with a signal 1/100 of the total, or covering only 0.01° of the 1° vertical subtense. For the two to one dynamic range of radiance levels,

the error is thus seen to be only 0.005° which is less than the expected phenomenological errors.

3.3.2.1 Description of Switched Field Edge Tracking Horizon Sensor

We examine, next, methods of implementing a field switching edge tracker. One system has been described in some detail in a paper by G. Falbel[14] which outlines the concept of the "FIRM" horizon scanner. About 1-1/2 years ago, Barnes Engineering Company began work on a piezoelectrically actuated frustrated internal reflection modulator (FIRM) intended for a variety of applications, including radiometry and horizon sensing, in which it would be possible to chop radiation without the need for moving parts (i.e., with motion of only a few microns required to produce full modulation) and with a minimum of power.

More recently, supported by the Company's independent R&D program, a complete horizon sensor was built using the "FIRM" principle. Upon completion of the engineering model, a thorough evaluation was made of this system, which revealed both encouraging and some very discouraging features.

---

[14]Gerald Falbel. "High Accuracy Horizon Sensor using FIRM," presented at the Symposium on Infrared Sensors for Spacecraft Guidance and Control, held at Barnes Engineering Company May 1965.

On the encouraging side is the fact that the edge tracking function, the search system, servo design, circuitry, readout, etc., function quite well. Furthermore, provided that the modulator works with an efficiency of at least 25%, good sensitivity is obtained with all indications that the figures referred to in Paragraph 3.3.2 above can be achieved.

On the discouraging side of the picture we have discovered some difficulties with the operation, in its present form, of the piezoelectrically modulated frustrated internal reflection modulator. In its present construction, we have observed a change in the separation of the optical elements due to dimensional changes in the barium titanate transducer. This resulted in a reduction in the gap separation for a given excitation field, with consequent decrease in modulation efficiency. The result of such decreased efficiency was the appearance of multiple ghost space fields and the possibility of aperture chop in the event that the optical elements do not have a homogeneous ambient temperature. Details of these problems with the modulator built for the engineering model horizon sensor are given in Appendix B of this report, since

these observations are only peripherally of interest in this study and other methods of edge tracking are available.

As part of its independent R&D effort, Barnes is continuing its work on the FIRM modulator. Various individual elements of this problem can be solved, e.g., the multiple field problem can be avoided through use of a different optical geometry in which the two prisms of the FIRM are identical and an exact symmetry exists in the path of rays reaching the detector in the open and closed positions of the gap. Because of the observed positional variations (creep) of the barium titanate transducer, we are also investigating a magnetic actuator for the FIRM prisms as a substitute for the piezoelectric elements. If a definite and complete solution to this problem is found within the next two or three months, the possible benefits of this accomplishment will be available to us for the system being contemplated.

3.3.2.2 FIRM using Magnetic Drive

Irrespective of the outcome of present design work on the piezoelectrically actuated FIRM field switching horizon sensor program, evaluation of the basic sensor concept has

demonstrated to us its potential for meeting the fundamental goals of the present program. Since other methods of field switching are available, we will next discuss several alternatives. One such system which uses components that have had wide use already and can be demonstrated to yield a very high reliability figure replaces the piezoelectric modulator with one which employs a magnetic drive to open and close the gap of two prisms which transmit or frustrate transmission of the incident energy. A new design with butting dove prisms avoids the "ghost" field problem. In other characteristics, this modulator is similar to the existing FIRM cell.

3.3.2.3 Field Switching Edge Tracker with Vibrating Reed Actuator

A detector's field of view may be switched back and forth between widely separated positions by means of a vibrating reed mechanism such as a tuning fork drive system. Such a tuning fork vibrator, apart from its wide use in precision oscillators and time standards, has had some considerable use as a light or radiation chopper in infrared systems. Among other systems, Barnes Engineering Company has been using such a modulator in its radiometric microscope.

A number of versions of field switching using a tuning fork vane actuator are described below.

3.3.2.3.1 Simple Field Switching Edge Sensing Device

This system has the simplest configuration and is applicable for earth or lunar missions. For earth applications, the accuracy can be somewhat improved by working in a narrow spectral band in the 15 micron CO_2 region, avoiding cloud lock-on. In the case of lunar missions, the accuracy is dependent on the S/N achievable for cold edges of the moon.

Various optical systems may be chosen for this system, only one version being shown by way of example. This uses the Cassegrain system already designed and built for the 13-155 horizon sensor system. The arrangement is shown in the sketch, Figure 3-24.

A dual mask in the focal plane defines two fields separated by some convenient angle, say 5°. These masks may define a field of view of 2° x 4° and must be precisely made and positioned. A vane actuated by a tuning fork tine does not require a precisely defined amplitude of oscillation. It simply opens one or the other of the masks to allow radiation

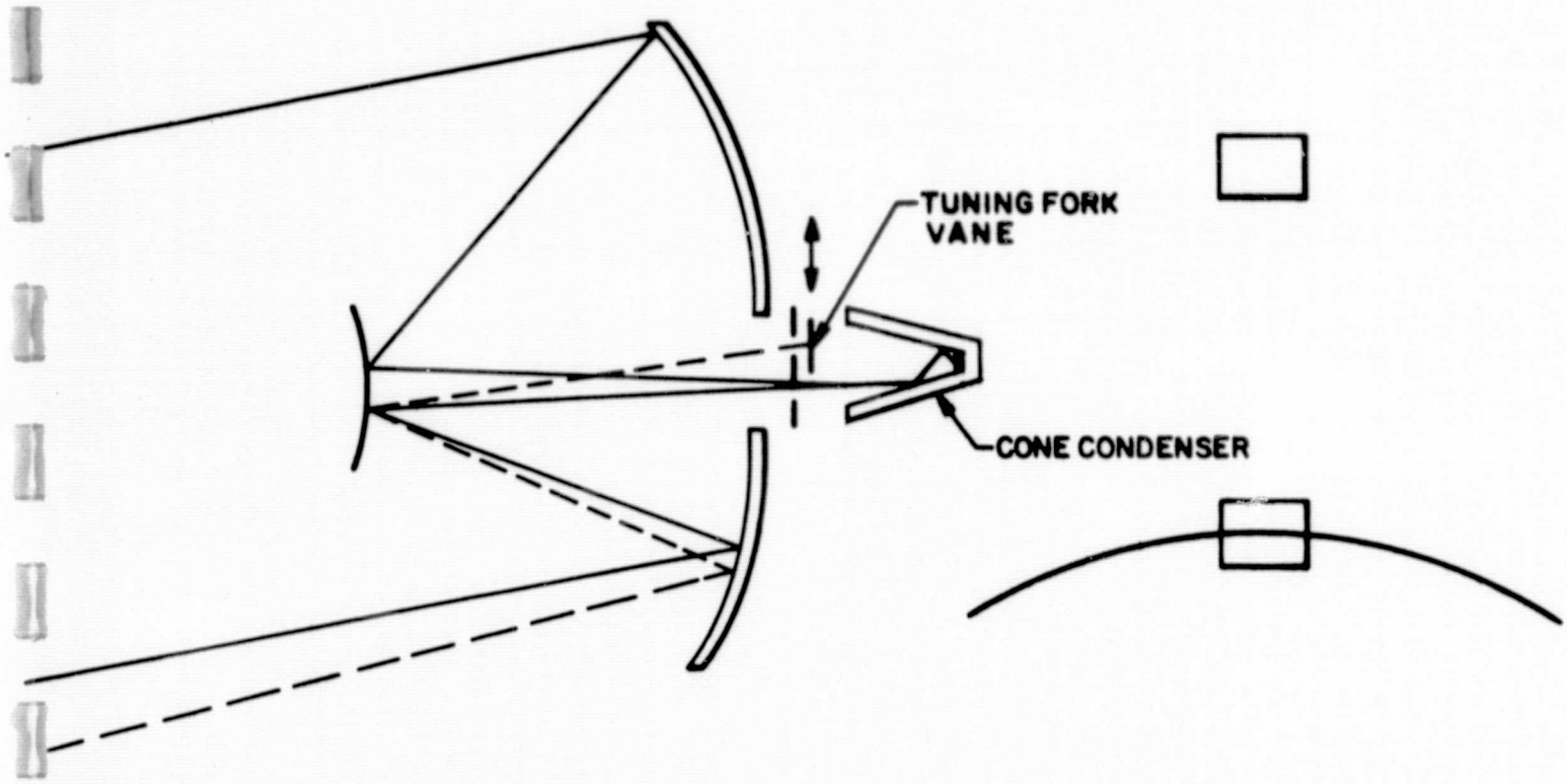

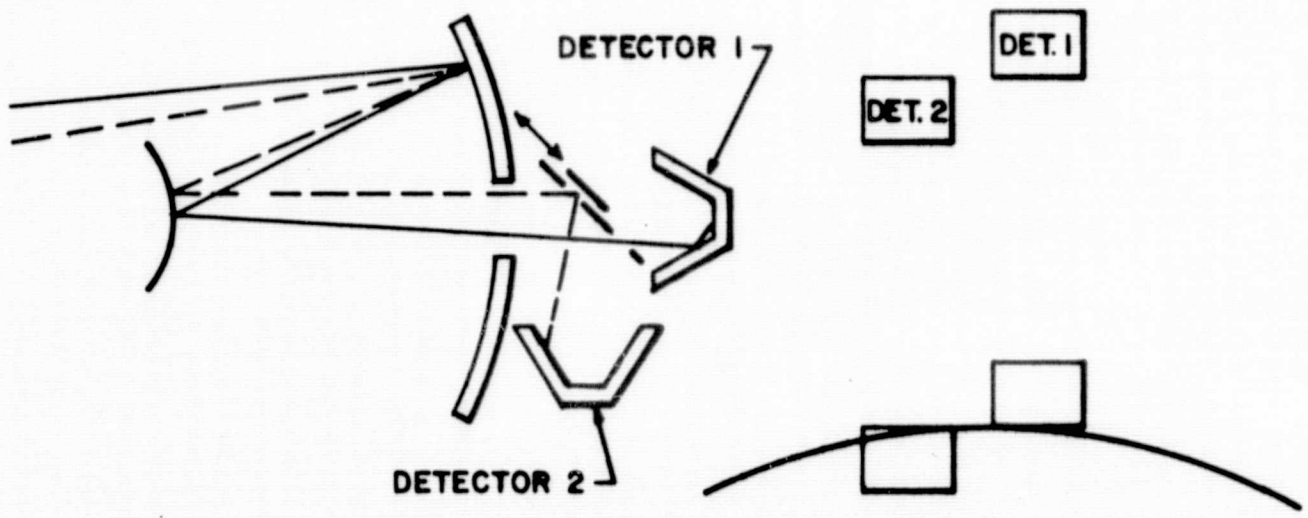

21756

Figure 3-24 FIELD SWITCHING EDGE TRACKER USING TUNING FORK MODULATOR

to be interrupted and reach the detector. An optical filter may be placed over the openings of the mask. Travel of the vane must be at least 2° or about 1 mm, which is quite simple by tuning fork standards (100 cps may be a convenient chop frequency). A condensing cone may be used to concentrate the energy on the detector and improve the system f/number. For the long wavelengths at which the cold side of the moon has its peak radiance, the condensing cone detector combination may be superior to a silicon-immersed detector. If a signal-to-noise ratio in excess of 20 is achieved for the 100°K portion of the moon (for the 2° x 4° field of view), then we should be able to "lock on" at a point within 0.1° of the planet edge. Higher planet temperatures would then cause slight errors as the horizon is acquired with the planet subtending a somewhat smaller portion at the bottom of the detector's field of view. Errors for low planet temperatures and errors due to the sun may present problems.

3.3.2.3.2 Dual Detector Field Switching System

A somewhat more sophisticated version of this system uses a second detector along with a time-shared vibrating vane chopper system. As shown in Figure 3-24, the second field of

view is displaced both in azimuth and elevation from the first field. This naturally multiplies the detector and associated electronics by two. However, it results in very significant advantages which may make it worthwhile in some applications:

(a) In the event that the sun appears in either field (it cannot appear in both as a result of the choice of greater than 1/2° displacement) the system can be made to ignore the output associated with the sun.

(b) The upper field output signal is normally in control of the torquer drive. The lower field output becomes a radiometric vernier correction signal which adjusts the precise level at which the upper detector is stationed with respect to the horizon. This will work properly only for a homogeneous radiance condition in the vicinity of the two fields.

(c) In the event of failure of either of the two signal channels, the electronics can be made to operate on the remaining one. If it switches over the lower field (as a result of a failure in the upper one), then an offset signal will automatically set the readout to a position 2° higher. We thus have complete redundancy in detector and electronics.

3.3.2.3.3 Single Detector Chopped Radiometric Balance System

A technique which is applicable for operation over a region of homogeneous radiance (for example, 15 micron CO_2 band) has some advantage in S/N over the methods above because of the fact that the target area illuminates one-half of the field of view when the system is correctly oriented. The chopper mask arrangement is shown in the sketch below.

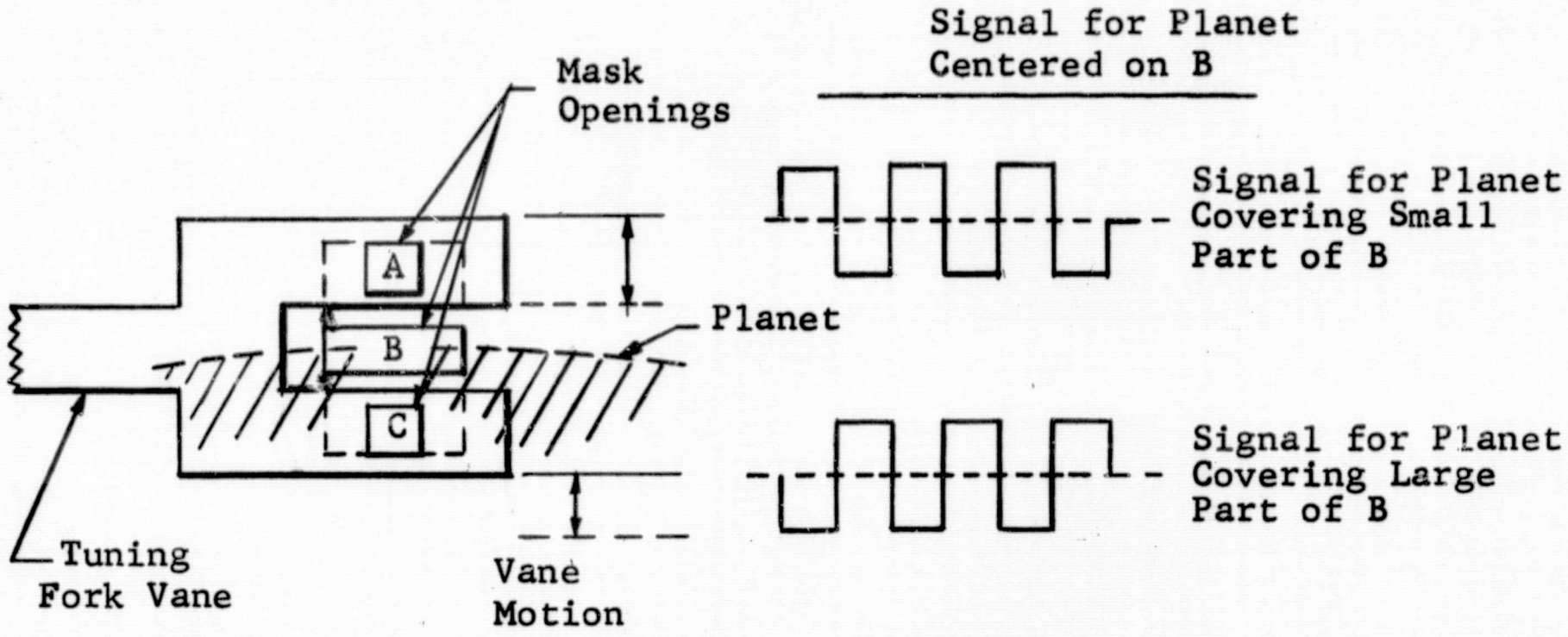

We can see that, in the position of the vane as shown, the lower half of window B is illuminated. When the vane is in the lower position, window C is fully illuminated, presumably from a target area of the same temperature.

Window C is exactly one-half of window B. The detector, which sees the dotted rectangle, gets the same amount of energy and a null output is created after demodulation. Other waveforms show the output under conditions off null for which the torquer is made to move in the appropriate direction. An output must be provided for this system in order to show when the planet has been acquired. A simply rectified output (not passing through the synchronous demodulator) will indicate acquisition, provided we always start our search from one extreme space.

In the case of lunar applications, possible local variations in radiance (craters) would make this system inaccurate. For lunar application, the other techniques described in this section are therefore more appropriate.

3.3.2.3.4 Local Radiance Disturbance Cancellation Schemes

The systems described in the previous section can achieve good accuracy if the region over which the sensor operates has a homogeneous radiance pattern. In the presence of such disturbances, e.g., craters on the moon or clouds on earth when viewing the radiance pattern in a broad spectral region, these systems become inaccurate. In view of the

availability of a moving vane (tuning fork or other vibrator), it is possible to average out to a large extent such local variations simply by exposing the detector to the small local radiance variations while the vibrator produces an azimuth averaging operation. This lateral motion may be performed by one tuning fork which, in addition, does the field switching discussed earlier. In this case, the lateral motion may take place at higher frequency so that the detector need not respond to the local radiance variations but instead puts out a signal representing the average radiance in a given region.

3.3.2.4 Field Switching Edge Tracker with Slow Spin Rotating Chopper

This system combines the advantages of the narrow bandwidth and consequent high signal-to-noise ratio of the field switching edge tracker (using reflecting optics) with the vibration immunity of a system in which the moving parts are constrained in bearings. In terms of the tracking function, the system is similar to other edge trackers, employing a closed loop servo system with a torquer drive. Insofar as the field switching function is concerned, the optical system is very similar to that which was used successfully on the

Mariner II Venus fly-by mission two-channel infrared radiometer which was made by Barnes Engineering Company. This radiometer employed a slow reflecting chopper which allowed a thermistor detector to view, alternately, two fields separated by a fairly large angle and permitted comparison of radiance on the planet with a field located in space at some fixed angle from the planet. The chopper rotation may be slow and selected as any convenient value within the time constant capability of the detector. The output may be synchronously demodulated and filtered to provide a very narrow bandwidth and a high signal-to-noise ratio for tracking on a planet edge having low radiance, such as the dark side of the moon. The basic scheme is seen in the sketch below.

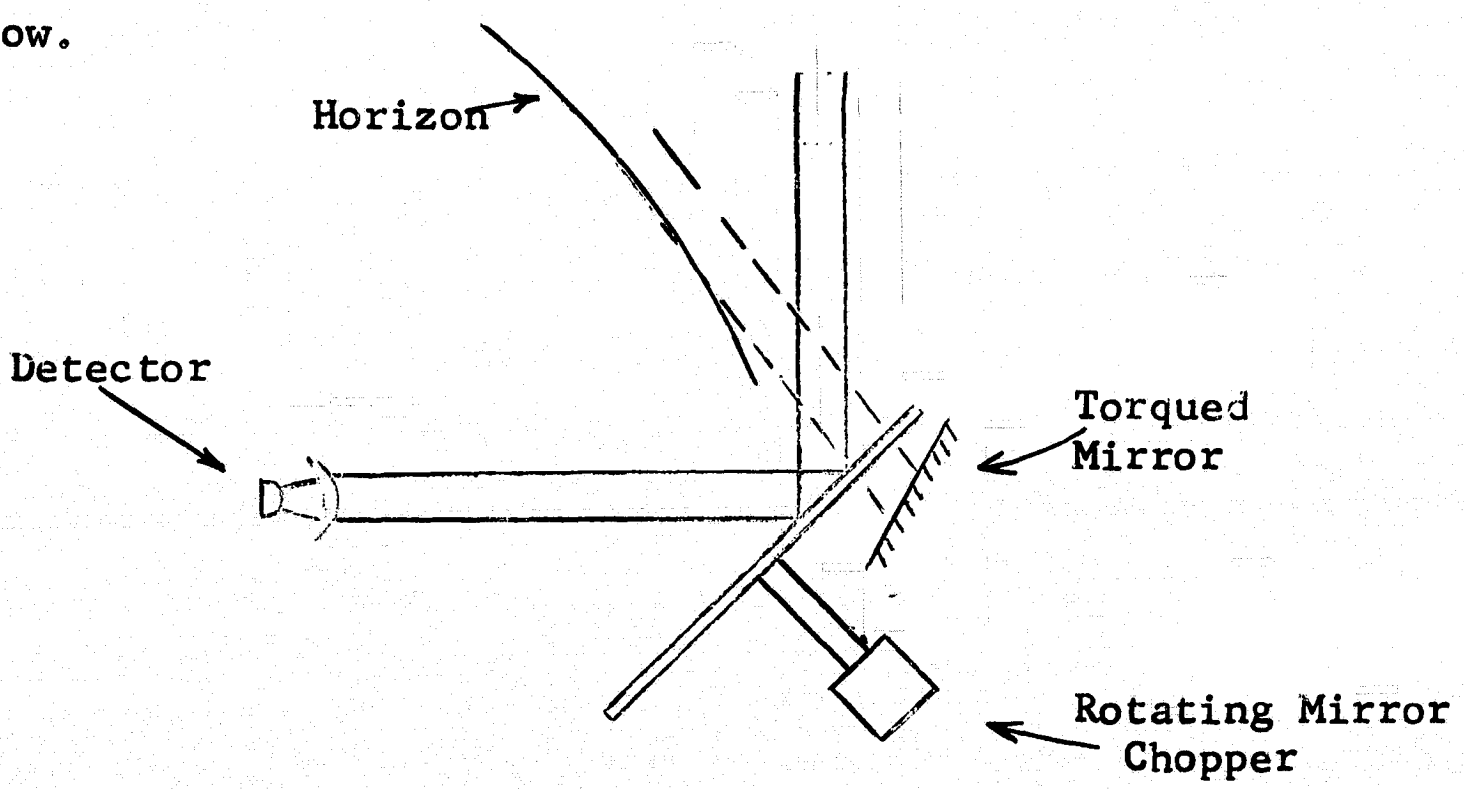

The principal difference between the Mariner radiometer optical system and the edge tracker being considered is the fact that mirror B, which in the radiometer application was kept in a permanently fixed position, will be the pivoting arm to perform the search and track function in the edge tracker and will be positioned by the torquer as controlled by the servo loop. If prime space is available on the spacecraft and a window can be used through which a wide field may be covered (as much as 180°), then a further refinement may be employed whereby two sensing positions may be tracked within one head using a single chopper. A sketch of this configuration is seen in Figure 3-25. Figure 3-26 is a block diagram of the processing.

A sample calculation of sensitivity for this system is shown in Section 3.3.2.5.

3.3.2.4.1 Problem Areas with Edge Trackers

We wish to examine next any conditions which may lead to difficulties with this approach to horizon sensing as with any other technique we have considered. The principal conditions we wish to examine are the following:

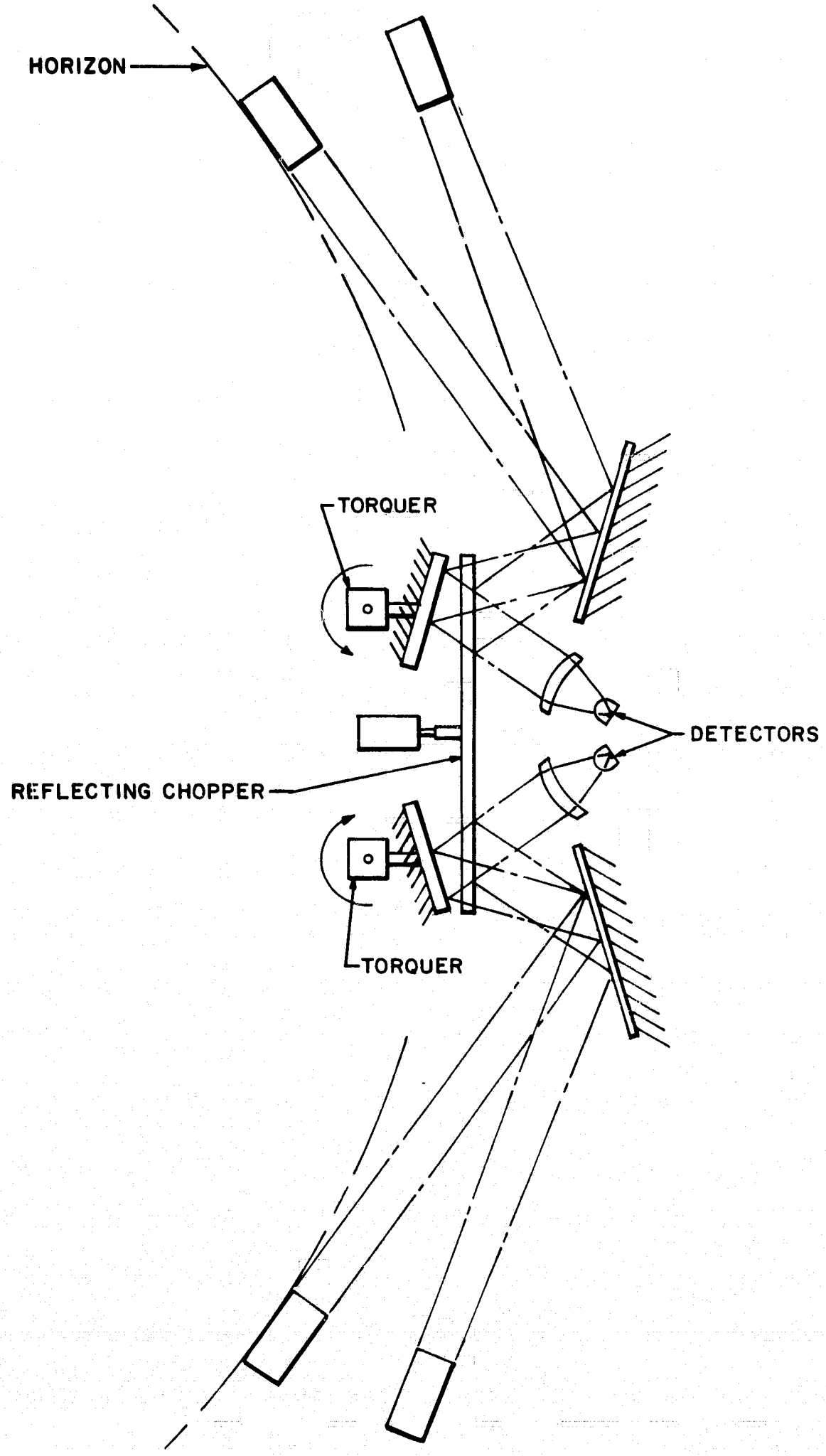

21758

Figure 3-25 SKETCH OF A SLOW SPIN ROTATING CHOPPER FIELD SWITCHING EDGE TRACKER

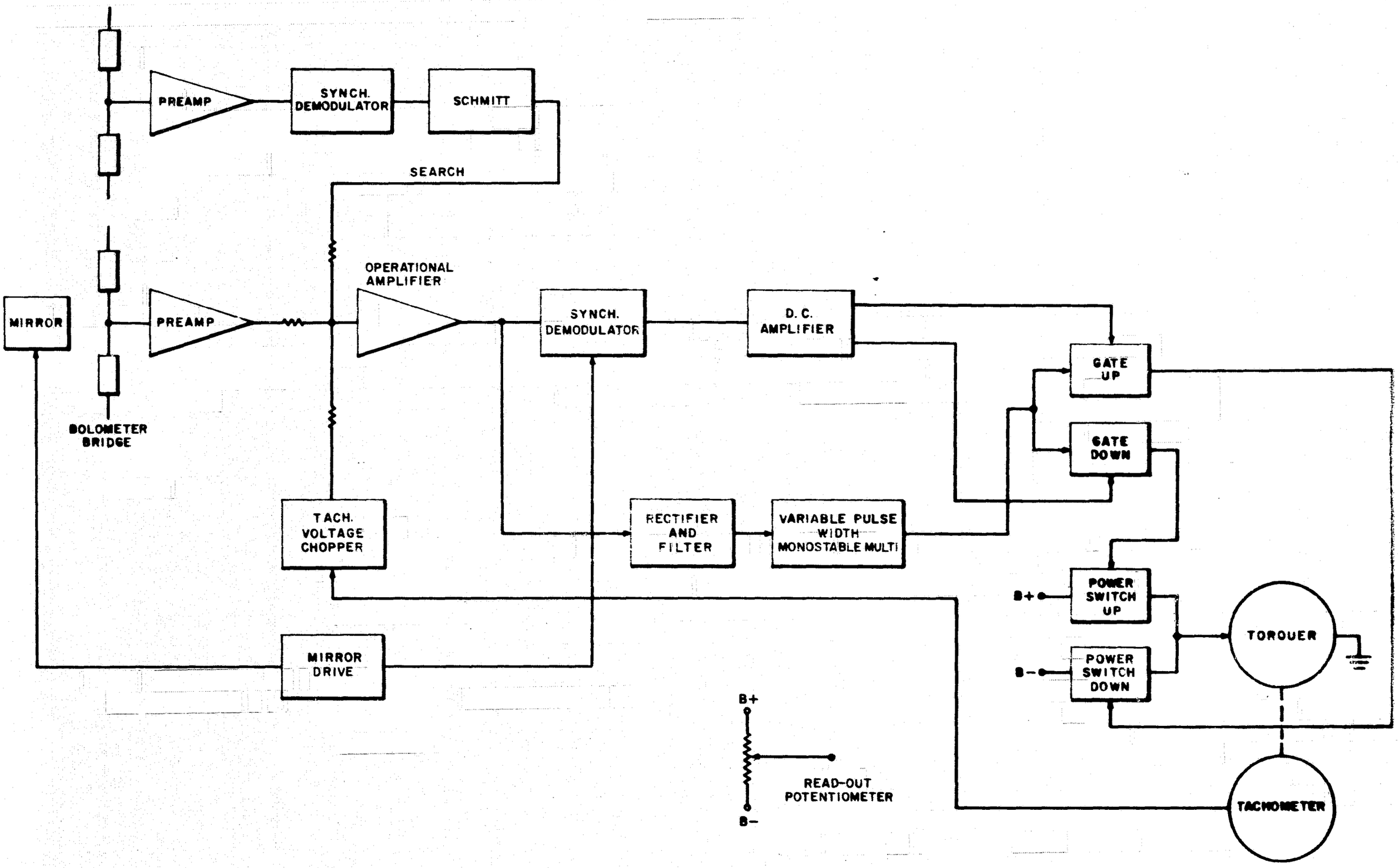

Figure 3-26 SWITCHING MIRROR ELECTRONICS 21759

(a) The possibility of the sun appearing in one of the fields of view of the sensor.

(b) Possibilities of aperture chop producing errors.

(c) Readout systems and their accuracy.

3.3.2.4.2 Sun Problem Elimination

The simple system sketched in Figure 3-25 may be upset by the possible presence of the sun in one of its fields of view. One solution to this problem is to install a second detector which is displaced from the first by an angle large enough so that the sun cannot be on both detectors simultaneously. Such an edge tracker is shown in Figure 3-27. It will be noted that two detectors separated by more than 2° in azimuth are used, each having a separate signal processing loop. This arrangement is used for a dual purpose:

(a) To prevent a false lock-on on the 1/2° sun or 2° earth (in lunar orbit use).

(b) To provide complete electronic redundancy of the signal amplification circuitry and thus greatly improve the reliability of the system.

The signal processing involves a servo loop into which a fixed downward bias is applied. This bias is bucked

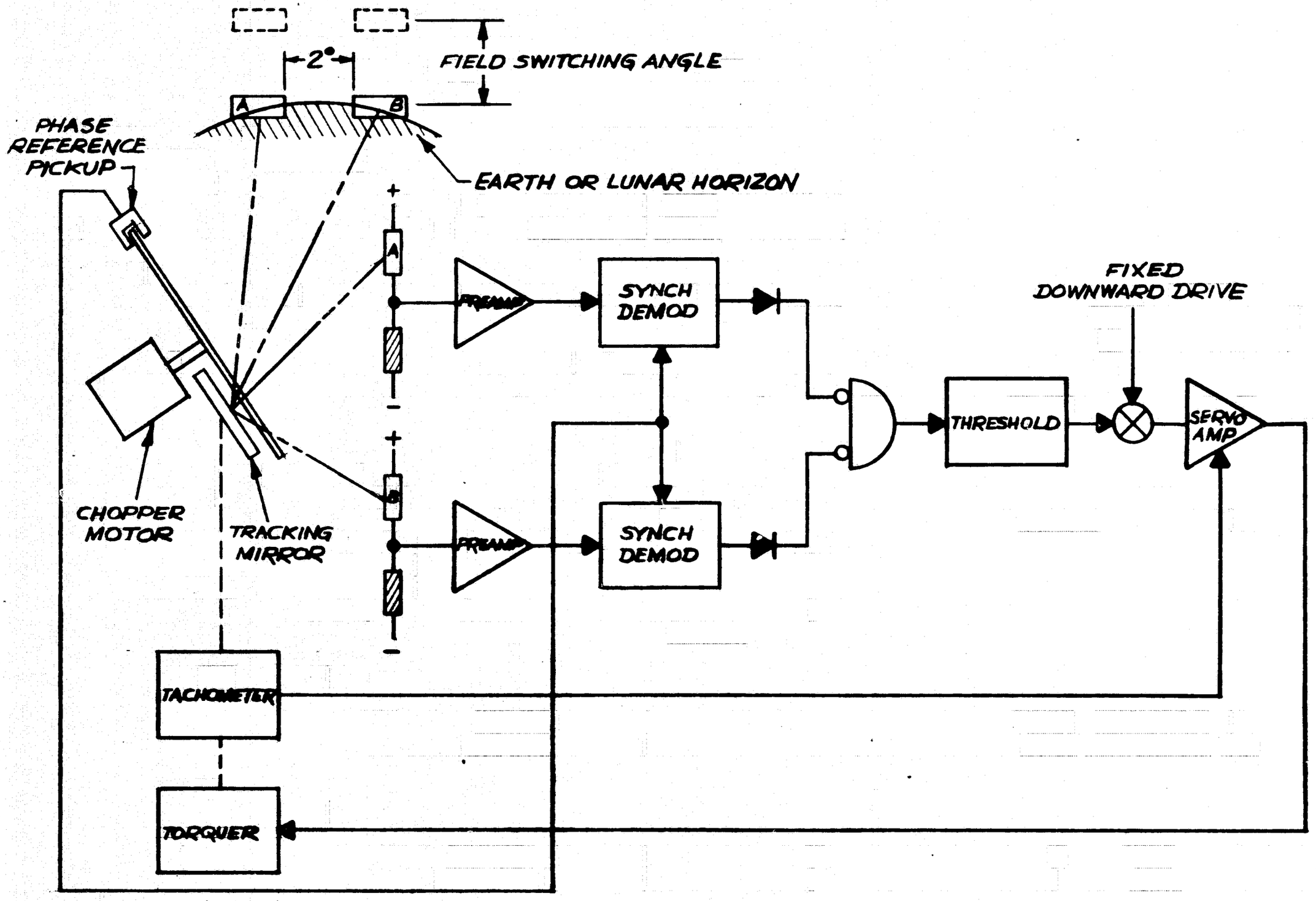

Fig. 3-27 CONFIGURATION OF FIELD SWITCHING EDGE TRACKER (ONE OF FOUR HEADS)

out by the signal generated when the bottom field position of both detectors intersects the planet. In order to prevent a false lock-on on the sun (or a 2° subtense earth when this sensor is used in a lunar orbit), a logic circuit does not disable the search mode until a signal is seen in both detectors.

Due to the 40 to 1 dynamic range of the lunar surface IR radiance, a "bang-bang" servo loop is used. This type of servo loop has the same stability characteristic independent of the 40 to 1 signal variation for the same angular indentation of the lunar horizon by the detector field of view.

This edge tracker configuration uses the same servo components that have been used in the FIRM horizon sensor. Due to the aforementioned developmental status of the FIRM cell, the field switching mechanism in this sensor would be a motor-driven mirror chopper, as shown in Figures 3-25 and 3-27.

3.3.2.4.3 Aperture Chop Considerations

In any sensitive radiometric system it is important to insure that the detector develop only signals representing variations in target area radiance and that it be insensitive to temperature differences in the optics, which may give rise

to a chopped signal just like that of the target. In the system sketched in Figure 3-25, we must make sure that the detector develops measurable chopped signals only from the target area radiance variations and not from internal sources. If the chopper blade and the tracking mirror had high emissivity and varied greatly in temperature, then the detector would be exposed alternately to the self-emission of the chopper blade and the tracker mirror and would develop a signal at the chopper frequency.

Our design calls for a highly reflective gold-coated chopper blade and tracking mirror (0.99 reflectivity is obtainable) and for an efficient thermal design which will insure a homogeneous temperature environment for the critical elements.

By way of illustration, let us suppose that the reflectivity has become degraded to a level where the emissivity of the surfaces is 1.5% and that a 1°C temperature differential exists between the two surfaces at a 25°C ambient temperature. The radiant emittance is:

$$W = \sigma\rho T^4$$

$$\text{and} \quad \frac{\Delta W}{\Delta T} = \sigma\rho T^3$$

Which, at 25°C is:

$$\rho \times 2 \times 10^{-4} \frac{\text{watts}}{\text{cm}^2\text{-ster}} \text{ per } °C$$

Since ρ, the emissivity, is 1.5%, the differential radiance

$$\frac{\Delta N}{°C} = 3 \times 10^{-6} \text{ watts/cm}^2\text{-ster}$$

Only about 20% of this energy is in the 20-40 micron region which a filter in front of the detector passes. The effective differential radiance becomes $0.2 \times 3 \times 10^{-6} = 6 \times 10^{-7}$ watts/cm^2-ster.

As we have computed earlier, a cool sector of the moon will have a radiance of about 10^{-4} watts/cm^2-ster in the 20-40 micron region. When one-tenth of this energy falls on the detector, an error of 0.1° ensues. Thus a radiance of 10^{-5} watts for the cold side of the moon will correspond to a 0.1° attitude error. The 1° temperature difference we have hypothesized will produce an error of $(6 \times 10^{-7})/(10^{-5}) = 1/16$ of this 0.1° value, or 0.006° which is negligible.

3.3.2.4.4 Readout System

The search mirror system shown in Figure 3-25 has the advantage of multiplying the optical field of view

displacement angle by two. Thus a 10° movement of this mirror produces a 20° sweep in space. The advantage in requiring small mechanical displacement is somewhat offset by the need for a more precise readout of the position of the tracking mirror. Since we require a 0.1° system accuracy, we must insure a superior readout resolution so that its error does not seriously degrade the system accuracy. Devices are available for obtaining the desired accuracy in either digital or analog form. Analog readout may be obtained to an accuracy of ±0.02° by means of an angular readout induction potentiometer made by Kearfott Division of General Precision. Optical encoders are also available to produce the desired readout accuracy in digital form from the Baldwin Piano Company.

3.3.2.5 Sensitivity Considerations for Field Switching Edge Tracker

As has been pointed out earlier, the field switching edge tracker requires the smallest electronic bandwidth of all the systems considered. This is so because no time is wasted in scanning over regions of planet or space in which there is no useful information to be obtained. The chopper frequency

may be selected pretty much at will and will probably be chosen in the vicinity below roll-off of the detector response. With the exception of the modulation efficiency and possible transmission factor, the various field switching systems would have the same sensitivity, bandwidth being chosen as small as possible within the constraints of system response requirements. In general, the available optical clear aperture will be somewhat more limited than in the case of the conical scan system because of the need for a search mirror motion whose dimensions must be kept within reasonable limits.

In our example of a sensitivity calculation, we will assume an all-reflecting system (using the chopper field switching approach) with a clear aperture of 5 cm^2 and an electrical bandwidth of 1 cps. Other parameters of the system are assumed as follows:

Field of View.....	1° x 5° $\omega = 1.52 \times 10^{-3}$ steradians
Detector Size.....	0.2 mm x 1 mm
Chop Frequency.....	20 cps
Switched Field of View Separation.....	> 6°

Optical Efficiency..... 0.5

Detector Size..... 0.1 x 0.5 mm immersed

Detector Time Constant..... 2 milliseconds

$$\text{Detector NEP} = 6.3 \times 10^{-10} \sqrt{0.05/2} = 10^{-10} \text{ watts/cycle}$$

Degradation Factors:

Noise Figure = 6 db	=	2
Bias Reduction	=	1.4
Rectification Loss	=	1.4
Thermistor Bridge Factor	=	1.4
Total	=	5.6

$$\text{Effective NEP} = 5.6 \times 10^{-10} \text{ watts}$$

For a 90°K lunar temperature, $\Delta N_{20\text{-}40\mu} = 4 \times 10^{-5} \frac{\text{watts}}{\text{cm}^2\text{-}\omega}$

$$P_D = \Delta N \; G \; A_0 \; \omega = 4 \times 10^{-5} \times .5 \times 5 \times 1.52 \times 10^{-3}$$

$$P_D = 1.52 \times 10^{-7}$$

The signal-to-noise ratio will be

$$\frac{S}{N} = \frac{P_D}{NEP} = \frac{1.52 \times 10^{-7}}{5.6 \times 10^{-10}} = 270$$

On the basis of peak-to-peak noise, this becomes 270/5 = 54/ cycle. For a 5 second integration time, noise is reduced

by $\sqrt{\frac{1}{1/2\pi\ 5\ \text{sec}}} \cong 5.5$, and the signal-to-noise ratio becomes 54 x 5.5 = 300.

Since the field of view is 1° vertically and we require a 0.1° accuracy, we must set our threshold level at a point where the system will track at 1/10 the detector subtense at the very edge of the detector. With 1/10 the detector illuminated, we obtain a S/N_{p-p} = 300/10 = 30, which is quite conservative and more than adequate.

3.3.2.6 Electronically Sampled Thermopile Edge Tracker

The all-electronic horizon sensor with its inherent advantage in eliminating all moving parts has been shown to require rather far reaching, time consuming, and costly changes in order to be capable of the accuracy desired for the present program. The FIRM sensor is likewise seen to require more development, resulting in a reliable modulator or, alternatively, a field switching method such as may be effected with a tuning fork vibrating vane.

In this section we will discuss an approach which utilizes certain elements and techniques of both systems which have been worked out and are considered to be reasonably successful. Such a system would use the torquer search and positioning system along with the readout method designed for

the field switching edge tracker and with electronically scanned thermopiles replacing the optically modulated thermistor detector.

By insuring a sufficiently large signal-to-noise ratio in such a system, one could attempt to track the edge of the planet at a position where the planet illuminates only a tiny extremity of the detector which may generate sufficient signal to exceed a threshold level determining the point at which the tracker stabilizes. It will be well to compute and examine the signal-to-noise ratio for a system with the required parameters. Assume the system to have a form such as is shown in Figure 3-28. The optics would consist of a 1-inch diameter collector with a speed of f/1. The thermopile detector would have to have the highest detectivity which we can obtain. Bismuth tellurium thermopiles which we have been evaluated for approximately one year have characteristics as follows:

Type.....	radial thermopile with 20 active and reference junctions
Specific Responsivity $\mathcal{R}'$	0.35 volt/watt/cm^2

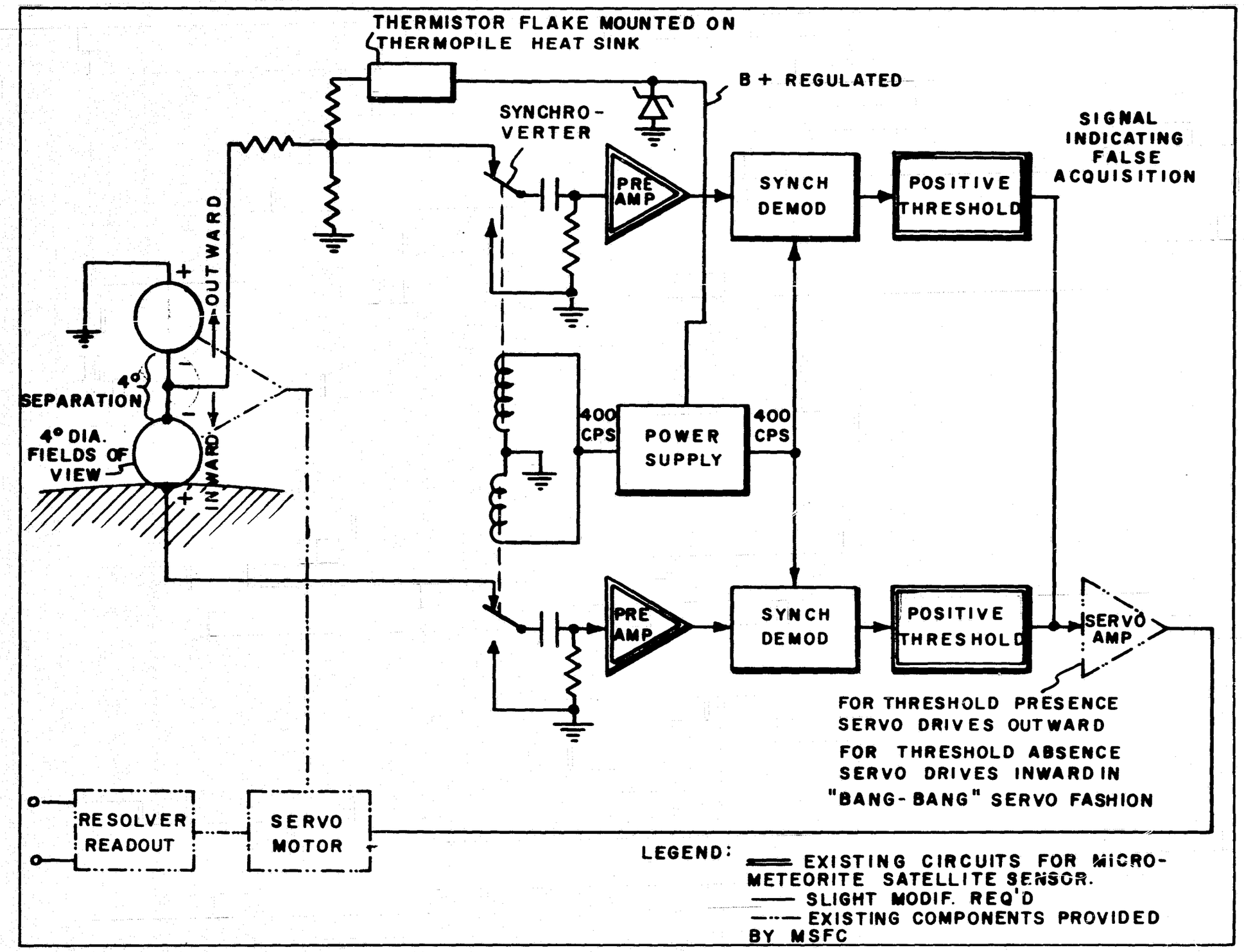

Figure 3-28 THERMOPILE EDGE TRACKING HORIZON SENSOR BLOCK DIAGRAM

Resistance..... ≈ 15,000 ohms

Time Constant..... 150 milliseconds

Size of Active Element.. 2.5 mm diameter

Detectivity..... 4×10^7 (cm-cps$^{1/2}$)/watt

The voltage developed for a detector fully illuminated from a 200°K earth is:

$$V_D = \frac{\pi}{4} \frac{\Delta N_{\lambda 1-\lambda 2} \Re' \epsilon}{f^2} = \frac{\pi}{4} \frac{2.8 \times 10^{-3} \times 0.6 \times 0.35 \times 0.6}{1} = 2.7 \times 10^{-4}$$

$$= 270 \ \mu V$$

Optical efficiency, ϵ, is assumed to be 0.6.

Since we require an accuracy of 0.1° or better and the detector subtends 2° in elevation, we must exceed a threshold level when only 1/20 of the detector is illuminated. This would result in a 13.5 microvolt signal. Peak-to-peak noise and drift will be of the order of 2 microvolts. We are thus left with a remaining S/N of about seven, which is considered satisfactory for operation against earth targets. Indeed, we could do even better by operating in the CO_2 band which would permit use of a radiation balance system in which half the detector may be illuminated rather than only one-tenth, as shown following:

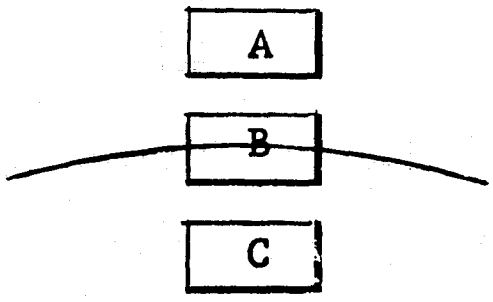

at the correct attitude

$$\frac{A - C}{2} = B - C$$

Next, we wish to examine possible use of this system for lunar use. For a possible 90°K temperature:

$$\Delta N_{\substack{90°K \\ 14\text{-}40\mu}} = 1.25 \times 10^{-4} \times 0.5$$

$$= 6.25 \times 10^{-5} \text{ watts/cm}^2\text{-ster}$$

The radiance in this spectral interval for a 200°K earth was 1.67×10^{-3}. We thus get only 3.7% of the energy we had available in the previous case and the new S/N would be reduced to 0.037 x 2.70 = 10 for a 2° fully illuminated detector. To obtain a 0.1° accuracy, the S/N is 0.5 which is clearly inadequate. The system accuracy for lunar application is at best of the order of 0.2° without allowing any safety margin. Improvements may be considered in several areas, including a faster optical system (f/0.5), detectors with more junctions and thus providing higher responsivity, and a more favorable detector geometry, perhaps with the detector subtending 1° x 10°.

4. REVIEW OF CHARACTERISTICS OF THE HORIZON SENSOR SYSTEMS DISCUSSED IN THIS STUDY REPORT

Table 4-1 summarizes the important performance parameters of some systems which have been discussed in the preceding sections. Some of the figures used are, of necessity, provisional. More exact figures could only be given after design, construction, and evaluation of the system. The table does, however, present an over-all view of the relative merits and potential of the various systems discussed, at least from the standpoint of technical performance factors. To this should be added such factors as development time, budgetary considerations, confidence level in the proposed system, and degree of experience with the technical and components required to translate the design to working hardware.

It is evident from Table 4-1 that we can expect to meet the design goals for accuracy with at least one version of the field switching edge tracker and with two versions of conical scan sensors.

Table 4-1 shows a substantial superiority of the field switching edge tracker in terms of S/N for the long integration time of 5 seconds. This signal-to-noise ratio

TABLE 4-1 Comparison of Characteristics of Various Earth/Lunar Horizon Sensors

	EARTH APPLICATION		LUNAR APPLICATION				PHYSICAL CHARACTERISTICS FOR ONE HEAD			
Type Sensor	S/N_{p-p} for 200°K Earth	Error	S/N_{p-p} for 90°K Moon	Error	Clear Aperture	Spectral Response	Size	Weight	Power	MTBF (hours)
Field Switching Edge Tracker with Thermistor Detector	6600 for total earth 660 at slice level	±0.05° limited by anomalies in radiance	300:1 for full illum. with 90°K moon 30:1 for illum of 1/10 of detector	±<0.1°	5 cm^2 1° x 5° FOV	20-40μ	6"D x 8"L	12 lbs	4 watts each head	42,000
Conical Scan (leading edge type)	750 for total earth signal 10 at slice level	±0.05° limited by anomalies in radiance	33 2:1 S/N at slice level	±0.1°	22 cm^2 1° x 3° FOV	20-40μ	6" dia x 6"L	12 lbs two heads plus mixer box	4 watts each head	42,500
Conical Scan with Slope Recognition (noise pred.)	90	±0.05°	4	±0.1°	22 cm^2 1° x 3° FOV	20-40μ	4-1/2" dia x 5-1/2"L	10 lbs two heads plus mixer box	4 watts each head	42,000
Field Switching Edge Tracker with Thermopile	7:1 for illum. of 1/10 of detector	0.1°	0.5 for illum of 1/10 of detector not satisfactory	0.2°	5 cm^2	20-40μ	500 cu.in.	12 lbs for 4 heads	3 watts 20 watts peak at maximum torque	60,000 est.
2nd Harmonic Type Edge Tracker	estimated 10:1 for 200°K earth	0.05°	not suitable due to craters		est. 3 cm^2	14-16μ for earth	5.5" x 5.6"	13 lbs.	8.5 watts	20,000 est.
All-Electronic Sampled Thermopile System	12:1	±0.5°	0.5	not suitable	13 cm^2	14-50μ	6" dia x 10"L	8 lbs per sector	15-20 watts	

is comfortably above what is necessary even for the lunar application to permit either an increase in response time should that be necessary or a possible reduction in the size of the collecting optics, or even both.

The two versions of conical scan sensors, whose prime characteristics have been tabulated, show an adequate signal-to-noise ratio for earth or lunar missions, though without as much flexibility in the scaling down of dimensions of the optics or increase in scan rate. A possible compensating feature of the conical scan sensor is a greater flexibility in search function, which may not be of great value in the present application. The sensor can be placed in a position to scan almost any angle that may be required and is relatively independent of altitude.

The field switching edge tracker is shown in Figure 3-25 and scans over an angle which is twice the angle displacement of the search mirror (due to angle multiplication of the mirror). The requirement of the present system for a 10° range of error signals plus the altitude variations which add approximately another 10° is easily met by the system as sketched in Figure 3-25

This range can be extended for a greater altitude range, though not quite as readily as with the conical scan sensor. If much greater search range is required, the size of the search mirror and chopper must be increased.

Physical characteristics of these systems, such as power consumption and volume, are likewise not too dissimilar and fall in the range of the design goals. The exact figures for these characteristics can only be established at a later date when the design is well under way.

The reliability of the three systems, following the criteria of reliability handbooks and discussed in more detail in Section 5, is so similar that it would require precise assignment of dissipation and stress levels and component selection before one could reach any conclusion as to which system has a higher Mean Time Before Failure (MTBF). Only through use of an auxiliary system with parallel redundancy can we expect to meet the 0.997 reliability for a 90-day mission which was cited as a design goal. No high accuracy infrared horizon sensor system which has as yet been built or which we can conceive at the present time alters the conclusion that independent parallel

redundancy must be provided to meet the 0.997 reliability figure.

We have attempted to show some of the differences, advantages, and disadvantages of the various horizon sensor systems which may be considered for the present application. The comparison was restricted to certain characteristics which are of concern in the Earth/Lunar Horizon Sensor application. For example, the mission is described as having a rather limited range of altitudes and attitude error. It therefore does not require very wide acquisition range and permits use of a limited range of search angle for the edge tracker and a rather narrow angle cone for the conical scan sensor (e.g., 37°). The optical design of the field switching edge tracker is eased by these considerations. Similarly, the response requirements are understood to be for a 5 second integration time which permits slow scan speeds in the case of the conical scan sensors and a narrow bandwidth for the edge tracker.

We have not emphasized such factors as the possibility of the sun appearing in the field of view of one of the sensors, possible physical location on the spacecraft of the sensor, and

the many other interface questions. We also did not go into details of the readout method and particular characteristics of the desired output signal.

Except for the possibility of the sun appearing at the very edge of the earth and grazing the detector field of view (for which no system provides adequate means for insuring absence of any sun error), means are at hand for deactivating or voiding data which is useless due to the effect of the sun. This applies to any of the systems to which we have given serious consideration. In the case of the conical scan sensors, a sweep across the field of the sun results in a blanked or voided output when the high amplitude narrow pulse produced by the sun is perceived by protection circuits which have been designed.

For the field switching edge tracker, a double flake detector is recommended for each optical system which provides both a means for avoiding the sun problem and a redundant output. Furthermore, for a system with four heads, only three will be required for attitude readout and the fourth one may be switched out. This was discussed in more detail in Section 3.3.2.4.

We have not questioned the use of thermistor detectors as the best choice for infrared horizon sensor systems--adequate justification for such a selection having been given in much of the literature on the subject.

Insofar as the motor is concerned, whether for the conical scan sensor or the field switching edge tracker, we feel that the low speeds contemplated will avoid the problems of excessive friction and wear. It will be necessary, however, to provide a lubricant reservoir such as was used in connection with the TIROS radiometers. It will be recalled that these motors functioned well over a period of more than a year in space with greater speeds and loads than are contemplated for this application.

Our experience in a number of these problem areas is well known, so that we can assign certain values to a confidence factor. It is known, for example, that over 150 Barnes conical scan horizon sensors have been flown in various space missions. The reliability record in these flights has been shown to be quite good.[15] The TIROS 5-channel radiometer,

---

[15]Lt. Col. William T. Jones and Kenneth A. Ward. "Performance of Horizon Sensor Systems in Earth Orbit," presented at the Symposium on Infrared Sensors for Spacecraft Guidance and Control, Barnes Engineering Company, May 1965.

with its motor designed for long life in space, and the Venus radiometer with its field switching system (comparing radiation from two separated regions of space and planet) likewise have had an excellent reliability record, though on a smaller scale in terms of number of units built. This latter experience with space motors indicates that it is possible to use certain special motors in a space environment without the requirement for vacuum sealing the sensor housing. This, in turn, eases the sensor mechanical and optical design and makes it unnecessary to provide a thick window with its inherent sealing problems.

5. RELIABILITY

5.1 General Reliability Considerations

Of all the specified design goals for the earth/lunar horizon sensor, the reliability figure sought is the most difficult to obtain. As has already been seen in the foregoing discussions the performance figures can be achieved in several sensor configurations. If we examine the reliability figures for all existing sensors we find them to fall very far short of the desired figure of a reliability of .997 for a 90 day mission. We wish to state at the outset that such a figure is not considered within the realm of the present state of the art without complete redundancy as applied to a sensor in which the most stringent care has been taken in all phases of a design which emphasizes utmost simplicity. Preliminary figures for a single system and one with parallel redundancy will be discussed in the paragraphs which follow.

Since the reliability or probability of successful mission completion $R_{(t)}$ is to be .997 and $R_{(t)} = e^{-\lambda t}$ where T = mission time and λ = Failure rate. The Mean Time Before Failure (MTBF) being the reciprocal of λ is to be approximately

700,000 hours, obviously a most difficult requirement. By way of example we can compare the MTBF for some of the existing sensors. The Status Report on Horizon Sensing[16] is helpful in this area and cites figures wherever they are available. The highest figure it quotes for any horizon sensor, other than static radiation balance types, is 25,000 hours which is an estimated and not computed figure. The Barnes Type 13-142A conical scan horizon sensor is shown in this report to have an MTBF of 20,000 hours. Recent improvements made on a standard type horizon sensor to be used for the BIOS satellite vehicle has essentially doubled this value. Such efforts still fall far short of the MTBF by a factor of about 50 which is desired for the present program. Disregarding any mechanical components, it would be difficult to meet this design goal even with a simple two-transistor preamplifier without some redundancy. Yet considerably more circuitry will obviously be required and active electronic components are unavoidable.

---

[16] Duncan, Wolfe, Oppel, and Burn, op. cit.

5.2 Mechanical Components

A primary consideration in the case of horizon sensors is the question of what elements of the system represent the greatest reliability risks. Insofar as mechanical components are concerned it can be shown that flexing members have certain advantages since they avoid frictional forces and attendant wear but that the latter can be reduced significantly by operation at low speeds.

A motor operating at high speed may generate considerable friction which, in time, will be a source of failure. By reducing the speed of rotation we reduce the frictional forces and rapidly improve the reliability which improves logarithmically with speed reduction. This is seen in Figure 5-1 which is a reliability plot taken from RADC-TR-58-111 Reliability Notebook, Dec. 1961, MIL-HDBK-217.

For low rotational speeds we see that the failure rate due to friction becomes negligible and, in the limit, the motor reliability becomes equivalent to that of a transformer.

In our case, if we consider the prospects for a conical scan sensor, a low rotational speed (e.g. 180 RPM as would be

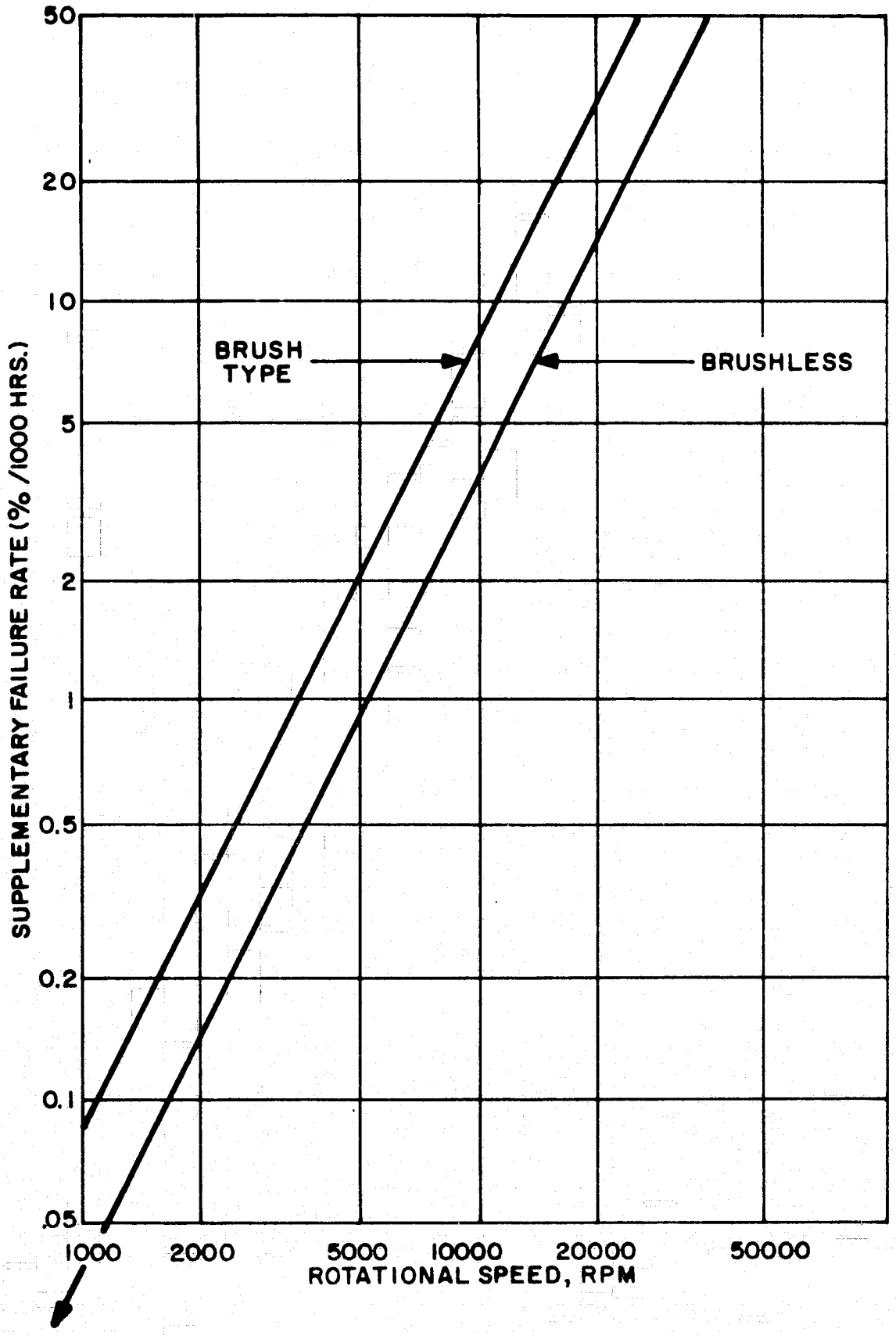

21760

Figure 5-1 SUPPLEMENTARY FAILURE RATES FOR MOTOR SPEEDS (FROM RADC HDBK 217)

desirable for other reasons in this application) would result in a reliability figure for the motor which is essentially the same as that of a torquer in an edge tracking sensor or a vibrating reed driver, etc. In such a design one would naturally keep the number and diameter of bearings small.

An additional problem would be that of providing the necessary lubrication for the moving parts. In the above reliability figures it is assumed that proper lubrication is available. For a very long mission, provision of adequate lubrication would be a serious problem. For a mission lasting 90 days the techniques presently available are considered to be quite adequate. Space motors in which a wick stores lubricant for an extended period of time have resulted in successful long life space missions. As an example the various TIROS satellites carrying five channel infrared radiometers have operated, at times for a year and one half with loads greater than contemplated for the present horizon sensor. The motor in the TIROS radiometers is geared to and drives five separate choppers each with its independent bearing. Motor speed for this radiometer is 2500 RPM. Therefore, for a relatively short mission

such as 90 days, the motor bearing lubrication problem should not be difficult to handle in the present application both operating life and motor speed being lower than in the case of TIROS application.

In the terms discussed above there appears to be no material difference in the reliability figures for the presently considered field switching edge tracker and the slow speed conical scan sensor.

5.3 Reliability of Electronics

We can consider, next, the reliability figures for the electronics which would be required for the various sensors considered. The figures compared are of course only provisional. They are necessarily based on very preliminary circuits and their assumed component requirements. In the next phase of this study, after more careful review of specific circuits, it will be possible to present more exact figures. The tentative figures given below are again based on Rome Air Development Center data.* The figures are based on the straightforward circuitry with an analog output. If

---

* RADC-TR-58-111 Reliability Notebook, Dec. 1961, MIL-HDBK-217

it is required to add digital outputs, additional circuitry would be required which would somewhat degrade the reliability figures. The reliability figures are based on circuitry as shown in the block diagrams, Figures 3-2b, 3-23a, 3-26. See tables on the following pages for the reliability figures.

5.4 Redundancy

Redundancy has been treated in a number of texts discussing reliability problems. The mathematical treatment will not be repeated here. It should suffice to take the results from a standard text.[17]

It is shown that for a parallel and independent redundant system in which two systems have the same reliability

$R_1(t) = R_2(t)$

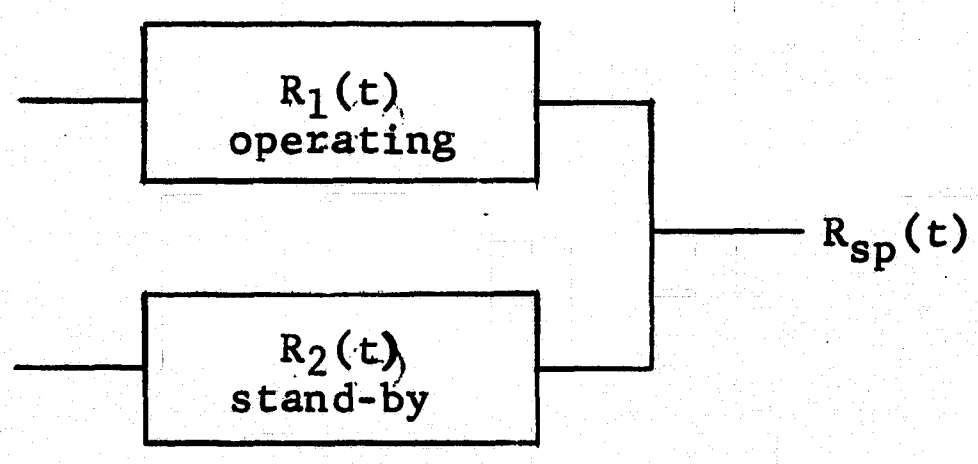

$$R_{sp}(t) = 2R_{(t)} - R^2_{(t)} = R_{(t)}\left[2 - R_{(t)}\right] = e^{-\lambda T}\,(2 - e^{-\lambda T})$$

---

[17] Bazovsky, Igor Reliability Theory and Practice, Prentice Hall, 1962

Then if one uses the exponential expansion:

$$e^{-\lambda T} = 1 - \lambda T + \frac{\lambda^2 T^2}{2!} - \frac{\lambda^3 T^3}{3!}$$

One can see that for values of $\lambda T < .1$, which is the case with our system, the series converges rapidly and can be simplified to an approximate form of $R_{(t)} \simeq 1 - \lambda T$

$$R_{sp(t)} \simeq 1 - \lambda^2 T^2$$

or, in the original equation $R_{(t)} = e^{-\lambda T}$, we may replace the failure rate λ by a new value of $\lambda_p(t) \approx \lambda^2 T$ for the completely and independently redundant system.

We may now examine the new reliability obtained through such redundancy. Assuming that we have picked a system and obtained a final design leading to an MTBF = 40,000 hours, we then have λ = 1/40,000 = 25 failures per million hours.

For a 90-day mission, we require about 2000 hours of operation.

The probability of failure for the redundant system with a 2000-hour operating time, $\lambda_p(t)T$, then becomes:

$$\lambda^2 T^2 = (2.5 \times 10^{-5})^2 \times 2000^2$$

$$= 2.5 \times 10^{-3}$$

This is equivalent to a reliability of 0.9975 which is slightly better than the required value. Additional components will be required for the decision circuitry to switch over from a possible inoperative system to the auxiliary unit. Alternatively, the decision to switch over from one system to another may be performed by an astronaut or even through ground command.

Since the method of instrumenting the desired reliability goes beyond the scope of the Phase IA study, we will defer further discussion and design of such redundancy to a later time.

CONICAL SCAN SYSTEM (LEADING EDGE TYPE)
RELIABILITY ESTIMATE
(see Figure 3-2b for block diagram)

Components	Failure Rate (x 10^{-6} f/hr)	Q x Fr (x 10^{-6} f/hr)	
Bias Supply			
2 transistors	0.25	0.50	
8 resistors	0.01	0.08	
6 capacitors	0.20	1.20	
2 zener diodes	0.15	0.30	
		2.08	= 2.08
Preamplifiers (2)			
6 transistors each	0.25	1.50	
12 resistors "	0.01	0.12	
3 capacitors "	0.20	0.60	
1 diode "	0.15	0.15	
		2.37 x 2	= 4.74
Schmitt Triggers (4)			
2 transistors each	0.25	0.50	
5 resistors "	0.01	0.05	
		0.55 x 4	= 2.20
Monostable Multivibrators (2)			
2 transistors each	0.25	0.50	
6 resistors "	0.01	0.06	
2 capacitors "	0.20	0.40	
		0.96 x 2	= 1.92
Gates (2)			
4 diodes each	0.15	0.60	
4 resistors each	0.01	0.04	
		0.64 x 2	= 1.28

Components	Failure Rate (x 10^{-6} f/hr)	Q x Fr (x 10^{-6} f/hr)	
Flip-Flops (2)			
2 transistors each	0.25	0.50	
7 resistors "	0.01	0.07	
2 capacitors "	0.20	0.40	
2 diodes "	0.15	0.30	
		1.27 x 2	= 2.54
± Reference and Integrator			
4 resistors	0.01	0.04	
1 capacitor	0.20	0.20	
2 zener diodes	0.15	0.30	
		0.54	= 0.54
Output Sampler			
1 transistor	0.25	0.25	
1 transformer	0.25	0.25	
3 resistors	0.01	0.03	
1 capacitor	0.20	0.20	
		0.73	= 0.73
Motor	3.00	3.00	= 3.00
Thermistor Bolometers (2)	0.375	0.75	= 0.75
Sun Correction Circuit			
4 transistors	0.25	1.00	
2 capacitors	0.20	0.40	
1 diode	0.15	0.15	
10 resistors	0.01	0.10	
		1.65	= 1.65

Components	Failure Rate ($\times 10^{-6}$ f/hr)	Q x Fr ($\times 10^{-6}$ f/hr)	
Power Supply			
2 transistors	0.25	0.50	
2 zener diodes	0.15	0.30	
2 capacitors	0.20	0.40	
4 rectifiers	0.15	0.60	
1 transformer	0.25	0.25	
6 resistors	0.01	0.06	
		2.11	= 2.11

Total Failure Rate/10^6 hours: 23.54

Mean Time Before Failure: 42,500 hours

PREDICTOR-DELAY SYSTEM RELIABILITY ESTIMATE

(see Fig. 3-23a for block diagram)

Components	Failure Rate ($\times 10^{-6}$ f/hr)	Q x Fr ($\times 10^{-6}$ f/hr)	
Bias Supply			
2 transistors	0.25	0.50	
8 resistors	0.01	0.08	
2 capacitors	0.20	0.40	
2 zener diodes	0.15	0.30	
		1.28	= 1.28
Preamplifier (1)			
6 transistors	0.25	1.50	
12 resistors	0.01	0.12	
3 capacitors	0.20	0.60	
1 diode	0.15	0.15	
		2.37	= 2.37
Predictor-Delay			
5 inductors	0.25	1.25	
5 capacitors	0.20	1.00	
12 resistors	0.01	0.12	
		2.37	= 2.37
Differential Post-Amplifier			
4 transistors	0.25	1.00	
10 resistors	0.01	0.10	
		1.10	= 1.10
D.C. Reference			
2 zener diodes	0.15	0.30	
2 resistors	0.01	0.02	
		0.32	= 0.32

Components	Failure Rate ($\times 10^{-6}$ f/hr)	Q x Fr ($\times 10^{-6}$ f/hr)	
Gates (3)			
4 diodes each	0.15	0.60	
6 resistors each	0.01	0.06	
		0.66 x 3	= 1.98
Integrators (2)			
1 capacitor each	0.20	0.20	
1 resistor "	0.01	0.01	
		0.21 x 2	= 0.42
Difference Amplifier			
4 transistors	0.25	1.00	
10 resistors	0.01	0.01	
		1.10	= 1.10
Monostable Multivibrators (2)			
2 transistors each	0.25	0.50	
6 resistors "	0.01	0.06	
2 capacitors "	0.20	0.40	
		0.96 x 2	= 1.92
Bistable Gate			
2 transistors	0.25	0.50	
13 resistors	0.01	0.13	
4 diodes	0.15	0.60	
2 capacitors	0.20	0.40	
		1.63	= 1.63
Read-Out Capacitor	0.25	0.25	= 0.25

Components	Failure Rate ($\times 10^{-6}$ f/hr)	Q x Fr ($\times 10^{-6}$ f/hr)	
Reference Pulse Generator			
1 lamp	0.70	0.70	
1 photo diode	0.25	0.25	
2 transistors	0.25	0.50	
8 resistors	0.01	0.08	
2 capacitors	0.20	0.40	
		1.93	= 1.93
Motor	3.00	3.00	= 3.00
Thermistor Bolometer (1)	0.375	0.375	= 0.375
Sun Correction Circuit			
4 transistors	0.25	1.00	
2 capacitors	0.20	0.40	
1 diode	0.15	0.15	
10 resistors	0.01	0.10	
		1.65	= 1.65
Power Supply			
2 transistors	0.25	0.50	
2 zener diodes	0.15	0.30	
2 capacitors	0.20	0.40	
4 rectifiers	0.15	0.60	
1 transformer	0.25	0.25	
6 resistors	0.01	0.06	
		2.11	= 2.11

Total Failure Rate/10^6 hours: 23.805

Mean Time Before Failure: 42,000 hours

SWITCHING MIRROR ELECTRONICS
RELIABILITY ESTIMATE
(see block diagram, Figure 3-26)

Components	Failure Rate (x 10^{-6} f/hr)	Q x Fr (x 10^{-6} f/hr)	
Bias Supply			
2 transistors	0.25	0.50	
8 resistors	0.01	0.08	
2 capacitors	0.20	0.40	
2 zener diodes	0.15	0.30	
		1.28	= 1.28
Preamplifiers (2)			
5 transistors each	0.25	1.25	
10 resistors "	0.01	0.10	
3 capacitors "	0.20	0.60	
1 diode	0.15	0.15	
		2.10 x 2	= 4.20
Operational Amplifier			
4 transistors	0.25	1.00	
2 capacitors	0.20	0.40	
10 resistors	0.01	0.10	
		1.50	= 1.50
Synchronous Demodulators (2)			
1 transistor each	0.25	0.25	
1 capacitor "	0.20	0.20	
3 resistors "	0.01	0.03	
		0.48 x 2	= 0.96

Components	Failure Rate ($\times 10^{-6}$ f/hr)	Q x Fr ($\times 10^{-6}$ f/hr)	
Schmitt Trigger			
2 transistors	0.25	0.50	
5 resistors	0.01	0.05	
		0.55	= 0.55
D.C. Amplifier			
4 transistors	0.25	1.00	
10 resistors	0.01	0.10	
		1.10	= 1.10
Gates (2)			
4 diodes each	0.15	0.60	
4 resistors each	0.01	0.04	
		0.64 x 2	= 1.28
Power Switches (2)			
1 transistor	0.25	0.25	
1 transformer	0.25	0.25	
2 resistors	0.01	0.02	
		0.52 x 2	= 1.04
Variable Pulse Width Monostable Multivibrator			
3 transistors	0.25	0.75	
2 capacitors	0.20	0.40	
1 diode	0.15	0.15	
10 resistors	0.01	0.10	
		1.40	= 1.40

Components	Failure Rate ($\times 10^{-6}$ f/hr)	Q x Fr ($\times 10^{-6}$ f/hr)	
Tachometer Chopper			
1 transistor	0.25	0.25	
2 capacitors	0.20	0.40	
5 resistors	0.01	0.05	
		0.70	= 0.70
Rectifier and Filter			
1 transformer	0.25	0.25	
2 diodes	0.15	0.30	
3 resistors	0.01	0.03	
2 capacitors	0.20	0.40	
		0.98	= 0.98
Mirror Drive Oscillator			
4 transistors	0.25	1.00	
1 transformer	0.25	0.25	
2 capacitors	0.20	0.40	
6 resistors	0.01	0.06	
		1.71	= 1.71
Torque Motor (assume use of motor as a tachometer readout through time sharing)	3.00	3.00	= 3.00
Thermistor Bolometer (3 flakes)	0.50	0.50	= 0.50
Read-Out Potentiometer	0.25	0.25	= 0.25
Sun Correction Circuit			
4 transistors	0.25	1.00	
2 capacitors	0.20	0.40	
1 diode	0.15	0.15	
10 resistors	0.01	0.10	
		1.65	= 1.65

Components	Failure Rate ($\times 10^{-6}$ f/hr)	Q x Fr ($\times 10^{-6}$ f/hr)	
Power Supply			
2 transistors	0.25	0.50	
2 zener diodes	0.15	0.30	
2 capacitors	0.20	0.40	
4 rectifiers	0.15	0.25	
1 transformer	0.25	0.25	
6 resistors	0.01	0.06	
		2.11	= 2.11

Total Failure Rate/10^6 hours: $\cong$ 24

Mean Time Before Failure: 42,000 hours

6. CONCLUSIONS AND RECOMMENDATIONS

The foregoing analyses and discussion have convinced us that the system best suited for the Earth/Lunar Horizon Sensor and which most readily meets the desired performance characteristics for this program is the edge tracker with field switching, as outlined in Section 3.3.2.4. We therefore recommend that Phase 1B of this program concentrate on the detail design of a horizon sensor based on this principle and that this design be carried on to the hardware stage and an engineering model of it be built in Phase II of this program.

This conclusion is based on a number of features and factors, the details of which have been discussed in earlier sections of this report:

(1) The signal-to-noise ratio is superior to that of any other system considered (with the exception of several variations in the mechanization of the same horizon sensing principle).

(2) The comfortable signal-to-noise ratio provides some flexibility in decreasing size and weight of the optics, speed-up of response times, and other parameters.

(3) Readout of the attitude error is simple and can be provided with equal ease either as a digital or analog output signal.

(4) The reliability figures for a single sensor are shown to be of the same order as those of certain conical scan sensors which could meet the sensitivity and accuracy goals. The reliability goals can only be met through redundancy.

(5) We suggest a dual detector configuration (as described in Section 3.3.2.4) with separate processing to both provide a means of avoiding errors due to the sun appearing in the field of one detector and also to improve the reliability.

(6) We also recommend edge tracking at four points, only three of which are needed to establish pitch and roll errors. The fourth edge tracking point provides redundant data and increased reliability.

(7) If it is possible to mount the sensor in a position to view fields separated by nearly 180°, then a single optical head may be used for tracking two edges of the planet and possibly four. This would represent a substantial saving in power, volume, and weight.

These conclusions and recommendations are based on the analyses and study which have been conducted for the past 2 months of this program and which are summarized in the data presented in earlier sections of this study report.

In Section 2 of this report we pointed out that the 20-40 micron spectral interval appears to be both a satisfactory and desirable range to use for both earth and lunar operation of the horizon sensor being considered. It will therefore be unnecessary to modify the optics or detector package when changing from an earth to a lunar mission. The only change which is foreseen is a new signal threshold setting for the two conditions. This may be accomplished by a simple switch which changes a resistance and effects a scale factor change.

In Section 3 we have discussed a large variety of horizon sensor concepts and systems, including the one we have recommended. Details of the optical and electronic system are presented along with a calculation of the energy expected for the earth and lunar missions and the resulting signal-to-noise ratios and accuracies.

Section 4 summarizes the important features of the various systems and points out the principal differences and

their significance for the intended application. Table 4-1 shows the important features of some of the systems which have been discussed.

Section 5 is concerned with the reliability of the various systems which, we feel, could meet the design goal of accuracy and sensitivity for this program.

We have also shown that two modified versions of a conical scan sensor are capable of meeting the basic requirements of accuracy and sensitivity for both earth and lunar missions and, with the same redundancy recommended for the edge tracker, can also be shown to attain the desired reliability figure. However, we feel that the sensitivity of these systems is inferior to that of the edge tracker and that the latter has more flexibility and growth potential. We also feel confident that we can execute the remaining phases of this program within the timetable which was set up in our proposal and which is part of the work statement of our contract.

One further recommendation which we make is that a meeting be held between the cognizant NASA, MSC authorities and Barnes Engineering Company technical personnel to discuss

the results of our study, obtain unanimity on the course chosen for the balance of the program, and resolve any interface problems concerning the sensors, spacecraft, and its mission in advance of commencement of the design and construction phases of this program.

A P P E N D I X A

Experimental Low Level Commutator for use with Electronic Scan Horizon Sensor

Experimental Low Level Commutator for use with Electronic Scan Horizon Sensor

A single-pole, five-throw MOS FET switch was constructed with the necessary associated electronics to demonstrate the feasibility of a solid-state, microvolt-level commutator. Incorporated therein were the necessary techniques to eliminate the dual problems relating to spurious thermal potentials and to amplifier saturation from commutation transition spikes.

The commutator was tested at -50°C, +25°C, and +90°C ambient temperatures. Spurious potentials generated within the commutator were less than ±1 microvolt over the test range of ambient temperature conditions. By refining the techniques utilized, these spurious potentials can be further reduced.

The basic commutator utilized five FET's. They were mounted on an isothermal test fixture designed to minimize temperature differences between each transistor and its associated leads. The five transistors were interconnected to function as a five-input, single-output commutator switch. Low-level d.c. input signals were provided thereto by five

associated logarithmic potentiometers and five subsequent 1000:1 attenuator networks. The output impedance of each attenuator network was 1000 ohms, which simulated the output impedances of the thermopile detectors that are eventually to be commutated.

A five-stage ring counter was used to sequentially provide -20 volt pulses to the gates of the FET commutator transistors. These pulses caused the transistors to be sequentially gated on, permitting their associated inputs to be sampled one at a time.

The transition spikes at the commutator output (caused by the capacitive coupling of leading and trailing edges of the gating drives through the FET gate to source and drain capacitances) were reduced in amplitude by means of a 0.0047 microfarad bypass capacitor. The resultant spikes were sufficiently small in amplitude so saturation did not occur in the subsequent low-level (approximately 1 microvolt input noise) 2800 gain signal amplifier. The amplifier's bandwidth (high and low frequency cut-offs of 3 and 3000 cps, respectively) was adequately wide to permit commutator

sampling times of 2 milliseconds duration to be accommodated without causing excessive "overshoots," signal "droops," or "stretching" of the transient commutator spike into the sampling period.

The sampling time of 2 milliseconds was obtained from an external "clock" square wave oscillator. This drove a 500 microsecond monostable multi-vibrator, and the leading edge of the resultant pulses therefrom were used to trigger the five-count ring counter.

The 500 microsecond pulse was also applied to a high level transistor switch which was connected, in series, between the signal amplifier's output and a subsequent low pass final output filter which set the system's upper frequency response limit to 800 cps. The pulse from the monostable multi-vibrator "opened" the series output switch simultaneously with the arrival of the input commutator transient "spike" and held it open for a period of 500 microseconds. This effectively prevented the amplified spurious gating pulse (which, referred to the input, decayed to under a microvolt in less than 150 microseconds) from being fed into the 800 cps low pass

output filter. The output switch was permitted to close for the 1.5 millisecond remainder of each 2 millisecond sample period, allowing the output filter to be driven to the amplified level of the input signal being sampled.

The system block diagram is shown in Figure A-1. Figure A-2 shows oscilloscope photographs of gating drive signals, transient "spike" waveshapes, and commutated signals taken at indicated points on the block diagram.

In the tests described, the 2 millisecond sampling time should not be regarded as a limit to the sampling rate which may be used. This rate was selected for convenience in the tests which we conducted. It may be readily changed to a 10 kc rate for the present application. However, it is still felt that switching at a megacycle rate, such as would be required if each detector element were sampled once every frame, is not presently feasible with the MOS FET switch. Instead, we recommend using this switching system to sample each element of one line at the frame rate and combining the line outputs at the final outputs to obtain the desired video signal. This technique is described in more detail in the body of the proposal.

An example of our successful use of low-level switching using the proposed "gating-off" technique with field effect devices is illustrated in the oscillographs of Figure A-2. A signal only 1/1000 the amplitude of the transient pulse is shown first in relation to the transient pulse and then with the transient pulse gated off. The difference is quite dramatic.

Scale factors are listed in the lower right hand corner of the figure.

Photograph A presents the voltage and time scales. Trace 1 is the preamplifier output pulse which is brought about by gating "off" FET_1 and, 30 microseconds later, gating "on" FET_2. Trace 5 is the "off" gating pulse on FET_1. Trace 6 is the "on" gating pulse on FET_2. The voltage transient in Trace 1 is about 3 millivolts referred to the input of the wide band preamp. It would be quite hopeless to try to read a few-microvolt signal through this transient without the aid of the gating technique described.

Photograph B shows that there is randomness as to the exact form, duration, and amplitude of the transient pulses

encountered. Trace 1 is the preamplifier output with a different time base. Note that the second pulse has a different appearance due to a different gate/source, gate/drain capacitance of the second FET. Trace 2 is the output of a post-amplifier with a gain of 6 and a phase inversion. The constant departure from the zero line, dwarfed by the large switching transient, represents a 150-microvolt signal which, by thermal imaging standards, is in itself quite large.

Photograph C, Trace 2 is the post-amplifier output with a 150-microvolt signal in one FET channel. Trace 7 shows synchronous pulses generated by a one-shot multi-vibrator which will be used for blanking the leading and trailing edge transients. The pulse duration is sufficiently long to outlast the longest transient pulses expected.

Photograph D, Trace 2 is preamplifier output showing a 20 microvolt signal with wide band noise. The transient pulse extends well beyond the upper and lower edges of the photograph. Trace 3 shows a 20 microvolt signal as seen at the output of the transient blanking circuit. The transient pulse, having been gated off, has disappeared.

Photograph E, Trace 3 is the same as above--20 microvolt signal with wide band noise after blanking. Again, the transient pulse, having been gated off, has disappeared. Trace 4 shows a 20 microvolt signal after an 800 cps low-pass filter network.

Note that we can easily distinguish one-microvolt levels with no disturbance from the switching transient which has a peak-to-peak amplitude of about ±2 millivolts referred to the input. This performance has been established over a range of ambient temperatures from -50°C to +90°C.

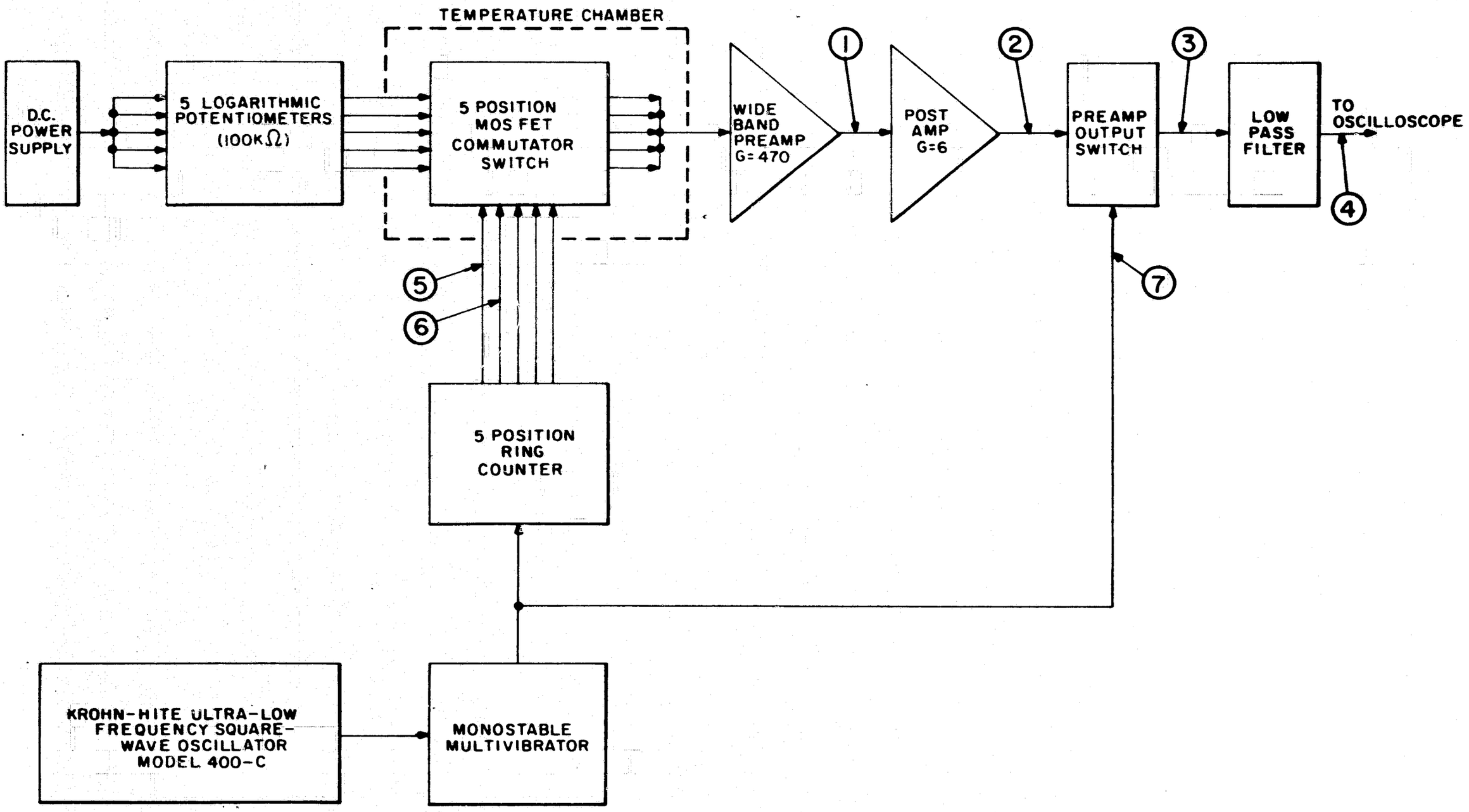

21628

Figure A-1 SYSTEM TO EVALUATE MOS FET TRANSISTORS, BLOCK DIAGRAM

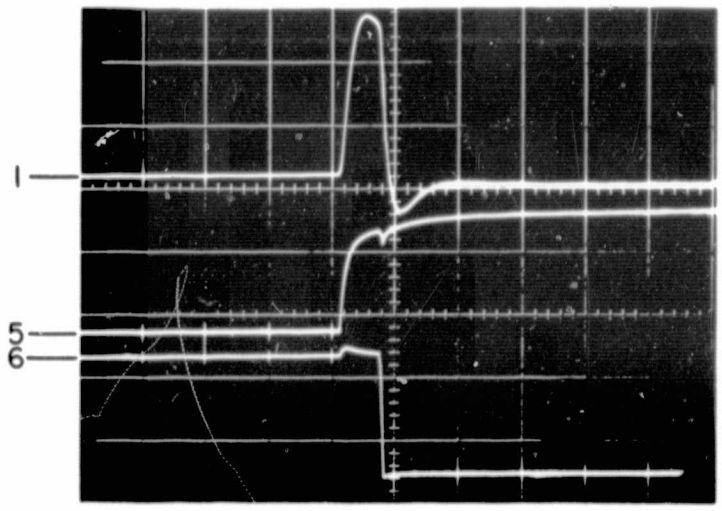

A

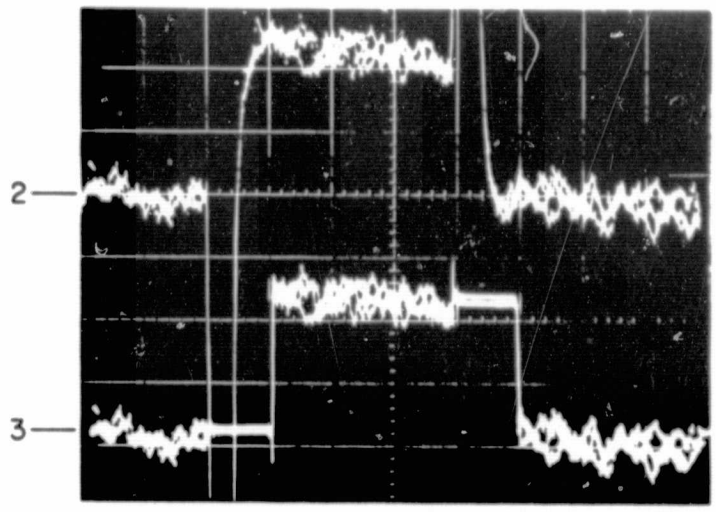

D

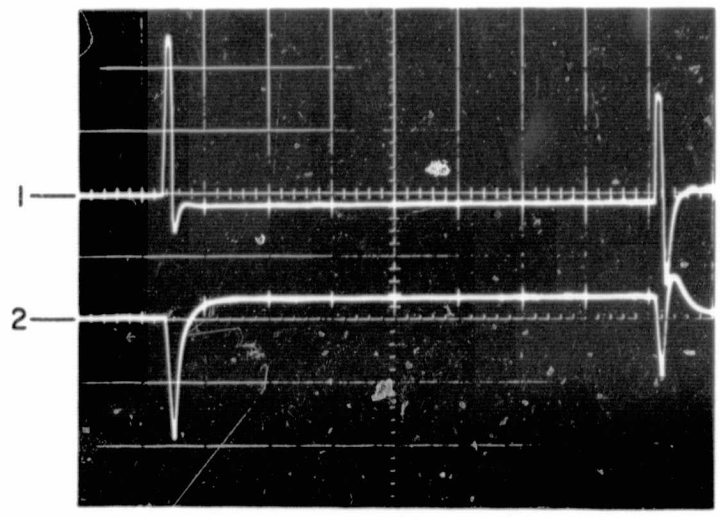

B

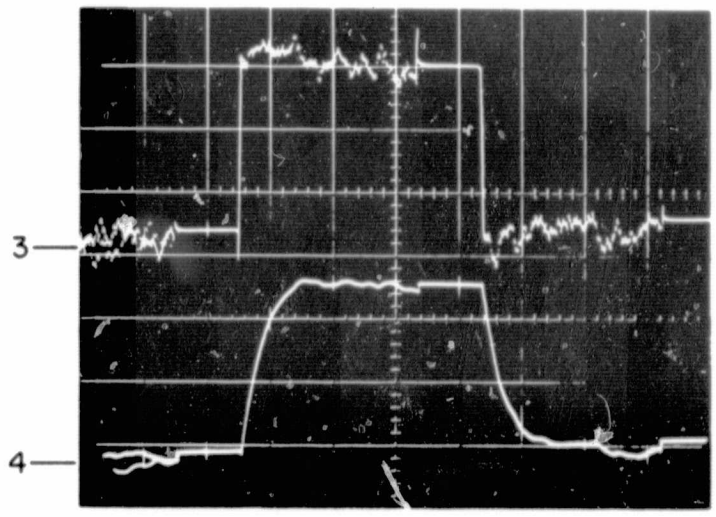

E

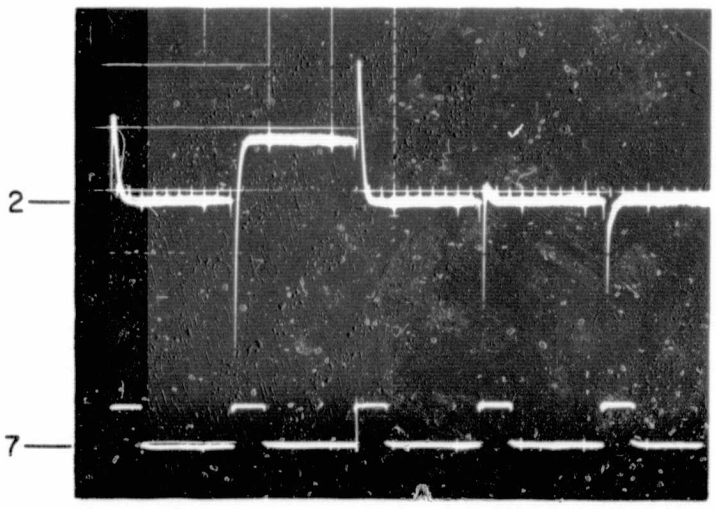

C

	REFERENCE (TO BLOCK DIA)	VERTICAL SCALE FACTOR	TIME BASE
A	1	0.5V / DIV.	50μ SEC / DIV.
	5	10V / DIV	50μ SEC / DIV
	6	10V / DIV	50μ SEC / DIV
B	1	0.5V / DIV	250μ SEC / DIV
	2	2.0V / DIV	250μ SEC / DIV
C	2	0.5V / DIV	1 MS / DIV
	7	20V / DIV	1 MS / DIV
D	2	10 MV / DIV	500μ SEC / DIV
	3	10 MV / DIV	500μ SEC / DIV
E	3	10 MV / DIV	500μ SEC / DIV
	4	10 MV / DIV	500μ SEC / DIV

21629

Figure A-2 WAVESHAPES AT VARIOUS POINTS INDICATED IN SYSTEM BLOCK DIAGRM

A P P E N D I X B

Description of Difficulties with the Present Piezoelectrically Actuated FIRM Component

Description of Difficulties with the Present Piezoelectrically Actuated FIRM Component

We discussed certain difficulties with the FIRM piezoelectric modulator in Section 3.1.3 while explaining the nature of the problems which we observed and possible solutions to them.

In this section we wish to outline the nature of these problems and the steps being taken to correct them.

Two sources of difficulty were uncovered: a reduction in modulation efficiency, and a group of auxiliary fields spaced at discrete intervals from the primary field.

(a) The gap problem identified with creep in the Barium Titanate transducer which resulted in a change in the gap between the FIRM optical elements. A change of about .5 microns in the open gap direction was observed over a period of about one month.

(b) Multiple fields in the FIRM cell. As is indicated in Figure 1, due to the double pass through the gap of the optical rays, multiple fields can exist in the FIRM, each field being of lower intensity. These multiple fields become a problem

only for the case where full chopping efficiency of the FIRM is not reached. However, it should be mentioned that, if all of the rays from the multiple fields do not get out of the FIRM cell aperture but are trapped within the cell, then the possibility of an ambient chop exists which would produce an erroneous signal when the FIRM horizon sensor was scanning cold space. As many as five separate fields of view have been detected in one of the FIRM cells—each field being less intense by approximately a factor of two. Further quantitative measurements of these auxiliary fields are being conducted. The effect of these auxiliary fields on system performance would be to make the system more susceptible to sun interference, since more than two fields are scanned in space. This multiple field problem can, of course, be cured if the FIRM can be made to modulate between total transmission and total extinction. Therefore, the elimination of this problem is tied in with the solution to obtain an adequate drive force to assure greater modulation efficiency.

Solutions are being investigated for both of the problems discussed above. The gap change is believed to be associated with dimensional changes in the Barium Titanate. A different drive mechanism using magnetic actuation is presently under consideration.

By making the FIRM cell with two butting prisms of identical geometry, we can avoid the multiple field problem. One configuration is shown below in which we have insured complete symmetry with no more than one reflection for each ray at the gap interface. In this design the FIRM cell is in a convergent beam and will employ smaller optical elements than would be needed at the aperture.

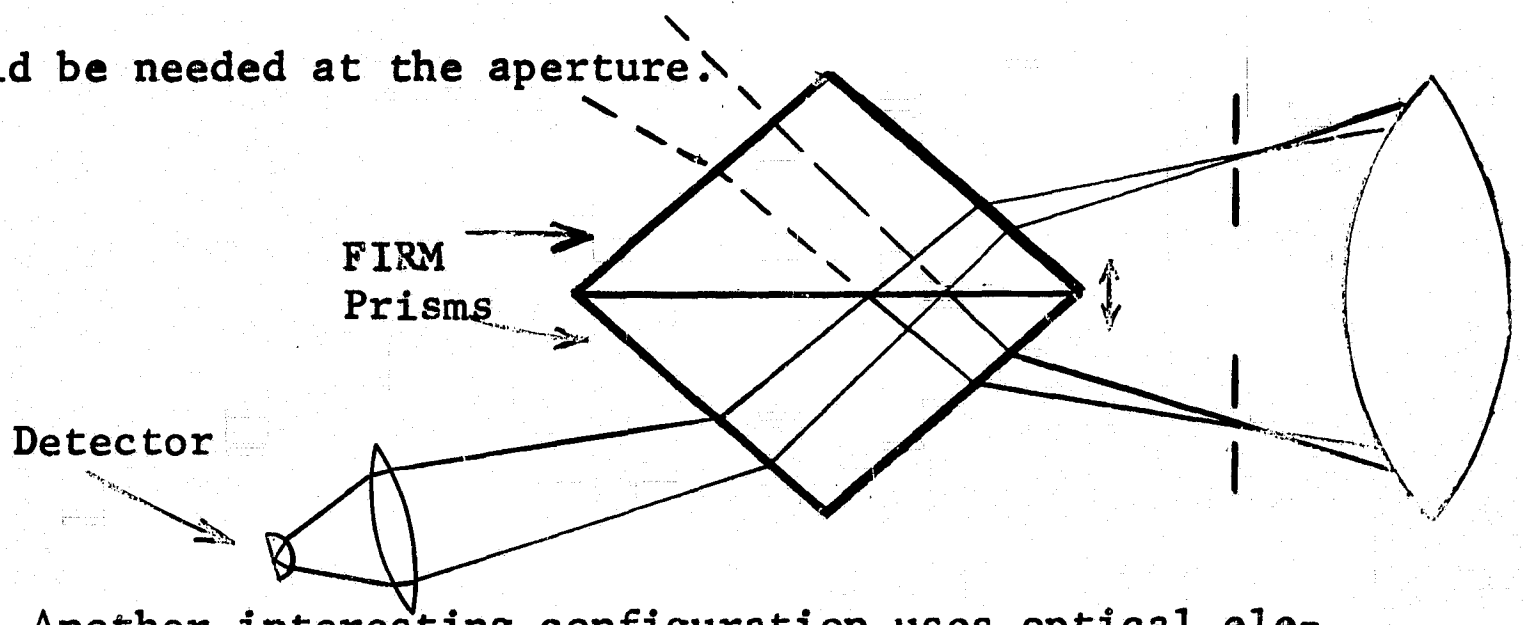

Another interesting configuration uses optical elements with convex surfaces to converge the incoming radiation to a focal point at the gap. It, therefore, requires contact

and modulation only in a small region of the optical elements thus easing the problem of obtaining a high modulation efficiency with negligibly small drive power.

If work presently being performed on these systems on the Company's R & D program yields satisfactory results in the next month or two, it may still be possible to incorporate a newly designed modulator into Earth/Lunar Horizon Sensor systems.

A P P E N D I X C

Explanation of Logic Circuit Operation for Sensor using Noise Prediction Processing

Explanation of Logic Circuit Operation for Sensor using Noise Prediction Processing

A few words of explanation may be in order to show how the processing electronics identifies the first and last horizon crossovers and thus measures the attitude with respect to a fixed optical reference point. The sketch below shows typical waveforms expected for an assumed horizon profile.

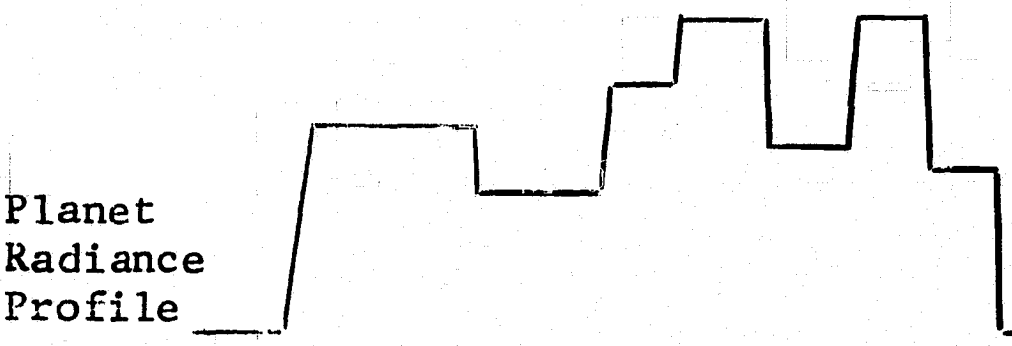

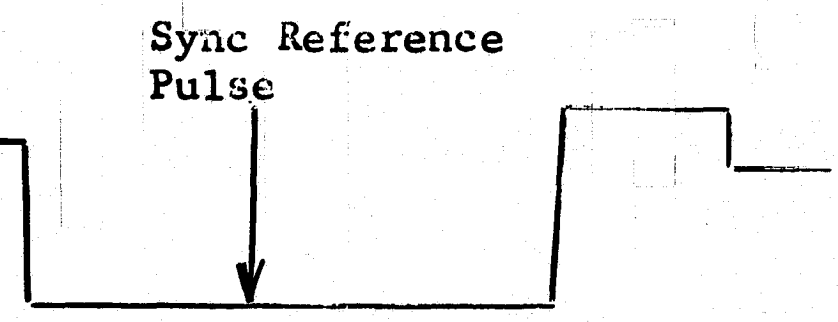

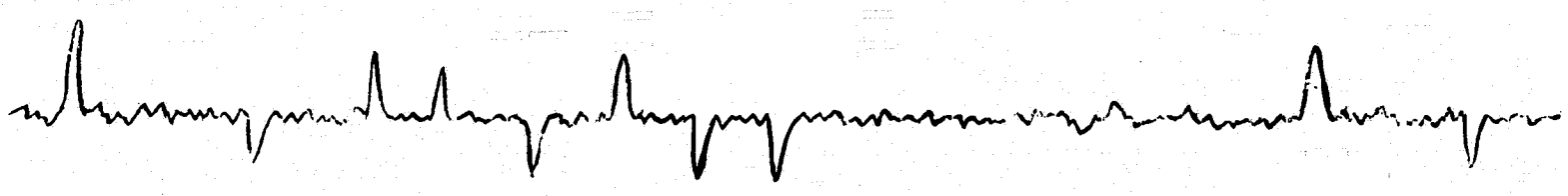

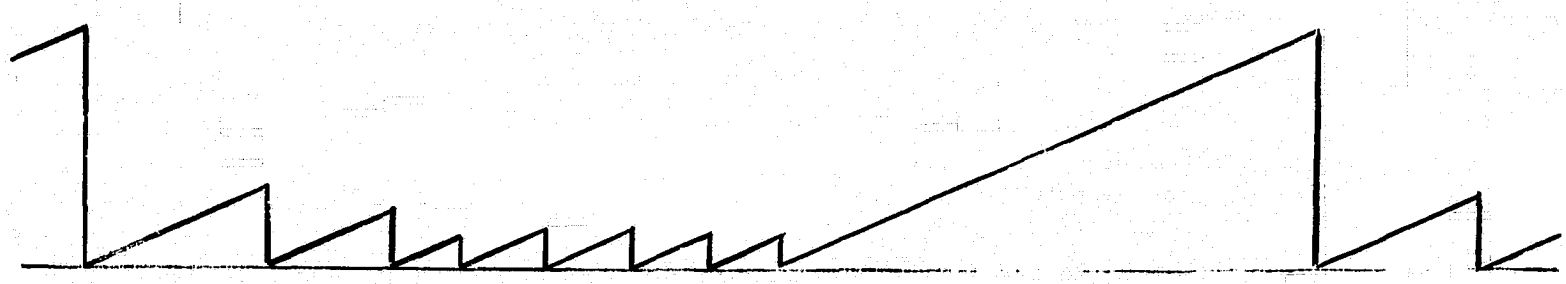

Roll — Sync Reference Arms Readout Gate

Pitch — Sync Reference Arms Readout and Inverts Slope

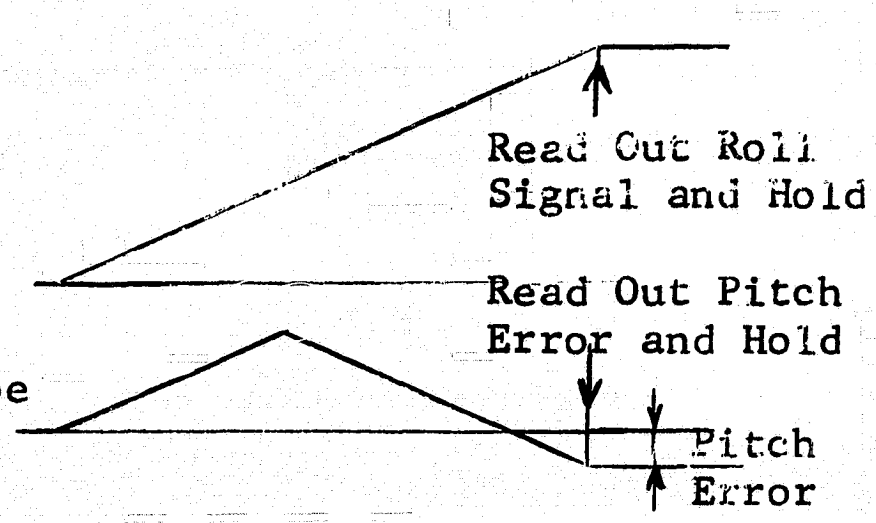

Roll error is the difference between the roll signals of two channels viewing opposite sides of the planet.

As is seen in the sketch, a ramp generator is started by each signal pulse exceeding a prescribed value. The next incoming pulse discharges the ramp output and starts a new one at zero. The value of the ramp output voltage is a measure of the time from the start of the ramp at zero volts. The last pulse when the detector field of view leaves the planet in its transition to space starts a ramp which continues uninterrupted except on command from a readout and hold gate.

A reference signal generated optically when the scan motor reaches the midpoint in the outer space scan performs two functions: It arms a gating circuit to ready it for actuation when the next pulse arrives (the crossover of the field of view from space to planet edge); and it also inverts the direction of one ramp in order to measure the difference in time between the trailing planet edge and the reference time and the leading planet edge and reference time (pitch). The closing of the gate by the first pulse (leading planet edge crossover) after the space reference pulse holds and isolates

the net difference in the rising and falling ramp voltage to provide the pitch readout.

Roll readout is obtained in a similar fashion except that no ramp direction reversal is required. The first planet crossover pulse turns on the gate (armed earlier by the reference pulse) and holds the charge representing the maximum ramp value. A difference amplifier compares this maximum ramp voltage emanating from two oppositely directed sensor heads and registers the difference as the roll error and provides both direction and magnitude attitude data.

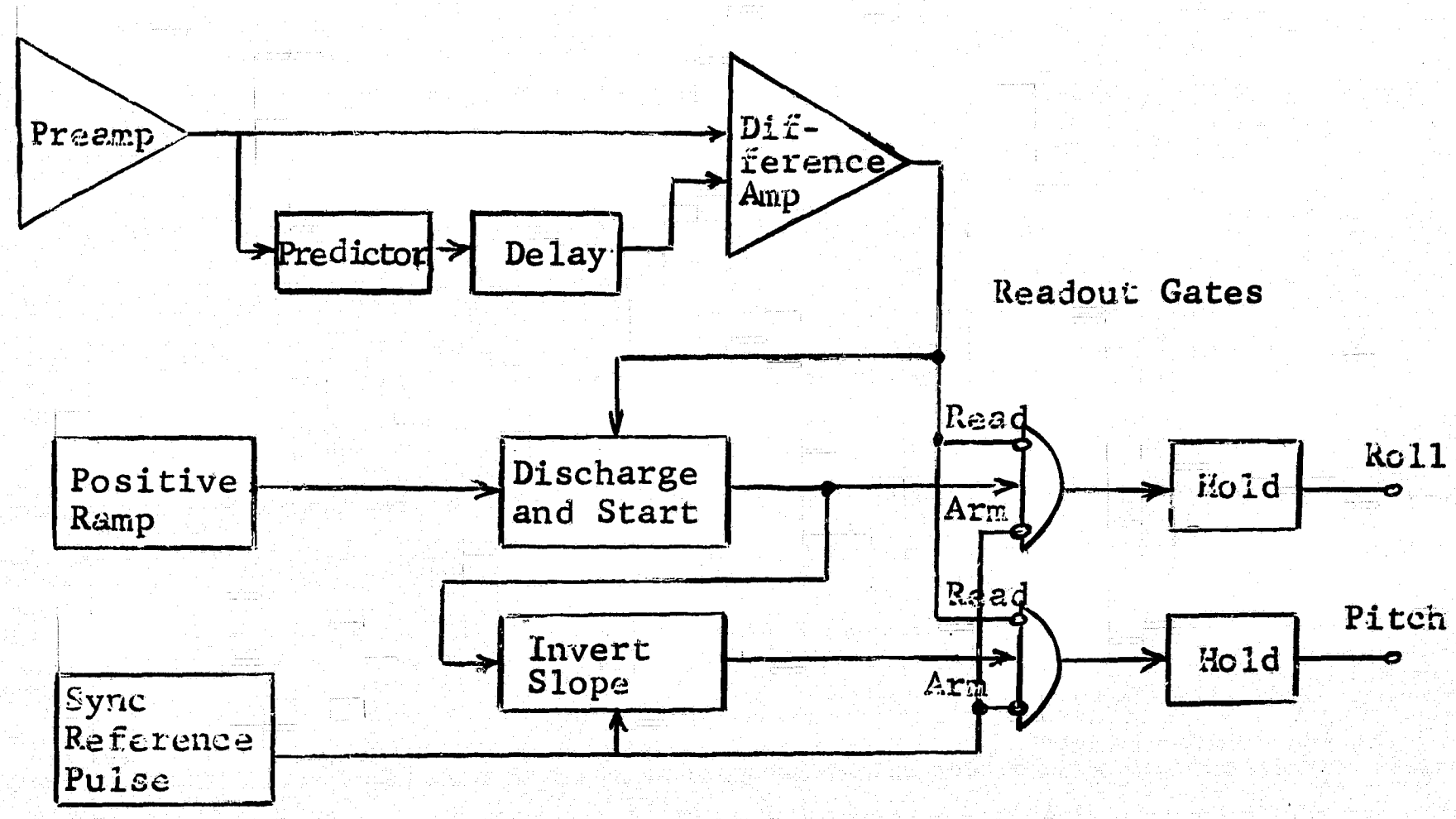

A P P E N D I X D

"Horizon Sensors for Vertical Stabilization of Satellites and Space Vehicles"

"Infrared Horizon Sensor Techniques for Lunar and Planetary Approaches"

"High Accuracy Horizon Sensor using FIRM"

"Electronic Scan Horizon Sensor"

"A High Accuracy Conical Scan Infrared Horizon Sensor Operating in the 15 Micron CO_2 Band"

BLANK PAGE

HORIZON SENSORS FOR VERTICAL STABILIZATION OF SATELLITES AND SPACE VEHICLES

by

Morris H. Arck and M. Monty Merlen

Reprinted from:
PROCEEDINGS
of the

National Specialists Meeting on Guidance of Aerospace Vehicles

BOSTON, MASSACHUSETTS

May 25-27, 1960

INSTITUTE OF THE AERONAUTICAL SCIENCES

HORIZON SENSORS FOR VERTICAL STABILIZATION OF SATELLITES AND SPACE VEHICLES

by
Morris H. Arck, Project Manager and M. Monty Merlen, Project Engineer
Horizon Sensor Systems
Barnes Engineering Company, Stamford, Connecticut

Introduction

The Local Vertical has long been used as a reference for navigation on the surface of the earth. With the launching of missiles and satellites, it has also come into importance as a reference for space navigation and for control of the attitude or orientation of space vehicles. The local vertical at any point near the surface of a celestial object is a straight line between the point and the center of the celestial object. If the body is a homogeneous sphere, the local vertical lies along a radius of the body. Under these conditions the local vertical has two properties by which it can be determined; it is perpendicular to the plane of the horizon as seen from the point of observation; and it coincides with the gravity vector through the point. At a point in space the local vertical is thus a direction relative to a nearby celestial body and it is not an absolute direction.

Gravity sensing systems determine the local vertical by detecting the direction of the gravity vector. Such systems are of limited use where in addition to the gravity vector the system experiences other forces due to accelerations. For an object in free-fall or for an orbiting body, where weightlessness occurs and the net force is zero, the gravity detector is useless.

Inertial guidance systems establish an absolute reference in space. With the proper data, the local vertical can be computed. The use of these systems is limited by their relative size and complexity. The required information is derived by computation, and the system is subject to drift.

The visible horizon is a convenient reference for establishing the local vertical. Its use is precluded at night or under obscuring weather conditions when the horizon is not clearly visible.

It will be shown that the infrared radiation received from the earth at a point in space clearly delineates the earth against its space background under all weather conditions and by day or night. By detecting this thermal horizon, the local vertical can be erected for objects in space flight. Attitude control of the pitch and roll axes of satellites or space vehicles may then be accomplished by reference to this vertical. For this purpose, horizon sensors have been developed with high sensitivity in the far-infrared spectrum. These sensors are compact units, completely automatic and passive in operation.

This paper describes several sensor systems, reviews the history of their development at Barnes Engineering Company and discusses the infrared and electro-optical techniques employed in their design.

Basic Principles

The Thermal Horizon

The infrared radiation received from the earth at a point in space is contributed by two sources: diffusely reflected radiation from the sun and thermal self-emission from the earth and its atmosphere. Essentially zero infrared radiation is received from the space background; the contribution from stars and distant planets is negligible compared with the earth's radiation. There is thus a sharp radiation discontinuity at the horizon, between the earth and space background which can be used both day and night for vertical position sensing.

Thermally-Emitted Radiation

As the horizon sensor scans across the earth's surface, it will receive thermally-emitted radiation and reflected solar radiation. The thermally-emitted radiation will come partly from the earth and partly from the atmosphere. The earth's contribution will be in spectral regions where the atmosphere is transparent; the atmosphere itself will radiate in the spectral regions where it is opaque. When one looks close to the horizon, the thickness of the air layer becomes very great, and theoretically the atmosphere defines the emission. The primary source of infrared emission in the atmosphere is the water vapor concentrated in the troposphere. The radiance seen at the horizon would be expected to be of a black body at the temperature of the top of the troposphere, or the tropopause. This temperature has been reported to vary between 220°K at the poles to 200°K at the equator. As we scan across the earth's surface toward the nadir, the effective black body temperature should increase since we see through less atmosphere and hence see more of the earth's surface, which is generally much warmer than the tropopause. Theoretically, the horizon discontinuity which must be detected is between black bodies at 0°K and 200°K. This represents a radiance difference of 0.003 watts-cm^2 - $steradian^{-1}$. The location of the horizon gradient should be well-defined and would be much steeper than any others to be expected, such as gradients across geographical features of the earth's surface. The steepness should not be deteriorated appreciably by the finite height of the atmosphere. One reason is that the gradient should occur primarily at the tropopause; another is that at operational altitudes the horizon is so distant that the vertical thickness of the atmosphere subtends only a fraction of a degree.

Reflected Solar Radiation

The accuracy with which the earth's infrared horizon can be determined is affected adversely by the presence of reflected solar radiation which

could produce other discontinuities from cloud edges, topographical features or the terminator (night-day division). Fortunately, spectral filtering can be used to separate reflected solar radiation from the earth's self-emission. Solar radiation has a color temperature of about 6000°K and appears almost entirely in the spectral region from 0.2 to 2.0 microns; the earth, at a much lower temperature, radiates in the long wavelength region beyond 5 microns. By using a filter which eliminates the short wavelengths and a thermal detector which has high sensitivity at long wavelengths, a system can be made almost completely independent of solar radiation. A suitable combination is a germanium filter and a thermistor detector. Germanium is completely opaque below 1.8 microns and transmits well between 1.8 and 20 microns. Figure 1 illustrates the spectral distribution of radiation received at a point in space from the earth and the transmission characteristics of germanium. The thermistor detector, itself, has a flat response over the entire region shown. About 92% of the reflected solar energy is removed by optical filtering; residual reflection effects are eliminated by signal-clipping techniques in electronic systems.

Historical Development of Horizon Sensors at Barnes Engineering Company

Barnes Engineering Company undertook development of horizon sensor systems in mid-1958 with the design and fabrication of Narrow Scan Angle Sensors for General Electric, MSVD, Philadelphia. Two different systems were developed in limited quantities. Each system consisted of three scanner heads and a central electronic mixer box which resolved the information from each head to yield both pitch and roll error signals. Each scanner head, in both system versions, employed a thermistor detector to sense the horizon. The earlier version employed a chopper wheel through which an 18° vertical by 1° horizontal field of view was examined. The horizon location was determined from the total radiation received, and stabilization was accomplished by comparing outputs from head-pairs. The three heads were mounted in the configuration shown in Figure 2. Thus, heads 1 and 2 yielded roll information while heads 2 and 3 yielded pitch information after the signals were processed in the mixer box. The later version utilized pulse-width information obtained from each scanning head by means of a Nipkow scanning wheel upon which a series of holes was arranged in a spiral path. The mounting of heads and combination of head-pairs were identical with the earlier version. Both versions were test-flown in THOR missiles with the sensor outputs monitored but not controlling. These tests extabilshed the existence of a reasonably sharp infrared horizon, but several deficiencies were disclosed, among them limited altitude capability and excessive bias power and lowered sensitivity resulting from the extremely large detectors required.

The successor to these earlier systems was designed under contract to General Electric, MSVD. Under this concept, two sensor heads comprised a system. Each sensor scanned space in a conical pattern with an apex angle of 78° to detect radiation discontinuities existing at the horizon. The operating principles of the conical scan sensor are discussed in a later section.

Subsequent development of horizon sensor models led to use of conical scan angles of 90 to 110°. These wider angles improved acquisition capabilities and increased the range of operational altitudes. One version, developed for ABMA, utilized a rotating mirror assembly with a 120° scan angle. This sensor is shown in Figure 3. As further developments incorporated more severe environmental requirements, the rotating mirror assembly was replaced by a rotating prism assembly, and the entire sensor package was complately sealed against external environments. The present sensor design is shown in exploded view in Figure 4. This configuration is used for sensors delivered to ABMA and for McDonnell Aircraft Corporation. For ready comparison, Table I lists the characteristics of some of the sensors developed.

Wide Angle Prism Scan Systems

The present wide angle horizon sensor, shown in Figures 4 and 5, is representative of the conical scan sensor which was designed to meet severe environmental specifications. Each sensor is a completely self-contained unit which is flange-mounted. The backbone of the unit is a circular baseplate which supports a rotating prism assembly, drive motor, synchronous choppers, a germanium-immersed detector and the entire signal-processing and power supply electronics. A cylindrical rear cover encloses the electronics. A metal front cover with a germanium window encloses the rotating mechanism. The unit is sealed with O-rings.

Before the operation of the horizon sensor is described, certain design features will be pointed out and explained.

(a) Sealing of the sensor unit was required in order to prevent moisture from entering during storage and during long hold-periods on the launch pad. As an adjunct, the sensor is pressurized with dry nitrogen at 3-5 psig.

(b) A centrifugal sun-shutter was provided for applications requiring an intermittent duty cycle with the output of the horizon sensor coupled to the reference gyros. In this application, the horizon sensor system operates for a relatively short time at periodic intervals. Its prime function is to correct the drift of reference gyros which operate continuously to keep the space vehicle properly oriented. Whereas the sun may be scanned with no damage to the detector, the energy of the sun concentrated for extended periods on a detector will cause it to deteriorate. The latter condition could occur during one of the "off" periods of the horizon sensor. Therefore, a sun-shutter is incorporated for this contingency. A centrifugal design has the advantages that it is self-activating, fail-safe, and

requires no additional power.

Horizon Sensing With a Conical Scan Sensor

Two horizon sensors, properly oriented in a space vehicle as shown in Figure 6, will establish a local vertical with respect to the earth. When the vehicle is oriented so that the earth is present in the scanning path of a sensor, there are two points at which each scan intersects the earth's horizon. The sensor detects the change in radiance level between the earth and space at the two horizon points. It then compares the time interval between alternate horizon crossovers with fixed references aligned with the space vehicle. From this, the sensor generates linear error signals proportional to the angle of tilt between the normal to the chord connecting the horizon crossover points and the fixed references. These error signals can be used to control attitude about one axis by a suitable reaction mechanism. By using two sensors, attitude control about both pitch and roll axes is possible.

Operation of Rotating Prism Sensor

The operation of the Rotating Prism Sensor will be described in terms of its scanning system and electronic circuitry.

Scanning System details, including the sensor optics and scan mechanism, can be seen in Figures 4 and 5. The infrared detector is fixed to the center of the circular plate, and its 2°x8° field of view extends through the circular opening in the center of the scanning assembly. The scanning prism deflects the detector field of view 55° from the normal. As the prism rotates it swings the line of signt around the axis of the sensor, generating a cone with an apex angle of 110°.

A drive motor geared to the scanning assembly rotates the scanning prism at 30 rps. Closely associated with the prism drive assembly is a reference signal generator. The output of this generator is a square wave signal at 30 cps; this is the fixed reference to which the detector horizon signals are compared. The reference generator is triggered by the interaction between a nagnetic pickup coil and a semi-circular steel vane embedded in the under surface of the scanning prism assembly gear. As the gear rotates, the vane passes over the pickup coil, generating reference pulses. These pulses trigger the phase reference generator to yield a phase-locked 30 cycle square wave.

The collecting optics consist of a germanium objective lens which focuses the radiation upon a thermistor detector attached to its rear surface. Germanium, in addition to its spectral filtering characteristics, is an ideal optical material because of its high index of refraction (4.0) and low dispersion. A fast lens can be made without excessive curvature. The detector is oriented so that its long dimension is parallel to the horizon during the conical scan, giving maximum resolution. Use of an immersed detector produces an optical gain almost equal to the index of refraction of the germanium. The principle of immersion (i.e., embedding a detector in the rear surface of a lens) is the same as for an oil-immersion microscope objective. In addition, the detector area for a given field of view is reduced, substantially reducing the bias power requirements.

The Infrared Detector consists of two thermistor (thermally sensitive resistor) elements connected in a bridge circuit as shown in Figure 7. One arm is the active flake which receives the incoming radiation; the other arm consists of a similar compensating flake which is shielded from external radiation. The two flakes are oppositely biased, and their junction is connected to the input of the preamplifier.

Radiation impinging upon the active flake will change its temperature and therefore its resistance. The junction voltage changes accordingly. The result of the radiation changes during a complete scan cycle is the generation of a rectangular wave signal at a 30 cps frequency.

Electronic Circuitry

The electronic circuits of the horizon sensor are shown in block diagram form in Figure 8. They combine transistor electronics and printed circuit techniques in a compact assembly. The individual circuit blocks are described in the following paragraphs.

The Preamplifier and Booster Amplifier provide impedance matching and raise the level of the detected signal. The junction of the thermistor flakes is direct-coupled to the input of the preamplifier. Direct-coupling provides good low-frequency response and prevents phase-shift. Feedback is used to stabilize gain and provide high-frequency boost compensation for the detector time constant in order to preserve the steepness of the sides of the rectangular radiation signal waveform. The booster amplifier simply provides additional gain.

The Signal-Centering Circuit assures that the output signal reflects only vehicle tilt. The amplifier output signal is limited in order to make the error signal dependent only upon horizon angle and independent of variations in the earth's radiance, detector sensitivity, amplifier gain, or power supply voltage. The amplitude limiter employed samples a thin horizontal slice from the rectangular waveform. This slice must be taken at a point of minimum phase variation. This condition occurs at the center of the waveform. Were an RC circuit used to couple the signal to the limiter, it would balance equal areas of the signal waveform above and below ground. Changes in the angle of horizon depression would then cause a

shift in the D-C signal level. Therefore, a signal centering circuit is employed before the limiters to assure that the same center slice is sampled for phase shift under all conditions. In this way the signal amplitudes rather than signal areas are balanced about ground.

The Phase Inverter and Limiter provide a clean push-pull signal for rectification. After centering, the signal next enters the first of a pair of cascaded feedback amplifiers, each of which acts as a limiter and phase inverter. The first stage output is a limited rectangular wave which swings 10 volts either side of a fixed 10-volt level. Part of the output signal is fed to another limiter amplifier substantially the same as the first where it is amplified and inverted to yield the mirror image of the output from the first section. The total output is a dual signal which then proceeds to a phase detector.

The Phase Reference Generator consists of a free-running multivibrator which is synchronized to the rotating prism motion by the reference pulses from the magnetic pickup. The resultant square wave is amplified and used to drive two high-speed SPDT synchronous switches (Syncroverters) which comprise the phase detector. Accurate phasing is assured by correct initial adjustment of the pickup vane.

The Phase Detector and Filter converts the limited push-pull signal into a proportional D-C error signal by synchronous rectification. The input signal is connected to one pair of stationary switch terminals, and the output is connected to the other pair. The moving contact arms are connected to capacitors and they are phased so that when one capacitor is sampling the input signal, the other is connected to the output terminals. The voltage transferred from input to output by each capacitor corresponds to the integrated charge accumulated during the previous sampling cycle. The principle is similar to that of the box-car integrator used in radar systems.

The iron vane of the scanning prism assembly is initially aligned so that switch-over of the synchronous switches occurs when the radial sector of the scanning beam crosses the vertical reference mark of the sensor; switch-back occurs 180° later. Thus, when a storage capacitor is connected to the signal input, it receives part of the sky radiation pulse and part of the earth radiation pulse. The capacitor is charged positively during the switched-in portion of the earth pulse and negatively during the switched-in portion of the sky pulse. If the sensor horizontal is parallel to the earth's horizon, each capacitor is negatively charged an amount equal to the positive charge, and its net charge is zero. If the sensor is tilted with respect to the horizon, the positive and negative charges placed on one capacitor during a sample period are no longer equal, and a net error signal is produced which indicates by its polarity and magnitude the direction and degree of tilt. Figure 9 illustrates the signal waveforms and the reference signal switch points for a centered and a tilted horizon respectively.

The D-C Output Amplifier isolates the sensor from the load circuits at the input of the D-C amplifier. The outputs of the phase detector are combined and filtered by an R-C network. The output of the amplifier may be adjusted for 0.1 to 1.0 volt per degree of tilt; for the sensor under discussion, it is approximately 0.3V per degree. The output transfer function is linear over the range of ±35° of tilt and is constant outside this range up to ± 90°.

The Void Signal Circuit puts out a "disregard output" signal under two conditions. Spurious error signals may be generated either when (a) the sun appears in the scan or (b) the horizon is lost because of vehicle perturbations. Void signals produced under these conditions trigger a logic circuit which indicates by its output that either of these effects prevail. This output is used to disconnect the D-C error output from the vehicle guidance system so as to prevent erroneous control by inherent system noise.

The Power Supply and Regulator Circuits derive all required operating voltages from the 400 cps, 115-volt supply. Semi-conductor regulator circuits supply the divers regulated voltages required by different portions of the system. The ABMA horizon sensor provides for 12Volt D-C input.

Outputs and Test Points A single multipin connector at the rear of the unit provides all the electrical connections to the sensor. In addition to the power input and error signal output, a number of test points are provided at this connector for use in check-out and troubleshooting.

Environmental Tests

The Wide Angle Horizon Sensor has successfully completed a Qualification Test Program, meeting severe environmental requirements of reduced pressure, temperature, humidity, acoustic noise, vibration, shock, and acceleration. These tests were designed to simulate environmental conditions encountered during missile launch and in flight.

Test Flight Results

Telemetered data from an ABMA horizon sensor mounted in a Jupiter missile yielded valuable information. Although the error signal output was not used for control purposes (control being delegated to a gyro stabilized platform during these tests), two output were monitored. One of the monitored signals was the unlimited preamplifier output signal which was observed to determine the earth-space radiance difference. The other

monitored signal was the error output. This was compared with the gyro platform attitude.

Information from the preamplifier output channel disclosed that the temperature difference at the earth-space horizon was approximately 275° K. This implies that the discontinuity is at the earth horizon rather than at the tropopause.

During the same tests, the error signal channel showed that the horizon sensor output over its linear range differed from the gyro-platform attitude output signal by no more than ±0.3°. This was a factor of three better than the design requirements of ±1.0°.

Conclusions

The Horizon Sensor demonstrates the feasibility of employing the infrared horizon as a reference for vertical stabilization. The systems have performed satisfactorily under the conditions encountered while placing and maintaining a vehicle in geocentric orbit. There are good reasons to believe that the same system can be used to establish a local vertical with respect to other celestial bodies in close proximity during space flight, for example, in moon approaches and landings.

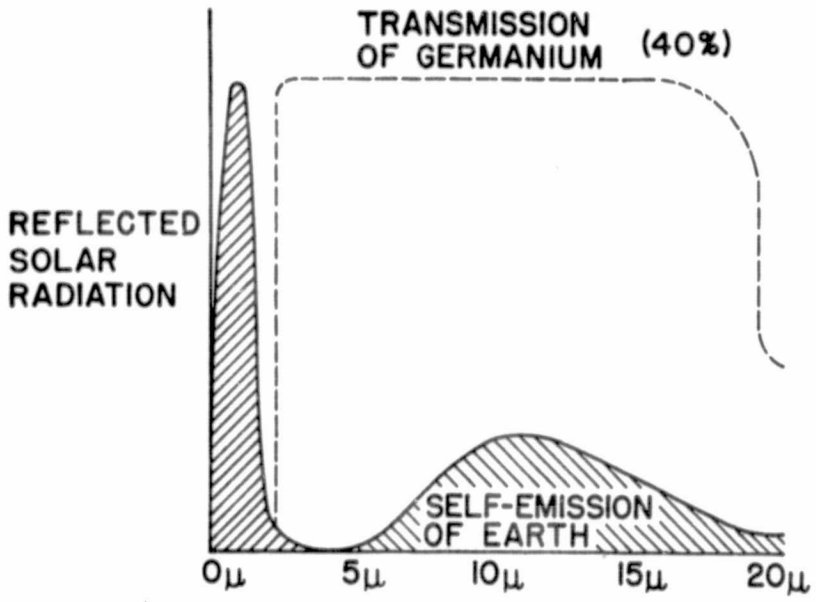

FIGURE 1-SPECTRAL DISTRIBUTION OF RADIATION

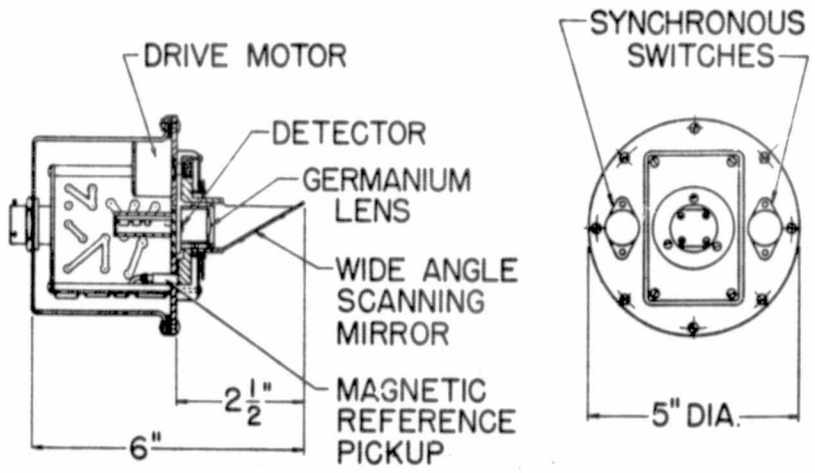

FIGURE 3-ROTATING MIRROR SCAN HORIZON SENSOR

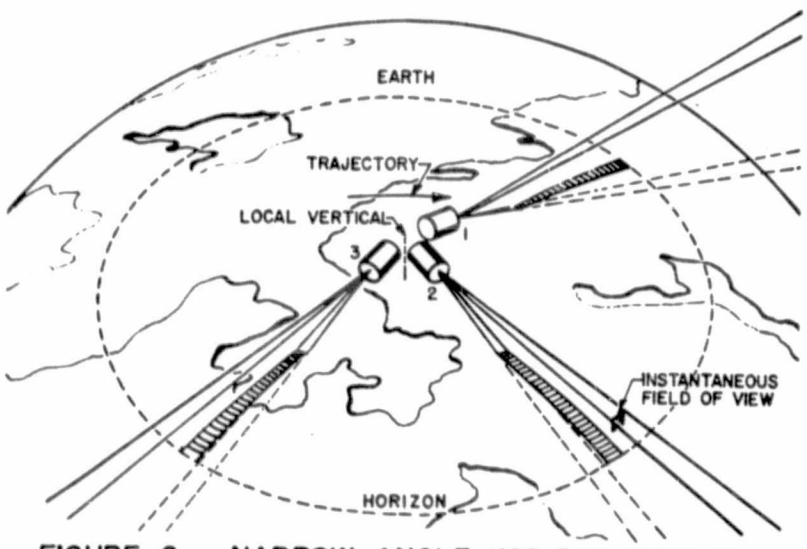

FIGURE 2. NARROW-ANGLE HORIZON SENSOR SYSTEM CONFIGURATION

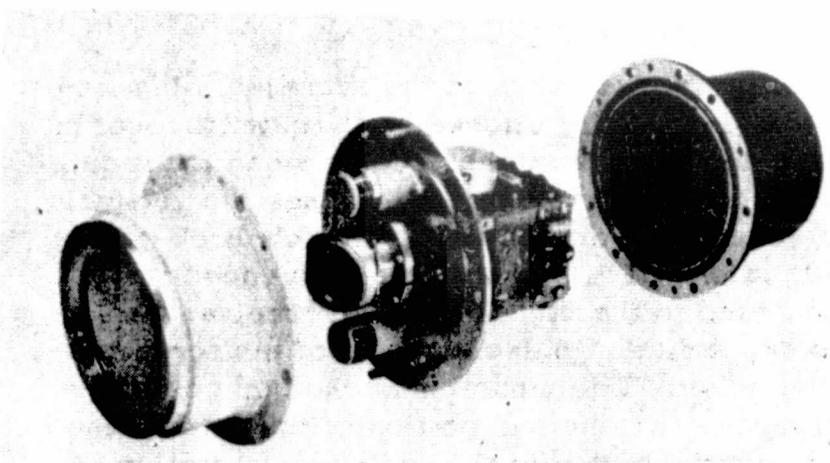

FIGURE 4-ROTATING PRISM SCAN HORIZON SENSOR

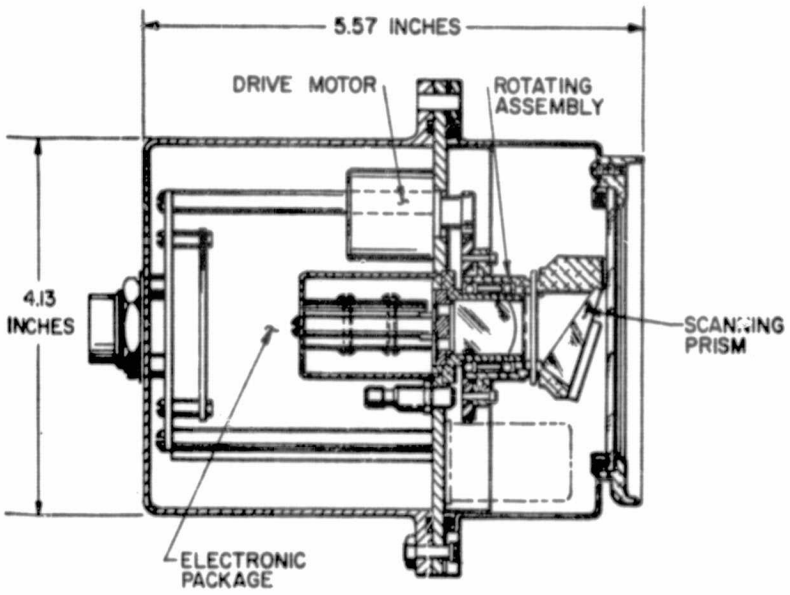

FIGURE 5. CROSS-SECTION OF ROTATING PRISM SCAN HORIZON SENSOR

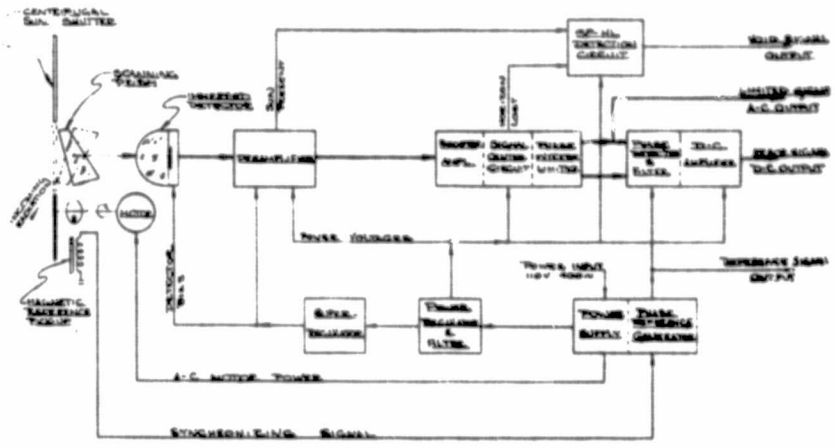

FIGURE 8 - BLOCK DIAGRAM OF ROTATING PRISM HORIZON SCANNER

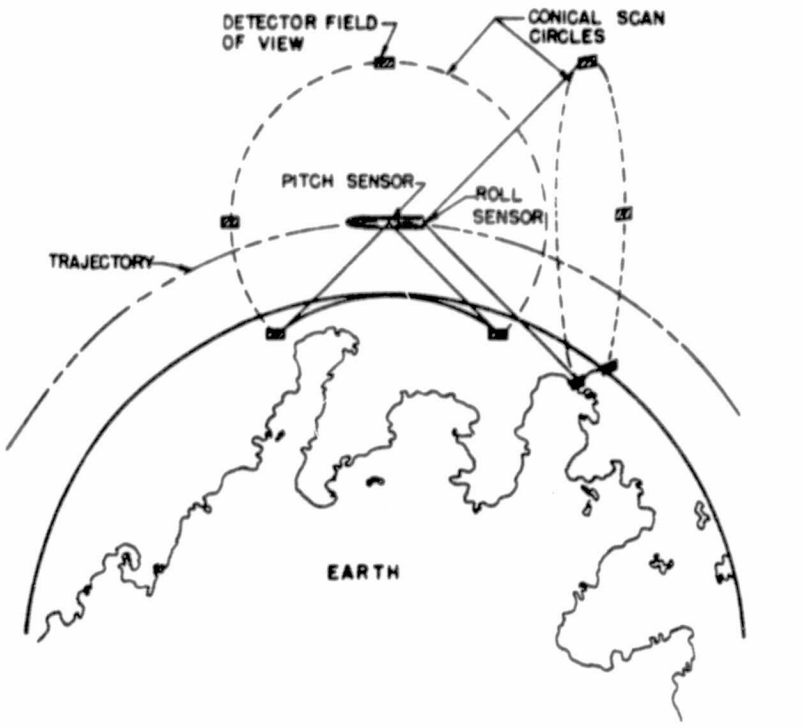

FIGURE 6 - INSTALLATION AND SCAN PATTERN OF CONICAL SCAN SENSOR

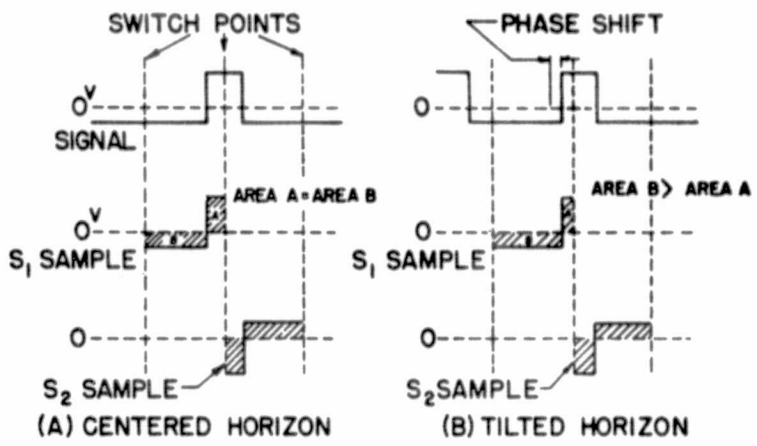

FIGURE 9 - CENTERED AND TILTED HORIZON WAVEFORMS

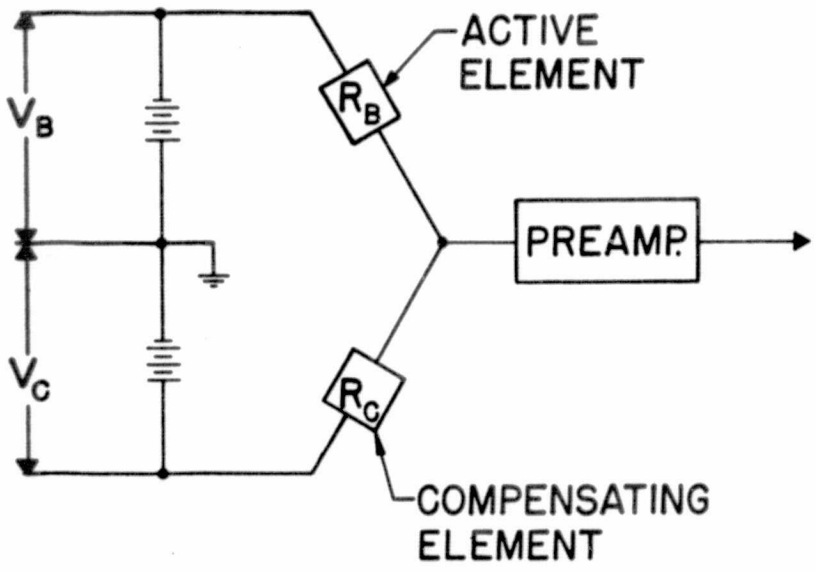

FIGURE 7 - THERMISTOR-DETECTOR BRIDGE CIRCUIT

TABLE I
Horizon Sensor Characteristics

MODEL	Contracting Agency or Firm	Field of View	Heads per System	Separate Electronics Package	Total Weight	Total Power Input	Rotational or Chop Rate	Scan Angle	Angular Accuracy	Environmentally Sealed
Narrow Angle-Amplitude	GE-MSVD	18° x 1°	3	1	23 lbs.	20 W.	200 cps	---	±1°	no
Narrow Angle Pulse Width	GE-MSVD	18° x 1° (1° x 1° unit)	3	1	23 lbs	20 W	10 cps	---	±1°	no
Wide Angle Prism Scan	GE-MSVD	2° x 8°	2	0	14 lbs	20 W	30 cps	78°	±1°	yes
Mirror Scan	ABMA	2° x 8°	2	0	5 lbs	8 W	30 cps	120°	±1°	no
Prism Scan	ABMA	2° x 8°	2	0	6.5 lbs	7 W	30 cps	110°	±0.3°	yes
Prism Scan	McDonnell Aircraft	2° x 8°	2	0	5.7 lbs	6 W	30 cps	110°	±0.5°	yes

Infrared and Electro-Optics
Components · Instruments · Systems

Barnes Engineering Company

30 Commerce Road · Stamford, Connecticut

INFRARED HORIZON SENSOR TECHNIQUES FOR LUNAR AND PLANETARY APPROACHES

Gerald Falbel, Technical Planning Staff
Robert W. Astheimer, Chief Engineer, Development Engineering
Barnes Engineering Company

Introduction

It is necessary to establish the attitude of most orbiting and interplanetary vehicles at various times with respect to some external coordinate system. This is usually accomplished by sensing the position of some combination of the sun, stars, or planets. If the object is at a distance such that it appears as a point, the sensor is called a star tracker, while if the planet is close enough so that a definite disc is perceptible, it is usually called a horizon sensor. In the latter case, the direction toward the center of the disc is desired. This paper will consider the problem of determining the horizon position by means of the thermal self-emission of the planets, particularly the earth, the moon, Mars, and Venus. The infrared emissive characteristics of these planets will be reviewed and various sensing techniques discussed. A comparison of the accuracy which may be achieved by the various methods is given.

In order to sense the position of a planet by its thermal self-emission reliably and with some degree of accuracy, three properties of the planet are desirable. First, it must be warm enough so that a detectable thermal discontinuity exists between the horizon and the space background. Second, for a good accuracy, this discontinuity or gradient should be very sharp; and lastly, system problems are simplified if the radiance is reasonably uniform over the surface of the planet. The last condition can sometimes be attained fairly satisfactorily by selecting the spectral region of operation.

A plot of the apparent temperature distribution[1] along a diametral scan of the earth, the moon, Mars, and Venus is shown in Figure 1. A logarithmic radiance scale for the total thermal emission is also shown since it is the radiance rather than the temperature which produces the received signal. Each object is assumed at half phase with the terminator bisecting the disc in order to illustrate the difference in signal level between the dark and sun illuminated sides. This figure is a great over-simplification but is useful for comparing the gross radiant characteristics of the four objects. It must be pointed out that these characteristics may be very different in restricted spectral regions, particularly in the absorption bands of atmospheric constituents; however, restricting the spectral region can only decrease the apparent radiance, although it may also reduce the dynamic range of signal that must be accepted.

A minimum detectable radiance level is shown at 0.1 milliwatts/cm^2-ster assuming an immersed thermistor detector with a 2-inch diameter collecting aperture, 20% optical efficiency, a $1^\circ \times 1^\circ$ field of view, a 250 cps bandwidth, and a signal 10 times rms noise. These are realistic parameters for a system as will be shown. It is seen that the horizon of all planets is readily detectable with such a system. We conclude then that all these planets have enough thermal emission to make infrared horizon sensors of reasonable aperture practical.

The accuracy with which the horizon can be determined will depend upon the steepness of the horizon gradient which is a function of the density and composition of the atmosphere. The moon, possessing no significant atmosphere, has an infinite gradient; and the ultimate accuracy is limited only by terrain irregularities. In a practical system, however, the detector noise would probably be a limiting factor because of the low temperature and emission from the dark edge.

The uncertainty caused by the fuzziness of the horizon discontinuity of a planet with an atmosphere is a function of altitude. At very low altitudes, the error could be quite large, while at high altitudes, the entire subtense of the atmosphere may become negligible. The earth is the only planet on which horizon sensors have been used, and considerable data has now been accumulated from Mercury and Discoverer vehicles with wide spectral band systems. The accuracy of these systems has generally been limited by the size of the detector field of view rather than the horizon gradient. A number of theoretical studies[2] have been made of the gradient to be expected in different spectral regions, some results of which are shown in Figure 2. The spectral regions of greatest interest are the CO_2 absorption band at 14 - 16 microns, the water vapor bands extending from 20 - 35 microns (and beyond), and the so-called transparent atmospheric "window" between 8 - 12 microns. It will be seen that the horizon gradient is quite sharp in the atmospheric window, but the range of signal level is greatest here because of cloud cover. Operation in the 14 - 16 micron CO_2 absorption band masks clouds and will present a very uniform signal, but the gradient will be more gradual, extending over almost 1° from an altitude of 400 miles. Accuracy at this altitude is probably limited to a few tenths of a degree by the indistinctness of the horizon itself.

Much less information is available regarding Mars and Venus. The atmosphere of Mars is fairly tenuous with few clouds and will probably not diffuse the horizon significantly even at low altitudes. Venus has a very dense atmosphere of unknown depth; however, the top of the cloud deck appears to be quite distinct and of uniform temperature. Therefore, a sharp gradient should exist in a spectral region where the clouds are opaque and the atmosphere above transparent.

One of the most troublesome problems in horizon sensing is caused by large variations in temperature or radiance over the surface. Some difficulties of this nature were experienced with early earth horizon sensors because of unexpectedly cold cloud tops associated with large storm areas. Spectral filtering and modifications of the electronic processing systems were required to achieve reliable operation for all weather conditions. The situation is much worse with the moon as indicated

in Figure 1. The radiant emission from the sun-baked side is 100 times greater than that from the dark side, and there are additional small "hot" and "cold" areas caused by sun-illuminated crater edges and shadows. These variations in signal strength may not only produce errors due to saturation and time constant effects but could cause the system to confuse the horizon with the terminator, since the terminator discontinuity is 50 times greater than the dark edge horizon discontinuity.

The planet Venus seems to present the easiest object for infrared horizon sensing, but the sharpness of the horizon gradient in various spectral regions, which depends upon the atmospheric structure, is still unknown.

Reflected solar radiation will be superimposed on the thermal self-emission of the sun-illuminated portions of all the planets. This is in general an unwanted disturbance and can be substantially removed by filtering out wavelengths shorter than 8 microns. Such filtering also greatly reduces the signal produced from direct viewing of the sun which could saturate the system or even damage the detector.

Detector Considerations

It has been shown that the range of apparent planetary temperatures to be sensed extends from 120°K to 380°K. Detectors sensitive to such thermal radiation must respond to long wavelengths from 8 to 40 microns. Photoconductive detectors highly sensitive in this region have been developed such as copper or zinc doped germanium[3] but these all must be cooled to temperatures in the neighborhood of liquid helium. Reliable cooling to these temperatures for long periods of time is presently impractical for space systems and often also for ground use because of logistic restrictions. The only suitable detectors are the thermal types, particularly thermistor and metal bolometers and thermocouples. Of these, the thermistor bolometer has found greatest use to date.

The thermal detectors[4] operate by virtue of the heating effect when incident radiation is absorbed on the sensitive element. The very small temperature change resulting effects some physical parameter such as the resistance which can be read out electrically. An inherent difficulty in the use of such detectors is the identification or separation of the temperature change caused by the desired radiation from the very much larger ambient temperature variations. For example, in a typical horizon sensor, the increase in radiation received when the field of view scans from space onto the earth increases the detector element temperature about .001°C. The sensor must be designed so that this temperature differential may be detected in spite of ambient temperature variations 10,000 to 100,000 times greater.

The most common way of separating the desired temperature change from unwanted internal effects is by optical-mechanical scanning or chopping. This modulates the external radiation signal at a relatively high frequency, while the internal signals are very slowly varying d.c. and can be removed by capacitance coupling to the electronic amplifier. It is important to notice that such modulation must be done on the radiation signal before detection and not on the electrical output. Electronic chopping will modulate both external and internal signals and is of no value in this respect.

Thermal detectors which depend upon a resistance change for signal generation, such as thermistor or metal bolometers, are more subject to internal temperature effects than thermocouple types. The reason for this is that in order to sense the resistance change a bias current must be used to convert it to a voltage signal. The desired signal thus appears as a very small change superimposed on the much larger bias voltage. Bridge arrangements of detector elements may be used to buck out the large bias voltage, but it is practically impossible to maintain the degree of balance necessary over a wide ambient temperature range. Optical modulation, of course, solves the problem since the d.c. bias voltage is filtered out, therefore these detectors are seldom used without optical modulation.

Thermocouple detectors do not require biasing and are thus free of this problem. The only voltage appearing is the thermoelectric EMF produced by the radiant heating of the junction, and this is not superimposed on a biasing voltage. Unmodulated optical systems are therefore feasible with thermocouple and thermopile detectors. However, even with these detectors, care must be taken in the design to eliminate spurious signals from internal temperature gradients and self-emission of optical parts.

The elimination of optical chopping and scanning mechanisms is highly desirable for space missions where very long life and low power are necessary. The spurious signals or drifts, inherent in unmodulated systems, make them relatively less accurate than optically scanned systems. Therefore, thermopile detectors are most suitable for low accuracy, long life applications such as antenna pointing.

Basic Sensing Techniques

The infrared emission characteristics of the planets and suitable detectors for sensing this radiation have been described. Such detectors must be employed in an optical arrangement to provide information from which the coordinates of the center of the planetary disc can be determined to the degree of accuracy desired. A complicating factor is that for most planetary objects the radiant emission will be highly non-uniform over the surface, and for high accuracy, the system must be independent of the radiance level.

A number of systems have been developed for this purpose. These can all be shown to be versions of three general categories which we shall designate as follows:

(1) Conical scan.

(2) Edge tracking.

(3) Radiometric balance.

The detector field of view and scan pattern associated with these techniques are shown in Figure 3. In the conical scan, which could also be called a wide field scan system, the instantaneous detector field is relatively small and is caused to scan through a large cone whose apex angle may be as much as 180°. With a 180° apex angle, the scan describes a great circle, although a more usual apex angle is between 50° to 120°. The detector signal generated will be an approximately rectangular waveshape repetitive at the scan frequency. This waveshape is usually limited in some fashion to eliminate amplitude dependence, and then position information is derived by a phase or pulse width comparison technique. Two sensors are used to generate pitch and roll attitude information.

Most horizon sensor systems flown to date have been of the conical scan type because it possesses a number of very significant advantages. It has excellent acquisition capability, attained without additional search modes because of the wide conical scan angle. The attitude information is derived from time characteristics of an amplitude limited waveshape and is therefore made insensitive to radiance variations over the surface of the planet, which as we have seen can be very large in some planets. Another advantage is that, because of the wide scan field, it is certain that some portion of the scan will leave the planet and view space. This provides an absolute zero radiance level against which any portion of any planet must give a positive contrast. Use can be made of this reference in setting limiting levels so as to prevent the system from confusing radiance discontinuities on the planetary surface, such as may be produced by the terminator or clouds, with the true horizon. This can be a serious problem with edge tracking systems as will be discussed in the next section. The primary disadvantage of the conical scan sensor is the need for high speed rotating elements which present life and lubrication difficulties in spaceborne applications.

Some sensors have been developed which combine the function of the two scanners by precessing the basic conical scan to produce a rosette or epicyclic pattern.[5] These systems may be considered essentially versions of the conical scan system and the same general remarks apply.

The basic concept of the edge tracking system is shown in Figure 3B. A small detector field of view is caused to lock onto the radiance discontinuity of the planetary disc. This is usually accomplished by oscillating the detector field through a small angle normal to the horizon edge and moving the entire sensor or the oscillating field until a balanced waveshape is obtained. Multiple sensor heads may be used, in which case at least three are necessary, or a single oscillating field may be caused to trace around the edge. In either case, the horizon position is determined by reading out the position of the center of the oscillating field with respect to spacecraft coordinates, i.e., angles θ_1, θ_2, θ_3, and θ_4, in Figure 3B.

For equivalent optics and detectors, this type of system will have a better signal-to-noise ratio than the conical scan because of narrower electronic bandwidth as will be discussed later. It leads to a much more complicated system however because of a separate search or edge tracking movement must be provided on each sensing head along with precision position readouts.

A high price is paid for this narrow bandwidth and consequent greater sensitivity. Without the wide scan motion, the previously mentioned space reference is lost and there is no way for the system to sense whether the signal is the true horizon or some other discontinuity such as a cloud edge or terminator which can be much greater than the horizon signal. Various devices such as auxiliary detectors may be employed to prevent locking on false edges, but they even further complicate the system. The edge tracking type of system would appear best suited for application where spectral filtering to an atmospheric absorption band can eliminate radiance variations over the planetary disc. An example for earth horizon sensing would be to filter to the narrow CO_2 absorption band at 15 microns. The increased detectivity of this type system would compensate for the large reduction in signal caused by the spectral filtering.

The former two systems are scanning types where the scan is usually accomplished by optical-mechanical means. It should be pointed out, however, that a stationary array of detectors could be used whose outputs are electronically sampled. For example, in a conical scan system, instead of mechanically causing a small detector field to scan over a wide circle, a stationary array of detector elements can be placed to view the same circle, and the array sequentially sampled electronically. Thermopile detectors with photosampling are particularly well suited for this technique, and a system of this type is being developed.

The radiometric balance type sensor is a non-scanning system and operates by comparing the radiation received from opposite portions of the planet. Very wide fields of view are used to achieve acquisition and also to average radiance variations over the surface. A typical arrangement of detector fields is shown in Figure 3C. Four wide angle stationary fields are employed designated a, b, c, and d; and attitude information is obtained by the difference in radiant power received from opposite fields, i.e., $P_c - P_a$ and $P_b - P_d$. This is obviously only correct if the planet is uniformly radiant, and therefore this system is only suitable for use with planets of uniform radiance such as Venus or where only approximate pointing information is necessary.

The great virtue of this system is its extreme simplicity and consequent high reliability. By using thermopile detectors no moving parts are necessary and very long life can be achieved. Non-uniform radiance effects can sometimes be minimized by spectral filtering. Also, by the use of an overlapping field scheme, to be described later, radiance variations can be cancelled at a specific altitude.

In the remainder of this paper, a more detailed description of these systems is given with an analysis of the accuracy each is capable of on

the planets of interest. Wherever possible, experimental results from existing horizon sensors are factored into this accuracy analysis.

Analysis of Errors for Various Horizon Sensing Techniques

This section will discuss the effect of the design parameters of various horizon sensor configurations on the achievable accuracy of these sensors. We will deal with three horizon sensing techniques:

(1) Conical scan technique.

(2) Edge tracking technique.

(3) Radiometric balance technique.

Conical Scan Technique

Mechanically Scanning Sensors Horizon sensors which obtain vehicle attitude indications based upon a wide angle conical scan have provided the largest source of flight test data. In this scanning technique, the instantaneous field of view defined by an infrared detector is scanned in space through the use of a motor-driven prism or mirror. When this scan intercepts a planet, the infrared emission from the planet causes a signal pulse to be generated which we shall hereafter refer to as the "planet pulse."

As was discussed previously, signals indicative of the vehicle attitude relative to the planet's local vertical are obtained based on the phase of this planet pulse relative to a mechanical reference point in the horizon sensor. In conical scan sensors, such as those used in the Mercury flights, this planet pulse phase indication is obtained by comparing the width of the "squared-up" planet pulse occurring before and after a reference point. This "squared-up" planet pulse is obtained by limit amplifying the pulses above a preset threshold level. The reference point is mechanically oriented such that it points toward the center of the planet when the sensor output is null.

It will be seen that for this signal processing concept the accuracy of such a conical scan sensor is determined by the time definition of the planet pulse edges. This uncertainty in planet pulse edge position can result from a number of error sources:

(1) System signal-to-noise ratio.

(2) Signal threshold level setting.

(3) Temperature differentials at opposite planet limbs.

(4) Detector-preamp time constant.

The system signal-to-noise ratio defines the amount of time jitter that will take place due to the presence of noise on the leading and trailing edges of the planet pulse. Most conical scan sensors have instantaneous fields of view subtending 1° - 2° in the scan direction and have scan rates of 20 to 30 per second, such that depending upon the scan cone apex angle the planet pulse rise times are of the order of 200 microseconds to 1 millisecond. The noise frequency components in this rise time period are smoothed by the 1 to 2 cycle low pass filter situated at the output of the sensors, such that it is only necessary that the threshold level be above the peak noise level expected during the period when the sensor scans space.

For a given optical system and spectral bandwidth, the achievable system signal-to-noise ratio is a function of the scanning speed and the infrared detector's field of view dimensions. The higher the scanning speed and the smaller the field of view dimension in the scan direction, the "sharper" the planet pulse edges become and therefore the higher the bandwidth that is required in order to maintain the fidelity of these short pulse rise and fall times.

The effect of temperature differentials at opposite planet limbs as well as that of the detector-preamp time constant is shown in Figure 4. This figure shows that the effect of temperature differentials at opposite planet limbs causes an asymmetric phase shift in the planet cross-over indication given at the time when the signal crosses the threshold on the leading and trailing edges of the planet pulse. This error occurs even if the detector-preamp time constant is much less than the horizon cross-over time for the finite field of view. Figure 4 also shows that an additional asymmetric phase shift error (whose asymmetry is accentuated by the temperature differential at opposite planet limbs) results if the detector-preamp time constant approaches or exceeds the horizon cross-over time (τ_c).

The presence of a cold cloud in the scan path (such as could be the case on the earth or Mars) can cause a large error if its radiance level is low enough to penetrate below the threshold and thus "chop out" a portion of the limit-amplified planet pulse. The resulting sensor error is then equivalent to the angular subtense of the cloud.

The threshold must therefore be set below the lowest dip in the planet pulse caused by a cloud or other cold area on the planet. Since cloud dips on the earth are equivalent to up to 80% of the peak "earth pulse" amplitude, the threshold is usually set at a fixed level equivalent to 10% to 20% of the peak pulse amplitude. If the threshold could always be maintained at 50% of peak amplitude level, the errors due to the detector-preamp time constant could be compensated for by inserting a fixed phase lag into the reference signal. However, this would require the physical elimination of cloud dips for operation.

The elimination by spectral filtering of cloud dips caused by all but extremely high altitude clouds has been theoretically[2] and experimentally[6] evaluated. In this technique, the sensor's spectral region is limited to the atmospheric CO_2 absorption region centered at 15 microns. However, although this technique could result in a "smooth" planet pulse when operated against the earth, there is approximately a 10 to 1 reduction in signal level produced by the resulting decrease

in spectral bandwidth. This results in a corresponding degradation in signal-to-noise ratio and thus affects the safety factor level for sensor operation, which is usually provided to allow for a possible signal-to-noise degradation with time. Furthermore, this technique is not applicable on the moon which has no atmosphere, and on Mars the altitudes of the various types of Martian clouds relative to the absorbing constituents of the Martian atmosphere are not yet clearly established.

We will therefore analyze the effect of these errors of the conical scan sensor on the basis of a 20% threshold level, since this technique is more generally applicable to all planets.

Let us take the following system parameters for a conical scanner such as has been used on the Mercury program.

γ = instantaneous field of view in scan direction = 2°

ϕ = scan cone apex angle = 110°

ω = scan rate = 30 scans per second

It can readily be shown that the horizon cross-over time, τ_c, can be expressed as

$$\tau_c = \frac{\gamma \csc \frac{\phi}{2}}{360 \times \omega} = 226 \text{ microseconds}$$

Since thermistor bolometers have time constants of approximately 2 milliseconds, a treble boost is required in the detector-preamp in order to make the detector-preamp effective time constant (τ_e) equal $\tau_c/2$.

This treble boost amplifies the system noise considerably and results in a practically achievable system peak-signal-to-peak-noise ratio of approximately 4:1 when scanning a 275°K earth. Based on experimental data, this signal-to-noise ratio results in a random error at the sensor output of approximately ±1/4°.

The phase lag in the planet pulse is approximately equal to $\tau_c/2$ or 1.2° and can be compensated out if it is the same on both the leading and trailing planet pulse edges. However, for the planet radiance profile and threshold setting shown in Figure 4, which would be the case if the sensor were scanning Mars, a phase shift difference of 1.2° occurs between the leading and trailing edges. Since this phase shift is averaged between the two edges, the resulting angular bias error is 0.6°.

This random error can be reduced by increasing the optical aperture and thus increasing the signal-to-noise ratio. The phase lag error can be reduced by reducing τ_e/τ_c. This can be accomplished by reducing ϕ, ω, or increasing γ all of which serve to increase τ_c. An increase in γ will, in addition, increase signal-to-noise ratio, but this may not necessarily improve the random error since the input ramp function produced by the horizon cross-over will subtend a larger angle.

We have dealt so far with a simple conical scan system. The errors discussed above can be reduced by using a different conical scan mode. An example of this is the four-leaved rosette scanner.[5] In this scanner, which was designed for planetary approaches to Mars and Venus, the IR detector's instantaneous field of view alternately sweeps forward and backward across the planet. This serves to cancel out the sensor errors due to asymmetric planet temperatures to at least a first order.

As is discussed previously, the dynamic range in infrared radiance between the hot side and the cold side of the moon is of the order of 100:1. This dynamic range can be reduced to 30:1 by setting the system's spectral response so that it is sensitive only above 15 microns. However, even for this improvement, in order to sense the 120°K cold side of the moon in its first or last quarter, the pulse threshold level would have to be set at less than 3% of the maximum planet pulse amplitude, and the sensor error produced by lunar temperature asymmetries would increase exponentially. Therefore, a simple conical scan horizon sensor using normal signal processing is not directly applicable for lunar operation if both the cold and hot side of the moon are to be simultaneously sensed. For the lunar case, a different scanning method is desirable in order to eliminate the "trailing edge error." This would involve the design of a scan which always entered the planet from space, or a so-called "space scan." Since this type of scan inherently eliminates the trailing edge of the planet pulse, the errors produced by planet temperature asymmetries can be greatly reduced. An all-electronic conical scan horizon sensor which uses this "space scan" principle is analyzed in the following section.

Electronic Scanning Sensor A conical scanning system which uses no moving parts is under development. This system uses a newly developed, solid-backed, vacuum-deposited thermopile[7] combined with a photomodulator technique.

In this sensor, several thermopiles are arranged in a closely adjacent array situated at the focus of an optical system. As is shown in Figure 5, when this array brackets the horizon edge, the thermopiles viewing the planet below the horizon will produce a higher d.c. signal than those viewing cold space above the horizon. The sequential closing of a light souce illuminated cadmium selenide photoconductive switch connected in series with each of these thermopiles thus effectively samples the signal output of each thermopile at the detector level. This effectively causes an instantaneous field of view defined by each thermopile to be scanned in space (in step function movements) by all-electronic means. Such a configuration has been mechanized in a breadboard model. This model consists of five linear thermopiles situated at the focus of a collecting mirror. These thermopiles are sequentially sampled by cadmium selenide photoconductors operated by ring-counter-driven neon bulbs as shown in Figure 6. By increasing the number of thermopile detectors, it can readily be seen that relatively large fields can thus be electronically scanned with an angular resolution determined by thermopile size and spacing. Work is presently being conducted on an all-electronic, wide-angle sensor with 50 or more thermopiles in

each of four optical heads situated 90° apart in azimuth. In this system, the instantaneous field of view in each optical head is scanned inwardly from space to the planet surface, thus achieving a "space scan."

A transfer function indicative of null axis angular displacement from a planet local vertical is obtained in this system by sensing the phase of the first horizon intersection (or positive-going signal) in each optical head.

Since the output of each thermopile in the array is sampled in a step function manner, the transfer function output of this type of scanner takes the form of a staircase versus angular deviation. This transfer function can be smoothed out by using an analog interpolation technique which senses the magnitude as well as the presence of the signal in each thermopile. By making a radiometric comparison between the signals present in the thermopile straddling the horizon edge and its adjacent thermopiles which are respectively fully above and fully below the horizon, a smooth transfer function can be produced.

By minimizing the elevation angular subtense of each thermopile in the array, the accuracy of the sensor is inherently limited only by the system sensitivity to the infrared radiance of the various planets.

The thermopile signal (e_t) generated in such a sensor for the coldest planet, namely, the 120°K dark side of the moon, can be computed for a typical sensor configuration using the following assumed system parameters. It can be shown that:

$$e_t = \frac{\pi}{4} \frac{\Re \eta}{(f)^2} N_\lambda \qquad (1)$$

where

$\Re$ = thermopile responsivity. Assuming a 2-inch focal length f/1 optical system, a linear array of 20 thermocouples can subtend 10° x .1°, thus making up one thermopile detector. Such a thermopile can provide a responsivity of .05 volts/watt-cm^2.

η = optical efficiency. Assuming a silicon window with the 15 micron cut-on, long-pass interference filter having a 70% average transmission between 15 - 40 microns, a 15% optical obscuration, and a 98.5% reflectivity for the gold-plated collecting mirror, the net optical efficiency is 0.58.

f = system f/number = 1

N_λ = radiance of a 120°K black body located within the 15 - 40 micron band, except for the 16 - 18 micron silicon absorption band = 1.9×10^{-4} watts/cm^2-steer

$\therefore$ e_t = 5.2 microvolts

The error sources discussed in the previous section also affect the accuracy of this type of sensor but to a degree limited by the elevation subtense of the elemental thermopile. In other words, for a 1.0° elevation subtense in the worst case of a 30:1 hot/cold radiance ratio for opposite planet horizons, it can readily be shown that the maximum error that can accrue is equivalent to one-half of the 1.0° elevation resolution.

The limiting case for these errors occurs when the noise level caused by either the peak Johnson noise level of the scanning circuitry or a "noise" voltage generated by random responsivity differences along the thermopile array. If a combination of these noise sources exceeds the threshold set for the horizon signal and this threshold is exceeded while the system is scanning cold space, an undesirable large error can result. For thermopiles viewing a space background, a relatively high quiescent d.c. level exists at their output. The quiescent d.c. voltage in a thermopile viewing a complete space background in the foregoing sensor can be obtained by evaluating equation (1) in essentially a "backward" direction. In other words, while we normally assume that the thermopile sees a hotter object than its ambient temperature, in this case the active thermopile junctions effectively see a background close to absolute zero through the optics. Therefore, for a 300°K ambient, since radiation interchange is bidirectional, the thermopile signal will be approximately equivalent to that obtained if its ambient were 0°K and it was seeing a 300°K extended source. Under these considerations, the thermopile output signal for the above sensor when viewing only space will be given by:

$$e_t = \frac{\pi}{4} \frac{\Re \eta}{f^2} \left(N_\lambda(0°K) - N_\lambda(300°K)\right)$$

where

N_λ (300°K) = the radiance equivalent to a 300°K black body within the 15 to 40 micron region

$\therefore$ e_t (quiescent) = -140 microvolts

It is quite difficult to closely match the responsivities of the relatively large number of thermopiles used in this type of sensor. Therefore, a 10% responsivity variance along the array would be intolerable considering the 5.2 microvolt signal generated by the cold edge of the moon. However, this thermopile quiescent voltage can be greatly reduced by using a radiative temperature offset technique which involves the mounting of a controlled heat source in the optical aperture. This heat source equally irradiates and "heats up" all of the active junctions in the array of thermopiles. The thermopile having the highest elevation angle in each optical head always sees space; it is thus used as a reference to control the output of the heat source so as to insure that all of the active junctions in the thermopile array closely approximate ambient temperature. With this closed loop radiative temperature offset, a 1 microvolt residual quiescent d.c. level is considered obtainable. Under these considerations, a 10% responsivity variance would produce a peak-to-peak noise of only 0.1 microvolt.

The Johnson noise of this system is primarily a function of the impedance of a closed photoconductive switch rather than the thermopile impedance. This is true since each pair of thermocouple junctions in the thermopile has an impedance of approximately 1 ohm, such that each elemental thermopile would then have an impedance of only 20 ohms. The lowest short circuit impedances of currently available cadmium selenide photoconductors are of the order of 500 ohms. Therefore, the effective Johnson noise generated in the scanning circuitry will be equivalent to that of a 500-ohm resistor. Assuming a 100-cycle noise bandwidth, this would be equivalent to a peak-to-peak Johnson noise of 0.15 microvolts.

Under these considerations if this Johnson noise level operation can be achieved, an excellent signal-to-noise ratio would result, and an accuracy on the moon of ±0.5° would be achievable. However, a problem area is presently being encountered in obtaining an adequate noise level reduction of the preamplifier input stage, thus making the system amplifier-noise limited. In addition, dynamic short circuit impedances of 500 ohms have not as yet been achieved for high-speed cadmium selenide photoconductors. Improvements in these areas are being investigated, and it is felt that accuracies of better than ±0.5° will ultimately be achieved against the moon.

Edge Tracking Horizon Sensors

In this horizon sensing technique, an infrared detector's instantaneous field of view is caused to oscillate in space about a horizon edge, thus providing tracking signals which can servo the orientation of the center of the oscillating scan, such that it points at the horizon edge. The errors produced in these sensors are subject to errors produced by their signal-to-noise ratio, servo errors, and angular readout problems. These sensors also have a problem caused by clouds or other intensity structure on the planet surface. For a given optical system and spectral bandwidth, the edge tracking sensor has an inherent advantage in signal-to-noise ratio over the conical scan sensor, since its scan moves through relatively small spatial angles such that its horizon cross-over time at a given scanning repetition rate is much lower than for the conical scan sensor. This reduces the required electrical bandwidth, thus reducing the system noise level. The effect of other factors such as detector-preamp time constant are also commensurately reduced due to the slower horizon cross-over time. These sensors usually require an acquisition mode in which the horizon edge is searched for. After acquisition, the angle to each horizon is read out by a servo resolver of some type. The angular accuracy of this resolver therefore must be factored into the accuracy of the entire sensor, and precise analog voltages for energizing these resolvers are usually required.

The edge tracking sensor also has an accuracy problem resulting from clouds or other temperature discontinuities on the planet surface. This comes about since this sensor tracks on the a.c. signal produced by viewing a temperature differential during its scan. Since the infrared detector must be capacity coupled to the preamplifier, the sensor cannot inherently discriminate between a temperature difference of 0°K to 200°K and a temperature difference of 200°K to 300°K. Furthermore, since the radiant emittance of a black body varies with the fourth power of its absolute temperature, the signal produced by a temperature difference of 200°K to 300°K is approximately four times that produced by a 0°K to 200°K temperature differential. (This can be related to a similar cloud condition in the conical scan sensor in which the detector signal can dip to a level equivalent to 20% of peak planet pulse amplitude.) Therefore, unless some absolute radiometric reference equivalent to the essentially 0°K of space is provided in the edge tracking sensor, this sensor could falsely lock on to cloud edges below the horizon and thus produce large errors.

By limiting the sensor's spectral response to the 14 to 16 micron atmospheric CO_2 absorption region, the effect of clouds could be minimized to a great extent if the sensor is to be used on earth. However, as is discussed previously, this technique is not applicable for operation against the moon which has no significant atmosphere or against Mars where this spectral cloud elimination is not as clearly defined. Therefore, unless some special techniques are inserted into the edge tracking concept, this sensor is not considered directly applicable for use on the moon or Mars.

If there is no cloud edge problem such as would be the case on Venus, the accuracy of this sensor is defined by the resolver-type readout usually required to define the elevation angle of the tracking axis in each optical head and the signal-to-noise ratio in the tracking loop.

The signal-to-noise ratio in the tracking loop can be related to the corresponding value in the conical scan sensor for the same optical parameters on the basis of the major reduction in electrical bandwidth required due to the slower horizon cross-over time. This can be shown by the following numerical example.

Assuming a ± 2° edge tracking scan at a 30-cycle rate, the horizon cross-over time for a 2° field of view in the scan direction is 5.5 milliseconds. Since this is a factor of 50 times lower than the corresponding value for the conical scan sensor, the required electrical bandwidth is also reduced by this factor. This major reduction eliminates the requirement for treble boost in the preamp since the 2 millisecond thermistor time constant is entirely adequate to minimize the phase lag in the horizon cross-over signal. The effective noise reduction which normally varies as the square root of the bandwidth is greater in this case because of the treble boost. Therefore, the 50:1 electrical bandwidth reduction results in a 30:1 reduction in the system noise level.

Quantitatively relating this to the conical scan sensor performance, it can be stated that an edge tracking sensor having the same optical parameters as a conical scan sensor will have a peak-signal-to-peak-noise ratio in the tracking loop of approximately 120:1 when viewing a 275°K planet. However, because of the aforementioned problem of false lock-ons on cloud edges, it is desirable to limit the sensor's

spectral region to the atmospheric CO_2 absorption band. This spectral limitation results in a reduction in signal of approximately 10:1. A further reduction in signal is produced due to the fact that since the earth, when viewed in the CO_2 band, is much colder[2] than 275 °K, thus resulting in approximately another factor of two in signal degradation. The net result of this is that an edge tracking sensor operating in the atmospheric CO_2 absorption region would probably have a peak-signal-to-peak noise ratio of approximately 6:1 which is of the same order of magnitude as that obtained in the conical scan sensor. The random accuracy of the two sensors when operated against the earth is thus approximately equivalent for the assumed optical parameters and is equal to ±1/4 °. The edge tracker has the advantage that there is no "trailing edge" error as with the simple conical scan sensor, such that different temperatures at opposite planet limbs do not contribute any significant error when compared with the above random error values. The other error contribution component in the edge tracker is the resolver angular readout. This error component can be held to less than 0.1° by using precision resolvers. Of course, these resolvers usually require precision drive voltages in order to utilize their angular accuracy. If the edge tracking sensor is used against Venus which has no cloud problem the spectral response can be again widened to the equivalent of the simple conical scan sensor, such that with the 234°K Venus cloud temperature the peak-signal-to-peak noise ratio would be approximately 60:1 and the random error would become essentially negligible. Therefore, for operation against Venus, the edge tracking sensor's accuracy is limited only by the resolver readout accuracy.

Radiometric Balance Sensors

The simplest horizon sensors are the radiometric balance types. In this sensor, the planet is optically divided into four quadrants defined by IR detector fields of view. The direction of the planet local vertical is indicated when the infrared radiances seen in opposite sensor fields are equal.

Depending upon the optical configuration, radiometric balance sensors can be used for attitude stabilization of high altitude aircraft, low altitude satellites, or interplanetary vehicles. A nominal dividing point between the various optical configurations occurs at a planet altitude of approximately 1000 miles. We will analyze the errors in a typical radiometric balance sensor designed for operation at planet altitudes above 1000 miles.

As shown in Figure 7, the optical configuration of this sensor design consists of a single unit casting made up of four cone optics set in quadrature. At the apex of each cone, a 20-element thermopile detector of the vacuum-deposited type[7] collects planet radiation that enters the cone's 35° diameter circular field of view. The cone axes are set at such an angle that the fields of opposite cones bisect the planet as shown in Figure 3C. The amount of field overlap desirable depends upon the altitude range for which the sensor is designed. In this design a 4° field overlap was chosen.

The signal outputs of opposite thermopiles are bucked out, and the difference is proportional to the angular deviation of the sensor from the local vertical.

This four-cone structure incorporates all of the sensor optical components in one compact unit. This is important since the whole system concept is based on a radiometric energy comparison. Uniform temperature of the optical surfaces seen by opposite thermopiles must be closely maintained or an angular error will result as will be discussed later.

A protective outer shell designed for minimum radiation interchange between it and the cones is also provided. It will be noted that all the detectors view the planet through a single silicon window. If two or four windows, situated at different angles to the sun, were used, each window could be differentially heated by the sun; and the resulting differential self-emission seen by opposite detectors could cause a sensor error. This window is also the spectral filter and is coated for transmission above 15 microns with an interference filter that has recently been developed by Optical Coating Laboratories, Inc. Since silicon transmits in the far infrared to beyond 100 microns, the system long wavelength spectral response will be limited only by the absorptivity of the thermopile's black coating. For small window thicknesses, the only silicon absorption band occurs between 16 and 18 microns. Therefore, a 15 to 40 micron bandpass (except for 16 to 18 microns) can be assumed.

The specific thermopile configuration used in this sensor is a circular array of thermocouple junctions as shown in Figure 8. Thermopiles of this type were fabricated and mounted in a breadboard model. These 20-element detectors exhibited a responsivity of 0.06 volts/watt/cm^2.

In this sensor, the pitch and roll signals are obtained by photomodulating and amplifying the differential d.c. thermopile signal which is proportional to the vehicle attitude and is obtained from a pair of thermopiles viewing opposite planet quadrants. The photomodulator consists of two cadmium selenide photoswitches illuminated by neon bulbs. By opening and closing these photoswitches, the microvolt level d.c. signal of the thermopile is thus electronically chopped and can be amplified with normal a.c. amplifiers. Through the use of this thermopile-photomodulator technique, no moving parts are required in this sensor.

In order to determine the accuracy potential of this radiometric balance sensor, a theoretical error analysis was conducted in which possible sources of error were examined and values for these errors, based to a large extent on experimental results, were assigned. The major sources of possible error are the following:

(1) Errors due to temperature differences in opposite planet quadrants - ϵ_1

(2) Errors due to drift in the thermopile signal modulator combination - ϵ_2

(3) Errors due to the sun in one field of the planet sensor - ϵ_3

(4) Errors due to responsivity differences in opposite thermopiles - ϵ_4

(5) Errors due to ambient temperature gradients in the optics seen by opposite thermopile detectors - ϵ_5

ϵ_1 - Errors due to Different Temperatures in Opposite Planet Quadrants These errors are due to a temperature gradient on the planet surface viewed by the sensor. These gradients can be caused by seasons, cloud cover, day-night differentials, etc. The magnitude of this effect depends on the specific planet viewed and the spectral interval of the sensor. As discussed previously, the planets in consideration emit infrared radiation equivalent to black body temperatures between 120°K and 300°K. Two basic approaches are open to the designer in the choice of a spectral interval so as to minimize the value of ϵ_1.

(1) Specify a spectral interval for the sensor located within a strong atmospheric absorption band (if the planet has an atmosphere) such that wide temperature extremes on the planet surface and those due to cloud cover are not seen by the sensor. An example of this is the atmospheric CO_2 absorption band on the earth centered at 15 microns.

(2) Set the system spectral response to wavelengths higher than the planet black body curve peak wavelength so that the planet radiance varies as a lower power of temperature.

The choice between these two approaches is based on a trade-off between the resulting value for ϵ_1 and other errors which are a function of the sensor's sensitivity. For example, if the CO_2 absorption region between 14.5 and 15.5 microns is used as in (1) above, the value of ϵ_1 can be expected to be minimized for an earth sensor, but due to the reduced spectral interval, a much lower signal is generated in the sensor per degree of tilt than would be the case if the sensor responded to a wide band of wavelengths above 15 microns. Therefore, the values of the other errors not related to system spectral response will be equivalent to larger angular offsets due to this reduction in transfer function scale factor.

Since the latter of the above spectral response characteristics is more generally applicable to all the planets, this radiometric balance sensor will be analyzed on the basis of a 15 to 40 micron spectral bandpass.

For this sensor configuration, the ϵ_1 values are a function of: (a) different infrared radiance ratios between opposite planet quadrants and (b) the altitude. The determination of these ϵ_1 values required the derivation of an equation for the areas of the planet seen in each thermopile's field as defined by the intersecting circles of Figure 3C. This equation was programmed on an LGP-30 computer and a family of error curves were computed. Planet subtense angles were varied from 10° to 40°, and opposite quadrant planet radiance ratios of 1.05:1, 1.2:1, 3:1, and 50:1 were assumed for Venus, earth, Mars, and the moon respectively. The resulting values of ϵ_1 for these planets are shown plotted vs. planet subtense angle in Figure 9 for comparison with other errors of this sensor.

For constant altitude operation, by using the orientation of the four-cone optics field of view as shown in Figure 10, the ϵ_1 error can be greatly reduced. In this configuration, the entire planet is seen by each detector such that temperature gradients on the planet surface do not contribute to null error. The effect of temperature differences at opposite planet limbs in this configuration would result in the asymmetric transfer function shown in Figure 10, but the ϵ_1 error at null would be essentially zero. However, it must be remembered that this configuration is for the special case of a circular orbit or for operation at one predesignated altitude in an approach trajectory. Above this predesignated altitude, the transfer function has a dead zone at null, and below this altitude, the transfer function has a double slope at null which may be intolerable for servo characteristics.

ϵ_2 - Errors due to Drift in the Thermopile-Photomodulator Combination This error can be computed as the angular equivalent to the measured drifts experienced with thermopile-photomodulator combinations.

The drift characteristics of a thermopile-photomodulator combination and a photomodulator by itself have been tested over an ambient temperature range for periods of several days using a continuously running chart recorder.

A circular detector-photomodulator combination, such as the one used in this sensor configuration, was tested over a 3-day period at laboratory ambient (which varied ±7°C over the measurement period). The total recorded drift was ±0.25 microvolts. Another thermopile-photomodulator test was conducted in a temperature chamber which was varied between +50°C and -25°C. Over this range at various soak temperatures, an offset of 0.5 microvolts with a variance of ±0.25 microvolts was measured.

The drift of the photomodulator alone, with a simulated thermopile input, was also tested at ambient temperature extremes of -56°C and +65°C. Only ±0.1 microvolt drift was experienced in these tests, showing that the photomodulator apparently contributes only a very small amount to the total system drift.

In view of the foregoing preliminary test data, it is expected that over a reasonable ambient temperature range in the space vacuum environment, a long-term drift of less than ±1 microvolt will be achievable with careful thermal design. We will now compute the angular error equivalent to this ±1 microvolt drift as follows.

An LGP-30 computation of this thermopile scale factor for various planet subtense angles was conducted using the equation derived for ϵ_1, and the resulting scale factor expressed in square degrees was converted to a thermopile output signal as shown by the following sample calculation.

Assuming a 250°K planet, its radiance in the 15 to 40 micron region ($N\lambda$) equals approximately 3.5×10^{-3} watts/cm^2/steradian.

For a 40° planet subtense, a 1° deviation from null produces a differential signal in a pair of opposite thermopiles equivalent to a planet solid angle (Ω) of 67.4 square degrees or approximately 2.04×10^{-2} steradians. The resulting differential irradiance (ΔH) at the sensor is given by:

$$\Delta H = N\lambda$$

$\Delta H = 7 \times 10^{-5}$ watts/cm^2 per angular degree of tilt from null.

The detector area magnification produced by the cone condenser has been discussed in the literature by Williamson[8] and Hanel.[9] As can be seen in Figure 11, the optical gain of a cone collector can be expressed as:

$$M = \frac{\rho R_1^2}{R_d^2}$$

$$M = \rho \csc^2 \left(\frac{\theta}{2}\right) \qquad (2)$$

where

ρ = reflective efficiency of the cone which is an integral function of: (a) the number of reflections of an optical ray bundle within the cone before it reaches the detector, (b) the area of the bundle, and (c) the reflectivity of the cone surface.

R_1 = distance from the cone apex to the truncation where the detector is mounted, or radius of the image polygon.

R_d = radius of the detector

θ = apex angle of the cone collector

Evaluating equation (2) for the assumed optical parameters, $\rho = .9$, $\theta = 35$

$$\therefore \quad M = 10$$

The differential irradiance of the detector H_d is therefore given by:

$$\Delta H_d = M \eta \Delta H$$

where

η = optical efficiency of the spectral filter. Using a thin silicon filter so as to minimize absorption, it is expected that an average transmission efficiency of 0.7 can be achieved in the 15 to 40 micron region. Due to the strong silicon absorption band between 16 to 18 microns which eliminates 20% of the radiance of a 250°K black body in the 15 to 40 micron region, the net filter efficiency will thus be approximately 0.7 x 0.8 or

$\eta = 0.56$

$$H_d = 3.9 \times 10^{-4} \text{ watts/cm}^2$$

The circular 20-element thermopile used in this sensor configuration has demonstrated a responsivity of 0.06 volts/watt/cm^2. The differential output voltage (e_t) of a pair of opposite thermopiles is:

$$e_t = 0.06 \times 3.9 \times 10^{-4}$$

e_t = 23 microvolts per angular degree of tilt from null

Therefore, at this planet altitude, a ±1 microvolt thermopile-photomodulator drift would be equivalent to a ϵ_2 value of ±0.045°.

A curve showing values of ϵ_2 versus planet subtense angle for earth, Venus, and dark Mars is shown in Figure 9 to obtain a comparison between the various sensor error magnitudes.

ϵ_3 - Errors due to the Sun in One Field of the Planet Sensor This error can be evaluated in a similar manner to that used for ϵ_2.

Between 15 and 40 microns, available data indicate that the sun's radiance approximates that of a 5000°K black body[10] and approximately equals 0.3 watts/cm^2-steradian.[11] The sun subtends approximately 1.16×10^{-4}, 5.9×10^{-5}, and 2.6×10^{-5} steradians, respectively, in the vicinity of Venus, earth, and Mars. The resulting values of ΔH for the sun in one field of the sensor when viewing these planets are respectively 3.5×10^{-5}, 1.8×10^{-5}, and 7.8×10^{-6} watts/cm^2. The remainder of the calculation is the same as for ϵ_2. The resulting values of ϵ_3 for this sensor are plotted in Figure 9 versus subtense angle altitude for these planets.

As can be seen in Figure 9, the value of ϵ_3 increases markedly for smaller subtense planets. This error can be reduced greatly by using four visible-region detectors viewing the same fields as the thermopiles. These detectors would be sensitive only to the sun's energy with negligible input from the planet albedo and would thus produce a signal which could be used to buck out the erroneous input of the sun in the thermopile signal. The inclusion of these visible detectors is usually required only for planet subtenses less than 30°.

ϵ_4 - Errors due to Responsivity Mis-Match in Opposite Thermopiles This error comes about if the responsivity of thermopiles viewing equal radiance opposite planet quadrants is not equal, thus producing a false output signal at the true null. In the sensor described, each thermopile views both the essentially 0°K of space and the planet surface. For small subtense planets, the major part of the thermopile's field of view is taken up by cold space.

For the worst case, where the entire field of the thermopile views cold space, a relatively large quiescent d.c. level exists at each thermopile output, as is discussed in the section describing the electronic scanning sensor.

Since the cone collector is an f/0.5 optical system, evaluating equation (1) "backwards"

for a 300°K ambient yields a thermopile quiescent output of:

$$e_t = \frac{\pi}{4} \frac{.06 \times 0.5}{(0.5)^2} (-6 \times 10^{-3})$$

$$= -560 \text{ microvolts}$$

Since only four thermopiles are involved in this radiometric balance sensor, their responsivities can be matched by trimming in the laboratory so that the only remaining variation would be due to aging. On the basis of responsivity tests of sample thermopiles conducted over a 3-month interval which showed no measurable change in responsivity, aging effects on thermopile responsivity are apparently insignificant.

However, as a safety factor, the compensating technique applied to the electronic scanning sensor involving the mounting of a small heat source in the sensor window can also be used in this sensor to minimize the effect of a possible responsivity mis-match due to aging. On the basis of the above considerations, it is expected that values of θ_4 can be held to less than 1/2° even in the worst case when an extremely small planet is viewed.

θ_5 - Errors due to Ambient Temperature Gradients Seen by Opposite Thermopile Detectors

This error signal will be produced due to radiance differences caused by temperature gradients in the optical surfaces viewed by a pair of opposite thermopiles.

In this sensor configuration, all of the thermopiles look out through approximately the same window area, so that temperature gradients in the window should have negligible effect. The main problem, if any, will come from differential emission by the inner surfaces of the cone optics. The emissivity of the gold-plated cone surface above 15 microns is 1.5%.

Assuming a 300°K ambient, the radiance change (ΔN) for a 1° temperature change at an emissivity of 1.5% is approximately 3×10^{-6} watts/cm^2-steradian, and since the cone optics are situated behind the optical filter, the detectors will see all of this radiation.

Since the thermopile sees the cone optic over a solid angle (Ω) of approximately 2.5 steradians, if opposite cones have temperatures different by 1°C, it can readily be shown that the differential thermopile signal will be:

$$e_t = \mathcal{R} \times \Delta N \times \Omega$$

$$e_t = \pm 0.45 \text{ microvolts}$$

For a 250°K, 40° subtense planet, which produces a thermopile scale factor of 24 microvolts per angular degree, ±0.45 microvolts would be equivalent to an θ_5 value of only ±0.019°.

Let us now thermally analyze this sensor design on a preliminary basis to determine the maximum temperature difference expected in opposite thermopile optics.

As can be seen in Figure 7, the four-cone optical assembly is a single aluminum casting conductively isolated from the window and the outer shell of the sensor. The heat dissipation of the electronics is conducted to the outer shell through the connector located on the axis of the cylindrical housing to assure transverse symmetry. The electronics' heat is also conductively transmitted symmetrically to the four-cone optical casting. However, the optic casting is conductively isolated from the shell; and its outer surface as well as the inner shell surface is gold plated with a 98.5% reflectivity in the far infrared region. Therefore, very little of the electronics' heat is radiatively transmitted from the optic casting to the shell, since the casting effectively "sees itself." For the same reason, very little heat from the shell is transmitted to the optic casting due to the 1.5% emissivity of the inner shell surface. Heat, due to solar absorption by the window, cannot directly affect the optic casting since this heat is conductively transmitted to the outer shell and to the vehicle.

Under these considerations, let us take the worst case of asymmetric solar heating of the sensor, in which the sun's rays are impinging normal to the axis of the cylindrical housing and determine the maximum steady state temperature difference (Δt) that can be sustained between opposite surfaces of the cylindrical shell. This can be expressed as:

$$\Delta t = \frac{A_s \, \alpha \, S \, \Delta x}{K \, a_{(shell)}}$$

where

A_s = projected area of shell relative to sun = 130 cm^2

α = solar absorptivity of shell conservatively assumed = 0.5 (usual values of α are 0.05 to 0.1)

S = solar constant = .137 watts/cm^2 (in earth vicinity)

$\Delta x_{(shell)}$ = length of thermally conductive element in shell = 5.5 inches

K = thermal conductivity of aluminum = 100 (Btu-ft/hr-ft^2-°F)

$a_{(shell)}$ = cross-sectional area of conductive heat flow path in shell = 0.0625 x 6 = 0.37 $(in)^2$

Converting to British units and evaluating:

$$t = 55°F = 31°C$$

A Δt of 31°C at an ambient temperature of 300°K is equivalent to a black body emitted radiant flux (W) of approximately 4×10^{-2} watts/cm^2.

Conservatively assuming an active radiation interchange area in the vicinity of each thermopile equal to 10 cm^2 with a 1.5% emissivity

of the gold-plated interior surfaces of the shell, we obtain a radiant power differential in opposite thermopile optics of:

$$P_{(optics)} = 4 \times 10^{-2} \times 10 \times 0.015 = 6 \times 10^{-3} \text{ watts}$$

This is equivalent to a temperature difference in opposite optics, $\Delta t_{(optics)}$, given by:

$$\Delta t_{(optics)} = \frac{P_{(optics)}\, \Delta x_{(optics)}}{K\, a_{(optics)}}$$

$$\Delta t_{(optics)} = .05^{\circ}F = .028^{\circ}C$$

It can therefore be readily seen that even in this worst case θ_5 will be negligible.

Conclusions

This paper has described various configurations of horizon sensors that are in existence or have been discussed in the literature. An error analysis has been conducted for each of these sensor configurations and accuracy values have been assigned relative to the planets Venus, earth, moon, and Mars. A summary of these accuracy capabilities of the various sensors is presented in Table I. It should be noted that the accuracy figures quoted in this table do not take into account the following error sources:

(1) Errors caused by variation in the horizon altitude in planets which have atmospheres.

(2) Errors due to topographic features on the planet.

Both of these error sources have a significant effect only at low planet altitudes (i.e., less than 500 miles). Furthermore, these effects are so complex that they comprise subject matter for another paper.

Acknowledgment

The authors gratefully acknowledge the valuable discussions helpful in the preparation of this paper held with Mr. M. Monty Merlen.

References

[1]Kuiper, G. P. and B. M. Middlehurst (Editors): Planets and Satellites: The Solar System III. University of Chicago Press, 1961.

[2]Hanel, R. A., W. R. Bandeen, and B. J. Conrath: "The Infrared Horizon of the Planet Earth," Journal of the Atmospheric Sciences, Vol. 20, No. 2, pp. 73-86, March, 1963.

[3]Potter, R. F. and W. L. Eisenman: Applied Optics 1, p. 567, 1962.

[4]DeWaard, R. and E. M. Wormser: Proc. IRE, Vol. 47, No. 9, pp. 1508-13, September, 1959.

[5]Wormser, E. M. and M. H. Arck: Proceedings of ARS Guidance Control and Navigation Conference, August 7-9, 1961.

[6]Haynie, W., J. Collinge, and E. P. Ertsgard: "Theory and Measurement of 15 Micron CO_2 Horizon Radiance from a Satellite," to be published in Proceedings of IRIS, May 6, 1963.

[7]Astheimer, R. W. and S. Weiner: "Solid Backed Evaporated Thermopile Radiation Detectors," to be published in Journal of the Optical Society of America.

[8]Williamson, Donald E: "Cone Channel Condenser Optics," Journal of the Optical Society of America, Vol. 42, No. 10, October, 1952.

[9]Hanel, Rudolph A: "A Low Resolution Unchopped Radiometer for Satellites," NASA Technical Note D-485.

[10]Shaw, John H: "The Radiation Environment of Interplanetary Space," Applied Optics, Vol. 1, No. 2, March, 1962.

[11]Pivovonsky, M. and M. Nagel: Tables of Black Body Radiation Functions. The Macmillan Company, 1961.

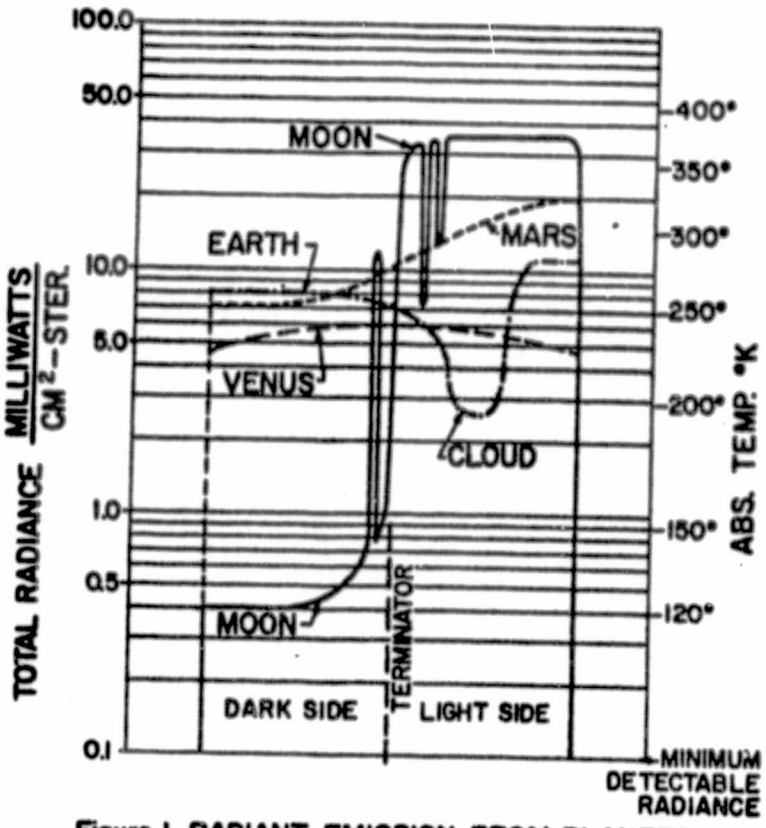

Figure 1 RADIANT EMISSION FROM PLANETS

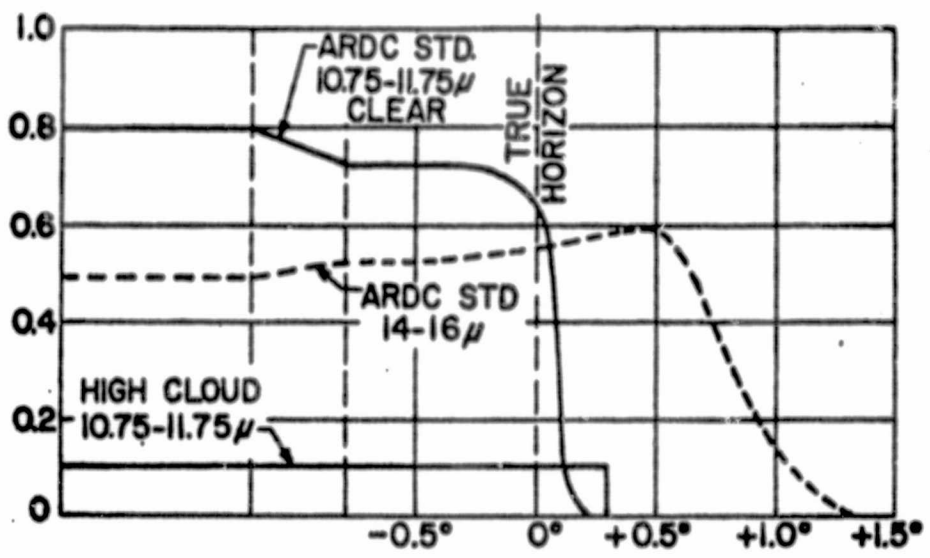

Figure 2 HORIZON GRADIENTS FROM 400 MILE ALTITUDE

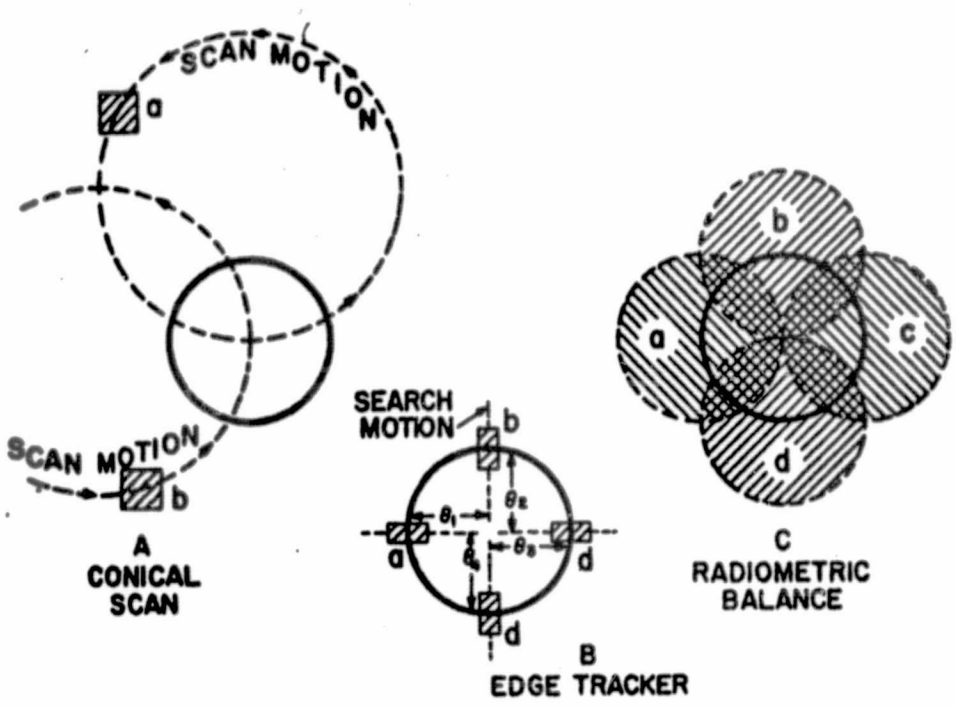

Figure 3 HORIZON SENSING TECHNIQUES

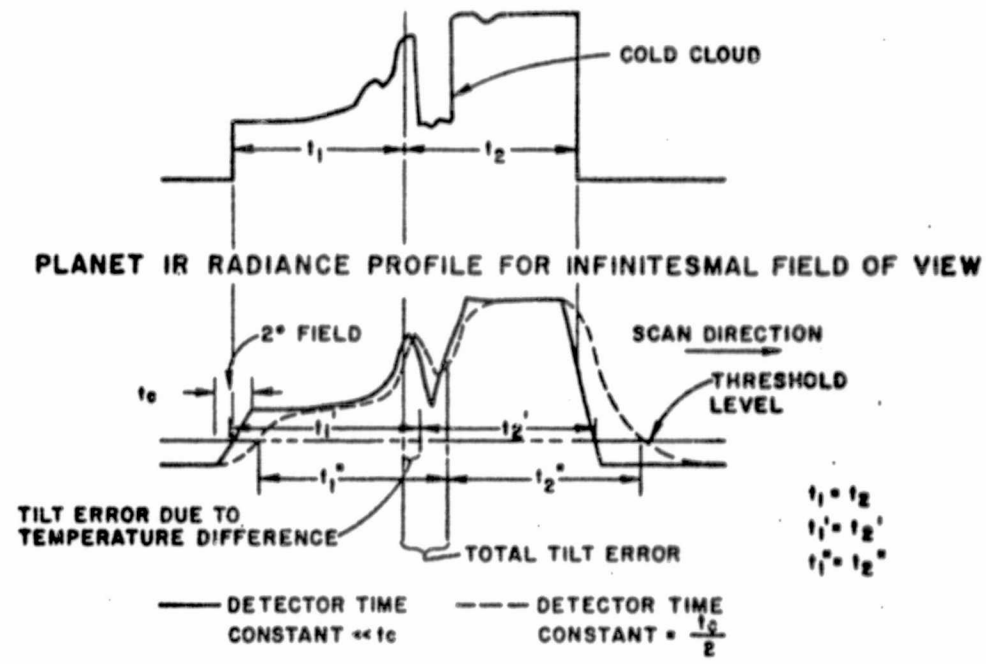

Figure 4 CONICAL SCAN SIGNAL WAVEFORMS

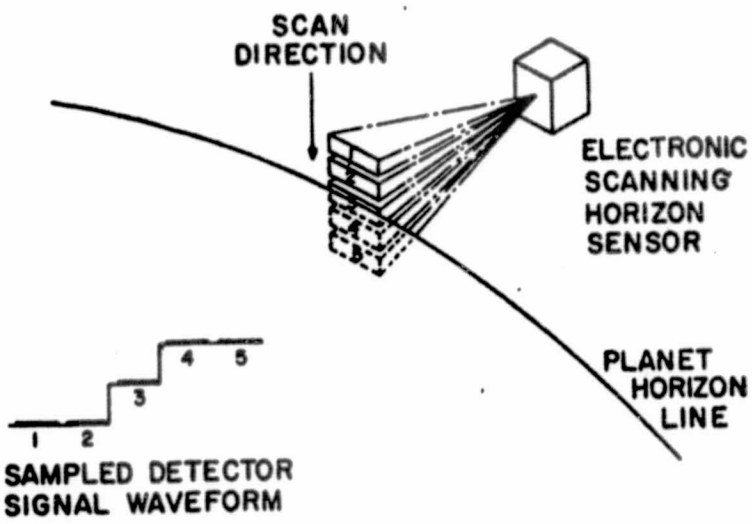

TRACKING SIGNAL GENERATION IN ELECTRONIC SCANNING HORIZON SENSOR

Figure 5

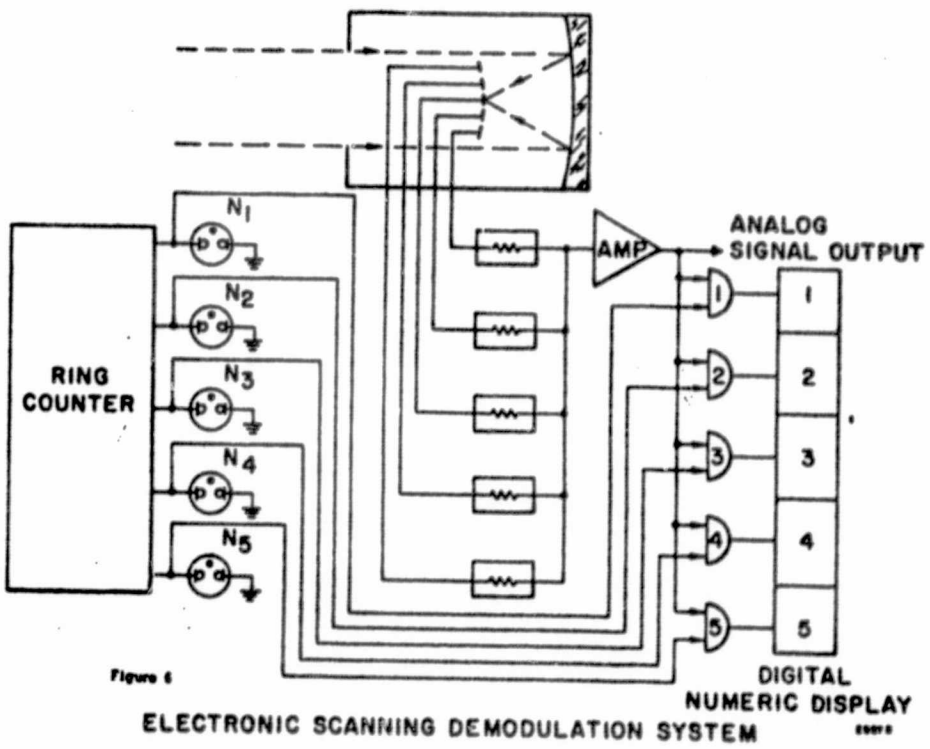

Figure 6

ELECTRONIC SCANNING DEMODULATION SYSTEM

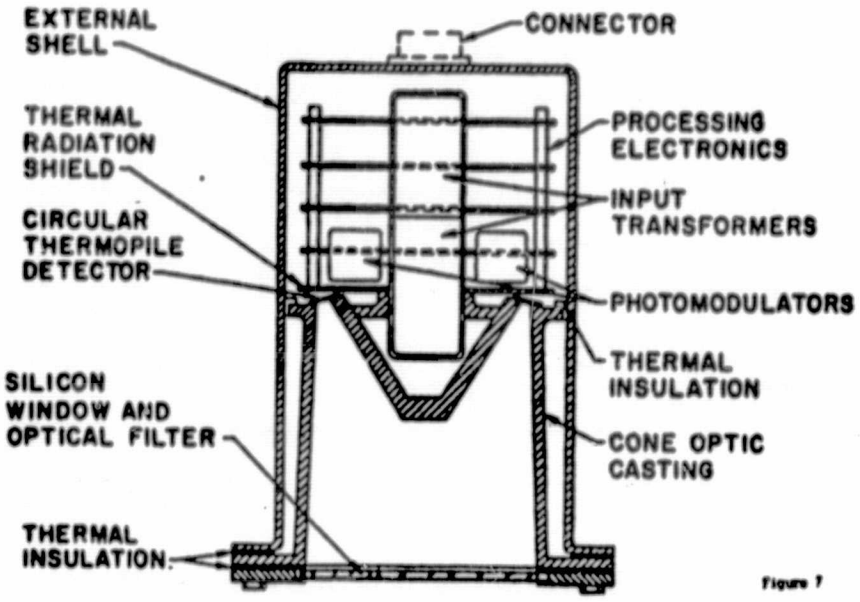

Figure 7

CONE OPTICS RADIOMETRIC BALANCE PLANET SENSOR

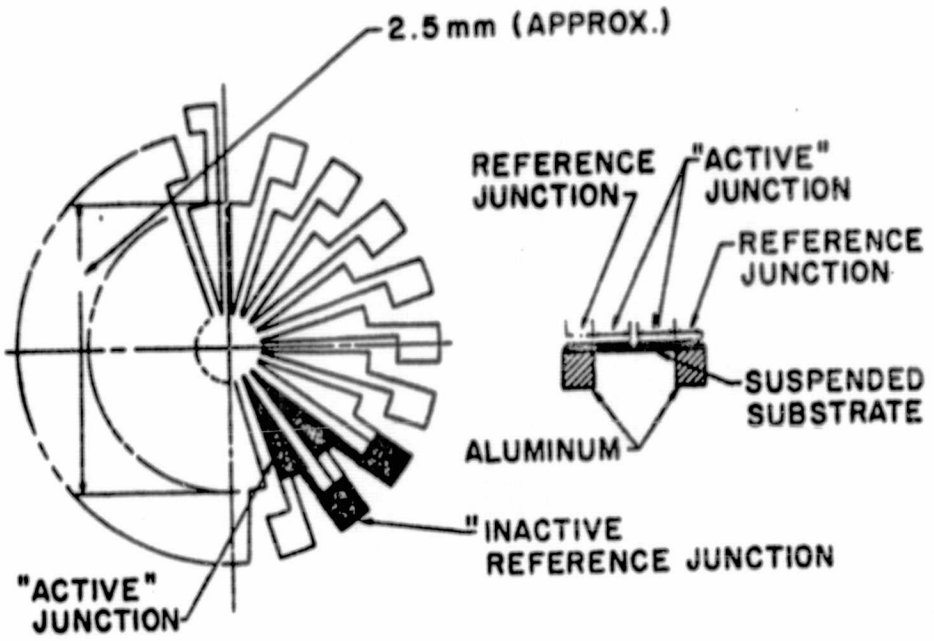

CIRCULAR THERMOPILE DETECTOR

Figure 8

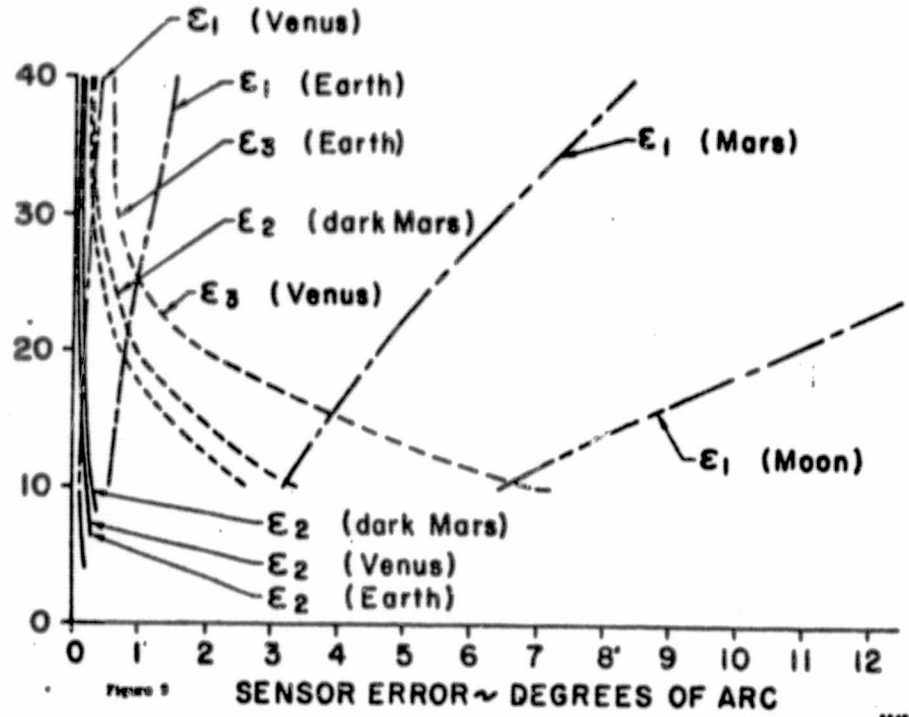

Figure 9

HIGH ALTITUDE SENSOR ERRORS FOR VARIOUS PLANETS

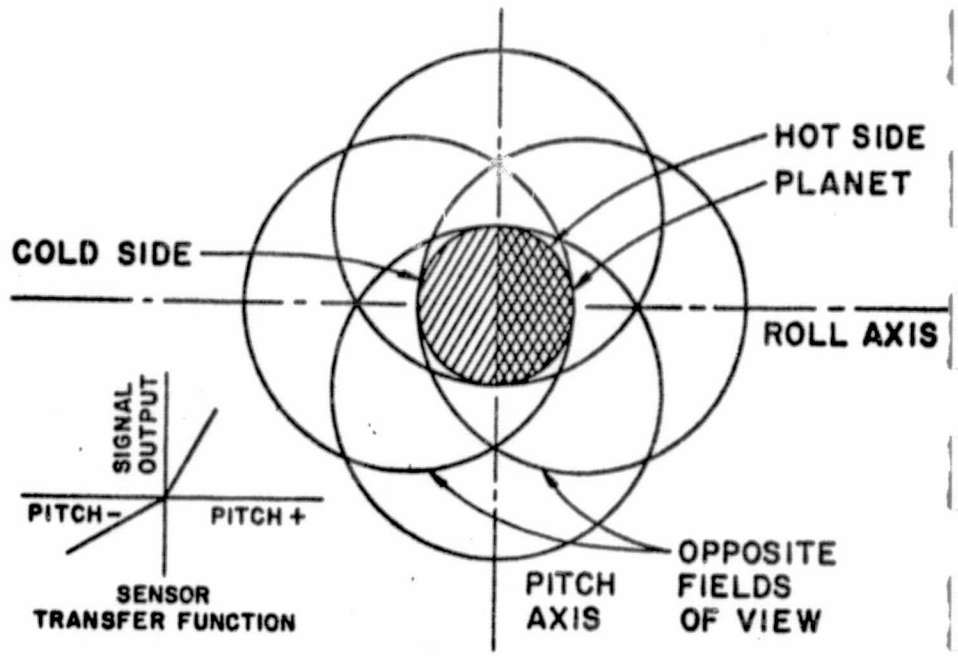

Figure 10

FIELD ARRANGEMENT TO MINIMIZE ε_1

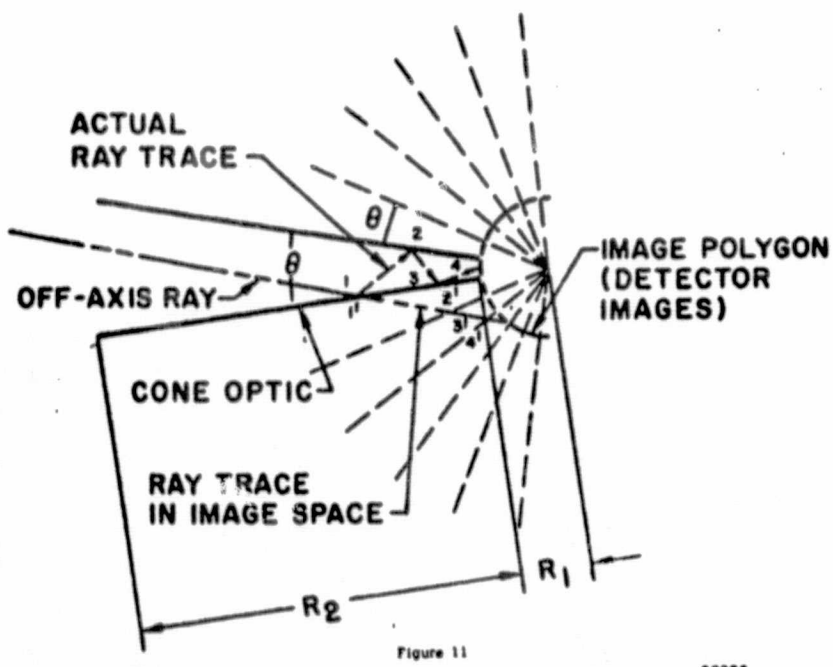

Figure 11

IMAGE POLYGON REPRESENTATION OF CONE

Horizon Sensor Type	Range of Accuracies Against Venus	Range of Accuracies Against Earth	Range of Accuracies Against Mars in First or Last Quarter Phase	Range of Accuracies Against Moon in First or Last Quarter Phase
Conical Scan Sensors				
(a) Simple Conical Scanner	±0.1° to ±0.5°*	±0.2° to ±0.5°*	±0.3° to ±1°*	Requires Elimination of Trailing Edge Error
(b) "Space Scan" Conical Scanner	±0.02° to ±0.1°*	<±0.1°*	±0.1° to ±0.3°*	<±0.5°
Edge Tracker	±0.05° to ±0.1°*	±0.1° to ±0.3°* (Atmospheric CO_2 band used)	Requires means for discrimination of true horizon edge from cloud edges	Requires means for discrimination of true horizon edge from crater edges
Radiometric Balance Sensor	±0.5° to ±2°**	±0.5° to ±2°**	±5° to ±10°**	Not applicable except for very coarse pointing

*Specific achievable accuracy is a function of optical parameters (i.e., size, weight)

**Specific achievable accuracy is a function of planet altitude and degree of sun error compensation used.

TABLE I

High-Accuracy Horizon Sensor Using FIRM

GERALD FALBEL
Barnes Engineering Company, Stamford, Connecticut

ABSTRACT

This paper discusses the design configuration and performance capabilities of a high-accuracy edge tracking horizon sensor operating in the 14- to 16-micron atmospheric CO_2 band. The edge scanning function is achieved without using mechanically moving parts.

At the heart of this horizon sensor system is a Frustrated Internal Reflection Modulator (FIRM) which produces optical modulation of the incoming infrared energy by piezoelectrically varying the spacing between two optical prisms. The history, design, and performance of the basic FIRM cell, which has been developed by Barnes, is discussed. It is concluded that this sensor will provide an accuracy better than ±0.01° in the laboratory and better than ±0.05° against the real earth horizon.

I. BACKGROUND AND DESCRIPTION OF THE FIRM TECHNIQUE

It is well known that if an optical ray within a material whose refractive index is greater than one impinges on a surface of that material at an angle greater than a certain value, depending upon the index, the ray will be totally internally reflected and will not emerge from the optical material. However, if another piece of the same optical material is moved closer than 0.1 wavelength of the aforementioned light ray, the ray will penetrate through the interface, and total internal reflection will be frustrated. The amount of this frustration will be a function of the spacing of the two optical elements. This phenomenon is discussed in greater detail in references 1, 2, and 3.

For the purposes of this paper, we will just briefly describe simple mechanizations of FIRM cells. One such configuration is an ambient chopper indicated in Figure 1. This is composed of two 20° germanium wedges with the interface spacing varied by piezoelectric driving elements. It will be noted in this figure

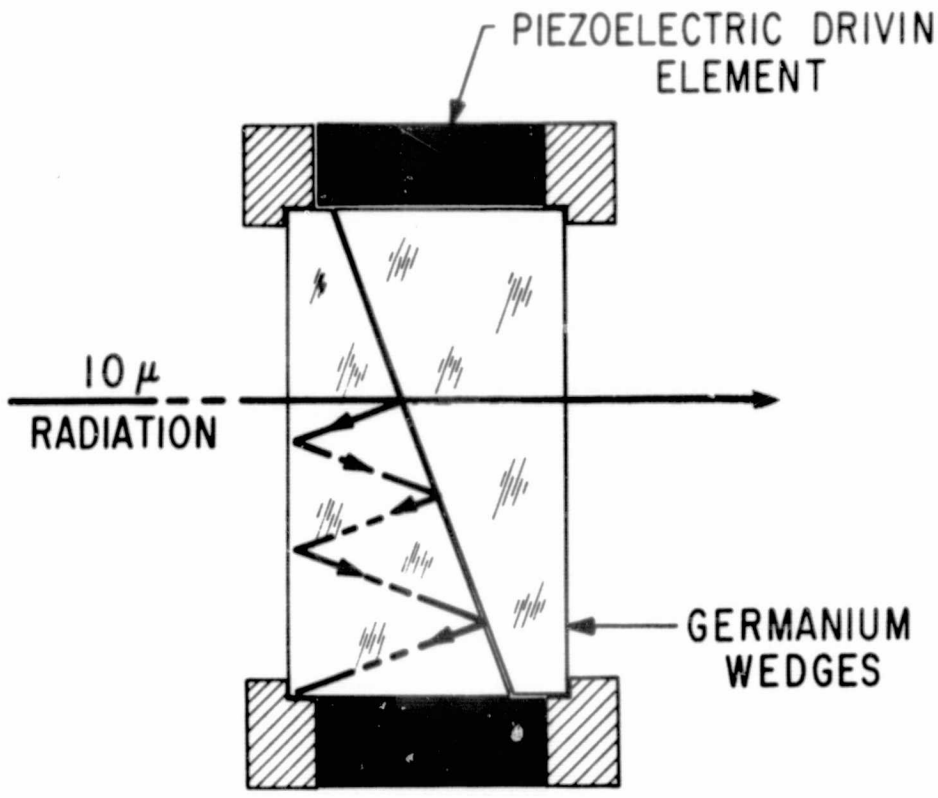

FIGURE 1. "FIRM" AMBIENT CHOPPER

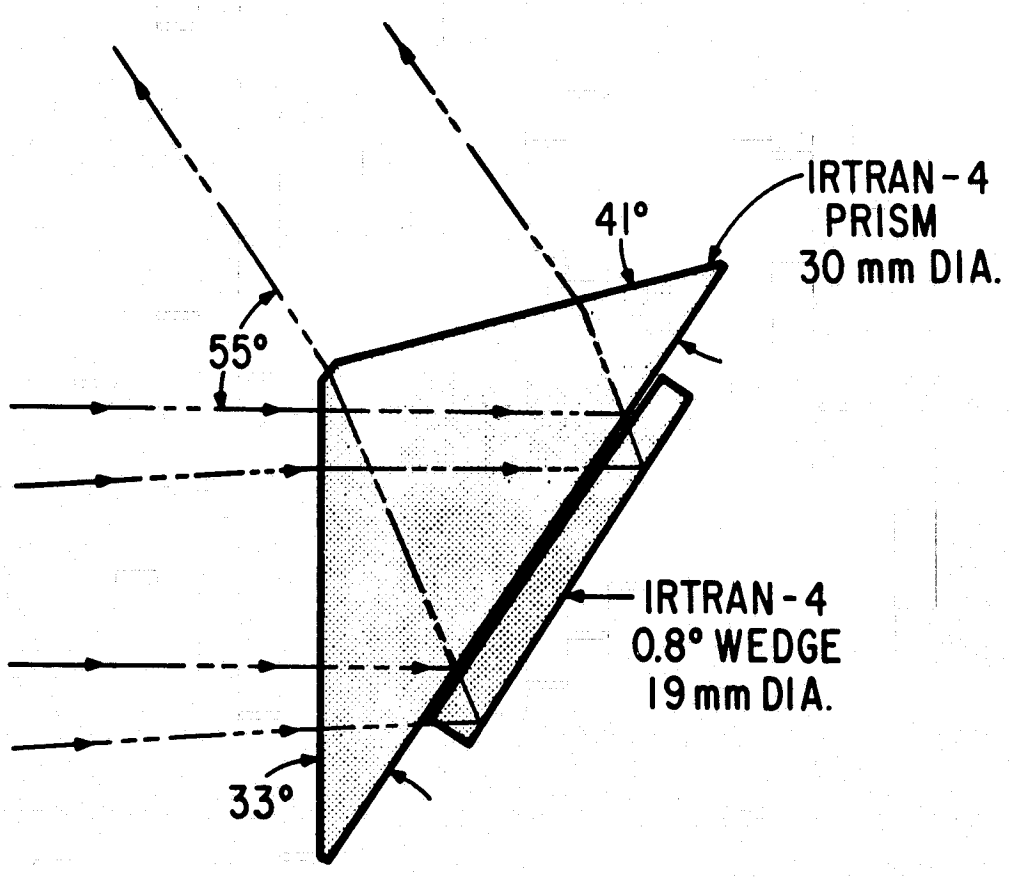

FIGURE 2. FIELD SWITCHING "FIRM" CELL

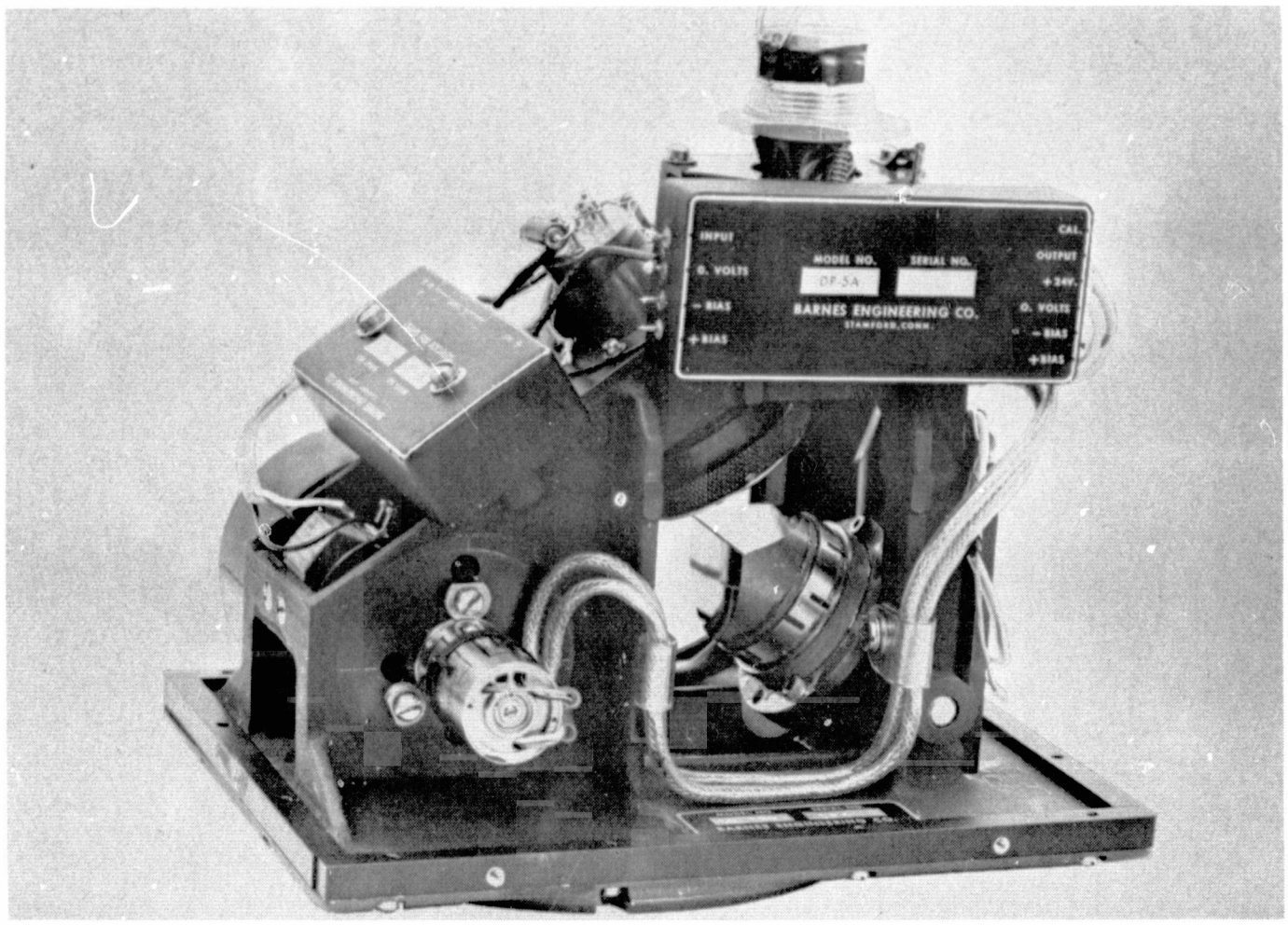

FIGURE 3. FEASIBILITY MODEL, "FIRM" HORIZON SENSOR

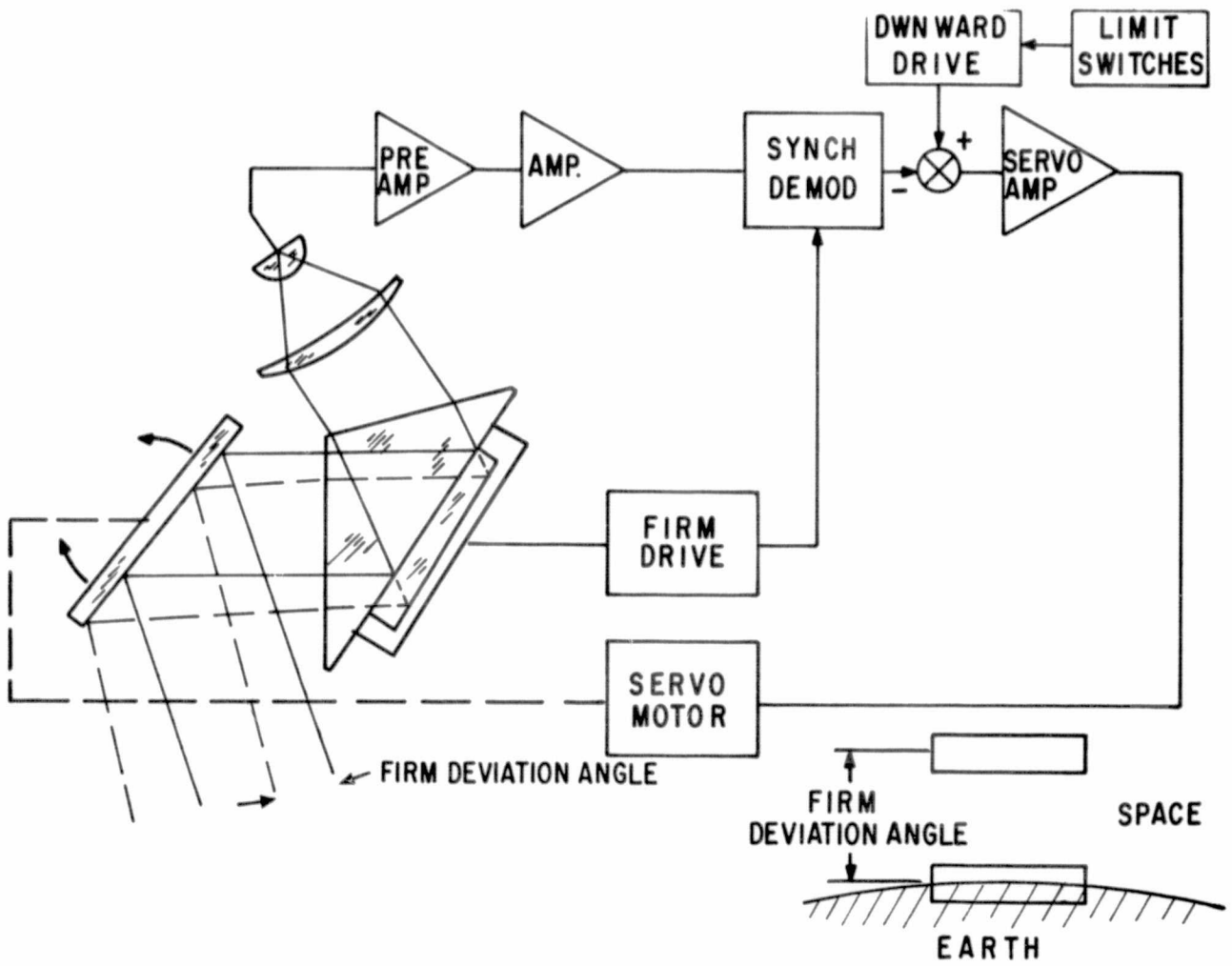

FIGURE 4. SIMPLIFIED "FIRM" HORIZON SENSOR

that 10-micron IR radiation is either allowed to transmit through the interface or is totally internally reflected and trapped within one wedge, depending upon the spacing between the two wedges.

A second unit of more direct interest in the horizon sensor application is a so-called field switching version of the FIRM cell. One configuration of this unit is indicated in Figure 2. In this case, the optical elements consist of a large prism and a small wedge.

In operation, this cell moves the field of view of an infrared detector between two discrete positions in space. The area between these two fields is not viewed. Therefore, this cell is not a scanner but a field of view switching device. This angle between the two fields is controllable by varying the angle of the small wedge shown in Figure 2. If the infrared energy seen in either of the field-of-view positions is equal, no a-c signal will be produced in the detector. Any a-c signal produced will therefore be proportional to the radiance difference between the two field of view positions.

A feasibility model, shown in Figure 3, of a horizon sensor using this field switching FIRM cell was constructed. In this case, the field switching FIRM cell replaced an oscillating mirror scan drive mechanism in an edge-tracking horizon sensor engineering model. The field switching FIRM cell deviated the field of a thermistor over the same 4° angle that it was previously scanned by the oscillating mirror. The basic concept of this feasibility model is indicated in block diagram form in Figure 4.

The horizon was tracked by letting the lower field-of-view position, shown in Figure 4, effectively "bounce" off the horizon edge. In this relatively simple edge-tracking system, a fixed downward drive voltage is applied to the servo, which thus searches for the horizon. When the lower field-of-view intersects the horizon a signal generated in the IR detector serves to buck out the downward drive in the servo and thus produces tracking. Such a system was fabricated. The tracking mirror servo was energized by the thermistor detector output, and rudimentary tracking of the horizon was obtained. A tight tracking loop could not be achieved because of the absence of rate feedback in this horizon sensor model.

Some preliminary environmental testing was conducted with this feasibility model. The ambient temperature was varied between -10° C and +50° C in an attempt to determine the effect of ambient temperature on the modulation efficiency of the FIRM cell. Encouraging results were obtained in this test: it was found that a total modulation variance of only 2:1 over this temperature range was obtained. Even this was a conservative figure since the short-wavelength infrared radiation used in the test is a much stronger function of the interface gap than would be the 14- to 16-micron radiation desirable for use in horizon sensors. The problems attendant to temperature compensation of the FIRM cell are discussed in more detail in reference 3.

This feasibility model was also subjected to a vibration test in two runs. The first of these was at 2 g's peak, 20 to 2000 cps; and the second at 5 g's peak,

20 to 2000 cps. The FIRM chop frequency in each of these runs was 60 cps, and no significant effect was seen in the chopped signal at any frequency in the vibration run, even when the vibration frequency was near 60 cps. The 5 g vibration limit was dictated by the breadboard nature of the horizon sensor rather than by the FIRM cell itself, and it is felt that considerably higher vibration amplitudes could have been applied to the FIRM cell itself. These higher vibration tests are planned for future FIRM units. However, these preliminary tests provided great encouragement insofar as the survival and operation of the FIRM cell in more severe environments is concerned.

II. DESIGN PARAMETERS OF THE HIGH ACCURACY FIRM HORIZON SENSOR

The FIRM horizon sensor that has been designed and fabricated is shown in Figure 5. The major design objectives of this sensor are the following:

(a) Accuracy of ±0.05°, including horizon anomalies;

(b) wide altitude range and tilt range capability;

(c) long life and high reliability operation in a space environment without requiring pressurization;

(d) high output frequency response capability.

In order to achieve a ±0.05° accuracy against the real horizon of the earth, the simple "bouncing" system discussed in the previous section would not suffice. Even in the 14- to 16-micron atmospheric CO_2 absorption band, the seasonal radiance variations that could be produced in opposite earth horizon limbs would result in an error exceeding ±0.1°. In order to achieve an over-all accuracy better than ±0.1°, these horizon radiance variations must be compensated for. In this regard, use was made of the work of Duncan[4] and Hanel[5], who have, on the basis of computer studies, postulated that a spatial horizon edge variance of only 0.05° will result if the radiance variations of opposite horizon limbs are normalized. In order to produce this normalizing function, we must effectively measure the local radiance in the vicinity of the horizon limb being tracked and correct the horizon declination angle in that head accordingly, in this sense performing an AGC function. Through the use of a dual thermistor detector in this horizon sensor, this normalization or AGC function is achieved at the detector itself. This is mechanized in a manner discussed in the following paragraph.

As with the simple "bouncing" horizon sensor system, the instantaneous field of view of the horizon sensor is defined by a thermistor flake. However, instead of using a single active flake, a dual flake, indicated by A and B in Figure 6, is used. This dual flake forms an "active-active" bolometer bridge. A horizon tracking signal is obtained by making the responsivity of the B portion of the dual flake half of the A portion. This is accomplished by inserting a compensating flake in the bridge which reduces the responsivity of the B flake by two. If the FIRM horizon sensor is viewing space in both of its field-of-view positions,

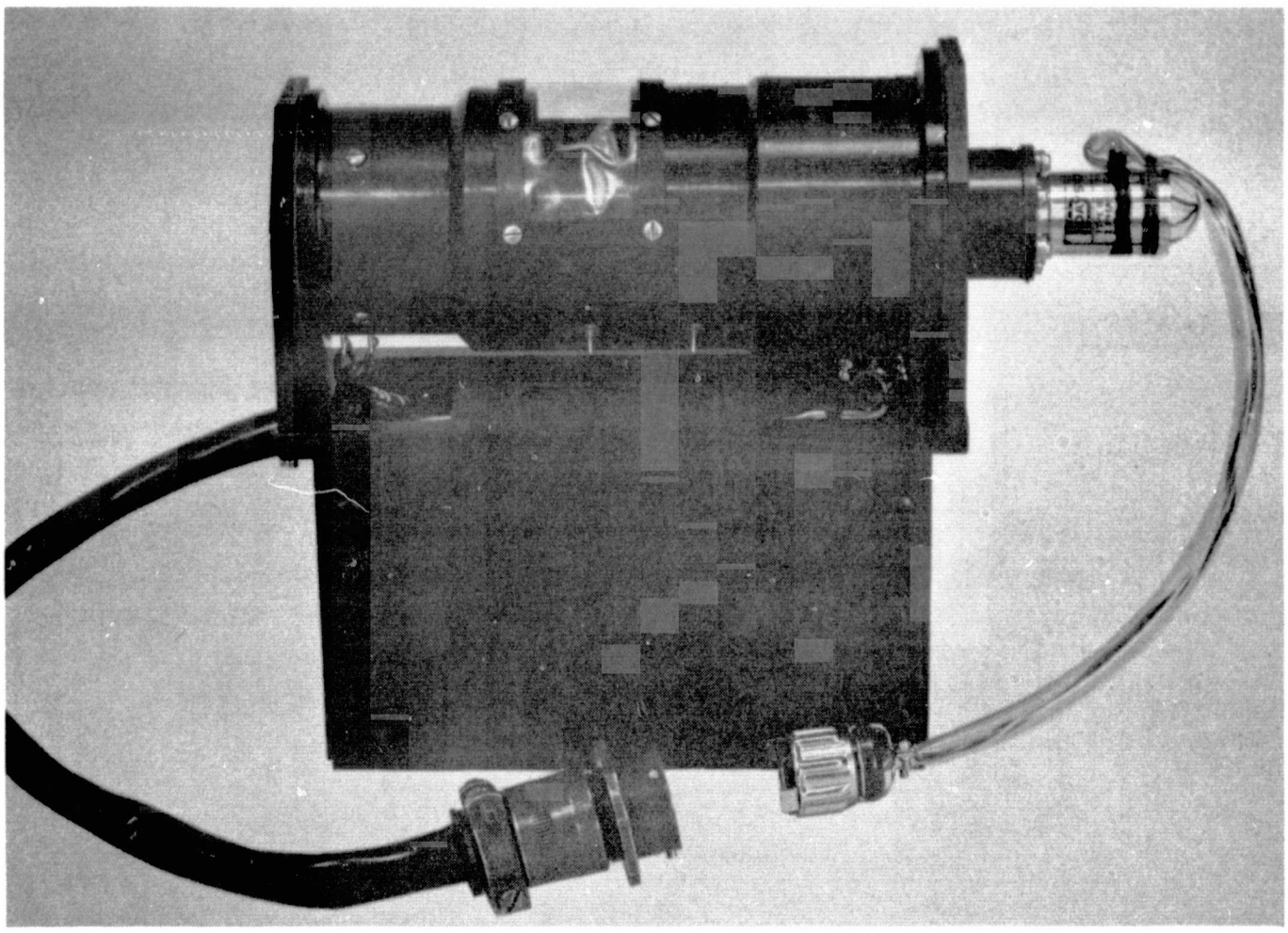

FIGURE 5. "FIRM" HORIZON SENSOR, ENGINEERING MODEL

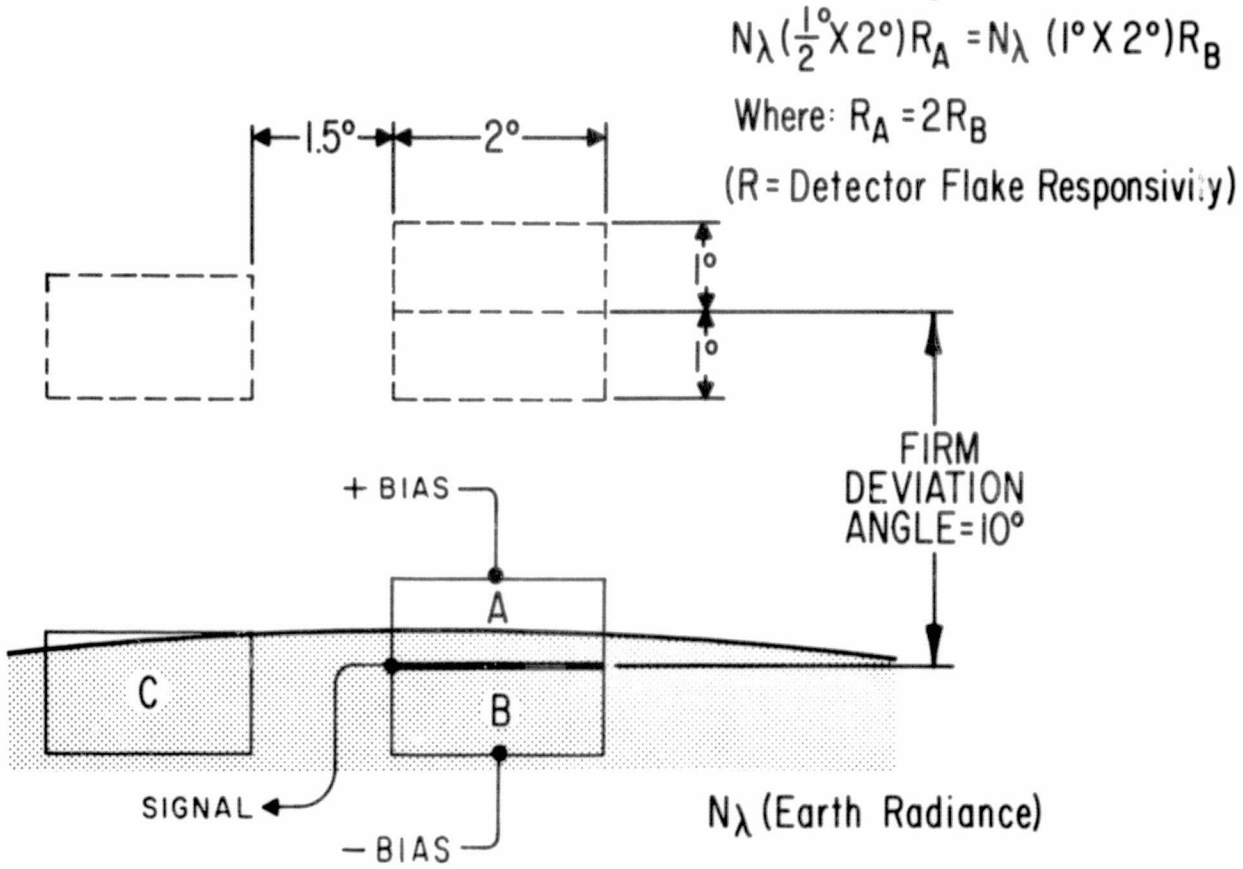

FIGURE 6. THERMISTOR DETECTOR ARRANGEMENT FOR EARTH RADIANCE COMPENSATION

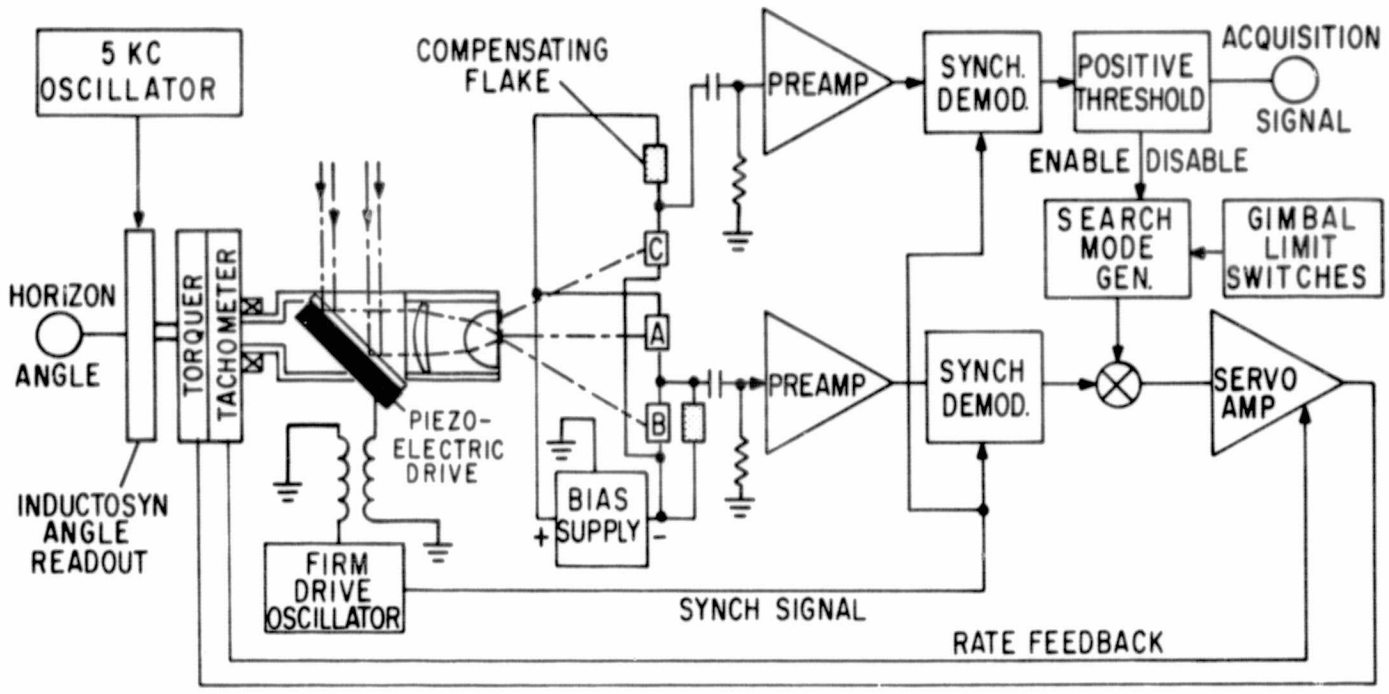

FIGURE 7. BLOCK DIAGRAM, "FIRM" HORIZON SENSOR SYSTEM (ONE OF FOUR HEADS)

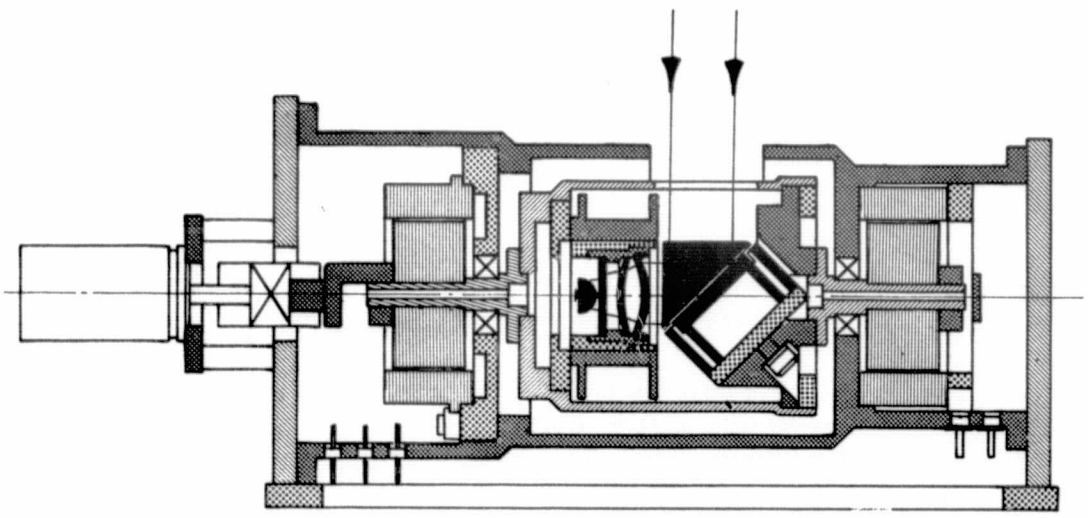

FIGURE 8. MECHANICAL LAYOUT OF "FIRM" HORIZON SENSOR

no α-c signal is generated, since irradiance on either the A or B flake does not vary. However, if the horizon is intersected in one of the field-of-view positions, α signal is generated in the A and B flakes as shown below:

$$V_A = N_\lambda \Omega_A \mathcal{R}_A \quad (1)$$

$$V_B = N_\lambda \Omega_B \mathcal{R}_B \quad (2)$$

where

V = output voltage of the thermistor flake

N_λ = earth radiance

Ω = solid angle of the detector flake subtended by the earth

$\mathcal{R}$ = responsivity of the flake.

Therefore, it can be seen that if $\mathcal{R}_A = 2\mathcal{R}_B$ α null condition will occur when the B-field is completely below the horizon but the earth subtends only half of the A-field. Furthermore, if both the A- and B-fields are below the horizon, one polarity of output signal will result, while if only the B-field is below the horizon, another polarity of output signal will result. In this way, the transfer function for the servo input is generated at the detector, and since N_λ (which is the earth radiance) appears in the equation for signals produced by both the A and B flakes, variations in N_λ should not affect the null position. The A-B bridge signal is processed as shown in Figure 7 and serves to position the fields of view of the A-B bridge so that they continuously track the horizon.

The C detector, which is mounted on the same immersion lens, has α dual function. One is to determine when the horizon is acquired, α function which is necessitated by the fact that the A-B bridge output is zero both when it is tracking the horizon and when it is looking at only space in both field positions. A second function of the C detector is the elimination of sun lock-on. This is achieved by the 1.5° azimuth separation angle between the A-B bridge and the C flake. Since the sun is only 0.5° in diameter and cannot be in two positions at once, it can produce α tracking signal but no acquisition signal, or an acquisition signal but no tracking signal. In either case, stable tracking of the sun above the horizon would not be achieved. For the case where the sun is just on the horizon, an error could be produced in one head. However, in this case, two-axis attitude information could be obtained from the three remaining heads which do not see the sun.

The mechanical configuration of the FIRM horizon sensor is illustrated in Figures 8 and 9. The entire optical system and preamp assembly of the horizon sensor are mounted on bearings and pivoted to track the horizon. This is achievable because there is no high speed moving part involved, and the system sensitivity is such that the optical aperture can be made small enough so that this type of optical

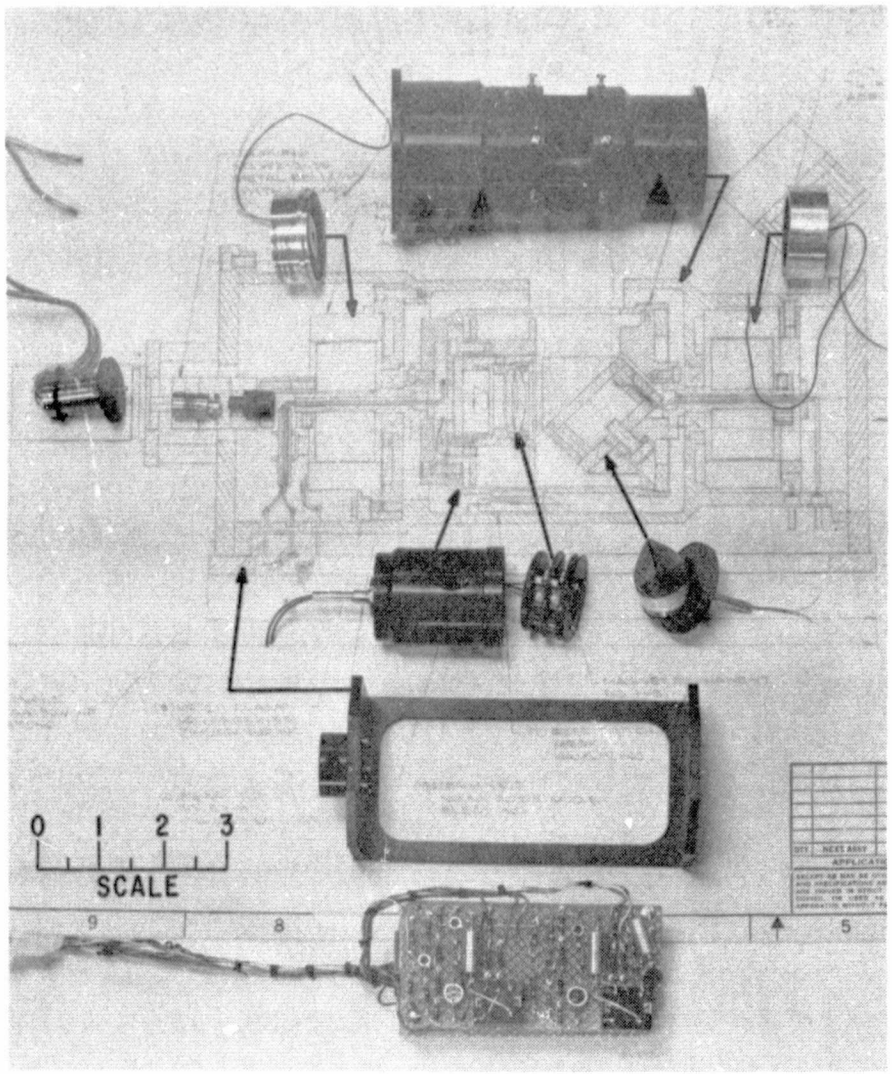

FIGURE 9. "FIRM" HORIZON SENSOR, DISASSEMBLED

mounting is feasible. The use of microcircuit preamps also reduces the size of the low-level electronics to such an extent that they can be housed in the pivot member. The use of a pivoted optical system has the following three advantages:

(a) The pivoted member is relatively light and has low inertia as compared to a comparable flat mirror that would have to pivot the optical field of view over 90°.

(b) In order to cover the desired 90° sector to provide wide altitude and tilt range performance, a pivoted flat mirror would be relatively large and would result in a commensurately large sensor head window.

(c) The use of a pivoted mirror requires twice the angular resolution for the shaft angle encoder than would be required with this system, since the flat mirror moves an optical beam through 2θ for θ rotation of its shaft.

In order to minimize power and eliminate any gears, a d-c brushless torquer and tachometer are used to drive the pivoted member. Although a resolver readout is shown in Figure 8, an ultimate system would use either a pair of inductosyn plates built into the pivot assembly (which would make the unit even smaller than that shown in Figure 8), or a 16-bit digital encoder could be attached to the shaft in a manner similar to that shown in Figure 8.

A complete sensor system is composed of four tracking heads, each of which includes all processing electronics except for the FIRM drive oscillator, inductosyn drive oscillator, and power supply. This power supply module is contained in a separate housing and drives all four heads and readouts.

III. PERFORMANCE PARAMETERS OF THE HIGH-ACCURACY FIRM HORIZON SENSOR

A. Accuracy

An over-all accuracy determination for any horizon sensor can be resolved into two main sources of error:

(a) Instrument errors (i.e., errors produced on a perfect horizon in the laboratory over the environmental range).

(b) Errors due to earth horizon spatial variation.

Of these errors the one more easily evaluated is the instrument accuracy. A brief discussion of these and of the CO_2 horizon variance error is presented below.

1. Instrument Accuracy

At this writing, the accuracy performance parameters of the prototype horizon sensor have not been completely evaluated. Therefore, this discussion will be limited to the expected performance based upon the nominal system

parameters. The errors produced by the FIRM horizon sensor in the laboratory against a perfect horizon will be a function of (1) system signal-to-noise ratio and (2) detector flake responsivity shift.

a. Random Noise Equivalent Angular Error

The following calculation determines the expected system signal-to-noise ratio when operating against a radiance in the laboratory equivalent to the minimum earth radiance in the atmospheric absorption region.

With a 0.5-inch diameter aperture and an effective system f/number of 0.21 produced by the detector immersion, the effective focal length is 2.7 mm. Therefore, a 1° x 2° field will be subtended by a thermistor flake having approximate dimensions of 0.05 x 0.1 mm.

Assuming a detector noise limiting condition, the Noise Equivalent Power Density (NEPD) of the system is given by:

$$NEPD = \frac{6.3 \times 10^{-10} \quad \frac{A_d \Delta f}{\tau}}{A_o \eta}$$

where

A_d = detector area in mm^2 = 0.005 or 5×10^{-3} mm^2

Δf = noise bandwidth = output bandwidth = 1 cps

τ = detector time constant in milliseconds = 2 milliseconds

A_o = aperture area = 1.2 cm^2

η = optical efficiency = (window transmission) x (FIRM transmission) x (CO_2 optical filter transmission) x (immersion lens transmission)

= 0.95 x 0.8 x 0.5 x 0.5 = 0.19.

The factor 6.3×10^{-10} is a thermistor figure of merit, while a factor of 3 is provided as a combined degradation factor for thermistor bridge factor, detector bias reduction required for wide ambient temperature range, preamp noise factor, etc.

$$\therefore NEPD = \frac{6.3 \times 10^{-10} \quad \frac{6.4 \times 10^{-3} \times 1}{2}}{1.2 \times 0.19} \times 3$$

$$= 4.8 \times 10^{-10} \text{ watts/cm}^2$$

With a field of view, Ω, of 1° x 2°, the received irradiance difference, ΔH, when the field of view in one FIRM position is entirely below the horizon is given by:

$$\Delta H = \Delta N_{\Delta\lambda}\, \Omega$$

where

$\Delta N_{\Delta\lambda}$ = minimum earth radiance between 14.2 and 15.8 microns

= 0.3×10^{-3} watts/cm^2-ster (See references 6, 7, 8)

$$\therefore \Delta H = 0.3 \times 10^{-3} \times 6.08 \times 10^{-4}$$

$$= 1.8 \times 10^{-7} \text{ watts/cm}^2$$

The peak signal-to-rms-noise ratio (S/N) will be given by:

$$\frac{S}{N} = \frac{\Delta H}{NEPD} = \frac{1.8 \times 10^{-7}}{4.8 \times 10^{-10}} = 374$$

Therefore, the rms or 1σ angular error of each head of the FIRM horizon sensor due to noise with a 1 cps output bandwidth will be 0.5/374 = 0.0013° or approximately 5 arc-seconds.

b. Errors due to Detector Flake Responsivity Shift

The second component of instrument error involves the responsivity match between the three thermistor flakes used in the FIRM horizon sensor signal processing. It will be seen from equations (1) and (2) that the responsivities ($\Re_A$ and $\Re_B$) of flakes A and B must track each other if null is to be maintained accurately. A change in responsivity in one half of the bridge will result in an offset of the bridge balance, and the horizon will be nulled at a difference elevation angle. The resulting null shift can be defined as: (percentage responsivity mis-match) x (field of view elevation subtense). For instance, for the 1° elevation subtense chosen for each thermistor field of view, a 10% responsivity mis-match would result in a 0.1° null shift. Therefore, in order to provide an accuracy better than 0.01°, the responsivities of flakes A and B must track each other to better than 1% with age and over the ambient temperature range. In addition, the resistances of flakes A and B and the compensator flake must be matched to 2%.

Encouraging results in the area of resistance and responsivity matching of thermistor flakes has been obtained experimentally at Barnes. It was found that over a temperature range of -10° C to +50° C the responsivity and resistance of two separate thermistor flakes matched to within 1%. In this case, the situation should be even better since the A-B bridge is in essence one flake, so that the characteristic of the thermistor material between the two halves of the flake should closely track.

It can therefore be seen that this second component of error will predominate insofar as the instrument accuracy is concerned. It is felt that with a suitable combination of parameters, the FIRM horizon sensor system can provide a 1σ accuracy of 0.01° if the horizon asymmetry errors are neglected.

2. Horizon Variance Error

As discussed in the foregoing section, extensive work on horizon profile has been performed by Duncan, Hanel, and Wark, among others. This work indicates that, if the horizon sensor is operated in the atmospheric CO_2 band and the seasonal radiance variation is compensated for, then the only remaining spatial variation is of the order of ±0.05° at an orbital altitude of 300 nautical miles. Therefore, if an instrument accuracy on the order of 0.01° is achieved, then the over-all accuracy of the FIRM horizon sensor system will be limited by these horizon variance errors and will amount to approximately ±0.05°.

IV. CONCLUSIONS AND PRESENT STATUS OF THE DESIGN

On the basis of the foregoing discussion, it is concluded that a horizon sensor using a FIRM cell can be successfully fabricated in both a simple configuration which is uncompensated for earth radiance variation and a more accurate configuration in which the earth radiance is compensated for at the detector level. The performance parameters of this earth radiance compensated FIRM horizon sensor are indicated in Table I, and where applicable, are based on direct measurements using the fabricated engineering model. At the writing of this paper, the engineering model is undergoing final debugging procedures while tracking a simulated earth horizon. All components of the system have been tested individually and are performing close to the design expectations. It is therefore expected that when the system debugging is completed the computed accuracy shown in Table I will be achieved experimentally.

Some comments about the peak power consumption and output bandwidth are pertinent. The peak power consumption was measured on the engineering model with the torquer at maximum torque, a condition which would never be held for any length of time for normal vehicle angular accelerations. In regard to the output bandwidth, since the torquer can provide 3 ounce-inches of torque, and the rotational moment of inertia of the pivoted assembly is relatively low, the sensor should be capable of providing an output frequency response greater than 10 cps. However, since the signal-to-noise calculation is based upon a 1 cps output, there will be a trade-off area in signal-to-noise ratio when higher output frequency response is desired. There is also the possibility of increased power consumption for a higher frequency response output. However, since the FIRM cell can be driven at any frequency up to 150 cps, the information theory limit for sensor output frequency response is essentially at 30 cps.

Therefore, in summary, it would appear that the primary advantages of this high accuracy FIRM horizon sensor are:

GENERAL CONFIGURATION	4 HEADS + POWER SUPPLY UNIT
TOTAL VOLUME	500 CU. IN (APPROX.)
TOTAL WEIGHT (4 HEADS + POWER SUPPLY)	15 LBS MEASURED PROTOTYPE WEIGHT WITH BREADBOARD ELECTRONICS 12 LBS (EXTRAPOLATED WEIGHT BY USING THIN WALL MAGNESIUM CASTING ETC.
TOTAL POWER CONSUMPTION	AVERAGE POWER (WHILE TRACKING) ≈ 3 WATTS PEAK POWER (MAX. TORQUE) ≈ 20 WATTS
COMPUTED HORIZON TRACKING ACCURACY	±.01° AGAINST PERFECT HORIZON IN LAB. ±.05° AGAINST REAL CO_2 HORIZON IN SPACE
OUTPUT CHARACTERISTICS	INDUCTOSYN ANALOG (20 ARC SEC RESOLUTION) OR 16 BIT DIGITAL
OUTPUT FREQUENCY RESPONSE CAPABILITY	>10 CPS

TABLE I. PERFORMANCE PARAMETERS OF "FIRM" SENSOR

(a) High accuracy capability against the real earth horizon;

(b) low power consumption during tracking;

(c) extremely long life in orbit environment;

(d) no requirement for pressurization;

(e) digital or analog readout;

(f) horizon angular rate readout directly available from the feedback tachometer.

[1] R. W. Astheimer, G. Falbel, and S. Minkowitz. "Infrared Modulation by Means of Frustrated Total Internal Reflection," presented at the Optical Society of America meeting, April 2, 1964.

[2] E. E. Hall. "The Penetration of Totally Reflected Light into the Rarer Medium," Phys. Rev., Vol. 1, No. 2, p. 73, 1902.

[3] G. Falbel and R. W. Astheimer. "IR Modulation, Field Deviation, and Spectral Scanning without Moving Parts Using Piezoelectric Drives," Proceedings of the Infrared Information Symposium, Vol. 10, No. 1, February 1965.

[4] John Duncan. "Horizon Indication Technique Providing 0.05° Accuracy at Low Satellite Altitudes," Proceedings of the Infrared Information Symposium, Vol. 9, No. 1, January 1964.

[5] R. A. Hanel, W. R. Bandeen, and B. J. Conrath. "The Infrared Horizon of the Planet Earth," Journal of the Atmospheric Sciences, Vol. 20, No. 2, pp. 73-86, March 1963.

[6] D. W. Wark, J. Alishouse, and G. Yamanoto. "Calculation of the Earth's Spectral Radiance for Large Zenith Angles," Meteorological Satellite Laboratory Report No. 21, October 1963.

[7] J. W. Burn. "The Application of the Spectral and Spatial Characteristics of the Earth's Infrared Horizon to Horizon Scanners," IEEE Transactions, August 1963.

[8] R. A. Hanel, W. R. Bandeen, and B. J. Conrath. "The Infrared Horizon of the Planet Earth," Report No. X-650-62-164, Goddard Space Flight Center, August 1963.

An Electronic-Scan Horizon Sensor

MONROE M. MERLEN, JEROME M. PASTERNAK AND DENTON PEARSALL
Barnes Engineering Company, Stamford, Connecticut

ABSTRACT

A system that utilizes a linear array of sequentially sampled Thermopile Detectors to provide scanning without moving parts is described. The techniques used to reduce system noise and eliminate spurious target signals are reviewed, along with simulated space environment test results. Potential future improvements in implementing the basic principles are evaluated.

I. INTRODUCTION

Today, in a time of expanding space exploration, there is a need for a reliable and passive means to establish a space vehicle's attitude with respect to an adjacent planetary body. One method of accomplishing this task is by the use of an infrared horizon scanner which uses the radiation discontinuity of the space-planet horizon to determine the vehicle's attitude. In presently accepted horizon scanners, a motor driven set of rotating optics moves the field of view (FOV) of a radiation sensing device in a set pattern across the planet's horizon. The resultant detector output signals vary as the FOV crosses the radiation discontinuity. These signals are used to establish the vehicle's attitude with respect to the adjacent planet.

The perfection of an electronic method of scanning the FOV would result in a completely solid-state horizon scanner. Such replacement of the mechanical scanning elements increases the possibility for a compact, long-life, universal horizon scanner. Barnes has developed suitable electronic scanning techniques.

Barnes has built a scanner unit employing these techniques. The unit is capable of determining a vehicle's attitude with respect to a wide range of planets (Earth, Mars, Venus) or Moon which vary in blackbody temperature (120°K and up) and angular subtense (2° to nearly 180°). It operates without interference from

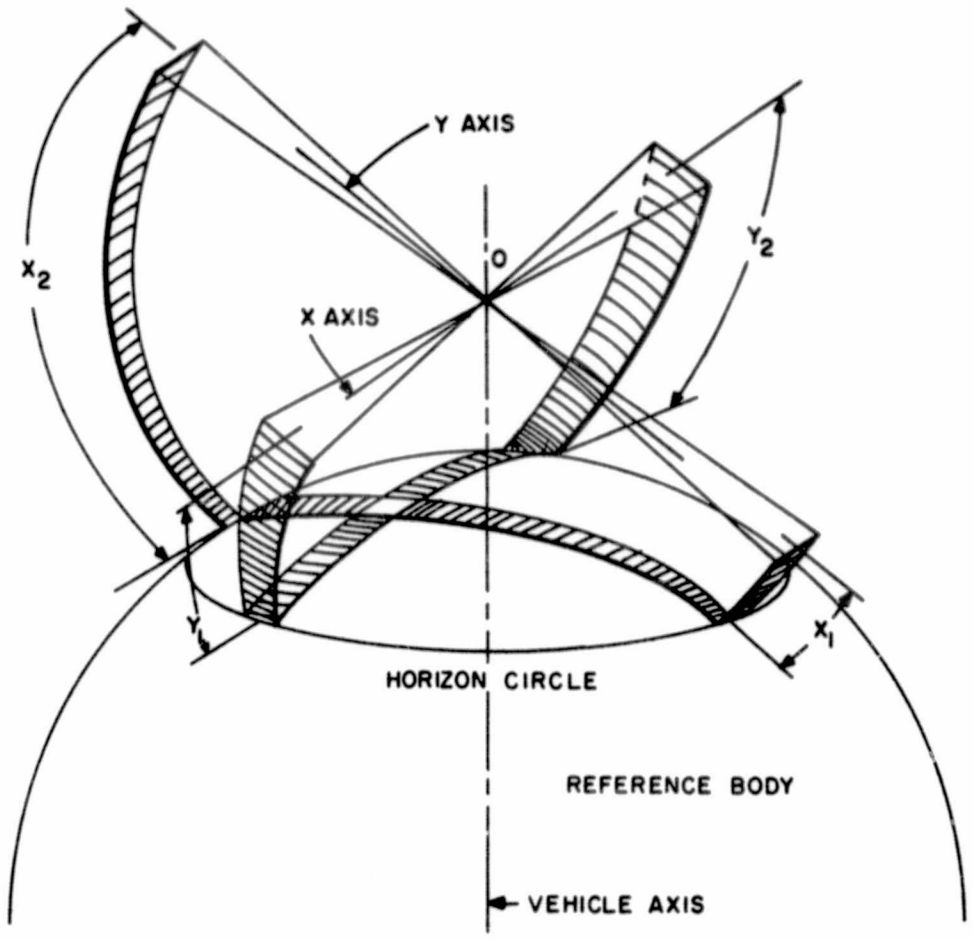

FIGURE 1A. SCAN CONFIGURATION

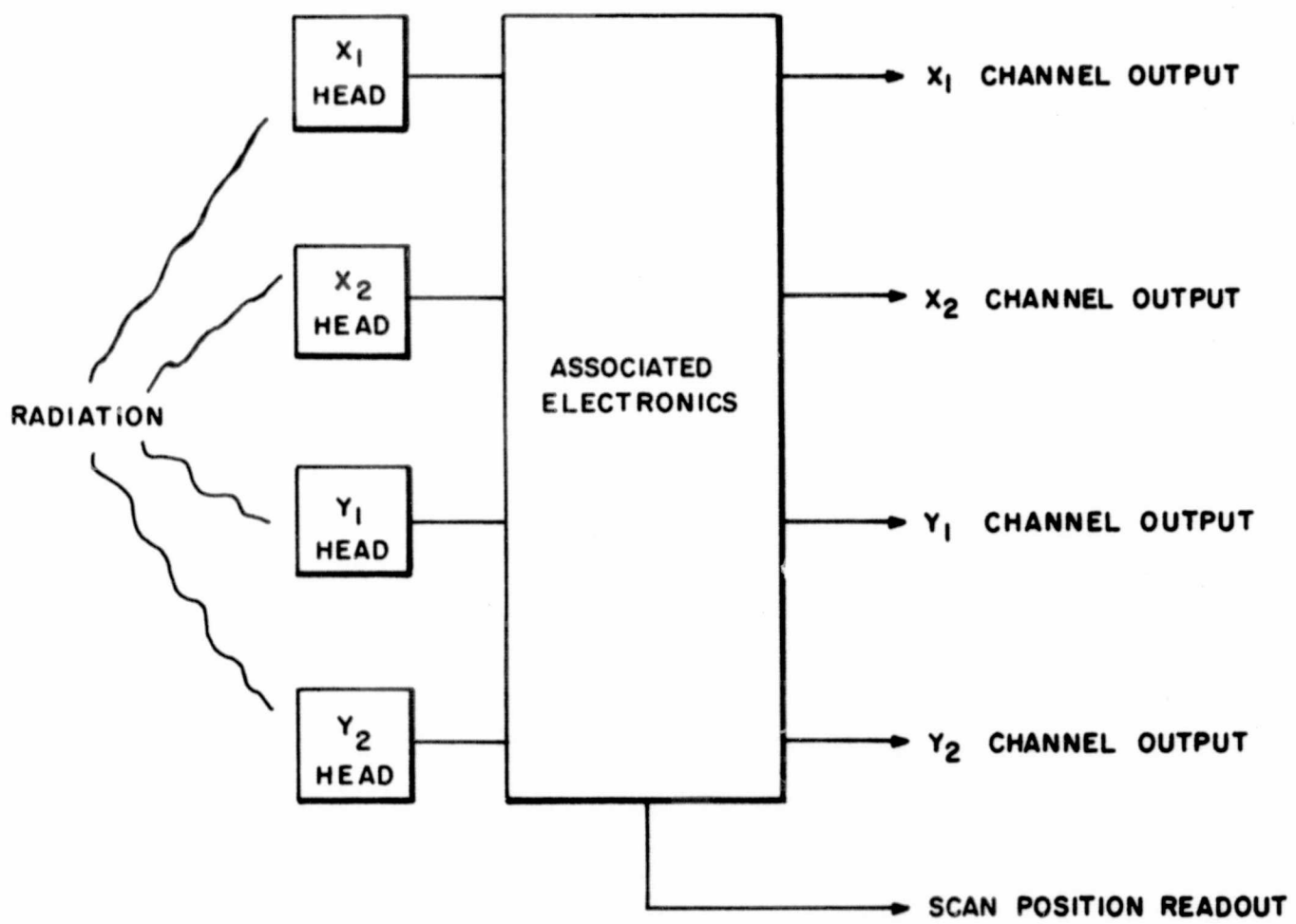

FIGURE 1B. SYSTEM BLOCK DIAGRAM

unwanted foreign bodies, and because no moving parts are used, a 3 year, 90% probability of success is realizable.

A. General Concept

The solid-state Lunar and Planetary Horizon Sensor system employs four, accurately defined, rectangular FOV's which are orthogonally projected into space (see Figures 1A and 1B). Each FOV is identified with one optical head in the overall system. In turn, the FOV of each head is segmented into discrete solid angles, which have a one-to-one correspondence with a set of radiation detectors in a linear array. The location of the thermal horizon within the segmented FOV is readily determined because those detectors of the array being irradiated by the energy from a planet have a different output signal than the detectors radiating energy into space. The detectors' outputs are directly and sequentially sampled by an electronic commutator. Thus, the necessary scanning is accomplished without utilizing any moving parts. This method of scanning has the benefits of digitalized processing initiated at the system's input.

The direction of scan from space-to-planet is used because space is a relatively uniform radiation source. Therefore, during any single space-to-planet scan, the first variation of radiation occurs when the planet's horizon is initially crossed. If the direction of scan were from planet to space, the planet's thermal gradients could produce confusion with the actual horizon crossover.

With subsequent electronic processing, attitude and altitude information is derived from the sequentially sampled detector outputs in each head. The serial information is in digital form but can be converted into an analog format. Formulations that indicate the nature of the processing are as follows:

$$\text{X axis attitude} = x_1 - x_2$$
$$\text{Y axis attitude} = y_1 - y_2$$
$$\text{Altitude information} = y_1 + y_2 = x_1 + x_2 = \text{a function of the angular diameter of the planet as seen from the vehicle} = \text{function of altitude}$$

where x_1 = number of detectors viewing space, or angular subtense segments sampled before sensing the thermal horizon in X1 sensing head FOV. Similarly, x_2, y_1, and y_2 are related to the FOV's of X2, Y1, and Y2 sensing heads.

The resolution accuracy of the above technique is limited by the size of the angular subtense of the individual field of view segments. However, the attitude and altitude functions depend only on the presence of the thermal horizon within the FOV and are not affected by the planet's magnitude, uniformity of radiation, or its angular subtense.

The sensor will function properly without interference from unwanted foreign (celestial) bodies in any of its FOV's. Rejection of signals from these bodies is accomplished by requiring a definite number of detectors, that have

planet radiation incident upon them, to be consecutively sampled before the sensor verifies the presence of a planet's horizon. If the angular subtense of the foreign body is less than the equivalent angular subtense corresponding to the required consecutively sampled detectors, the signal from the unwanted body is dismissed. As in the case of the desired planet, the magnitude of signal from the interferring body is of no consequence.

The above concepts were used to develop and design the Lunar and Planetary Horizon Sensor at Barnes.

B. Present Instrument

The Barnes solid-state sensor has the following elements associated with each of the four FOV's: an optical system to focus the energy on the detectors; an array of small, sensitive radiation detectors with the ability to discern the radiation difference between space (4°K) and the cold side of the moon (120°K); a low-noise electronic commutator to sequentially sample the detector output signals; a low-noise amplifier to process amplitude and time-varying low-level detector outputs; and an amplitude-time threshold circuit to provide the foreign body discrimination capability.

An uncorrected Schmidt optical system with 90° coverage is used to focus an image of the horizon on the detector array. The detector array consists of solid-backed thermopiles. These produce an output voltage (μv) proportional to the difference between radiation incident on and radiation from their surfaces. A photocommutator is used for sequential sampling of the thermopile output voltages. (Neon bulbs and photo-resistors are the basic elements of this low-noise, solid-state, commutator). The commutator output signal is fed to a compression amplifier.

The compression amplifier processes the dynamic microvolt signals without serious interference from noise. It also has a unique filtering arrangement that automatically varies the amplifier's effective bandwidth as a function of the instantaneous signal intensity. A subsequent threshold level comparator circuit is used to determine whether the amplifier's output signal is above or below a preset level. This output is coupled to a spill-over counter. The counter produces a d-c output only when a predetermined number of consecutive signal samples have remained above the setting of the amplitude threshold level. The output from this spillover counter comprises the final output from a single signal channel of the Lunar and Planetary Horizon Sensor.

II. SIGNAL PROCESSING

The electronic processing of the signal will be discussed in two phases. First, the fundamental concept will be reviewed and second, the details required to implement the fundamental concept will be described.

Figure 2A shows the fundamental concept of signal processing and an idealized d-c referenced signal output from a single scanning head. The d-c reference for the system is obtained by simultaneously shorting the input and output of the amplifier to ground during the last five steps in the commutator.

Since the net radiation interchange between space and the thermopile is out from the detector to space, a negative d-c voltage was selected to indicate this condition. Note that the most negative signals are produced by the "space-viewing" detectors, and the signals produced by "planet-viewing" detectors are always more positive. Therefore the location of the horizon can be determined by establishing the threshold level amplitude slightly more positive than the space level.

There are a number of problems not indicated by the foregoing idealized presentation. The magnitude of the negative space voltage varies with the detector's ambient temperature. The higher the temperature, the greater the radiation loss to space, hence the larger the negative voltage. This precludes the usage of a fixed voltage threshold. Also space-viewing detector outputs could vary ±20% during one scan, due to differences in individual detector responsivities. These spurious variations in sequential detector outputs could be confused with actual planet signals.

If the net radiation interchanges of space-viewing thermopiles were made equal to zero for all operating conditions, the preceding problems would be eliminated. The net radiation power on space-viewing detectors can be made equal to zero by using a small heated radiation source. This source must be equally seen by all detectors. It must also have a net radiation interchange with the thermopiles that is positive and equal in magnitude to offset the effective interchange between each detector and space. Furthermore, by using such a source, the outputs from all the detectors, would effectively be referenced to zero volts, thereby permitting a fixed amplitude threshold setting to be used.

In the actual system, a small temperature-controlled radiation source, that obscures only a small percentage of the system's entrance aperture, achieves the aforementioned results. The input power to this heated source is made proportional to the negative signal outputs from the first ten detectors of a scan by means of an electronic sample-hold servo. Under normal operating conditions these detectors will be viewing space. Figure 2B shows this modified arrangement with its idealized output.

Figure 2B would not be practical as a universal sensor that has to operate with respect to many celestial bodies whose angular subtense and radiation intensities varied widely. To accommodate the universal condition, the signal amplifier would require an extremely low-frequency cut-on in order to prevent excessive signal droop or overshoot. Extended low-frequency response is undesirable mainly because a transistor amplifier's noise increases at low-frequency, and, this noise could produce false signals. By keeping the signal pulse duration as short as possible, the low-frequency response requirement can be reduced.

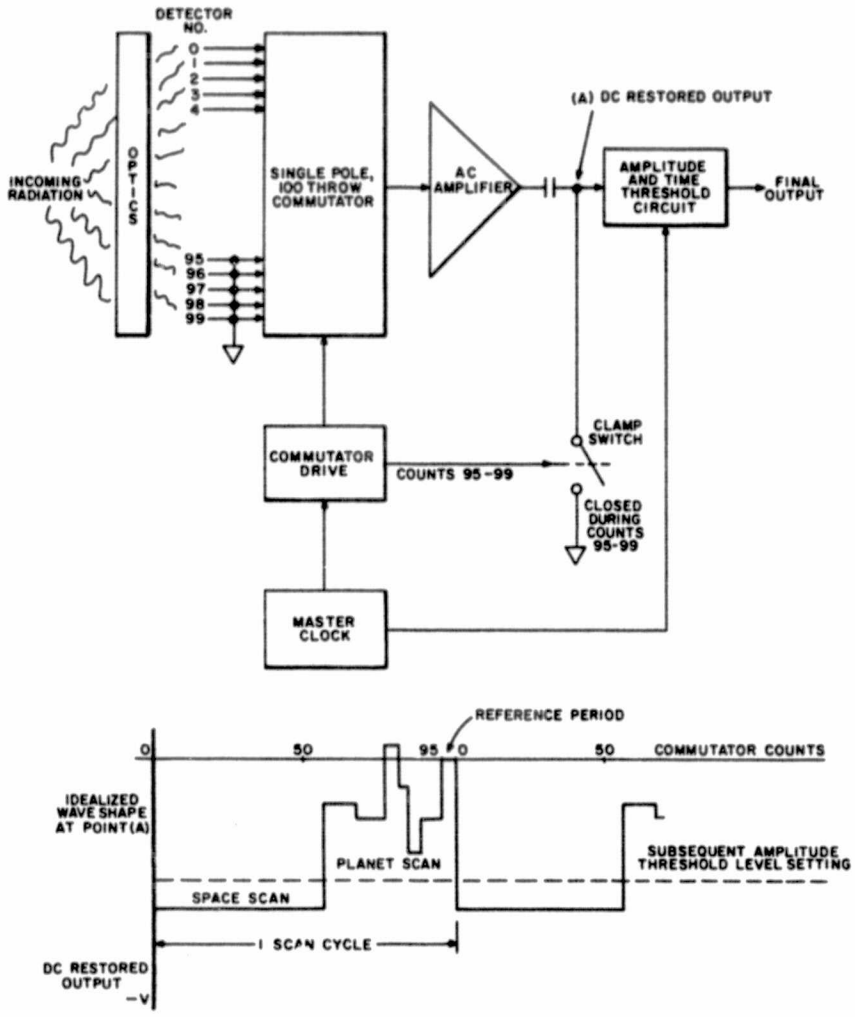

FIGURE 2A. BLOCK DIAGRAM FOR FUNDAMENTAL CONCEPT

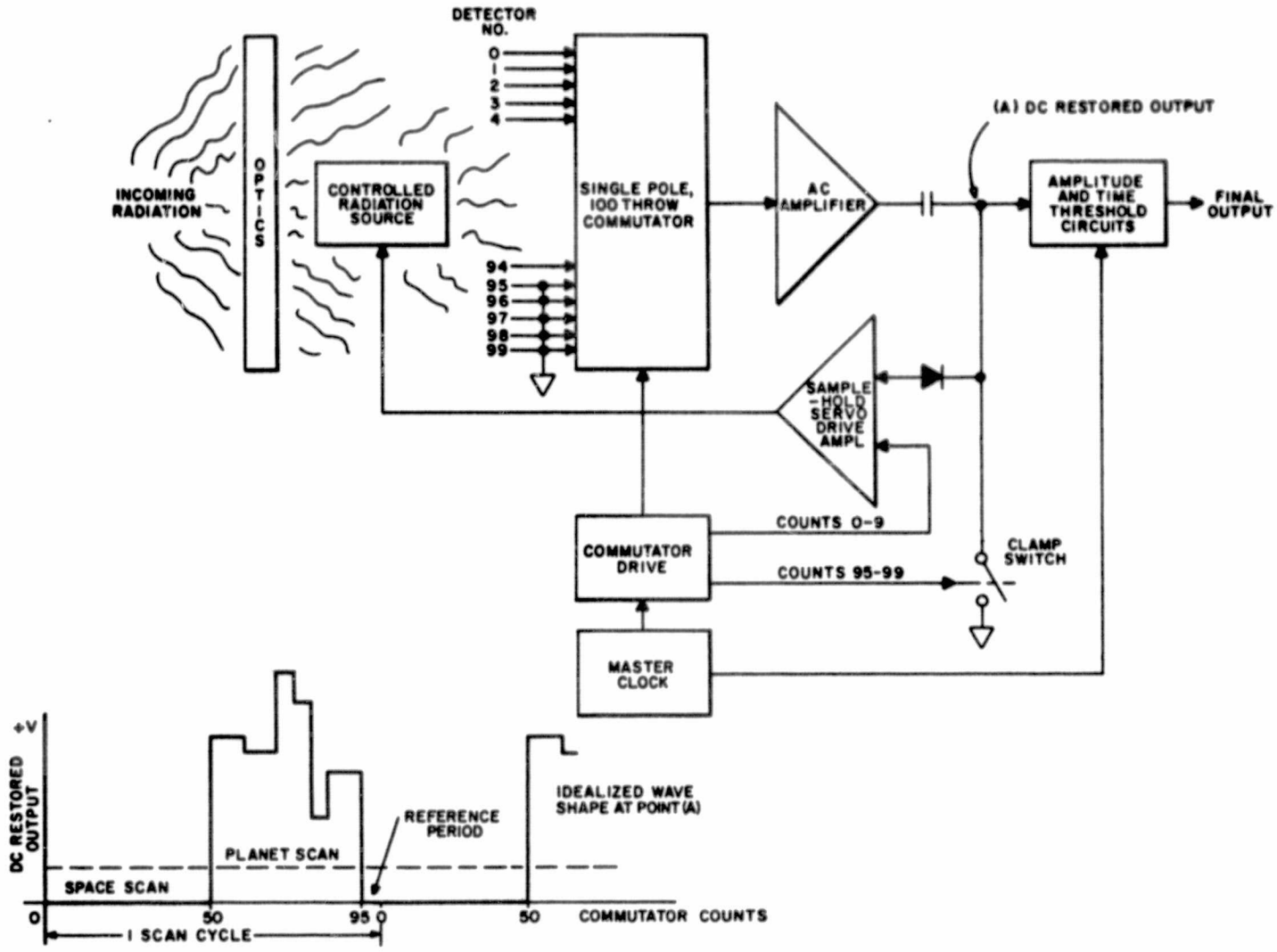

FIGURE 2B. BLOCK DIAGRAM FOR MODIFIED ARRANGEMENT

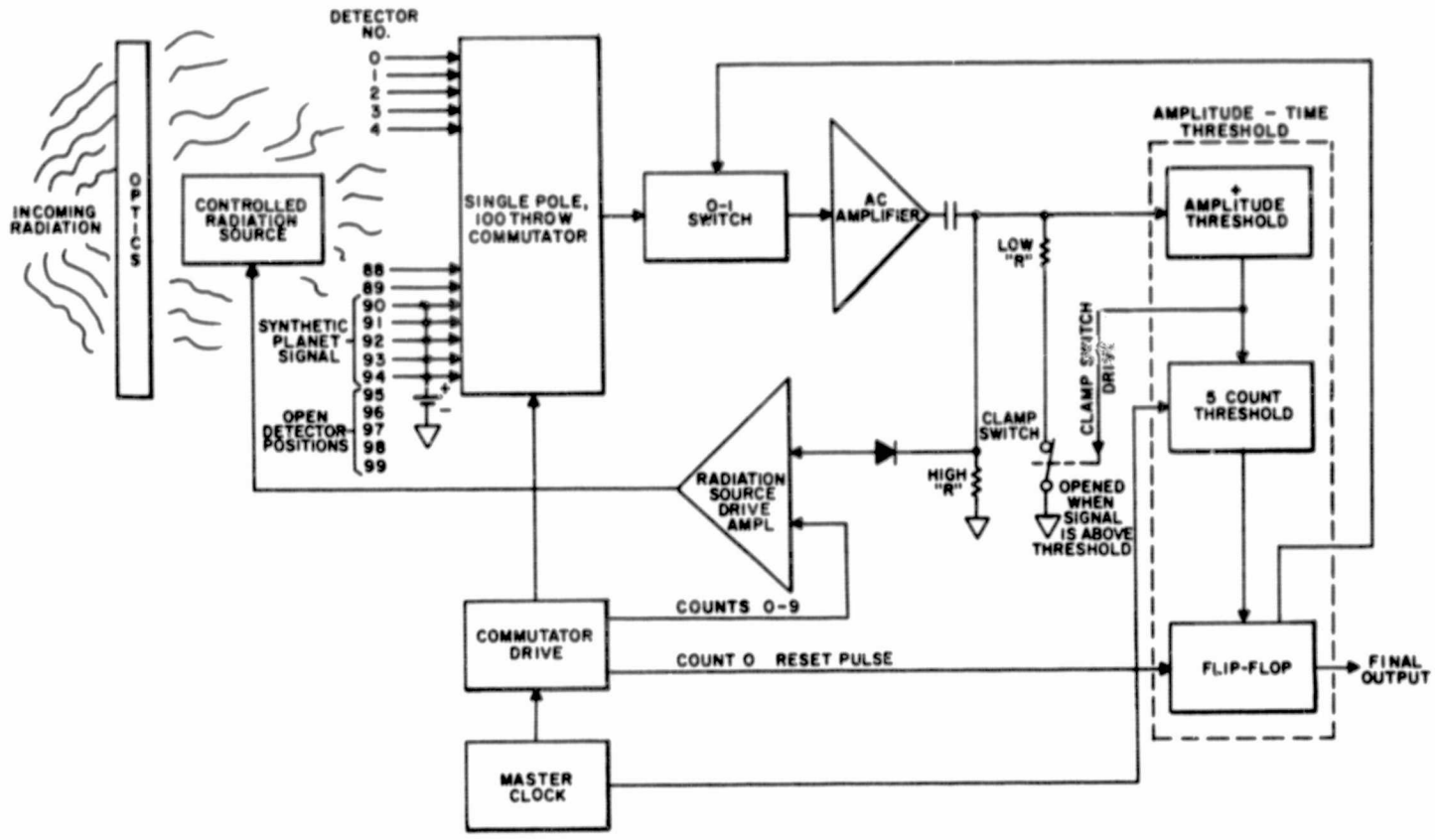

FIGURE 3. BLOCK DIAGRAM OF FINAL CONFIGURATION (ONE HEAD)

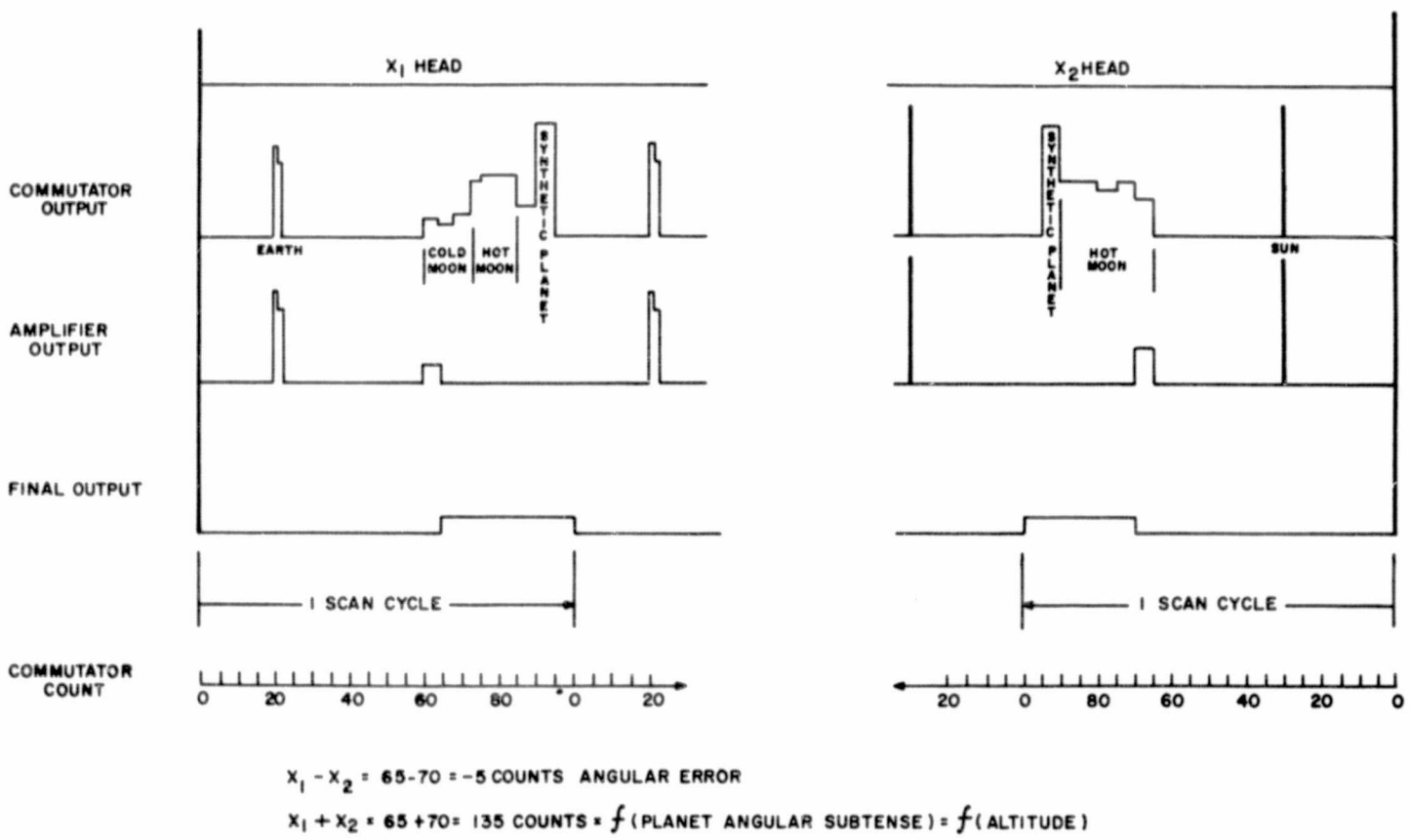

$X_1 - X_2$ = 65-70 = -5 COUNTS ANGULAR ERROR

$X_1 + X_2$ = 65+70= 135 COUNTS = f (PLANET ANGULAR SUBTENSE) = f (ALTITUDE)

FIGURE 4. TYPICAL SENSOR OUTPUTS IN VICINITY OF THE MOON

In the present system, shortening of the pulse duration was accomplished by using a "0-1" switch. This switch disconnects the amplifier's input from the commutator output, and, reconnects it to a zero-volt reference after planet verification is achieved. Thus the maximum signal pulse width that the amplifier has to process is limited to the number of counts required for horizon crossing confirmation. The confining of the signal pulse width in this manner is logical and convenient. During any single scan of a FOV, no further useful attitude information is obtained after verification of the planet horizon crossover occurs. The remainder of the scan time can therefore be utilized to zero-reference the amplifier.

The low-frequency noise problem was further reduced by varying, with signal amplitude, the cut-on frequency of an R-C high-pass filter at the amplifier's output. This was done by varying the "R" via the subsequent amplitude threshold circuit to achieve two states: (1) for signals below the threshold, the cut-on is relatively high but still capable of responding to the initial step input signal from the planet horizon; and (2) for signals above the threshold, the cut-on is extended downward to prevent excessive signal pulse droop, and subsequent overshoot. Thus, for low-amplitude signal conditions, where the signal-to-noise ratio is important, the effective bandwidth of the amplifier is reduced without hindering the system's response to the signal.

By returning the aforementioned variable "R" element to zero volts, the amplifier's output is automatically referenced to zero volts through a low resistance value whenever the signal is below the threshold level. This combination of the "0-1" switch and the variable high-pass filter offers a more effective means to d-c reference the system than that indicated in Figures 2A and 2B. With this method, the clamping function is maintained during practically the entire scan interval and not just during the final portion.

It should be noted that a predetermined minimum number of detectors must receive the planet signal for the proper referencing operation to be achieved by the improved method described. Under certain operational situations, large angular vehicle tilts may preclude fulfilling this necessary requirement. By applying a d-c potential to a number of commutator positions just subsequent to the final detector being sampled, a synthetic planet signal is produced at the commutator output. Since triggering of the threshold circuit is necessary for d-c referencing, the synthetic signal will perform this function if no adequate planet signal is obtained prior to its occurrence during the scan interval.

The final configuration for one head and its associated signal processing channel is shown in block diagram form in Figure 3. Typical commutator outputs, amplifier outputs and final outputs are shown in Figure 4. A photograph of a prototype optical scanning head assembly and its associated commutator deck is shown in Figure 5. Details of the controlled radiation source can be seen in Figure 6.

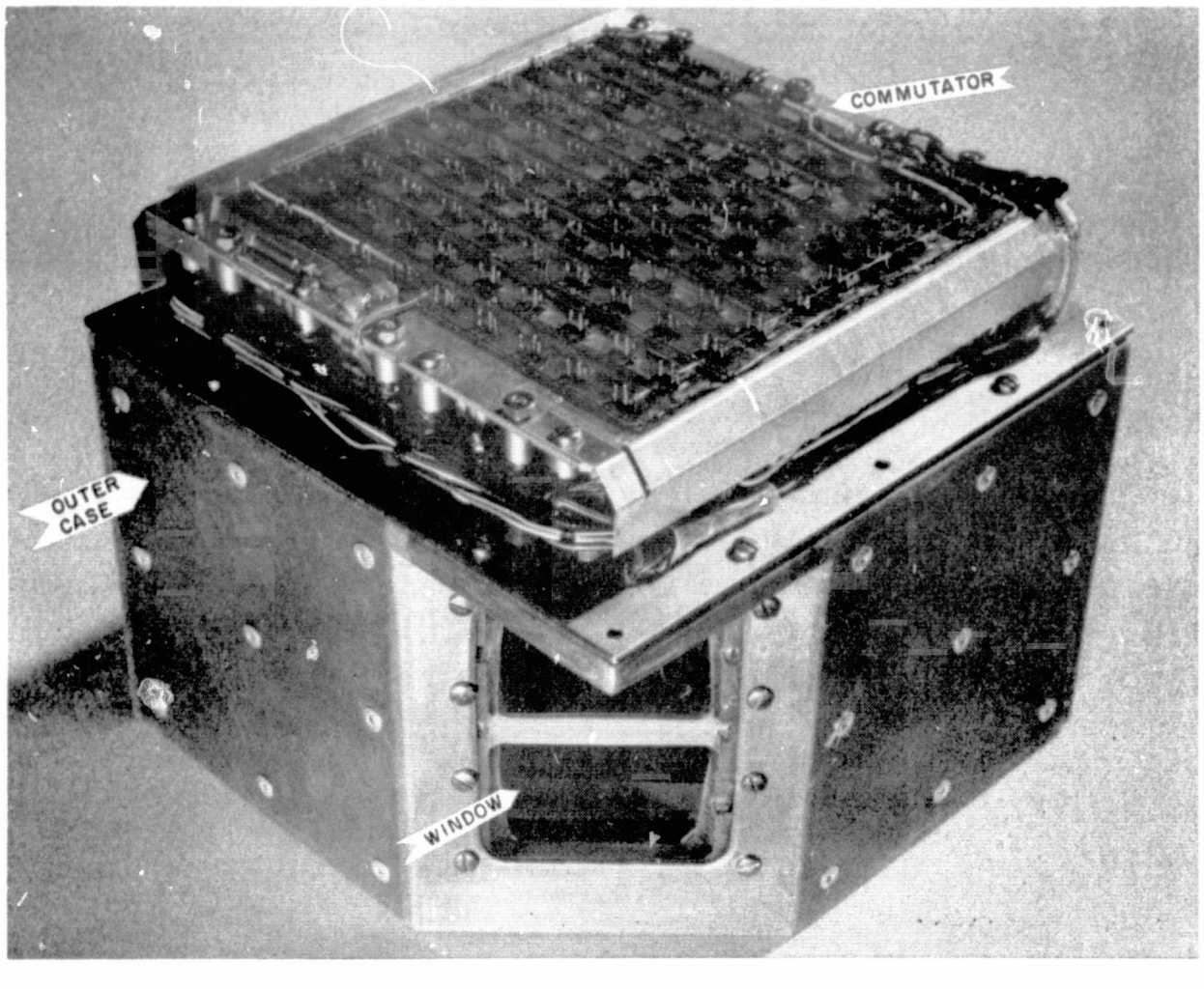

FIGURE 5. PROTOTYPE OPTICAL HEAD ASSEMBLY WITH COMMUTATOR COVER REMOVED

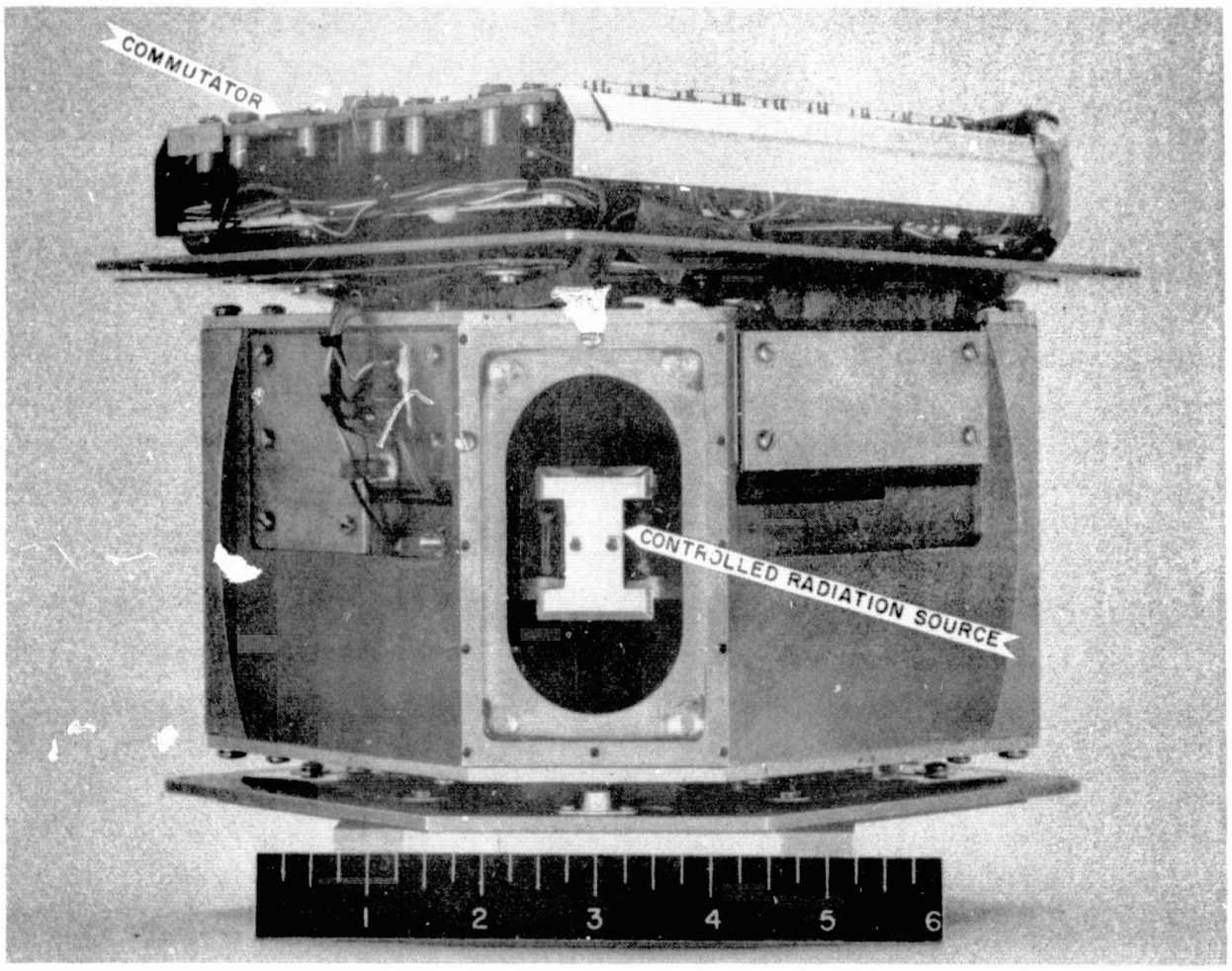

FIGURE 6. PROTOTYPE OPTICAL HEAD ASSEMBLY WITH OUTER CASE AND WINDOW REMOVED

III. PARAMETERS OF PRESENT UNIT

The present system has been designed as a wide-field, universal scanner which can be used to supply altitude and two-axis attitude information with respect to the Moon, Earth, Mars or Venus. Some of the existing limits on its parameters can be easily modified, but in most cases it will involve a sacrifice of other parameters. For example, a reduction in weight and size can be achieved by eliminating lunar operation requirements, reducing accuracy, or decreasing the FOV. A list of the system's parameters, as they presently exist are enumerated below:

TABLE I - PARAMETERS OF A TWO-AXIS SYSTEM

Number of Optical Heads	2 per axis, 4 per system
Scanned FOV per head	10° x 81° (could be expanded to 10° x 90°)
Segmented solid angle associated with individual detector	0.9 x 10°
Detectors per head/array	90 (with 10° x 81° FOV) 100 (with 10° x 90° FOV)
Spectral Response	14μ to 50μ
Weight Per Head	6 lbs.
Auxiliary Electronics (master clock, commutator drive, and threshold devices)	One per system
Weight	1 lb.
Resolution (digital)	1°
System Accuracy	±0.5°
Operational Planet Size	22° to 170° (with 10° x 81° field of view per head) 5° to 170° (with 10° x 90° field of view per head)
Threshold Settings	
Set for Planet Temperature	100°K
Set for Planet Angular Subtense	5°
Time per Single Scan	300 milliseconds
Signal Outputs*	Four separate outputs (one from each field of view)
Reference Output**	+10 volt pulses, synchronized with scanning
System Power Requirements	
220 vdc	7.5 watts
+28 vdc (in vacuum)	5.5 watts
+28 vdc (in laboratory)	15.0 watts
-28 vdc	0.5 watts

TABLE I - PARAMETERS OF A TWO-AXIS SYSTEM (Contd.)

System Weight	25 lbs.
Stabilization Time	3 minutes
Operational Environment	Space Vacuum
Operating Temperature Range	-40°C to +60°C
Scanning Head Dimensions (each head)	6.5" x 6.5" x 6.5"

* These outputs consist of repetitive rectangular pulses, 0 vdc during space scan, +10 vdc subsequent to verified horizon crossover for remainder of scan.

** By relating the signal outputs to the scan position readout pulses, altitude and attitude can be determined.

IV. TEST RESULTS

The present system was developed by Barnes for Jet Propulsion Laboratories in Pasadena, California. (J.P.L. contract No. 950470 under NAS 7-100). A prototype single sector scanning head was tested in a space environment test chamber at the J.P.L. facilities during October 1964.

The scanner operated satisfactorily over a wide range of ambient temperatures with various simulated target conditions. Only one minor problem was encountered, due to the non-similar spectral response of five of the ninety detectors being commutated. This spectral mismatch was probably due to improper blackening of the five affected detectors.

The delivered system utilized a window that transmitted radiation beyond 14 microns. This prevented the short-wavelength energy, from the sun and "hot" targets, from reaching the thermopile detectors in the array. The long-wavelength energy from "cold" targets, however, was passed without attenuation. In this way, the dynamic range of signals that the system had to accommodate was reduced.

The scanner's controlled radiation source (which was used to offset the detectors' 14 micron and beyond radiation loss to space) predominantly emitted at wavelengths shorter than 14 microns. The aforementioned spectral response mismatch caused detectors fifty through fifty four in the 90 detector array to produce a five-microvolt spurious output. In spite of this difficulty, the delivered system could have operated against the Earth, Mars, or Venus. Only in the case of the moon (where minimum signals of 2 microvolts are anticipated) would operation have been precluded.

The foregoing problem could be corrected by replacing the defective bank of five detectors. Another more sophisticated and universal solution, which is presently being implemented, would not require spectral matching of the detectors. This solution involves replacing the present offset heat source, that emits "black body" radiation, with one that selectively emits energy having wavelengths longer

than 14 microns. Because the energy received by the detectors from the selectively emitting offset radiation source will have nearly the same spectral distribution as the energy loss to space, the spectral response of the individual detectors in the array should no longer be significant. Further tests will be conducted after this change is implemented to corroborate the effectiveness of this solution to the problem.

V. PLANNED PRODUCT IMPROVEMENTS

One major improvement is presently being investigated and breadboard tested with successful results. This is the use of an MOS field-effect transistor (FET) commutator between the detectors and the amplifier. The FET approach has several distinct advantages over the photocommutator presently being used. It will permit an extension of the operating temperature range of the sensor, a reduction in the total system power requirement to about 3 watts, and an increase in the scanning rate. The use of these transistors, in an integrated package form, would result in a significant reduction in size and weight.

Another anticipated area of weight reduction involves the scanner head mechanical structure and collecting mirror. In the delivered system these were fabricated of aluminum. By utilizing ribbed rigidized magnesium castings for the structural members, and fabricating the collecting mirror by a replicating process, the weight of each scanning head can be reduced to three pounds.

Further reduction in system weight and power requirements can be achieved by substituting microminiature integrated circuits for the standard printed circuits presently used in the electronic processing package. This approach also has the advantage of yielding improved reliability. In addition, a high level of redundancy can be incorporated into an integrated system with a negligible increase in weight or power consumption.

BLANK PAGE

A High-Accuracy Conical Scan Horizon Sensor Operating in the 15μ CO_2 Band

FRANK SCHWARZ, KENNETH A. WARD, and THOMAS FALK
Barnes Engineering Company, Stamford, Connecticut

ABSTRACT

The accuracy of most present operational horizon sensors is limited by variations in the horizon gradient. A technique is described for overcoming this limitation by sensing only radiation emitted by atmospheric carbon dioxide, electronically measuring the slope of the horizon gradient, and automatically applying an appropriate correction. A laboratory model of such a system has been constructed and tested with a CO_2 band horizon simulator. The laboratory model was evaluated using a pyroelectric detector with a scanner operating at 20 rps as well as one using a thermistor bolometer in a system with a 3 rps scan rate. Results show that a nearly tenfold improvement in accuracy should be possible by this technique.

I. INTRODUCTION

Infrared horizon sensors, since their development in the early phases of our space exploits, have undergone continual evolutionary development. The development of the conical scan sensor, which in itself represented a major advancement over other techniques developed earlier, went through numerious stages of refinement in optics, electronic processing techniques and mechanical design. Of particular importance has been the achievement of greater accuracy in determining the local vertical. Earliest sensors used the broadest spectral response conveniently obtainable. Since the optical elements were generally made of Germanium the spectral response had, as a rule, the normal 1.8μ to 20μ transmission characteristic of pure Germanium. It was realized fairly early that it would be advantageous to restrict the spectral response in order to reduce the large variations in signal amplitude which arise from solar reflections and scatter, clouds, etc.

In recent years the various refinements in sensor characteristics and electronic processing techniques reached the stage at which the accuracy achievable has become limited principally by the characteristics or profile of the Earth's horizon. This being the case, further improvements in the accuracy of sensors could only be obtained through recognition of this fact and use of particular properties of the horizon gradient.

The sensor to be described in this paper represents one solution to the problem of obtaining improved accuracy. It uses proven principles and hardware that has been refined through application of new knowledge and newly developed techniques. It achieves a significant improvement both in accuracy and sensitivity. Performance of a laboratory model will be presented at the end of this paper.

By way of example, the sensor which will be described uses the well-known conical scan system which was developed in 1958-1959 in the early years of our venture into space. Over three hundred sensors of this basic conical scan design have been built by Barnes Engineering Company and a good many of these have been flown in various space missions.

The salient features of the sensor to be described in some detail in this paper are the following:

1. Use of the 15μ CO_2 band to make the Earth or planet appear as a target of relatively uniform radiance.

2. An electronic technique for establishing a horizon edge which is symmetrical about the local vertical and permits accurate determination of attitude.

3. Improvement in Signal to Noise ratio to permit use of a narrow spectral band at 15μ. This improvement is obtained in either of two ways:

   a) A slowing down of the scan speed, which narrows the electronic bandwidth to a range more within the thermistor detector response time domain.

   b) Use of a pyroelectric detector whose detectivity is essentially constant to higher frequencies and with which a 20 cps scan rate may be used.

II. INFRARED CHARACTERISTICS OF THE EARTH'S HORIZON

Early horizon sensor data consisted chiefly of telemetered signals from horizon scanners, some of which were flown as early as 1958. The data showed that the Earth's profile, when viewed in the broad infrared radiation spectrum, is complex. Very large variations in signal amplitude resulted from radiation

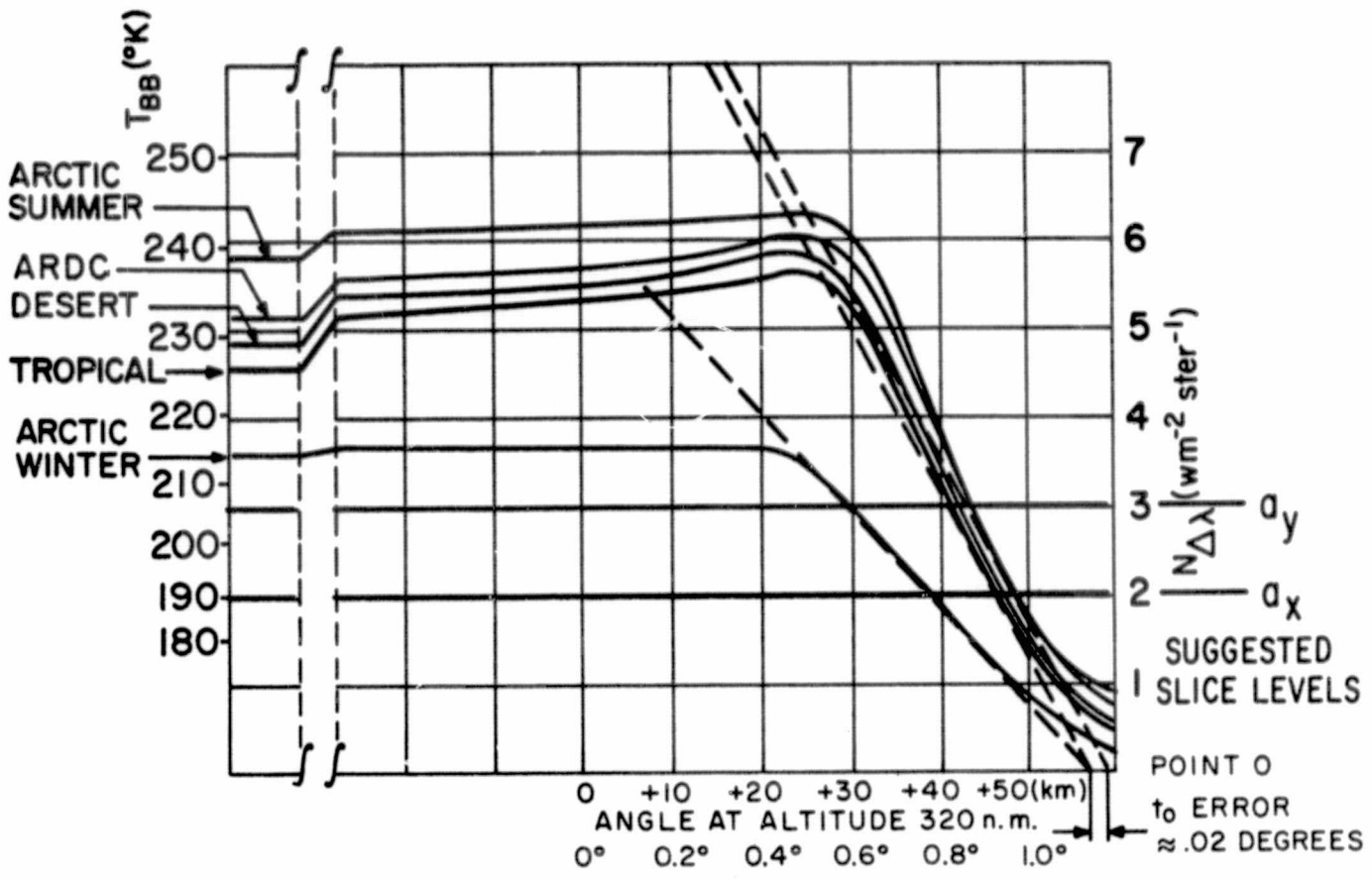

FIGURE 1. HORIZON PROFILE CURVES FOR 14-16μ CO_2 BAND

from cold cloud tops and reflections and scatter of solar radiation. A number of studies and experiments have been conducted more recently in order to obtain a better picture of the Earth's radiation profile in various portions of the electromagnetic spectrum.

III. USE OF THE CO_2 BAND

Data presented by a number of researchers, including Wark,[1] Burn,[2] Hanel[3] and others,[4,5] show that in the 15μ CO_2 band, the Earth's horizon looks uniform and is devoid of the cloud effects which plague us when we use a broad range of the IR Spectrum. Our own studies, drawing heavily on the data presented in the references cited, show how much error results when we use particular sensor parameters for a horizon scanner operating in the 15μ CO_2 band.

The TIROS VII meteorological satellite, which has been in orbit since June 1963, was equipped with a 5-channel radiometer, one of whose thermistor detectors measured radiation in the 15μ CO_2 band. Data from this channel has been analyzed by Goddard Space Flight Center scientists and others. The 5° x 5° field of view employed does not permit detailed determination of horizon profiles, but the radiance levels obtained can be compared with computed values. The agreement between Goddard SFC computed values (Hanel, Bandeen and Conrath[3]) and the values actually measured is excellent, confirming the validity of the curves shown in Figure 1. This is a conclusion reached in several reports published, including W. R. Bandeen, M. Halev, and I. Strange in a NASA Report, X-651-64-218, titled "A Radiation Climatology in the Visible and Infrared from the Tiros Meteorological Satellites."

A unique feature of the horizon profile in a narrow band CO_2 spectral range is illustrated in Figure 1. If we draw the slope lines of the family of horizon profile curves passing through selected fixed values of amplitude (which we have called a_Y and a_X), the lines would intersect in close proximity to Point 0 in the figure. It follows that if we can measure and correct for a slope difference for any scan position that we may encounter under worst geographic and seasonal conditions, we can establish the position of Point 0 to a very high order of accuracy. While the Point 0 should not be construed to correspond to the true Earth horizon, it is important that we keep in mind the fact that Point 0 is symmetrically located at the two horizon crossover positions with respect to the local vertical regardless of the radiance level encountered at either horizon edge crossing. Figure 2 shows this symmetry of Point 0 about the local vertical drawn to a scale which is appropriate for the parameters listed including slope changes produced by a finite field of view and detector response time.

A technique developed for accomplishing this slope correction will be described. Analytical as well as laboratory experimental results show that the pitch and roll outputs for a system operating in the CO_2 band may be corrected to an accuracy of about 0.05° with reference to the local vertical.

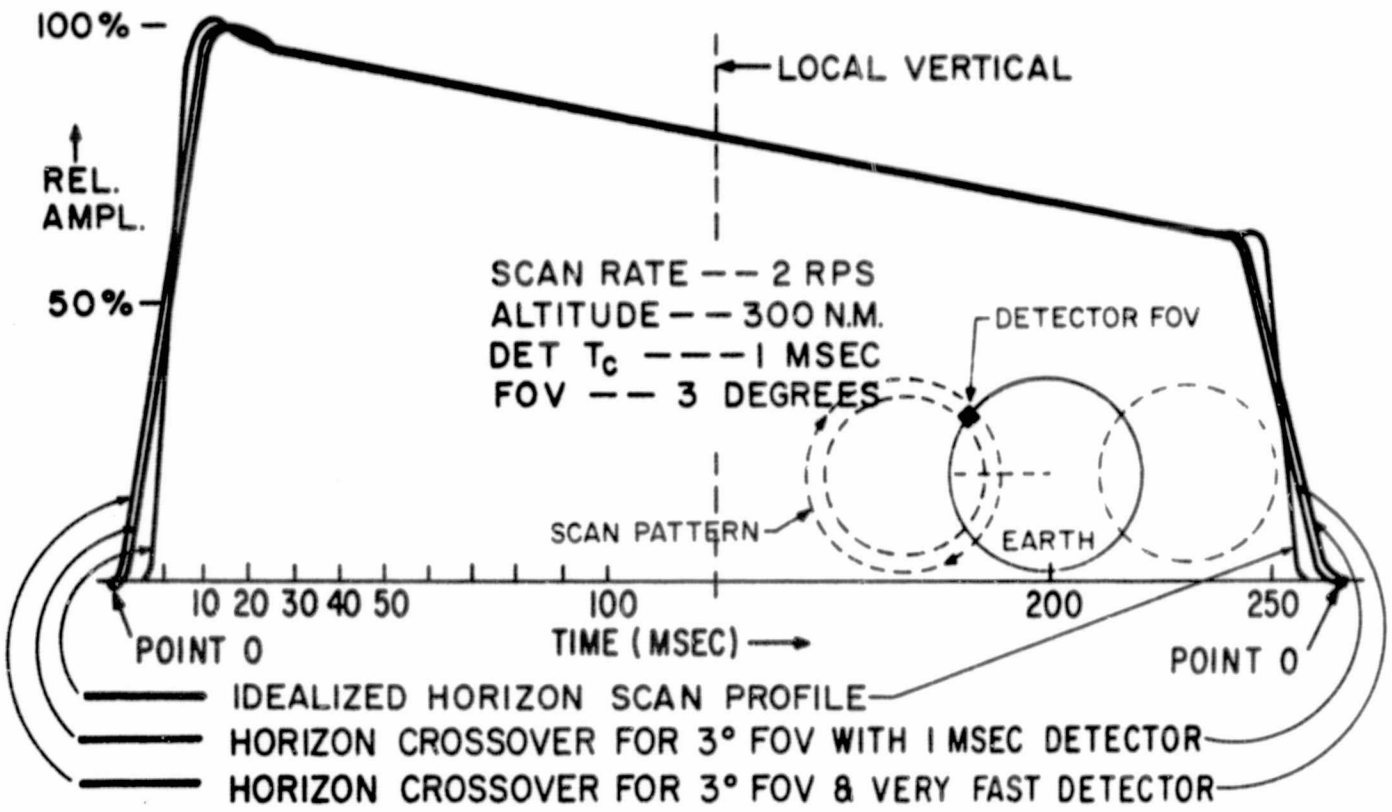

FIGURE 2. HORIZON SCAN PROFILE

An RPC 4000 computer has been programmed to compute the errors which will result when we use particular sensor parameters including field-of-view, detector time constant, scan angle, altitude, etc., all of which normally affect the accuracy of the local vertical determination. An error analysis was performed with the computer programmed to use CO_2 band radiance levels obtained with the TIROS VII Radiometer on November 4, 1963. Considering a sensor system with a detector whose time constant is four times faster than the horizon crossover time for a 3° x 3° field of view, the system errors, before correction, amount to about ±0.5 degree of pitch output. After correction, the maximum error is reduced to 0.05 degree. (See Figure 3, in which the error after the slope correction is shown on an expanded scale.) It should be pointed out that, although the treatment below deals fairly specifically with conical scan sensors, the technique developed for bringing about a correction in pitch and roll error works equally well with edge tracking sensors and other systems where a slope correction is desirable.

IV. ELECTRONICS PROCESSING TECHNIQUE FOR TWO-SLICE CORRECTION SYSTEM

A. Normal Processing (Pitch Channel)

The standard conical scan horizon sensor processing electronics should produce a normalized constant amplitude pulse starting at the time the field of view first crosses the horizon and terminating when the scan leaves the Earth's horizon. The duration of this constant amplitude pulse and its position with relation to a reference pulse representing the vehicle vertical optical position, provide the roll and pitch error data. The method of accomplishing this is shown in Figure 4, where a slice level, a_y, must be exceeded before the normalized earth pulse is generated by a Schmitt trigger circuit. The output of the electronic switch is fed to an integrator which has zero output when the two areas are equal and a measured error output when the areas are not equal due to a change in pitch angle. In practice, the value of slice level in a wide spectral band system may have to be much lower than is shown in the figure; perhaps lower than a_x to avoid possible drop-out of the limited pulse in the presence of cold clouds.

B. Correction Signal Processing (Pitch Channel)

To derive the correction signal, a second slice level at a lower amplitude, designated a_x, is used to trigger a second Schmitt type circuit, as will be described in the next section. By using two slice levels and generating a constant amplitude pulse whose duration is inversely proportional to the slope of the horizon profile in the region of the two slice levels (for a constant scan rate), we obtain a measure of slope which can be used to correct the pitch or roll errors regardless of geographic regions and equivalent horizon temperatures over which the scan occurs.

The mathematical formulation for this is shown in Figure 5, which is an expanded horizon slope dealing with only one edge. The equations show from slope and similar triangle determinations that a correction factor $t_4 - t_o$ may be

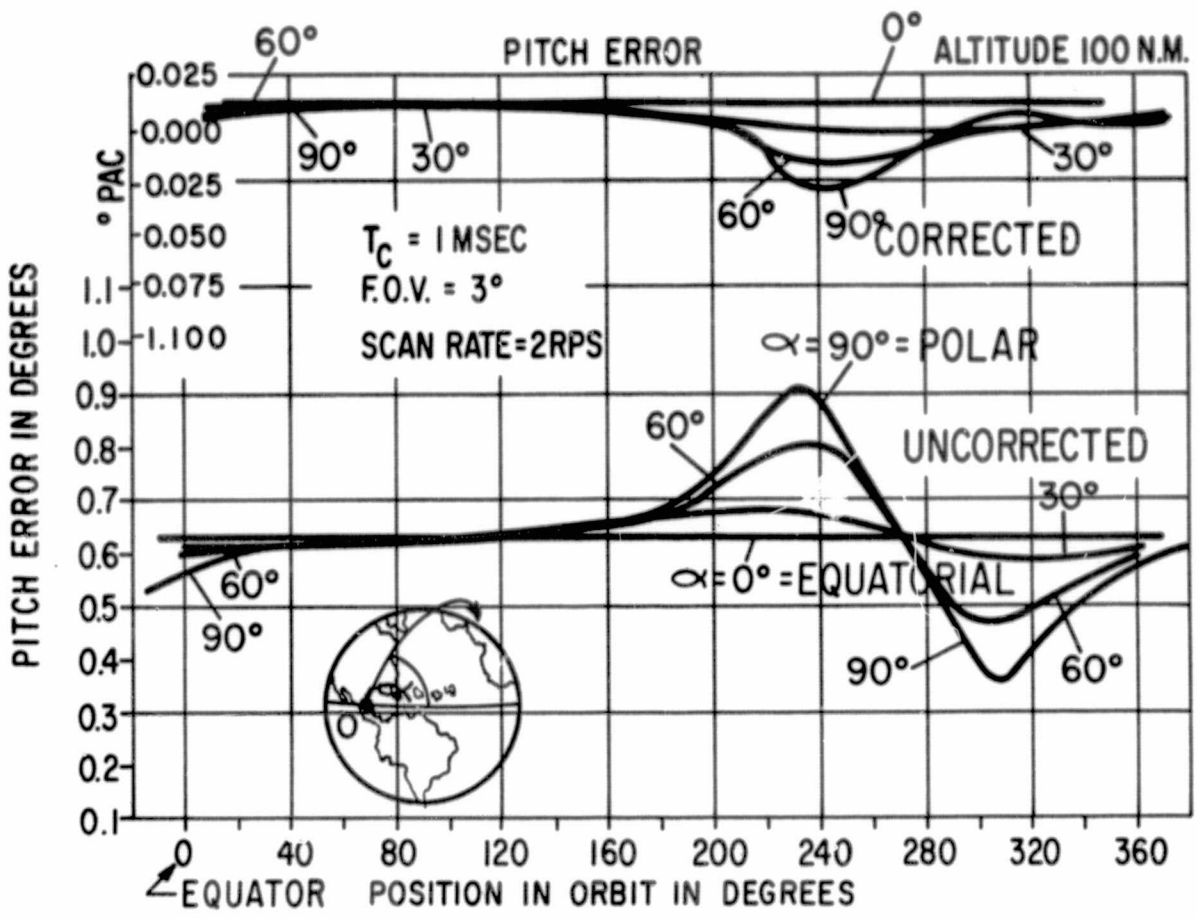

FIGURE 3. MAXIMUM ERRORS FOR STANDARD AND CORRECTED CO_2 BAND HORIZON SCANNER

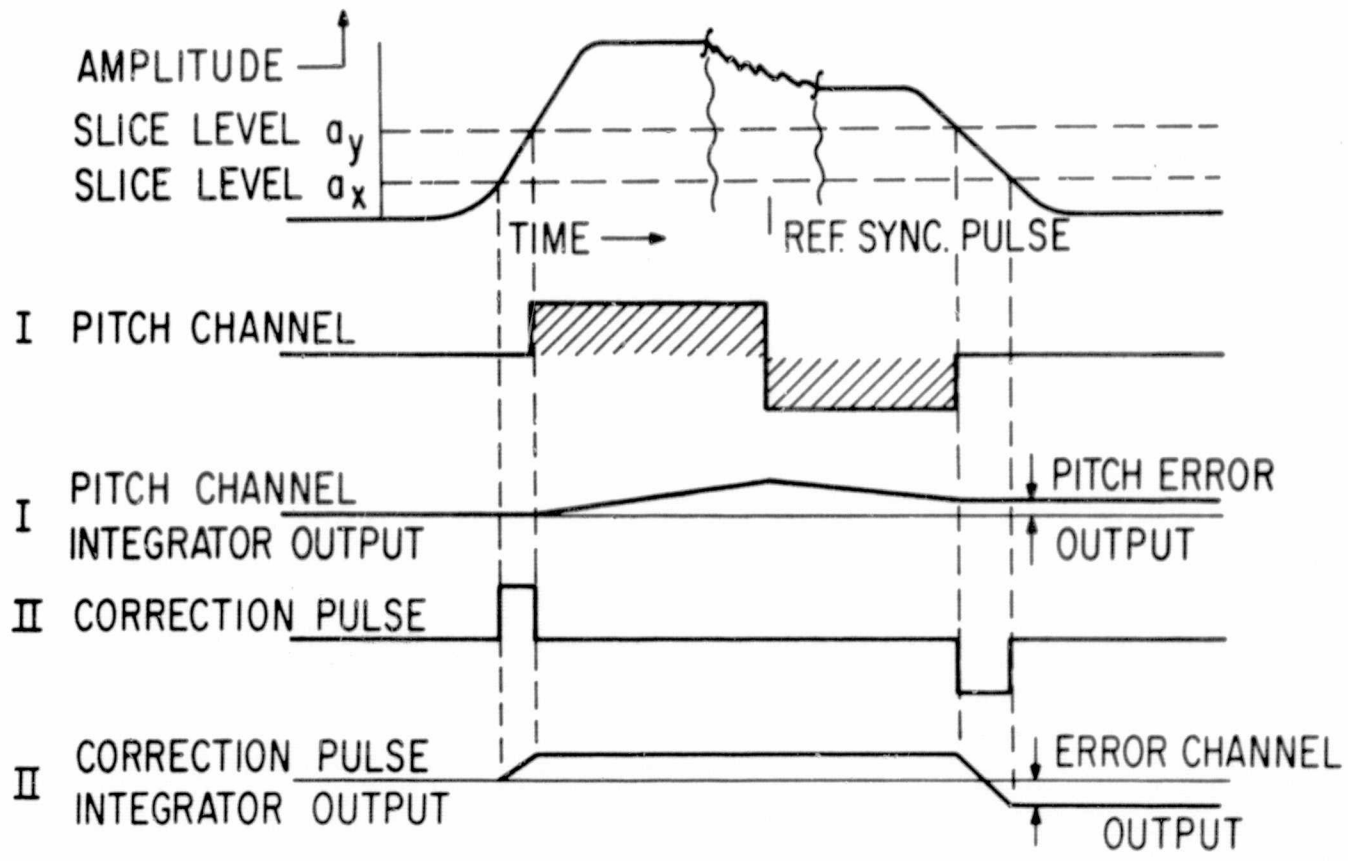

FIGURE 4. SIGNAL PROCESSING FOR HIGH ACCURACY CO_2 BAND HORIZON SCANNER

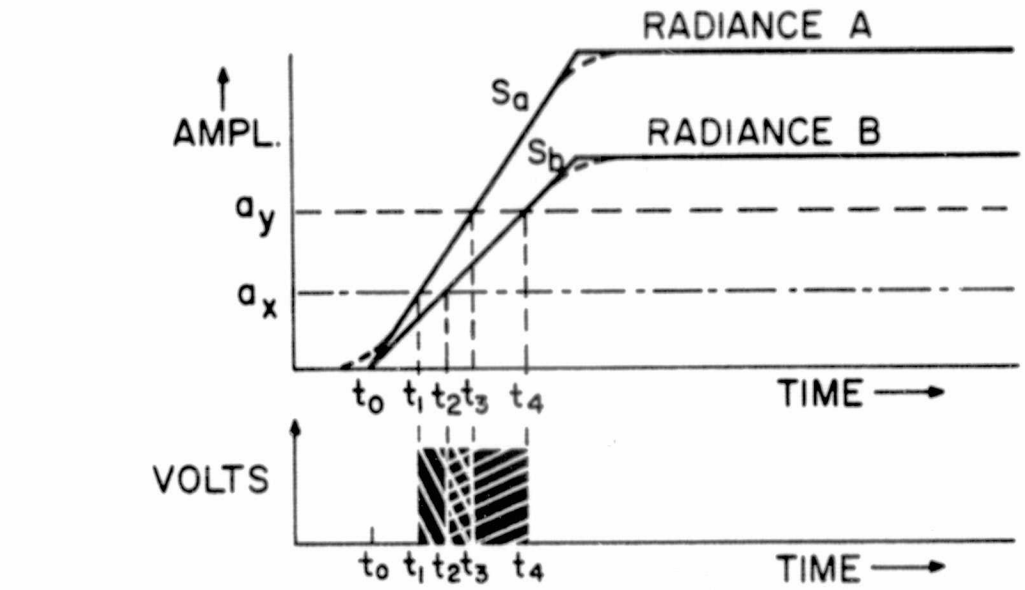

FOR RADIANCE LEVEL A:

$$\text{SLOPE } S_a = \frac{a_y}{t_3 - t_0} = \frac{a_y - a_x}{t_3 - t_1}$$

$$\text{CORRECTION REQUIRED} = t_3 - t_0 = \underbrace{t_3 - t_1}_{\text{MEASURED PULSE DURATION}} \underbrace{\left(\frac{a_y}{a_y - a_x}\right)}_{\text{SCALE FACTOR}}$$

FOR RADIANCE LEVEL B:

$$\text{SLOPE } S_b = \frac{a_y}{t_4 - t_0} = \frac{a_y - a_x}{t_4 - t_2}$$

$$\text{CORRECTION REQUIRED} = t_4 - t_0 = t_4 - t_2 \left(\frac{a_y}{a_y - a_x}\right)$$

FIGURE 5. PRINCIPLES OF ERROR CORRECTION PROCESSING

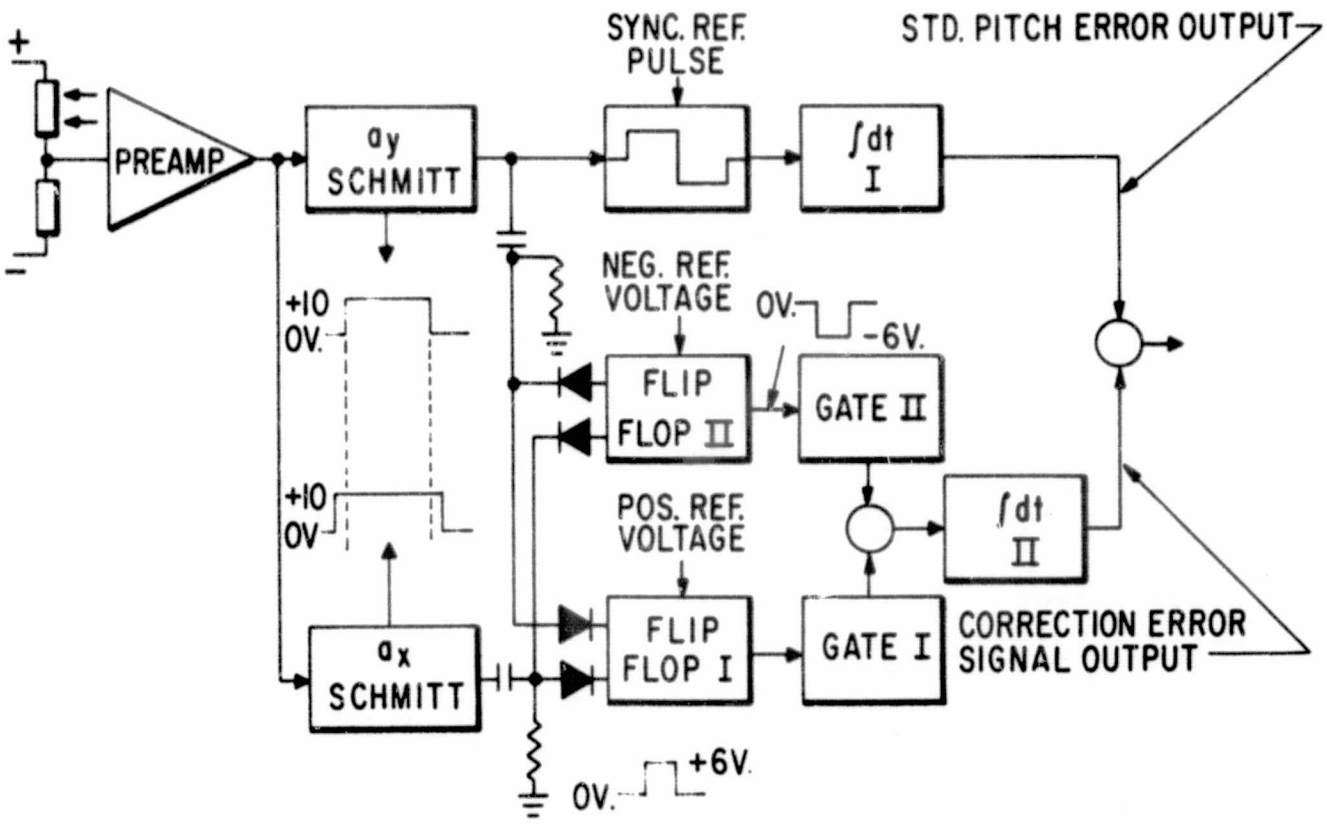

FIGURE 6. CO_2 BAND HORIZON SCANNER BLOCK DIAGRAM

obtained in the standard, single slice level processing procedure. The correction pulse adds to the normalized earth scan pulse the amount required to stretch the total pulse to the Points 0 at the two edges of the horizon over which the scan occurred.

C. Processing Circuitry; Analog Approach

To implement the concepts of the improved accuracy horizon scanner, we require, basically, the original circuits used for normal pitch and roll processing, plus a few elements to produce the error correction outputs which will be integrated with the common pitch and roll output signals. We will limit the discussion primarily to the circuitry which provides the error correction, the more standard processing having been covered in papers and articles prepared previously by M. Arck and M. Merlen[6].

The block diagram, Figure 6, shows the nature of the processing circuitry which is required. The standard circuits are shown in a somewhat simplified form, pointing out only the principal blocks for the pitch error channel. The higher slice level, for example, is achieved by setting the threshold level of a modified Schmitt trigger circuit to a convenient level, say 50% of expected 240° K target. The output of this trigger is a fixed amplitude square pulse of a duration which corresponds to the earth scan period of the sensor from the time of a_y threshold crossover at the leading edge to its crossover at the trailing edge of the earth scan. It is the output of this circuit which is further processed and used as the pitch output in the more conventional horizon scanners. For roll error output, it is compared with a similar pulse from a second head.

A second and identical Schmitt type circuit is used for the error correction channel in the present system. This trigger is set to a lower threshold value, a_x, which may be conveniently adjusted to be 25% of the expected 240° K target temperature preamplifier output signal level. The output of this trigger circuit is again a constant-amplitude pulse but it is of longer duration because it is initiated and terminated at a lower signal level of the earth scan. The Schmitt type circuits used are of a design which insures that hysteresis in their switching cycle is made negligibly small. The leading pulse of Schmitt a_x is next fed to one input of Flip-Flop I, whose output is thus made to go positive. As soon as Schmitt a_y starts its normalized earth pulse, a signal from its output is fed to the second (disabling) input of Flip-Flop I, thus turning off its output pulse. This output I is thus seen to be a pulse of standard amplitude and of a duration corresponding to the time between amplifier output signal crossover of the threshold levels a_x and a_y. The pulse duration is thus a measure of the slope of the leading edge of the earth scan cycle. In an analogous fashion, Flip-Flop II generates a negative pulse of a duration corresponding to the trailing earth scan pulse's time differential in crossing over the threshold levels a_x and a_y. This pulse is a measure of the trailing edge slope, and will be used to apply the desired correction voltage to precisely define the local vertical.

Pitch output is obtained in the conventional scanner by inverting the polarity of the normalized earth scan pulse on a command from the reference signal generator.

The reference pulse occurs at midpoint during the earth scan when there is no pitch error. The waveform thus generated will have equal areas for both the positive- and the negative-going portions. After going through an integrator ($\int dt$ I), zero pitch error output is produced. Error outputs different from zero occur when the reference pulse divides the earth pulse into unequal areas.

Similarly, the outputs of Flip-Flops I and II are positive- and negative-going equal-amplitude pulses of a duration representative of the slope of the horizon edge profiles. After going through Gates I and II, the pulses are fed to an inegrator ($\int dt$ II) whose output is a measure of the pitch correction. This error correction output is summed with the pitch output error signal to provide the highly accurate output.

In similar fashion the roll error may be corrected through subtraction of the two-slice-level error output pulses.

A feature of this error correction system which results in a significant improvement in signal-to-noise ratio is a scheme for gating "on" at least the lower slice level processing circuit at only those times when it is expected that a signal will be received from the detector as it crosses over the horizon. Since we know approximately at what point in the scan cycle the horizon edge will be scanned, it is relatively simple to activate the sensitive, low-threshold level circuit only at those times when it is expected that a signal will be received.

By restricting the time duration of the "acceptable" positive pulses to a minimum determined by the longest expected horizon crossover time and resetting the positive flip-flop for pulses that last longer than this pre-set interval, we can effectively discriminate against noise-triggering during most of the scan period.

D. Digital Circuitry

The techniques described above, while discussed in the form of analog circuitry, are equally adaptable to digital use. An optical pulse generating encoder, mounted on the periphery of the scan mechanism, provides a pulse train or code. In this method of processing, the preamplifier output signal, upon reaching the first slice level, initiates an up-count. The up-count is terminated when the second slice level is crossed. In an exactly analogous fashion, a similar down-count is produced at the trailing edge of the earth scan, subtracting from the accumulated leading edge count. The net difference in counts represents the error correction. A similar up and down count is produced for the conventional pitch (or roll) signals, commencing upon the crossing of the second threshold level a_y, inverting the count upon receiving the reference signal pulse and terminating the subtraction upon crossing the a_y level at the trailing edge of the earth scan. Upon adding the remainder pulses from the normal pitch (or roll) output to the correction pulse remainder we obtain the final, high-accuracy-error output.

V. LABORATORY MODEL SENSOR

Two sensors have been constructed and tested to demonstrate the value of this edge correction technique; each has particular merits in specific applications:

(a) One uses the 20 cps scan speed and scan mechanism of conical scan sensors of current design but substitutes a pyroelectric detector for the immersed thermistor bolometer.

(b) A second version uses the standard thermistor bolometer but uses a hollow-shaft, multiple-pole, motor to operate at a greatly reduced scanning speed. This choice is dictated by the parallel need in all horizon sensors of a high order of sensitivity and rapid response to permit precise determination of the crossover point of a sharply defined edge. Present conical scan horizon sensors, using thermistor bolometers with time constants of several milliseconds, use lead networks in the processing electronics in order to obtain a rise time equivalent to that of a 300μsec. response source. Such compensation results in a severe reduction in signal-to-noise ratio.

A. Pyroelectric Detector with 20 CPS Scan

A pyroelectric detector operating at frequencies beyond its thermal electrical time constant has a sensitivity which is essentially independent of frequency up to the frequency at which the amplifier short circuit noise becomes a limiting factor. This is so because the detector, which behaves like a pure capacitor, shunts out Johnson noise generated at the amplifier input, causing the noise voltage to decay at a rate of 6 dB/octave of frequency. The responsivity beyond the thermal constant of the detector likewise falls off at 6 dB/octave. The signal-to-noise ratio for equal noise bandwidth thus remains constant so long as the noise keeps falling at the 6 dB/octave rate. This is shown in the paper presented here by S. Weiner, and it is seen that a satisfactorily high detectivity is achieved up to frequencies of 1000 cps.

A pyroelectric detector was incorporated into an engineering model of the conical scan sensor for two reasons: its signal-to-noise characteristic and the frequency compensation possible to simulate a 300μsec. time constant. This occurred without degradation of its sensitivity per unit bandwidth. Because this sensor maintains a 20 cps scan speed, the available system error output rate is greater than that of the slower version described below.

B. Slow Scan Sensor Using Thermistor Detector and a Hollow-Shaft Motor Scan Drive

A second version of conical scan sensor, also adapted to demonstrate the edge correction technique, uses a standard immersed thermistor bolometer. In this sensor the optical element, a venetian blind reflector, may scan at about 3 rps because it is mounted directly to the rotor of a hollow-shaft multipole motor. This construction eliminates the gearing between the motor and the optical elements. As a result of the lowered speed and by eliminating gears and all bearings except those of the motor, wear is decreased substantially and the reliability of the mechanism is improved. Figure 7 shows the scanning head of the laboratory model sensor.

To evaluate the performance of the sensors, the optical heads were mounted in the horizon simulator shown in Figure 8. A heated plate source can be adjusted to provide the equivalent of a 240° K CO_2 band atmosphere temperature or other temperatures as desired. Signal-to-noise ratio measurements were made with both sensors for radiance values equivalent to 240° K and 200° K CO_2 band atmosphere temperatures. The data is shown in Table I below.

In order to simulate a lower equivalent radiation level at one edge of the horizon scan (as may occur when scanning over the arctic winter regions), an attenuating screen was introduced at the horizon simulator edge. The radiation

TABLE I — COMPARISON OF PYROELECTRIC AND THERMISTOR SENSORS

Parameter	Pyroelectric Detector System	Thermistor Detector System
Scan Rate	20 RPS	3 RPS
Spectral Response	14 to 16μ	14 to 16μ
Clear Area of Objective	8 cm^2	8 cm^2
Field of View	2° x 4°	2° x 4°
Detector Area	1 x 2 mm	0.2 mm x 0.4 mm Germanium immersed
Detector Time Constant	0.5 sec. compensated to 0.3 msec.	3 msec.
Detector Sensitivity	NEP (500K, 500, 1) = 10^{-9} Watts Detector Operating at Room Temperature	NEP (500K, 100, 1) = 0.36×10^{-9} Watts
Preamplifier Bandwidth	0.5 to 500 cps	0.05 to 400 cps
Signal (Peak) Noise (RMS) for 240° K radiance in 14 to 16μ band before slice level	67 (13.4 for p-p noise)	250 (50 for p-p noise)
Slice Levels	20% and 40% of maximum signal pulse from 240° K horizon	
S/N p-p at lower slice level	2.7	10
Minimum Effective Temperature*	190° K	165° K

* The lowest CO_2 band atmosphere temperature for which the correction system is effective. Below this temperature the system will function without the benefit of the edge correction system with an accuracy similar to that of a standard conical scan sensor.

FIGURE 7. EXPERIMENTAL CO_2 BAND SENSOR HEAD

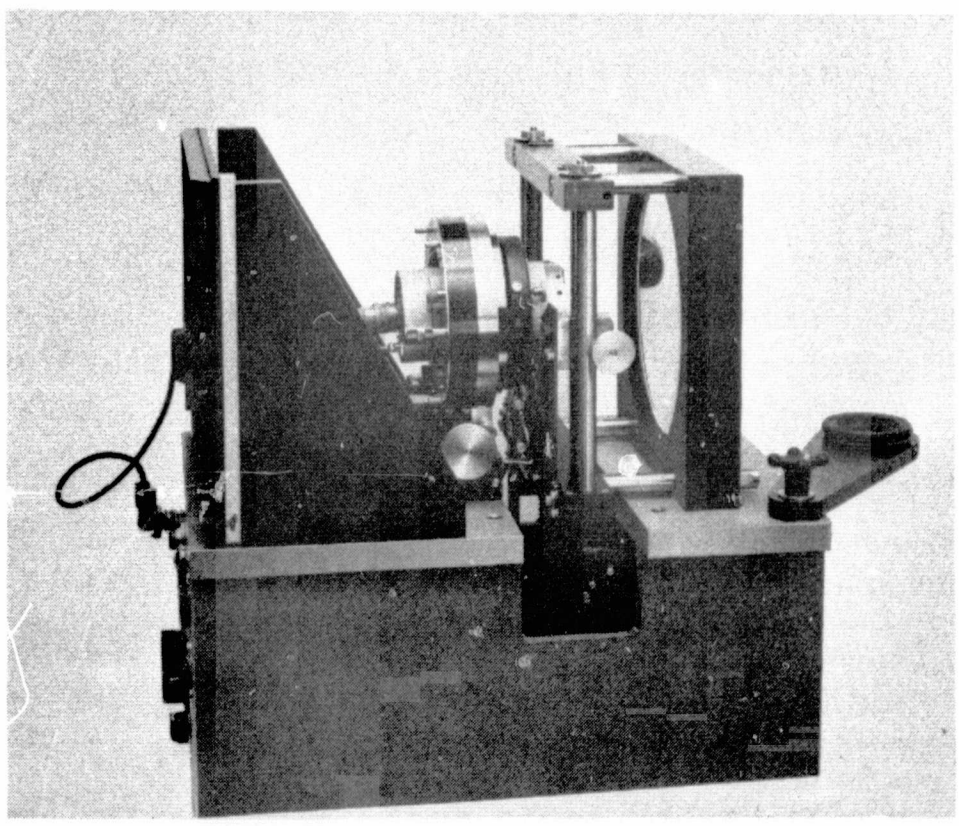

FIGURE 8. EXPERIMENTAL CO_2 BAND SENSOR MOUNTED IN LABORATORY SIMULATOR

received by the detector from this region had an equivalent CO_2 temperature of 210°K (the highest value having been 240°K). While such a system of attenuation of radiance at one side of the scan does not have the characteristic gradient of the horizon profile curves, the finite field of view of the sensor makes the transition a gradual one. In the absence of correcting circuitry, scanning over these regions of dissimilar radiance results in an error in the conventional pitch output of about 0.5 angular degree. On adding the correction channel output signal to the conventional pitch output the error is reduced to about 0.03°.

The data in Table I shows that the thermistor detector system operating at 3 RPS is somewhat superior to the pyroelectric detector system operating at 20 rps. However, it should be remembered that it will have a poorer error output response time. With a scanner operating in the narrow 15μ CO_2 band and a 20 rps scan rate, the required sensitivity cannot be achieved without some changes such as increased size of the optical collector or the substitution of detectors capable of increased response time. Among detectors which do not require cooling to liquid gas temperatures, the pyroelectric detector appears to be an excellent choice.

[1] D. Q. Wark, J. Alishouse, G. Yamamoto, "Variation of the Infrared Spectral Radiance Near the Limb of the Earth," Appl. Opt., February 1964.

[2] J. W. Burn, "The Application of the Spectral and Spatial Characteristics of the Earth's Infrared Horizon to Horizon Scanners," IEEE Trans., August 1963.

[3] R. Hanel, W. R. Bandeen and Conrath, "The Infrared Horizon of the Planet Earth," Rept. X650-62-164 Goddard Space Flight Center, August 1963.

[4] W. Nordberg, W. R. Bandeen, G. Warnecke, V. Kunde, "Stratospheric Temperature Patterns Based on Radiometric Measurements from the TIROS VII Satellite," Rept. X651-64-115 NASA Goddard Space Flight Center.

[5] D. E. Ehlers, "Temperature Measurement of Earth and Clouds from a Satellite," Second Symposium on Remote Sensing Environment, University of Michigan, Ann Arbor, Michigan, October 15-17, 1964.

[6] M. Arck and M. M. Merlen, "Horizon Sensors for Vertical Stabilization of Satellites and Space Vehicles," National Specialists Meeting on Guidance of Aero-Space Vehicles, Boston, Massachusetts, May 25-27, 1960.

[7] J. Duncan, "Horizon Detection Techniques Providing .05° Accuracy at Low Satellite Altitudes," Paper given at 10th National Infrared Information Symposium 1-3 October 1963, Ft. Monmouth, New Jersey.